Spring 5-15-2019

Quantifying Lithochemical Diversity of Martian Materials using Hierarchical Clustering and a Similarity Index for Classification

Michael Conner Bouchard
Washington University in St. Louis

WASHINGTON UNIVERSITY IN ST. LOUIS

Department of Earth and Planetary Sciences

Dissertation Examination Committee:
Bradley Jolliff, Chair
Raymond Arvidson
Robert Dymek
William McKinnon
Scott McLennan

Quantifying Lithochemical Diversity of Martian Materials using Hierarchical Clustering and a Similarity Index for Classification

by

Michael Conner Bouchard

A dissertation presented to
The Graduate School
of Washington University in
partial fulfillment of the
requirements for the degree
of Doctor of Philosophy

May 2019
St. Louis, Missouri

Table of Contents

List of Figures v

List of Tables vii

Acknowledgments viii

Abstract of the Dissertation x

Chapter 1: The Statistical Grouping Model: Methodologies, Theory, and Justification of Multivariate Statistical Analysis of Geochemical Datasets 1

1.1 Data Sets 1

1.2 Hierarchical Clustering 4

1.3 Similarity Index 10

1.4 Multivariate Statistical Analysis of Geochemical Data 13

1.5 Statement of Labor & Copyright and Permissions 16

1.6 References 17

Chapter 2: A Systematic Method for Classifying and Grouping Late Noachian and Early Hesperian Rock Targets Analyzed by the Mars Exploration Rover Opportunity at Endeavour Crater, Mars 22

2.1 Introduction 23

2.2 Methods 27

2.2.1 Dust and Soil Contamination 34

2.2.2 Hierarchical Clustering 35

2.2.3 Similarity Index 36

2.2.4 Previous Modeling 37

2.3 Results 39

2.3.1 Cluster Grouping with SO_3 and Cl Included 40

2.3.2 Cluster Grouping with SO_3 and Cl Excluded 50

2.3.3 Similarity Index Values 51

2.4 Discussion 55

2.4.1 Meridiani Rock Diversity and Model Validation 55

2.4.2 Endeavour Rim Rock Suite Variation and Interpretations 59

2.4.2.1 Two Burns Groups: 59

2.4.2.2 Shoemaker and Grasberg Formations: 60

2.4.2.3 The Copper Cliff/Matijevic unconformity: 61
2.4.2.4 Matijevic formation and erratic rocks: 61
2.4.3 Meridiani Rocks vs Martian Meteorites 63
2.5 Conclusions 65
2.6 References 68
Chapter 3: Rock Suites of Endeavour Crater, Mars: Comparing Perseverance Valley, Spirit of St. Louis, and Marathon Valley 73
3.1 Introduction 74
3.1.1 Perseverance Valley 76
3.1.2 Spirit of St. Louis & Marathon Valley 78
3.1.3 Pre-Endeavour Impact Lithology 80
3.1.4 Occurrence of "Blue" Rocks 81
3.2 Data & Methods 86
3.3 Lithochemical Rock Suites of Perseverance Valley 88
3.3.1 Perseverance Valley Floor Fill Material 92
3.3.2 Ysleta Del Sur Type Outcrop 93
3.3.3 San Miguel Type "Blue" Rocks (Cobbles & Outcrops) 97
3.3.4 Pitted, Silica-Rich Outcrop 100
3.4 Discussion 104
3.4.1 Relationships to Suites Outside of Perseverance Valley 104
3.4.2 Perseverance Valley Formation Mechanisms 107
3.4.3 Perseverance Valley Formation Model 111
3.5 Conclusion 112
3.6 References 113
Chapter 4: Lithochemical Diversity of Martian Crustal Materials as Represented by Rover APXS and Martian Meteorite Bulk Chemistry 119
4.1 Introduction 121
4.2 Data & Methods 131
4.2.1 Data Sets 131
4.2.2 Methods 134
4.3 Resulting Rock Suites 139
4.3.1 Martian Meteorites 139
4.3.2 Gusev Crater 143

4.3.3 Gale Crater 145
4.3.4 Endeavour Crater and Meridiani Planum 149
4.4 Discussion 153
4.4.1 Martian Meteorites 153
4.4.2 Gusev Crater 155
4.4.3 Gale Crater 158
4.4.4 Endeavour Crater and Meridiani Planum 161
4.4.5 Elemental Composition Comparisons 166
4.5 Conclusion 169
4.6 References 173
Appendix 181

List of Figures

Figure 1.1: Hierarchical Cluster Schematic ……...……...…19

Figure 1.2: Internal Data Geometry ……...……...……21

Figure 1.3: Example Hierarchical Cluster …….……...…22

Figure 1.4: Aitchison Cluster Comparison ……...…29

Figure 2.1: Opportunity Rover Traverse ...……...…38

Figure 2.2: Statistical Grouping Model …….……...…40

Figure 2.3: Cluster with SO_3 and Cl ….…….……...…54

Figure 2.4: Cluster without SO_3 and Cl ….…….……..…..…….…….56

Figure 2.5: Target Images: Burns …….…….……...…58

Figure 2.6: Target Images: Grasberg and Shoemaker ……...……...…60

Figure 2.7: Target Images: Matijevic and Erratics ……...…61

Figure 2.8: TAS Diagram …….…….……...…69

Figure 3.1: Opportunity Rover Traverse ...……...…88

Figure 3.2: Perseverance Valley Overview …...……...…90

Figure 3.3: Marathon Valley Overview ….…….……...……...…91

Figure 3.4: Spirit of St. Louis Pancam …...….…….…….93

Figure 3.5: Red Zones ……...……...…….……...…94

Figure 3.6: Blue Rocks ……...……...……..95-96

Figure 3.7: Tholeiitic Composition Plot ……...…….……...…97

Figure 3.8: Marathon Valley Overlook …….……..…….……..…98

Figure 3.9: Perseverance Valley Target Locator …….……...101

Figure 3.10: MI Target Images ……..……...…..107

Figure 3.11: Composition Plots ……..……...…….....109

Figure 3.12: Ysleta Del Sur …….……..…….....110

Figure 3.13: Pitted Rocks …….……..…….....114

Figure 3.14: Cluster with SO_3 and Cl ...……..……...…….....115

Figure 3.15: Cluster without SO_3 and Cl ...……..……..…….....116

Figure 3.16: Summary Clusters ……..……...…….....119

Figure 3.17: Perseverance Valley Structure ..…….....123

Figure 3.18: Endeavour Crater Graben ….....……....124

Figure 4.1: Cluster with SO_3 and Cl ……...……...…….....154

Figure 4.2: Cluster without SO_3 and Cl …….....…….....155

Figure 4.3: Crust Ratio Plot ……...…….……...…….....178

Figure 4.4: Fe/Mn Mantle Ratio Plot ……....…..…….…….……...180

Figure 4.5: Tholeiitic Magma Plot ….……...…..…….....181

List of Tables

Table 1.1: Example Data Set with SO_3 and Cl 17

Table 1.2: Example Data Set Standardized for Variance 20

Table 1.3: Similarity Index Matrix with SO_3 and Cl 25

Table 1.4: Example Data Set Transformed with Aitchison Geometry..... 27-28

Table 2.1: Selected Target Compositions 41-42

Table 2.2: Summary of Selected Targets One 43-44

Table 2.3: Summary of Selected Targets Two 45-46

Table 2.4: Similarity Index with SO_3 and Cl 67

Table 2.5: Similarity Index without SO_3 and Cl 68

Table 2.6: Average Formation Compositions 71

Table 2.7: Normative Mineralogies 76

Table 3.1: Selected Target Summary and Compositions 102-104

Table 3.2: Perseverance Valley Rock Suites 105

Table 3.3: Three Component Mixing Model of Valley Floor Material 108

Table 3.4: Similarity Indexes 112

Table 4.1: Representative Composition Summary 135-142

Table 4.2: Representative Compositions with SO_3 and Cl 143-144

Table 4.3: Representative Compositions without SO_3 and Cl 144-145

Table 4.4: Similarity Indexes with SO_3 and Cl 149-150

Table 4.5: Similarity Indexes without SO_3 and Cl 151-152

Acknowledgments

First and foremost, this work would not have been possible without the encouragement, resources, and guidance of Brad Jolliff. He took a chance on a bright eyed undergraduate and turned him into a scientist. The lessons learned taking classes from and teaching with the faculty of the Earth and Planetary Sciences Department and the cheery conversations and supportive attitude of the department staff contributed greatly to my development and experiences at Washington University in St. Louis. The moral, emotional, and gustatory support of my extended network of family, friends, and community sustained me through some of the toughest times, while my parents and siblings formed a rock for me in one of the most challenging endeavors in life to this point.

A personal thank you to the members of my PhD cohort; Scott Beeler, Roger Bryant, Melody Eimer, Joss Richardson, Xiaochen Mao, and Kelsey Prissel. Their comradery and support, through the thick and thin of this process, made it a bearable and much more enjoyable period of my life. Finally, a thank you to Julie Schneider, who struggled with me through the toughest time period of both our programs with grace and love.

This work would not have been possible without the financial support from JPL subcontract JPL1536058 to B. Jolliff, the NASA Earth and Space Science Fellowship grant #80NSSC17K0490 to M. Bouchard, and support through research fellowships and teaching assistantships from Washington University in St. Louis.

Michael C. Bouchard
April 5th 2019

Dedicated to my parents.

Abstract of the Dissertation

Quantifying Lithochemical Diversity of Martian Materials using Hierarchical Clustering and a Similarity Index for Classification

by

Michael C. Bouchard

Doctor of Philosophy in Earth and Planetary Sciences

Washington University in St. Louis, 2019

Professor Bradley Jolliff, Chair

We are currently living in the golden age of robotic exploration of Mars, with a continued robotic presence there since 1997. Next to Earth, Mars is the planet about which we have gathered the most geologic information. Unlike Earth, Mars does not appear to have plate tectonics, and the planet's primary and secondary crust is dominated by basalts. Understanding the compositional diversity of the materials that make up the martian crust will give us a better insight into the geologic processes that formed the planet and its subsequent evolution. One large and growing source of martian surface compositions is the Alpha Particle X-Ray Spectrometer, an in-situ instrument that has been carried on three Mars rovers, Spirit, Opportunity, and Curiosity. This instrument has measured elemental compositions for martian rocks and soils across three separate terrains on Mars. This dissertation seeks to characterize the diversity and quantify the similarities of compositions of rocks and rock suites as reported in the APXS datasets as well as published compositions of the martian meteorites. The careful application of multivariate statistics allows for a rigorous assessment of these diverse compositions to explore possible compositional groupings and primary and secondary relationships. To this end, a

statistical grouping model comprised of hierarchical clustering and a similarity index, informed by image analysis and ground-truth in-situ Mars exploration, is applied to the data.

Verification of models is essential as statistics can provide spurious results. In Chapter 2, I apply the statistical grouping model to a set of well characterized Opportunity APXS data. These datasets have significant covariant information, such as geographic relationships, rock textures, geologic context, Pancam spectra, and established working hypotheses about local geology. Chapter 2 also explores how the statistical model works relative to compositions of rocks that have undergone different surface treatment by the rock abrasion tool (RAT) on Opportunity. I also test the model sensitivity to dust/soil contamination. The model is able to reproduce several well-known relationships among the Endeavour crater and Meridiani Planum lithologies, as well as produce some new geologic interpretations. New interpretations include: The Meridiani Plains Burns formation is compositionally diverse enough to parse into two superclusters, mostly along the lines of surface coatings. Analysis of the data by excluding S and Cl, some Burns formation rock compositions are similar to the Endeavour crater Shoemaker impact breccias. The clastic Grasberg formation is compositionally homogenous across two temporally distinct units and is most similar to the Shoemaker impact breccia in the Endeavour crater rim segments. These relationships support a local erosional origin instead of a distal ash origin. The lowest member of the Shoemaker breccia, the Copper Cliff unit, is compositionally similar to the pre-Endeavour Matijevic formation and contains Matijevic-type spherules, indicating that this unit contains eroded Matijevic materials. The Matijevic formation is compositionally distinct from other Endeavour materials but is similar to the “blue” (in Pancam false color) basaltic rocks Marquette Island and Margaret Brush. As a final example, the new

regolith breccia class of martian meteorites (NWA 7034/7475) is the only class of martian meteorite to represent common martian surface compositions in the APXS data sets.

Chapter 3 expands the analysis to data collected by Opportunity within Perseverance Valley, using the statistical grouping model to classify lithologies and compare them to rock suites examined elsewhere along the Endeavour crater rim. The model establishes four rock lithologies within the valley, making it the most lithologically diverse location since the rover's first exploration of Endeavour crater at Cape York. The lithologies include: a clast-poor impact breccia that forms the walls of the valley, an outcrop of resistant basaltic rocks that appear "blue" in false color Pancam imagery, an outcrop of pitted rocks that are some of the most silica-rich materials examined by Opportunity, and the valley floor material that comprises a loose regolith mixture of impact breccia, Meridiani soil, and "blue" rocks, implying a trough filled with locally mass-wasted materials. The "blue" rocks are similar enough in composition and texture to be classified as members of the lithology of "blue" rocks observed on the rim overlooking Marathon Valley, an outcrop that is also co-located with a pitted, silica-rich rock unit. This similarity, combined with the lateral offset of units across the valley, indicates that Perseverance Valley is a graben, formed along a radial impact fault that lowered the "blue" and pitted rocks ~80 meters to their current position. Evidence for aqueous alteration and modern aeolian erosion rounds out the valley's history, and a formation model for Perseverance Valley, as supported by observations and lithologic relationships exposed by the statistical grouping model, is presented.

The fourth and final chapter of this dissertation expands the statistical grouping model to include representative lithologies from all three of the landings sites where an APXS was deployed, Meridiani Planum and Endeavour crater (Opportunity), Gusev crater (Spirit), and Gale crater (Curiosity). This study also includes a set of representative martian meteorite compositions

to best establish what these data sets, APXS compositions and published martian meteorite compositions, can tell us about the lithochemical diversity of the martian crust. The basalts of Gusev crater divide into three discrete classes along the lines of geography, pointing to limited mixing across units. In general, Gusev plains basalts are most similar to Endeavour crater materials, and they share a distinctive Fe/Mn mantle compositional trend compared to that of the Shergottite basalts. Unlike Gusev rocks, the sedimentary rocks of Gale crater mostly do not cluster along geographic lines, but where they do, they appear to be related by a common sediment source (Bathurst and Bell Island). Gale crater has two primary igneous protoliths that are especially alkaline in composition (Jake M and Clinton). All three rover locations include relatively silica-rich lithologies, which have some of the most dissimilar compositions across all of the data sets. Some of these silica enrichments are likely due to secondary processes (Endeavour pitted rocks, and Greenhorn Gale class), but for those that may be indicative of primary silica enrichments (ALH 84001, Clinton Gale erratic, and Buckskin Gale class) their SiO_2 vs FeO/MgO ratios could be indicative of a magma evolutionary trend, potentially that of a hydrous, calc-alkaline source. Considering compositions from all of the data sets, the Endeavour crater Grasberg formation composition is still more similar to the average Shoemaker formation composition than to any of the other rock suites represented in the analyses. The “blue” rocks of Endeavour crater can be subdivided into different rock suites, and the “blue” rock suite that is interpreted here to be pre-Endeavour impact (including the Perseverance Valley and Marathon Valley overlook “blue” rocks) is similar enough to the pre-Endeavour clastic Matijevic formation that it is possible the Matijevic formation represents a lithified sedimentary rock formed from eroded pre-Endeavour “blue” rocks. The Meridiani plains erratic, Marquette Island, is also a member of this pre-Endeavour “blue” rock class. Owing to its position on top of the Burns

formation, Marquette Island must have been excavated from a younger, larger crater, such as Iazu or Bopolu, indicating the pre-Endeavour “blue” suite of rocks may be continuous across tens of kilometers and could represent the Noachian cratered terrain underling the Burns formation of Meridiani Planum, some of the oldest rocks examined in-situ on Mars.

The application of this specifically tuned statistical grouping model provides new insights into the geochemical relationships between rock suites within, and across sites on Mars. It provides a rapid and quantitative tool for assessing large numbers of targets at once, and can help to provide a better understanding of the geologic units and context of the landing sites, as well as comparing and contextualizing the APXS data set with martian meteorites to better understand the diversity of the martian crust.

Chapter 1: The Statistical Grouping Model: Methodologies, Theory, and Justification of Multivariate Statistical Analysis of Geochemical Datasets

The exploratory data analysis performed in this dissertation relies on a custom designed statistical grouping model. This model provides a rapid and informative analysis tool for the large data set of rock and soil compositions across Mars as collected by the Alpha Particle X-Ray Spectrometer (APXS) carried on the Spirit, Opportunity, and Curiosity rovers (Gellert et al., 2006; Rieder et al., 2004; Rieder et al., 2003) (example Table 1.1). The model contains two prongs, hierarchical clustering, and a similarity index (SI). The model results are then investigated and enhanced with Panoramic Camera and Microscopic Images for contextual and textural interpretations (Bell et al., 2006; Bell et al., 2003; Herkenhoff et al., 2006; Herkenhoff et al., 2003). Specific details of the model's procedure, application, and validation are presented in chapter two. Here I provide a broader background on the specific statistical techniques used in this model.

1.1 Data Sets

One particularly rich surface data set is the Alpha Particle X-Ray Spectrometer (APXS), an in-situ instrument that measures rock and soil bulk elemental compositions through PIXE and

Alpha particle scattering (Gellert et al., 2004; Gellert et al., 2006; Rieder et al., 2004; Rieder et al., 2003). The APXS was one of the key chemistry instruments carried on both of the Mars Exploration Rovers (MER) Spirit and Opportunity, and an APXS is currently active on the Mars Science Laboratory rover, Curiosity. Together these instruments have built up a data base of almost 1,500 APXS analyses across three different landing sites on Mars and over a total of more than 70 kilometers of rover distance. This data set provides a unique opportunity to compare in-situ analyzed martian materials not only due to the quantity of analyses but also due to the fact that three separate missions have carried essentially the same instrument built and calibrated by the same group (Gellert et al., 2004; Gellert et al., 2006; Rieder et al., 2004; Rieder et al., 2003).

The APXS utilizes a curium-224 source for alpha particle emission and X-ray excitation housed in the sensor head (Rieder et al., 2004; Rieder et al., 2003). The spectrometer was designed to measure both the returned alpha particles and X-rays caused by electron transfer. The Alpha particles returned are the result of Rutherford Backscattering, an inelastic collision with elemental nuclei which results in a loss of energy, however due to interference from the CO_2 environment and the Ti sputtering shield hindering returning alpha particles, the energy was reduced below measurement certainty (Gellert et al., 2006).The MER APXS thus relies principally on its X-ray spectroscopy. The X-rays returning to the sensors are both reflected from the incident radiation and the orbital changes of the target's electrons allowing the instrument to operate on both X-ray fluorescence (XRF) and particle induced X-ray emission (PIXE) (Gellert et al., 2006). This combination of methods allows the team to confidently report elements of atomic mass 23-80 (Gellert et al., 2006). The X-ray energy spectrum and the alpha particle's loss of energy are diagnostic to the molecule's elemental weight and electron structure and are used to identify the sample site's composition as reported in oxide weight percents.

Rock textures are investigated by examining Panoramic Camera (Pancam) and Microscopic Imager (MI) images. The Pancam is an objective, stereo, remote sensing imager that provides high resolution color images and is mounted on the principal viewing mast of Opportunity (Bell et al., 2003; Bell et al., 2006; Squyres et al., 2003). The Pancam is capable of recovering high definition images at a variety of eight filters in combination which provides valuable spectral and contextual information. The L257 (753, 535, and 432 nm) false-color filter configuration is commonly used by the team to enhance textual contrast, and these images were used in this study to provide geologic context for the sample sites. The MI is a fixed focus camera that can acquire images at a spatial resolution of 30 microns/pixel over a wavelength range of 400-700 nm (Herkenhoff et al., 2003). Many of the MI images included in this paper are seam corrected mosaics of four MI images stitched together by the MI team and are used to provide a "hand lens" level petrologic look at the rock types. Each APXS target has complementary Pancam and MI imagery. A subset of APXS data is included in this chapter to illustrate procedure of the statistical grouping model (Table 1.1), while detailed studies and interpretation of model results are presented in the following chapters.

Martian meteorites provide another valuable source of martian compositions. The young achondrites were determined to have originated from Mars due to trapped gases of martian atmospheric composition (Bogard & Johnson, 1983; Bogard, Nyquist, & Johnson, 1984; Owen et al., 1977). While martian meteorites are not representative of the predominate martian surface materials as observed by robotic exploration (McSween, Taylor, & Wyatt, 2009), a new class of martian meteorite, that of the regolith breccia (eg: NWA 7034/7475/7533), is more representative of martian surface materials (Agee et al., 2013; Beck et al., 2015; Cannon,

Mustard, & Agee, 2015; Humayun et al., 2013; Udry, Lunning, McSween, & Bodnar, 2014; Wittmann et al., 2015).

Table 1.1: Example of an input into the statistical grouping model, a subset of Opportunity rover APXS target compositions from the rim of Endeavour crater. These targets include rocks from Perseverance Valley (PV: San Miguel "blue" rocks, Ysleta Del Sur, Pitted rocks, PV floor fill), Marathon Valley (MV: MV "blue" rocks, MV purple rocks), the Spirit of St. Louis feature (SoSL: SoSL floor fill, SoSL red zone), averages of the Endeavour crater rim lithologies (Matijevic, Shoemaker, and Grasberg formations), an average of Meridiani Planum soils and sulfate sandstones (average soil and Burns formation), and two targets analyzed between Cape Tribulation and Cape Byron (Ogallala and Julesburg). This subset is used in this chapter to illustrate an introduction to the statistical grouping model. Detailed geologic context and analysis of these targets is carried out in chapter 3.

Target Name	**SiO_2**	**TiO_2**	**Al_2O_3**	**Cr_2O_3**	**FeO**	**MnO**	**MgO**	**CaO**	**Na_2O**	**K_2O**	**P_2O_5**	**SO_3**	**Cl**
San Miguel Blue Rocks	46.98	0.64	11.6	0.26	13.9	0.37	8.9	5.71	2.34	0.24	0.93	5.52	1.05
Ysleta Del Sur	46.44	0.68	10.43	0.21	14.67	0.15	9.94	5.53	2.27	0.27	0.28	6.11	1.06
Pitted Rocks	57.79	0.70	13.73	0.05	8.23	0.22	4.28	5.75	2.9	0.26	1.39	3.12	0.69
PV Floor Fill	46.15	0.71	10.07	0.3	16.07	0.28	7.5	6.48	2.33	0.36	0.89	7.10	0.87
MV Blue Rocks	48.81	0.72	12.49	0.24	13.99	0.28	9.62	6.04	2.55	0.33	1.04	3.01	0.50
MV Purple Rocks	51.82	0.69	17.59	0.03	9.66	0.17	4.31	8.05	2.96	0.33	0.86	2.96	0.49
SoSL Floor Fill	43.82	0.79	9.35	0.20	16.09	0.29	7.21	6.08	2.32	0.33	1.00	11.07	1.03
SoSL Red Zone	54.98	0.75	10.64	0.28	10.28	0.18	5.64	5.27	2.15	0.36	0.85	7.07	0.96
Matijevic Avg n=6	48.8	0.87	10.02	0.28	15.96	0.33	8.13	5.96	2.34	0.36	0.98	4.93	0.89
Shoemaker Avg n=15	45.2	1.05	9.24	0.22	17.91	0.46	7.83	6.29	2.39	0.48	1.16	6.51	1.09
Ogallala	47.92	0.86	8.16	0.23	20.24	0.24	4.16	5.77	1.78	0.58	1.06	8.68	0.75
Grasberg Avg n=5	45.22	0.98	8.26	0.27	19.24	0.2	5.11	5.98	2.2	0.72	1.11	8.85	1.70
Julesburg	43.25	0.63	8.26	0.19	17.75	0.24	5.8	7.88	1.71	0.38	0.85	13.46	0.63
Burns Avg n=15	38.08	0.78	6.48	0.19	15.94	0.29	7.38	5.48	1.74	0.55	1.03	20.94	1.00
Average Soil n=9	45.3	1.1	9	0.4	19.2	0.4	7.4	7	2.2	0.5	0.9	5.8	0.6

1.2 Hierarchical Clustering

The first step of the statistical grouping model uses hierarchical clustering to establish subclusters and superclusters of rock targets to be further examined as potential related rock suites. Hierarchical clustering is an iterative statistical tool used to organize large datasets according to internal similarities of attributes (Xu & Wunsch II, 2009). It is an unsupervised form of data exploration, which means there is no need for prior grouping information. It works by creating a distance matrix (n x n) of the sum of the squared differences of the attributes of

each case (Van den Boogaart & Tolosana-Delgado, 2011). In this model the cases are the APXS or martian meteorite compositions, and their quantitative attributes are defined as the percentages of each element or oxide by weight.

Clustering can either be agglomerative, iteratively grouping together the most similar targets, or divisive, iteratively separating the most dissimilar targets. Since this study is interested in linkages between similar compositions, and less so the specific linkages of a highly dissimilar composition, agglomerative clustering was selected. Both approaches rely on calculating a distance metric between cases, such as euclidean, minkowski, manhattan, and maximum distance matrices. This study utilizes a euclidean distance matrix.

Once distances are established, they must be linked. Linkage techniques include: the nearest neighbor, farthest neighbor, group average, ward, or centroid approach. The nearest neighbor technique for fusing agglomerative clusters together defines the distance between two groups as the distance between the two closest cases, while the furthest neighbor technique defines this distance as the distance between the two furthest cases. The group average technique defines the distance between clusters as the mean between all of the individual cases and then replaces these cases with the average of those cases, while centroid replaces them with the centroid of those cases. The nearest and farthest neighbor distance metrics have a tendency to become driven by extreme outliers in data sets. There was no discernable difference in model outputs between implementing the group average vs. the centroid metric, so group average was selected because of its similarity to the standardization step applied in the similarity indexing step of the model, and its slight advantage in processing time.

For the group average approach, the Euclidian distance matrix is used to determine which two cases are the most alike. The two most similar cases are grouped together, and their values are replaced by their combined average (Figure 1.1). The test is run again recursively until the number of cases has been reduced to one. This "agglomeration" progressively decreases the field of cases by grouping them into families. When the process is complete these families have all been linked and can be displayed as a single dendrogram.

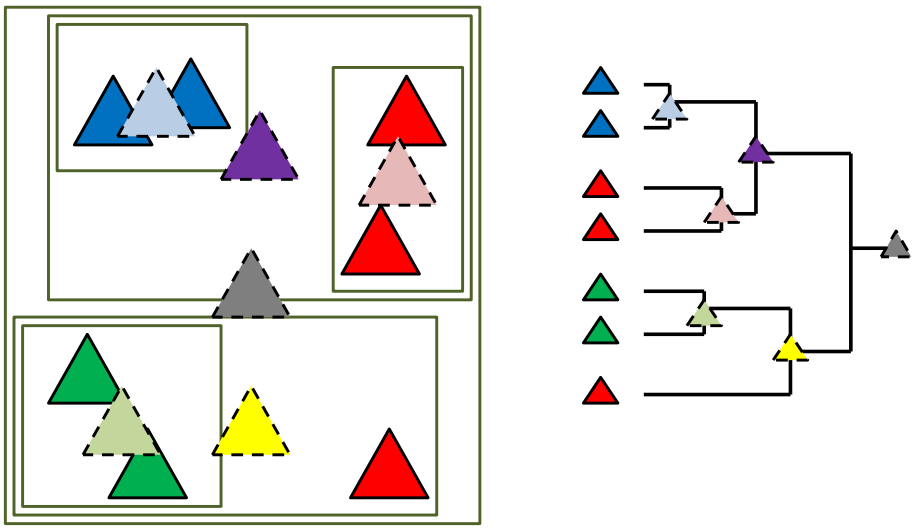

Figure 1.1: Schematic representation of a two-dimensional data set being combined into a dendrogram by an agglomerative, euclidean, group average, hierarchical cluster.

Hierarchical clustering tends to be driven by the cases with the largest absoluter variance (i.e., SiO_2, SO_3, and Al_2O_3); to reduce this effect, I first standardize the data for variance by subtracting the lowest oxide value and dividing by the range of oxides values (Table 1.2). This standardization technique has been shown to provide the best recovery of the underlying data's structure across varied parameters and clustering methods (Milligan & Cooper, 1988). This standardization for variance is notable because it maintains the data set's internal multi-

dimension geometry (Figure 1.2). Gasnault et al. (2010) employed a similar standardization step before applying multivariate statistics to martian geochemical data.

$$X_{std} = \frac{X - Min(X)}{Max(X) - Min(X)}$$

Table 1.2: Subset of APXS targets from Table 1.1, standardized for elemental variance. The range across each oxide now ranges from 0-1.0.

Target Name	**SiO_2**	**TiO_2**	**Al_2O_3**	**Cr_2O_3**	**FeO**	**MnO**	**MgO**	**CaO**	**Na_2O**	**K_2O**	**P_2O_5**	**SO_3**	**Cl**
San Miguel Blue Rocks	0.45	0.02	0.46	0.62	0.47	0.71	0.82	0.16	0.50	0.00	0.59	0.14	0.46
Ysleta Del Sur	0.42	0.11	0.36	0.49	0.54	0.00	1.00	0.09	0.45	0.06	0.00	0.18	0.47
Pitted Rocks	1.00	0.15	0.65	0.05	0.00	0.23	0.02	0.17	0.95	0.04	1.00	0.01	0.17
PV Floor Fill	0.41	0.17	0.32	0.73	0.65	0.42	0.58	0.44	0.50	0.25	0.55	0.23	0.31
MV Blue Rocks	0.54	0.19	0.54	0.57	0.48	0.42	0.94	0.28	0.67	0.19	0.68	0.00	0.01
MV Purple Rocks	0.70	0.13	1.00	0.00	0.12	0.06	0.03	1.00	1.00	0.19	0.52	0.00	0.00
SoSL Floor Fill	0.29	0.34	0.26	0.46	0.65	0.45	0.53	0.29	0.49	0.19	0.65	0.45	0.45
SoSL Red Zone	0.86	0.26	0.37	0.68	0.17	0.10	0.26	0.00	0.35	0.25	0.51	0.23	0.39
Matijevic Avg n=6	0.54	0.51	0.32	0.68	0.64	0.58	0.69	0.25	0.50	0.25	0.63	0.11	0.33
Shoemaker Avg n=15	0.36	0.89	0.25	0.51	0.81	1.00	0.63	0.37	0.54	0.50	0.79	0.20	0.50
Ogallala	0.50	0.49	0.15	0.54	1.00	0.29	0.00	0.18	0.06	0.71	0.70	0.32	0.21
Grasberg Avg n=5	0.36	0.74	0.16	0.65	0.92	0.16	0.16	0.26	0.39	1.00	0.75	0.33	1.00
Julesburg	0.26	0.00	0.16	0.43	0.79	0.29	0.28	0.94	0.00	0.29	0.51	0.58	0.12
Burns Avg n=15	0.00	0.32	0.00	0.43	0.64	0.45	0.56	0.08	0.02	0.65	0.68	1.00	0.42
Average Soil n=9	0.37	1.00	0.23	1.00	0.91	0.81	0.56	0.62	0.39	0.54	0.56	0.16	0.09

All clusters prepared for this paper used agglomerate, group average clustering (Figure 1.3), and the hierarchical clustering package utilized in the software, *R*, was verified by calculating the distance matrixes (sum of squared Euclidian differences) in Excel and recreating each step of the clustering algorithm for a selected subset of data. Clusters generated in this manner matched those exported from the cluster algorithm in *R*.


SiO2
TiO2
Al2O3
Cr2O3
FeO
MnO
MgO
CaO
Na2O
K2O
P2O5
SO3
Cl


SiO2_var
TiO2_var
Al2O3_var
Cr2O3_var
FeO_var
MnO_var
MgO_var
CaO_var
Na2O_var
K2O_var
P2O5_var
SO3_var
Cl_var

Figure 1.2: These two plots represent the internal data geometry as 78 two-element combinations of the 13 oxide weight percentage values in Table 1.1. The plot on top is the data "as is" (Table 1.1), and the plot on bottom is after the data has been standardized for variance (1.2). The compositional range changes between the two plots; as seen here, the integrity of the internal data geometry is maintained.

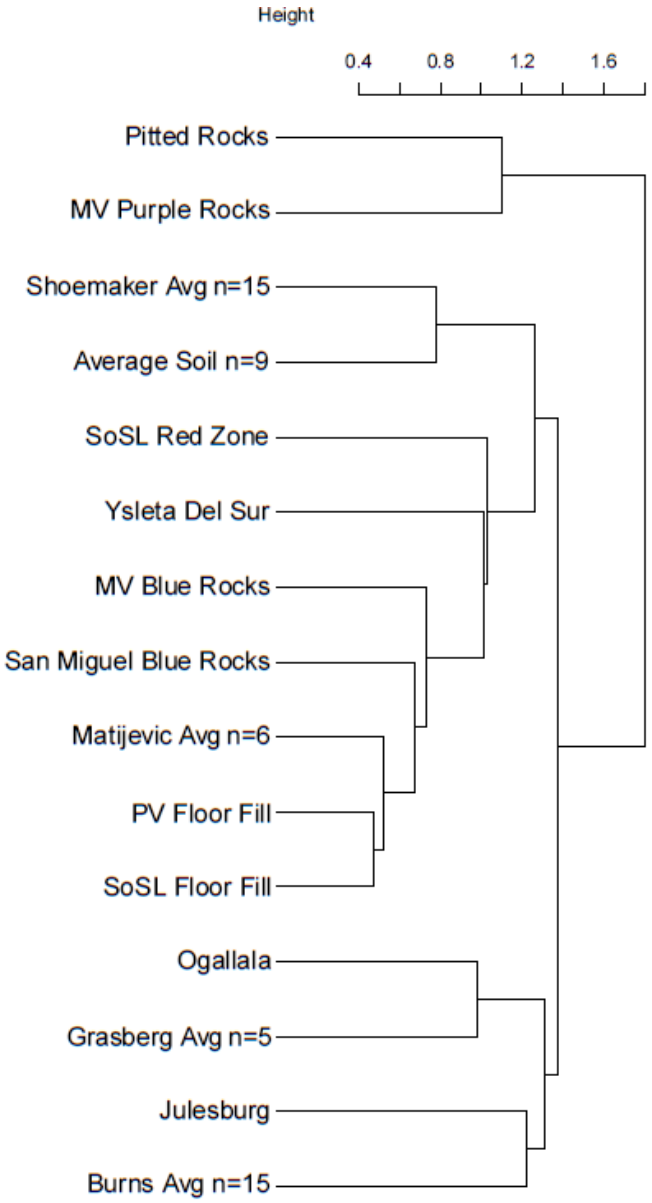

Figure 1.3: Example of an agglomerative, euclidean distance, group average, hierarchical cluster generated from the input of Table 1.2. Note the clustering of the Shoemaker formation, which comprises impact breccias in Endeavour crater, and the average Meridiani soil composition. Both compositions representing similar local geologic unit average compositions, compared to the clustering of the generally dissimilar, but silica-rich Perseverance Valley "pitted rocks" and Marathon Valley "purple rocks" (Chapter 3).

Other multivariate sorting methods can - and have been - applied to geochemical datasets including K-means clustering and principal component analysis. K-means clustering requires a number of output clusters to be selected prior to the analysis. This predetermination of the number of clusters makes K-means a supervised clustering algorithm, compared to the unsupervised hierarchical clustering algorithm. Limiting the number of clusters causes K-means clustering to be less exploratory, and it does not handle data outliers well. For example, when tested on Chapter 1 data sets, K-means clustering grouped the Endeavour basaltic erratic Bounce Rock (which has been compared to martian meteorite EETA 79001 lithology B, (Zipfel et al., 2011)) with the sulfate-sandstone Burns formation of Meridiani Planum, while hierarchical clustering allowed the Bounce Rock erratic to be an outlier loosely linked with EETA 79001 lithology B.

1.3 Similarity Index

The hierarchical clustering method provides a rapid classification scheme, but clustering of the late stage, most dissimilar targets, may be misleading. The next step in the statistical grouping model developed for this dissertation is an error weighted, χ^2 deviation technique. This approach is used to asses a goodness of fit for the clustering, as well as to generate an independent metric with which to quantify similarity of compositions on a target by target basis. The χ^2 approach compares two cases (rock compositions A and B) by dividing the oxide weight percent difference by their average and an appropriate weighting factor (*un*) (modified from (Korotev, Haskin, & Jolliff, 1995). These weighting factors were scaled based on the average APXS instrument measurement precision for each oxide measurement within each cluster as reported in the Planetary Data System (SiO_2: 0.02, TiO_2: 0.15, Al_2O_3: 0.03, Cr_2O_3: 0.2, FeO:

0.02, MnO: 0.1, MgO: 0.03, CaO: 0.02, Na_2O: 0.2, K_2O: 0.2, P_2O_5: 0.1). This factor makes the model unique in that it is specifically weighted for the APXS instrument precision, with slightly greater weight given to oxides that are known to a higher level of certainty. This value is squared to generate an effective absolute value, and summed across each attribute/oxide. The resulting error-weighted, sum-of-squared differences, χ^2 deviations, are used as a unit-less Similarity Index (SI).

$$\chi^2 = \sum_{i=1}^{n} \left[\frac{(A_i - B_i)}{\left(\frac{A_i + B_i}{2} * un\right)} \right]^2$$

Comparisons using this index are done using the 12 major and minor oxides and Cl, as well as with SO_3 and Cl removed and the bulk composition renormalized to 100%. Most alteration occurring at the surface of Mars appears essentially to be isochemical alteration, mainly addition of S and Cl (McLennan, 2012; McLennan & Grotzinger, 2008; Ming, Morris, & Clark, 2008; Morris & Klingelhöfer, 2008). Moreover, the relatively unaltered igneous martian meteorites S content is well below 1 wt%. By removing SO_3 and Cl and renormalizing a composition to 100% we can attempt to compare potential protolith compositions. However, we recognize the assumption of isochemical alteration may not always be correct. Since SO_3 has a high variance (~0 to ~20 wt%), removing it causes all SI values to become more similar. By using a *reduced* χ^2 (dividing χ^2 by *n*, either 13 or 11) we can more directly compare the SI values across both data sets (with and without S and Cl).

$$\chi^2_r = \frac{\chi^2}{n}$$

A perfect SI match would yield a χ^2 value of zero, while multiple APXS measurements on the same target would give SI values <20 (i.e., 1-2 across three analysis of Sergeant Charles Floyd all RAT-brushed, and 8-24 across three Steno targets, unbrushed, brushed, and RAT abraded). However, it can only compare between two cases at a time, the antitheses of the cluster analysis. Results of the SI analysis are reported in SI matrices throughout the dissertation and appendixes (e.g., Table 1.3).

Table 1.3: Matrix of SI values comparing compositions in Table 1.1 (with SO_3 and Cl included). The lower the value, the more similar the compositions are (ie, floor of the Endeavour crater Perseverance Valley has an SI of 45 with the general Endeavour crater impact breccia of the Shoemaker formation), the higher the SI value, the more dissimilar the compositions are (ie, the unique and silica-rich pitted rocks of Perseverance Valley SI's are all >1,000).

	SMB	YDS	PtR	PVF	MVB	MVP	SSLF	SSLR	Mtjv	Shoe	Og	Grs	Jls	Brns	Soil
San Miguel Blue Rocks	0	143	1525	252	517	1573	279	1165	105	250	629	465	859	1457	487
Ysleta Del Sur		0	1683	431	718	1809	412	1257	281	411	672	571	973	1399	653
Pitted Rocks			0	1703	1401	1684	1765	2148	1487	1754	1661	1688	2137	2670	1872
PV Floor Fill				0	550	1405	99	1196	123	45	585	281	340	1639	119
MV Blue Rocks					0	1364	609	1557	474	607	1029	842	1020	1863	714
MV Purple Rocks						0	1623	1578	1538	1589	1896	1655	1501	2829	1498
SoSL Floor Fill							0	1325	216	92	530	186	344	1435	276
SoSL Red Zone								0	1202	1330	1647	1373	1494	2342	1406
Matijevic Avg n=6									0	113	540	350	673	1565	262
Shoemaker Avg n=15										0	535	215	397	1625	122
Ogallala											0	445	845	1726	682
Grasberg Avg n=5												0	432	1587	390
Julesburg													0	1801	248
Burns Avg n=15														0	1852
Average Soil n=9															0

1.4 Multivariate Statistical Analysis of Geochemical Data

Geochemical data are inherently multivariate and compositional data, in part by definition, are proportional. The relative proportions of geochemical data, whether mineral, chemical, or volume/mass/molecule/elemental percentages, contains useful information. Proportions are useful in geologic analysis since they permit the study of materials across a range of relative quantities and are often indicative of primary formation and/or secondary alteration processes.

Multivariate statistics has not only been a staple toolset in general geologic data exploration (Koch Jr. & Link, 1971), but has been used to much success in the exploration data analysis of martian materials, including but not limited to: hierarchical clustering (Bouchard & Jolliff, 2018; Farrand et al., 2014; Mittlefehldt et al., 2018), error weighted χ^2 deviations (Adcock, Udry, Hausrath, & Tschauner, 2018; Bouchard & Jolliff, 2018; McLennan et al., 2005; Udry et al., 2014), least squares mixing models (Larsen, Arvidson, Jolliff, & Clark, 2000), and correspondence analysis (Arvidson & al., 2011; Arvidson et al., 2010; Arvidson et al., 2008; Larsen et al., 2000).

In the realm of pure mathematics multivariate statistics are traditionally not applied to proportional data sets because of issues with forced closure, abnormal distributions of bounded range data, and subcompositional coherence. Compositional data are inherently sub-compositions of something. Even the APXS oxide weight-percent data does not represent the *true* complete content of a given material (i.e., lacking low-concentration components that might be below detection limits), but the dominant measured components are still normalized to a proportion of 100%. This normalization causes induced correlations in the data, or forced closure (Van den Boogaart & Tolosana-Delgado, 2011). In this manner each component of a

composition is dependent on the others, as raising one value will force the others to be lessened. Issues with the application of traditional multivariate statistics to compositional data sets goes back to the 19th century (Pearson, 1897) and was investigated more thoroughly in the 1970's and 80's (Butler, 1978; Butler, 1979; Chayes & Trochimczyk, 1978; Pawlowsky-Glahn, 1984). One seminal paper resulting from that investigation was Aitchison's 1986 work.

Aitchison (1986) demands that the analysis of compositional data be carried out such that the results do not dependent on the presence of irrelevant components, now known as the principle of subcompositional coherence. This principle implies that similar results should be able to be attained as subsets of the composition are examined (Van den Boogaart & Tolosana-Delgado, 2011). Aitchison suggested that statistical methods derived for interval scale data can reliably be applied to compositions if they are first transformed on a log-ratio scale, thus removing the data from a closed-proportional space (Aitchison, 1986). Despite its mathematical rigor, the uniqueness and complexity of this transformation has resulted in the Aitchison's simplex geometry often being ignored in geologic work (Van den Boogaart & Tolosana-Delgado, 2011).

One transformation, the Aitchison distance (1986) is recommended to generate the requisite distance matrix for generating hierarchical clusters (Van den Boogaart & Tolosana-Delgado, 2011). This statistical grouping model validation with Opportunity data and is described in detail in chapter 2. This model does not invoke Aitchison simplex geometry, but I did calculate the Aitchison distance matrix (Table 1.4) of data subsets, passed them through the model, and compared the outputs.

Table 1.4: Here the APXs targets from Table 1.1 have been transformed with Aitchison simplex geometry.

Target Name	**SiO_2**	**TiO_2**	**Al_2O_3**	**Cr_2O_3**	**FeO**	**MnO**	**MgO**	**CaO**	**Na_2O**	**K_2O**	**P_2O_5**	**SO_3**	**Cl**
San Miguel Blue Rocks	0.48	0.01	0.12	0.00	0.14	0.00	0.09	0.06	0.02	0.00	0.01	0.06	0.01

Ysleta Del Sur	0.47	0.01	0.11	0.00	0.15	0.00	0.10	0.06	0.02	0.00	0.00	0.06	0.01
Pitted Rocks	0.58	0.01	0.14	0.00	0.08	0.00	0.04	0.06	0.03	0.00	0.01	0.03	0.01
PV Floor Fill	0.47	0.01	0.10	0.00	0.16	0.00	0.08	0.07	0.02	0.00	0.01	0.07	0.01
MV Blue Rocks	0.49	0.01	0.13	0.00	0.14	0.00	0.10	0.06	0.03	0.00	0.01	0.03	0.01
MV Purple Rocks	0.52	0.01	0.18	0.00	0.10	0.00	0.04	0.08	0.03	0.00	0.01	0.03	0.00
SoSL Floor Fill	0.44	0.01	0.09	0.00	0.16	0.00	0.07	0.06	0.02	0.00	0.01	0.11	0.01
SoSL Red Zone	0.55	0.01	0.11	0.00	0.10	0.00	0.06	0.05	0.02	0.00	0.01	0.07	0.01
Matijevic Avg n=6	0.49	0.01	0.10	0.00	0.16	0.00	0.08	0.06	0.02	0.00	0.01	0.05	0.01
Shoemaker Avg n=15	0.45	0.01	0.09	0.00	0.18	0.00	0.08	0.06	0.02	0.00	0.01	0.07	0.01
Ogallala	0.48	0.01	0.08	0.00	0.20	0.00	0.04	0.06	0.02	0.01	0.01	0.09	0.01
Grasberg Avg n=5	0.45	0.01	0.08	0.00	0.19	0.00	0.05	0.06	0.02	0.01	0.01	0.09	0.02
Julesburg	0.43	0.01	0.08	0.00	0.18	0.00	0.06	0.08	0.02	0.00	0.01	0.13	0.01
Burns Avg n=15	0.38	0.01	0.06	0.00	0.16	0.00	0.07	0.05	0.02	0.01	0.01	0.21	0.01
Average Soil n=9	0.45	0.01	0.09	0.00	0.19	0.00	0.07	0.07	0.02	0.01	0.01	0.06	0.01

The resulting clusters are similar to outputs generated without the Aitchison geometry, with most targets clustering in the same subclusters, and dissimilar outliers remained outliers (Figure 1.4). However, there are some differences in linkage geometry, and some of these differences appear to even be counterintuitive (Figure 1.4). This could be in part due to the Aitchison geometry's minimization of some elements, including MnO which can be an important indicator of differences in primary mantle compositions and/or secondary alteration. The pre-clustering data standardization procedure used in this statistical grouping model (described in section 1.2, Table 1.2) prevents the cluster algorithm from being driven by the values with the highest variance (SiO_2, SO_3, Al_2O_3, etc.), maintains the integrity of the data's internal geometry (Figure 1.2), and transforms each target's composition out of a closed, proportional data set. These reasons drive its adoption in the model over Aitchison geometry.

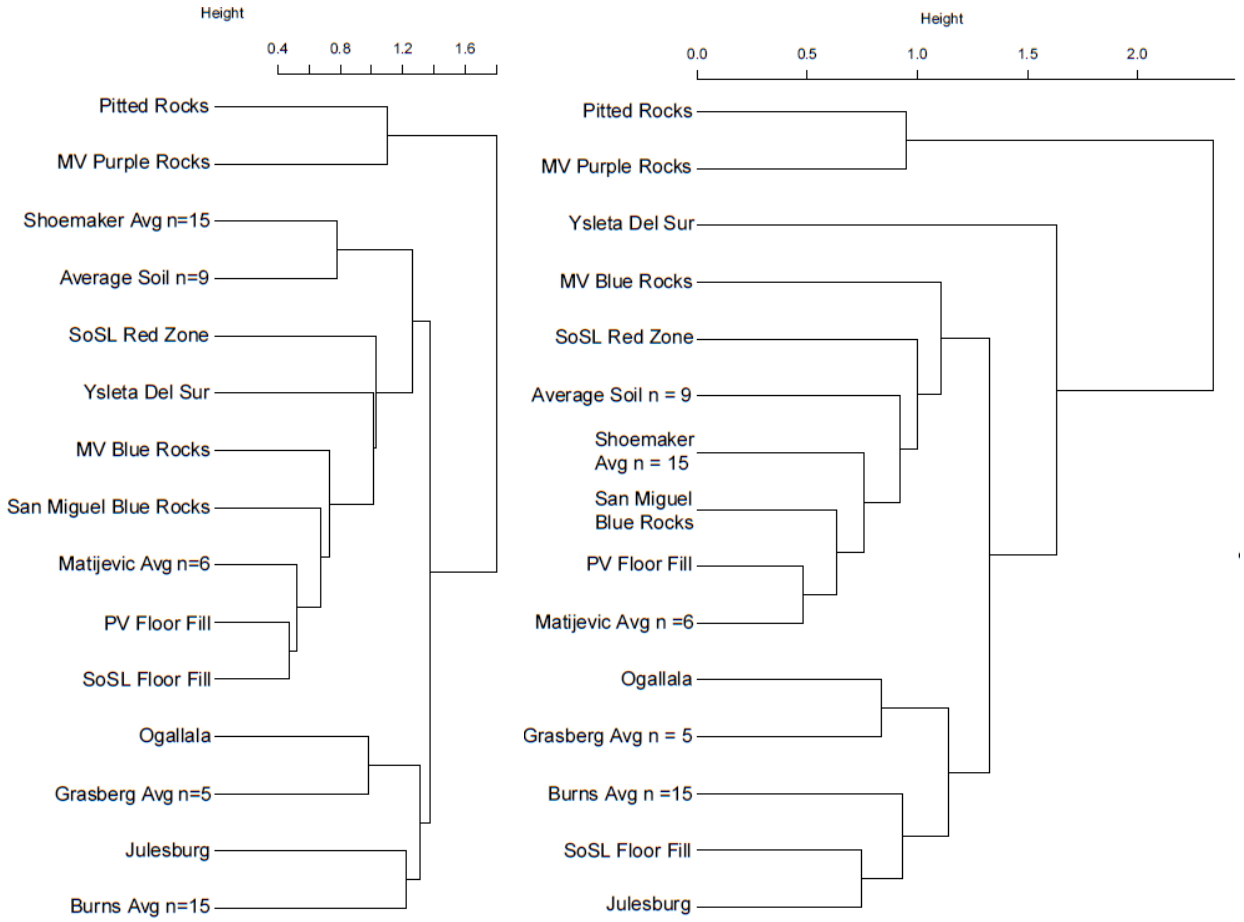

Figure 1.4: Agglomerative, euclidean distance, group average, hierarchical clusters generated from data standardized for variance as shown in Table 1.2 (left) and data with the Aitchison distance geometry as shown in Table 1.4 (right). In both clusters, the silica-rich targets group together off of the rest of the data set. Both clusters have a loose, dissimilar supercluster containing the Grasberg and Burns formation compositions, but the Aitchison geometry cluster includes the Spirit of St. Louis floor fill composition with them. A composition that is a much more similar (SI: 99) to the Perseverance Valley floor fill than the Julesburg target (SI: 344), an example of the occasionally spurious connections in the Aitchison geometry clusters.

1.5 Statement of Labor & Copyright and Permissions

Funding for this research was supplied through NASA Earth and Space Sciences Fellowship grant 80NSSC17K0490 to Michael Bouchard, JPL subcontract JPL 1536058 to Dr. Bradley Jolliff, and the Washington University in St. Louis Earth and Planetary Sciences (EPS) department's graduate research fellowship and teaching assistantships. APXS data was collected and curated by the APXS operations team, and partially supplied to the Planetary Data System maintained at the Geosciences Node at Washington University in St. Louis. Additional APXS

data was provided courtesy of Dr. Ralf Gellert, University of Guelph. Early motivations for this dissertation research and access to Mars Exploration Rover operations, data, and science discussions was guided by dissertation chair Dr. Bradley Jolliff. Model context, development, testing, validation, application, and interpretation was performed by the dissertation author and benefited from discussion with the dissertation committee, and the Mars Exploration Rovers science team.

Chapter 2 of this dissertation has been published in the *Journal of Geophysical Research: Planets* (Bouchard & Jolliff, 2018). The research was published as an open access journal article under the terms of the *Creative Commons Attribution-NonCommercial-NoDerivatives License*. This license permits the article's use and distribution in any medium, provided the original work is properly cited and its use is non-commercial and no modifications are made. Text and figures of chapter 2 have been formatted according to guidelines of the graduate school of Washington University in St. Louis pertaining to dissertation requirements, but no adaptations to the content have been made.

Chapter 2 open access publication website:

https://agupubs.onlinelibrary.wiley.com/doi/10.1029/2018JE005631

1.6 References

Adcock, C. T., Udry, A., Hausrath, E. M., & Tschauner, O. (2018). Craters of the Moon National Monument basalts as unshocked compositional and weathering analogs for martian rocks and meteorites. *American Mineralogist, 103*, 502-516. doi:10.2138/am-2018-6193

Agee, C. B., Wilson, N. V., McCubbin, F. M., Ziegler, K., Polyak, V. J., Sharp, Z. D., . . . Elardo, S. M. (2013). Unique meteorite from early Amazonian Mars: Water-rich basaltic breccia Northwest Africa 7034. *Science, 339*(6121).

Aitchison, J. (1986). *The statistical analysis of compositional data*. UK: Chapman & Hall, Ltd.

Arvidson, R. E., & al., e. (2011). Opportunity Mars Rover mission: Overview and selected results from Purgatory ripple to traverses to Endeavour crater. *Journal of Geophysical Research, 116*, E00F15. doi:10.1029/2010JE003746

Arvidson, R. E., Bell III, J. F., Bellutta, P., Cabrol, N. A., Catalano, J. G., Cohen, J., . . . Yen, A. S. (2010). Spirit Mars Rover Mission: Overview and selected results from the northern Home Plate Winter Haven to the side of Scamander crater. *Journal of Geophysical Research: Planets, 115*(E00F03).

Arvidson, R. E., Ruff, S. W., Morris, R. V., Ming, D. W., Crumpler, L. S., Yen, A. S., . . . McLennan, S. M. (2008). Spirit Mars Rover Mission to the Columbia Hills, Gusev Crater: Mission overview and selected results from the Cumberland Ridge to Home Plate. *Journal of Geophysical Research, 113*, E12S33. doi:10.1029/2008JE003183

Beck, P., Pommerol, A., Zanda, B., Remusat, L., Göpel, C., Hewins, R., . . . Chevrier, V. F. (2015). A Noachian source region for the "Black Beauty" meteorite, and a source lithology for Mars surface hydrated dust? . *Earth and Planetary Science Letters, 427*, 104-111. doi:10.1016/j.epsl.2015.06.033

Bell, J. F., III, Joseph, J., Sohl-Dickstein, J. N., Arneson, H. M., Johnson, M. J., Lemmon, M. T., & Savransky, D. (2006). In-flight calibration and performance of the Mars Exploration Rover Panoramic Camera (Pancam) instruments. *J. Geophys. Res., 111*(E2), 38. doi:10.1029/2005JE002444

Bell, J. F., III, Squyres, S. W., Herkenhoff, K. E., Maki, J. N., Arneson, H. M., Brown, D., . . . Wadsworth, M. (2003). Mars Exploration Rover Athena Panoramic Camera (Pancam) investigation. *J. Geophys. Res., 108*(E12). doi:10.1029/2003JE002070

Bogard, D. D., & Johnson, P. (1983). Martian Gases in an Antarctic Meteorite? *Science, 221*(4611), 651-654.

Bogard, D. D., Nyquist, L. E., & Johnson, P. (1984). Noble gas contents of shergottites and implications for the Martian origin of SNC meteorites. *Geochimica et Cosmochimica Acta, 48*(9), 1723-1739. doi:http://dx.doi.org/10.1016/0016-7037(84)90028-0

Bouchard, M. C., & Jolliff, B. L. (2018). A systematic method for classifying and grouping late Noachian and early Hesperian rock targets analyzed by the Mars Exploration Rover Opportunity at Endeavour crater, Mars. *Journal of Geophysical Research: Planets, 123*. doi:10.1029/2018JE005631

Butler, J. C. (1978). Visual bias in R-mode dendrograms due to the effect of closure. *Math. Geol., 10*, 243-252.

Butler, J. C. (1979). The effects of closure on the moments of a distribution. *Journal of the International Association for Mathematical Geology, 11*(1), 75-84. doi:10.1007/BF01043247

Cannon, K. M., Mustard, J. F., & Agee, C. B. (2015). Evidence for a widespread basaltic breccia component in the martian low-albedo regions from the reflectance spectrum of Northwest Africa 7034. *Icarus, 252*, 150-153. doi:10.1016/j.icarus.2015.01.016

Chayes, F., & Trochimczyk, J. (1978). An effect of closure on the structure of principal components. *Mathematical Geology, 10*(4), 323-333.

Farrand, W. H., Bell III, J. F., Johnson, J. R., Rice, M. S., Jolliff, B. L., & Arvidson, R. E. (2014). Observations of rock spectral classes by the Oppotunity rover's Pancam on nothern Cape York and on Matijevic Hill, Endeavour Crater, Mars. *Journal of Geophysical Research: Planets, 119*, 2349-2369. doi:10.1002/2014JE004641

Gasnault, O., Taylor, G. J., Karunatillake, S., Dohm, J., Newsom, H., Forni, O., . . . Boynton, W. V. (2010). Quantitative geochemical mapping of martian elemental provinces. *Icarus, 207*, 226-247. doi:10.1016/i.icarus.2009.11.010

Gellert, R., Rieder, R., Anderson, R. C., Brückner, J., Clark, B. C., Dreibus, G., . . . Zipfel, J. (2004). Chemistry of rocks and soils in Gusev Crater from the alpha particle X-ray spectrometer. *Science, 305*, 829-832.

Gellert, R., Rieder, R., Brückner, J., Clark, B. C., Dreibus, G., Klingelhöfer, G., . . . Squyres, S. W. (2006). Alpha Particle X-Ray Spectrometer (APXS): Results from Gusev crater and calibration report. *Journal of Geophysical Research: Planets, 111*(E02S05), 1-32. doi:10.1029/2005JE002555

Herkenhoff, K. E., Squyres, S. W., Anderson, R., Archinal, B. A., Arvidson, R. E., Barrett, J. M., . . . Yen, A. (2006). Overview of the Microscopic Imager Investigation during Spirit's first 450 sols in Gusev crater. *J. Geophys. Res., 111*(E2). doi:10.1029/2005JE002574

Herkenhoff, K. E., Squyres, S. W., Bell III, J. F., Maki, J. N., Arneson, H. M., Bertelsen, P., . . . Wadsworth, M. V. (2003). Athena Microscopic Imager investigation. *Journal of Geophysical Research: Planets, 108*(E12), ROV 6-1 - ROV 6-23. doi:10.1029/2003JE002076

Humayun, M., Nemchin, A., Zanda, B., Hewins, R. H., Grange, M., Kennedy, A., . . . Deldicque, D. (2013). Origin and age of the earliest Martian crust from meteroite NWA 7533. *Nature, 503*, 513-516.

Koch Jr., G. S., & Link, R. F. (1971). *Statistical Analysis of Geologic Data* (Vol. 1 and 2). New York: Dover Publications Inc.

Korotev, R. L., Haskin, L. A., & Jolliff, B. L. (1995). A simulated geochemical rover mission to the Taurus-Littrow valley of the Moon. *Journal of Geophysical Research: Planets, 100*(E7), 14,403-414,420.

Larsen, K., Arvidson, R. E., Jolliff, B. L., & Clark, B. E. (2000). Correspondence and least squares analyses of soil and rock compositions for the Viking Lander 1 and Pathfinder landing sites. *Journal of Geophysical Research, 105*(E12), 29207-29221.

McLennan, S. M. (2012). Geochemistry of Sedimentary Processes on Mars. In J. P. Grotzinger & R. E. Milliken (Eds.), *Sedimentary Geology of Mars* (Vol. 102, pp. 119-138): SEPM Spec.

McLennan, S. M., Bell, J. F., III, Calvin, W. M., Christensen, P. R., Clark, B. C., de Souza, P. A., . . . Yen, A. (2005). Provenance and diagenesis of the evaporite-bearing Burns formation, Meridiani Planum, Mars. *Earth and Planetary Science Letters, 240*, 95-121.

McLennan, S. M., & Grotzinger, J. P. (2008). The sedimentary rock cycle of Mars. In J. Bell (Ed.), *The Martian Surface: Composition, Mineralogy and Physical Properties* (pp. 541-577). Cambridge: Cambridge University Press.

McSween, H. Y., Taylor, G. J., & Wyatt, M. B. (2009). Elemental Composition of the Martian Crust. *Science, 324*(736), 736-739. doi:10.1126/science.1165871

Milligan, G. W., & Cooper, M. C. (1988). A study of standardization of variables in cluster analysis. *Journal of Classification, 5*, 181-204.

Ming, D. W., Morris, R. V., & Clark, B. C. (2008). Aqueous alteration on Mars. In J. Bell (Ed.), *The Martian Surface: Composition, Mineralogy and Physical Properties* (pp. 519-540). Cambridge: Cambridge University Press.

Mittlefehldt, D. W., Gellert, R., VanBommel, S. J., Ming, D. W., Yen, A. S., Clark, B. C., . . . Rice, J. W. (2018). Diverse Lithologies and Alteration Events on the Rim of Noachian-Aged Endeavour Crater, Meridiani Planum, Mars: In-Situ Compositional Evidence. *Journal of Geophysical Research: Planets*(123). doi:10.1002/2017JE005474

Morris, R. V., & Klingelhöfer, G. (2008). Iron mineralogy and aqueous alteration on Mars from the MER Mössbauer spectrometers. In J. Bell (Ed.), *The Martian Surface: Composition, Mineralogy and Physical Properties* (pp. 339-365). Cambridge: Cambridge University Press.

Owen, T., Biemann, K., Rushneck, D. R., Biller, J. E., Howarth, D. W., & Lafleur, A. L. (1977). The composition of the atmosphere at the surface of Mars. *Journal of Geophysical Research (1896-1977), 82*(28), 4635-4639. doi:10.1029/JS082i028p04635

Pawlowsky-Glahn, V. (1984). On spurious spatial covariance between variables of constant sum. *Science de la Terre, S´erie Informatique, 21*, 107-113.

Pearson, K. (1897). Mathematical contributions to the theory of evolution.—On a form of spurious correlation which may arise when indices are used in the measurement of organs. *Proceedings of the Royal Society of London, 60*(359-367), 489-498. doi:10.1098/rspl.1896.0076

Rieder, R., Gellert, R., Anderson, R. C., Brückner, J., Clark, B. C., Dreibus, G., . . . Zipfel, J. (2004). Chemistry of Rocks and Soils at Meridiani Planum from the Alpha Particle X-ray Spectrometer *Science, 306*(5702), 1746-1749.

Rieder, R., Gellert, R., Brückner, J., Klingelhöfer, G., Dreibus, G., Yen, A., & Squyres, S. W. (2003). The new Athena alpha particle X-ray spectrometer for the Mars Exploration Rovers. *J. Geophys. Res., 108*(E12). doi:10.1029/2003JE002150

Squyres, S. W., Arvidson, R. E., Baumgartner, E. T., Bell, J. F., III, Christensen, P. R., Gorevan, S., . . . Romero, R. A. (2003). Athena Mars rover science investigation. *Journal of Geophysical Research, 108*(E12). doi:10.1029/2003JE002121

Udry, A., Lunning, N. G., McSween, H. Y., & Bodnar, R. J. (2014). Petrogenesis of a vitrophyre in the martian meteorite breccia NWA 7034. *Geochimica et Cosmochimica Acta, 141*, 281-293. doi:10.1016/j.gca.2014.06.026

Van den Boogaart, K. G., & Tolosana-Delgado, R. (2011). *Analyzing Compositional Data with R*: Springer.

Wittmann, A., Korotev, R. L., Jolliff, B. L., Irving, A. J., Moser, D. E., Barker, I., & Rumble III, D. (2015). Petrography and composition of Martian regolith breccia meteorite Northwest Africa 7475. *The Meteoritical Society, 50*(2), 326-352.

Xu, R., & Wunsch II, D. C. (2009). *Clustering*: Institute of Electrical and Electronics Engineers.

Zipfel, J., Schröder, C., Jollif, B. L., Gellert, R., Herkenhoff, K. E., Rieder, R., . . . Yen, A. S. (2011). Bounce Rock—A shergottite-like basalt encountered at Meridiani Planum, Mars. *Meteoritics & Planetary Science, 46*(Nr 1), 1–20. doi:10.1111/j.1945-5100.2010.01127.

Chapter 2: A Systematic Method for Classifying and Grouping Late Noachian and Early Hesperian Rock Targets Analyzed by the Mars Exploration Rover Opportunity at Endeavour Crater, Mars

Michael C. Bouchard[1]
Bradley L. Jolliff[1]

[1]Department of Earth and Planetary Sciences, Washington University in St. Louis, Campus Box 1169, 1 Brookings Drive, St. Louis, Missouri 63130-4899

Published: October 5th 2018, *Journal of Geophysical Research: Planets*, 123
Open Access: https://agupubs.onlinelibrary.wiley.com/doi/10.1029/2018JE005631
Doi:10.1029/2018/JE005631

Abstract

The Mars rover Opportunity has collected in-situ compositional data with the Alpha Particle X-Ray Spectrometer at almost 500 sites. To analyze these data, hierarchical clustering analysis and an error-weighted similarity index are applied to a subset of 57 APXS target compositions and selected martian meteorites. Hierarchical clustering provides a rapid first approximation of compositional relationships whereas the error-weighted similarity index provides an in-depth and quantifiable comparison of individual composition pairs. These analyses are combined into a statistical grouping model that provides insight into lithologic relationships and is critically informed by examination of Panoramic Camera and Microscopic Imager images. Major lithologies are (1) the Burns formation sulfate sandstones, (2) Shoemaker impact breccias (Endeavour crater ejecta/rim deposits), (3) the morphologically distinct Grasberg formation, associated with Endeavour crater rim deposits, (4) the Matijevic formation, an

exposure interpreted to be Endeavour crater target rocks, and (5) erratics or other rocks that do not cluster with groups 1-4. The Grasberg formation is more similar to the Shoemaker formation than any other formation, and thus likely incorporated eroded Shoemaker material. The lowest Shoemaker member (Copper Cliff breccia) may contain material from the pre- impact Matijevic formation. The Matijevic formation is the most chemically distinct formation and is most similar to the volcanic erratic rock "Marquette Island." Clustering and similarity index values also show that regolith breccia martian meteorites (represented by the NWA 7475/7034 paired meteorites) are similar in bulk composition to Mars surface materials at Meridiani, especially the Matijevic formation.

2.1 Introduction

The Mars Exploration Rover (MER) Opportunity has been operating on the surface of Mars since January of 2004, assessing the water history, past environmental conditions, and habitability of those conditions (Arvidson et al., 2004; Arvidson et al., 2003; Squyres et al., 2003; Squyres, et al., 2004). Along its traverse from landing at Eagle crater (Squyres et al., 2004) and across Meridiani Planum, the rover and MER team has documented in detail the laterally continuous, sulfate-salt-rich, siliciclastic sedimentary rocks (Clark, et al., 2005b) of the Burns formation, first documented in Eagle crater (Grotzinger et al., 2005; McLennan et al., 2005). The Burns formation is considered to be of late Noachian or early Hesperian age (Squyres & Knoll, 2005), and is characterized as roughly half reworked siliciclastic debris and half chemical evaporite minerals (McLennan et al., 2005), with sedimentary structures of eolian dune and interdune facies, eolian dune sand sheets, and dry eolian dune fields with large-scale cross-bedding (Grotzinger et al., 2005).

As of this writing, the rover continues to explore the rim of the 22 km diameter, late Noachian aged, Endeavour crater (Squyres et al., 2012) (Fig. 2.1). This location provided the first opportunity for investigation of rock units older than the Burns formation, which was the main rock unit investigated by Opportunity up to that point. Upon reaching the rim of Endeavour crater at Cape York (sol 2681), the rover investigated a diversity of rock types including the Endeavour impact breccias of the Shoemaker formation, the post-impact clastic Grasberg formation, which forms a prominent bench surrounding Endeavour crater rim segments such as Cape York (Arvidson et al., 2014; Crumpler et al., 2015; Squyres et al., 2012), the pre-impact Matijevic formation identified at Matijevic Hill on Cape York (Arvidson et al., 2014; Crumpler et al., 2015), basaltic erratic rocks such as Bounce Rock (Zipfel et al., 2011) and Marquette Island (Mittlefehldt et al., 2010), and distinctive float rocks such as Tickbush at Solander Point. For the time period covered by this paper (up to sol 3812), the rover had analyzed several hundred targets with the Athena Science Payload instruments on the Instrument Deployment Device (IDD). At this time the rover can no longer use its Mössbauer Spectrometer and Mini-Thermal Emission Spectrometer; however, the Alpha Particle X-Ray Spectrometer (APXS), Panoramic Camera (Pancam), Microscopic Imager (MI), and Rock Abrasion Tool (RAT) still provide in-situ rock and soil (no organics implied) compositions and images (Arvidson et al., 2014; Squyres et al., 2003, 2012; Yen et al., 2005).

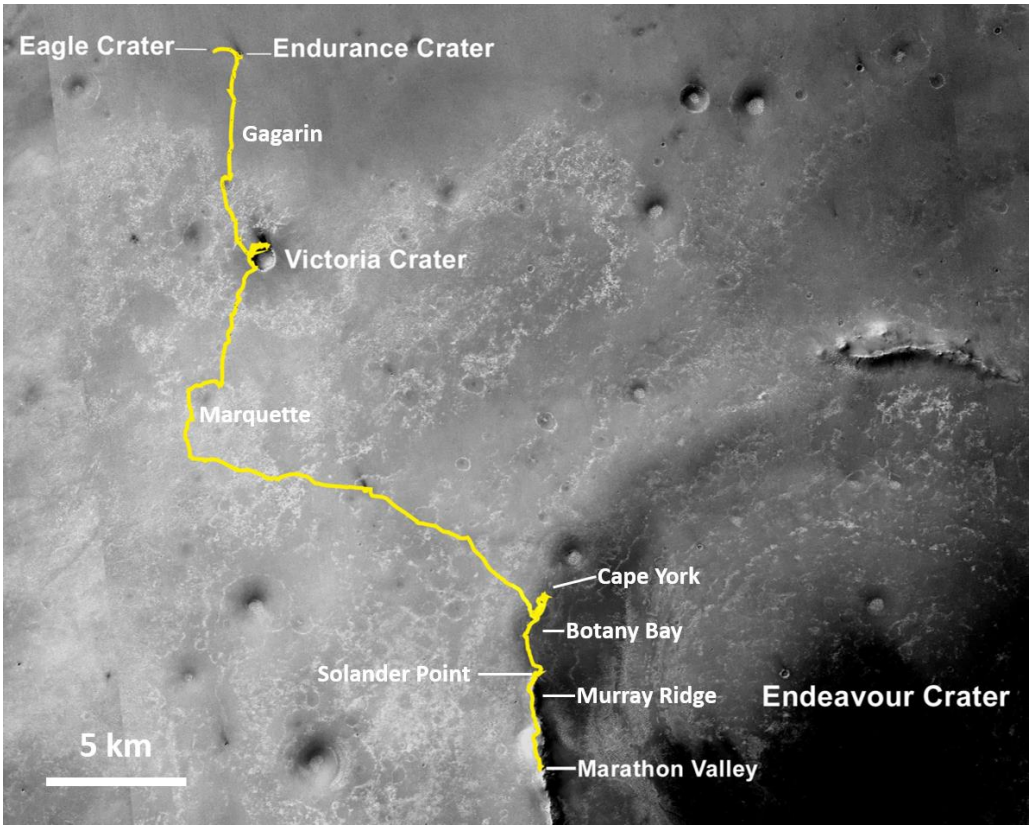

Figure 2.1 The rover Opportunity's 42 km traverse from landing in Eagle Crater, across the Burns formation sulfate sandstones of Meridiani Planum, to the rim of Endeavour Crater at Cape York where the clastic Grasberg formation, the Shoemaker impact breccia and the pre-impact Matijevic formation were first identified (sol 0 - 4000). Image source: *NASA/JPL-Caltech/MSSS/NMMNHS*

These Endeavour rim rocks are Opportunity's first look into materials as old as the late Noachian and could provide information to help constrain the climatic shift from a phyllosilicate-dominated aqueous regime to a more acidic environment indicated by extensive sulfate materials (Bibring et al., 2006). However, as a consequence of the quantity of targets, discerning relationships among different rocks and rock compositions analyzed at different times during the mission can be challenging. Moreover, variable coatings of weathered rock rinds or soil or dust contamination can obscure underlying rock compositions and compositional relationships (Stein et al., 2018; VanBommel et al., 2016, 2017).

In this paper, we present a methodology to quantify similarities in rock major and minor element compositions as analyzed by the APXS, coupled with Pancam and MI observations, in order to better understand the litho-chemical diversity in these late Noachian and early Hesperian rocks. The methodology combines a hierarchical clustering analysis, a quantitative compositional similarity index, and an image comparison into an informed statistical grouping model. Our objective is to provide a framework for rapid and quantitative assessment for relating specific rocks to others analyzed previously during the mission. Correspondence analysis has previously been used to explain relationships in martian surface data, and while our method does not directly explore causes of variance in groups of targets, they are complementary to these approaches (Arvidson et al., 2011; Arvidson, et al., 2006; Larsen, et al., 2000). We also use our method to compare rock compositions determined using the APXS to compositions of martian meteorites for which bulk major-element compositions (e.g., as determined by XRF) are available. The shergottite, nakhlite, and chassignite meteorites are not considered representative of the martian crustal surface (McSween Jr., et al., 2009), but here we compare the compositions of the well-known shergottites EETA 79001 lithology B and Zagami to one of the Meridiani Plains basaltic erratics, Bounce Rock. We also include the composition of a recently discovered regolith breccia meteorites represented by the paired meteorites NWA 7475/7034 for comparison with various groups of rocks analyzed by Opportunity (Bouchard & Jolliff, 2016). The results presented in this paper provide an independent perspective and complement results reported by Mittlefehldt et al. (2018).

2.2 Methods

This paper uses three data sets and two statistical techniques to assess compositional and chemical relationships between rocks encountered along the rover traverse (Fig. 2.2). The chemical data set consists of target compositional data measured by the APXS and reported in the Planetary Data System (PDS) (Gellert et al., 2006), and in other published literature (Arvidson et al., 2014; Clark, et al., 2005a; Lodders, 1998; Rieder et al., 2004; Squyres et al., 2012; Wittmann et al., 2015; Zipfel et al., 2011) (Table 2.1). The oxides detectable by the APXS make up the major rock-forming minerals. Relationships indicated by the APXS data are then assessed using Pancam and MI images.

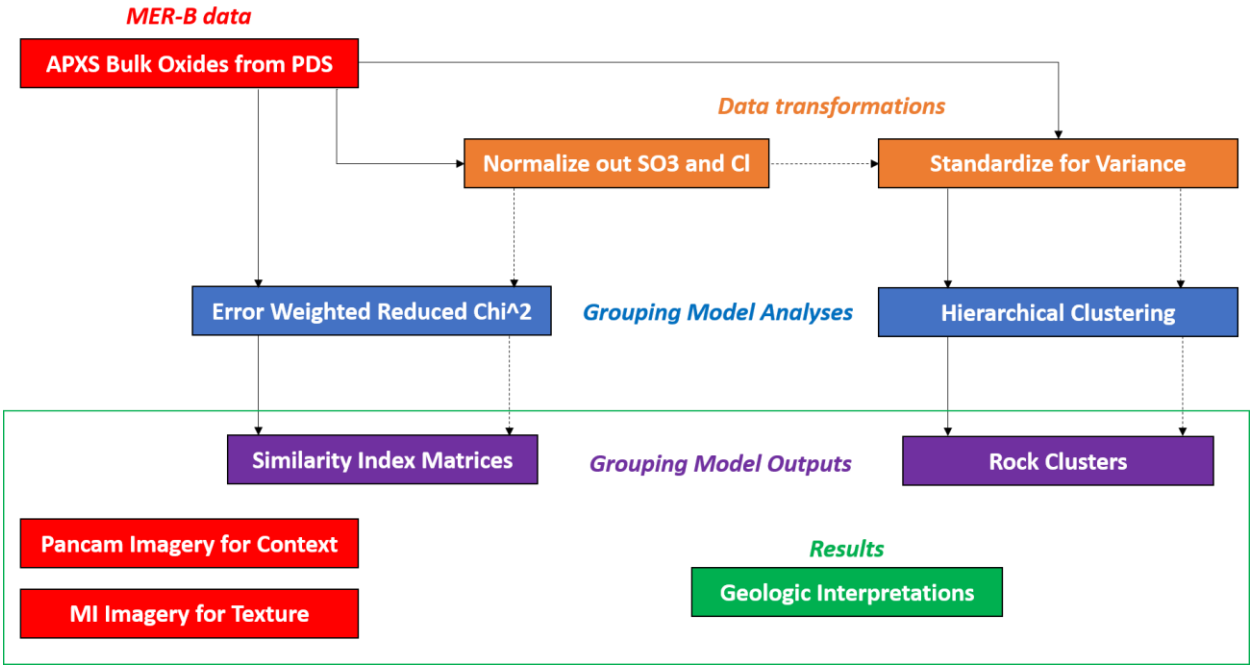

Figure 2.2 Data processing pipeline of the statistical grouping model. The three data sets are represented in red. The bulk chemistry of the rock and soil targets is from the PDS and is processed both including SO_3 and Cl (solid lines) and with SO_3 and Cl removed and normalized to 100% (dashed lines). The bulk chemical data are compared using the two statistical methods (blue) of an error weighted reduced χ^2 similarity index, and hierarchical clustering. The data is standardized to reduce the impact of different variances between elements before performing the hierarchical clustering. The matrices of index values and clusters are interpreted alongside contextual and textural imagery (red) to classify the rock groupings and relationship.

The first step in our analysis is to sort the APXS major and minor element compositional data using an agglomerative, group average, hierarchical clustering technique (see also Mittlefehldt et al., 2018). This form of statistical analysis allows for large, multivariate data sets to be sorted quickly according to internal similarities in the data (Xu & Wunsch II, 2009). However, there are some limitations to cluster analysis such as the disproportionate effect of high variance values and the difficulty in comparing targets that are paired late in the cluster analysis to individual targets that were clustered earlier in the analysis. Consequently, we developed a second comparison method that enables a more direct assessment of the similarity of two compositions and enables assessment of which compositional parameters are most important in the comparison. This "similarity index" (SI) is essentially an error-weighted sum-of-squares of differences in compositions, and is expressed as a reduced χ^2 value, which we use as the metric of similarity. By comparing each individual target composition to each of the others, we are able to quantitatively interrogate relationships between specific targets and reveal which elements contribute the most to deviations. We present these values as a SI-value matrix for organizing and examining these compositional relationships. Pancam imagery of the target rocks is used to establish geologic context for the targets, while MI imagery is used to compare specific rock fabric and textures. Targets within a common cluster are compared to evaluate possible petrologic relationships.

Table 2.1: Compositions of selected APXS targets from the PDS and reference data. Ni, Zn, and Br are not included in the statistical grouping model but are reported here for reference.

Sol	type*	Target Name	SiO_2	TiO_2	Al_2O_3	Cr_2O_3	FeO	MnO	MgO	CaO	Na_2O	K_2O	P_2O_5	SO_3	Cl	SUM	Ni	Zn	Br
36	RR	Guadalupe	36.2	0.7	5.9	0.2	14.8	0.3	8.5	4.9	1.7	0.5	1.0	24.9	0.50	99.9	589	324	30
68	RR	BounceRock Case	51.6	0.7	10.5	0.1	14.4	0.4	6.8	12.1	1.7	0.1	0.9	0.6	0.10	100.0	81	38	39
108	RR	LionStone Numa	37.2	0.8	6.2	0.2	14.3	0.3	8.8	5.0	1.7	0.6	1.0	22.8	0.91	99.9	572	415	268
155	RR	Kettlestone	36.2	0.8	5.9	0.2	15.2	0.3	8.6	4.9	1.5	0.6	1.0	23.0	1.75	99.9	644	346	19
184	RR	MacKenzie	43.0	0.9	7.3	0.2	15.6	0.3	5.4	4.6	1.9	0.7	1.2	17.0	1.90	100.0	546	447	9
400	RU	Gagarin RU	41.0	0.9	7.5	0.2	16.2	0.3	7.2	5.5	2.0	0.6	1.0	16.5	0.98	100.0	543	450	73
401	RB	Gagarin RB	38.3	0.8	6.7	0.2	15.2	0.3	7.3	5.4	1.8	0.6	1.0	21.5	0.92	99.9	574	405	67
403	RR	Gagarin RR	32.6	0.7	4.9	0.2	15.9	0.4	7.3	5.8	1.4	0.5	1.1	28.6	0.61	99.9	585	436	54
642	CU	Antistasi	47.4	1.1	11.4	0.2	16.5	0.3	7.6	6.9	2.5	0.5	1.1	3.7	0.53	99.9	899	189	35
1311	RU	Steno RU	39.4	0.8	7.0	0.2	16.7	0.3	7.5	5.3	1.9	0.5	1.0	18.4	0.87	99.9	563	506	34
1313	RB	Steno RB	36.3	0.7	6.0	0.2	16.4	0.3	7.4	5.4	1.6	0.5	1.0	23.2	0.80	99.9	580	567	47

1316	RR	Steno RR	34.4	0.7	5.3	0.2	16.1	0.3	7.2	5.6	1.5	0.5	1.0	26.4	0.68	100.0	523	507	22
2070	RB	Marquette PeckBay 1	46.1	0.6	11.5	0.5	16.6	0.4	12.0	5.7	2.5	0.4	1.0	2.3	0.43	100.0	319	182	26
2075	RB	Marquette IslingtonBay	47.0	0.6	12.3	0.5	16.3	0.4	9.7	5.7	2.5	0.5	0.8	3.3	0.50	99.9	310	182	31
2486	RB	LuisDeTorres	39.3	0.8	6.9	0.2	16.2	0.3	7.1	5.7	1.9	0.5	1.0	19.1	0.82	100.0	570	464	176
2669	RU	Gibraltar	41.8	0.8	7.8	0.2	16.9	0.3	7.4	6.2	2.1	0.6	1.0	13.7	1.01	99.9	426	414	498
2696	RU	Tisdale 2 Timmins 3	45.4	1.1	10.1	0.2	18.8	0.2	6.2	5.9	2.5	0.5	1.2	6.5	1.00	99.8	2030	710	377
2701	RU	Tisdale 2 Shaw 2	45.2	1.1	8.6	0.2	20.7	0.5	6.0	5.2	2.1	0.6	2.2	5.9	1.21	99.7	770	1853	1324
2722-6	RR	Salisbury 1 (CL matrix)	45.5	1.1	8.8	0.3	20.1	0.5	8.8	6.8	2.7	0.4	1.0	3.1	0.90	100.0	482	246	124
2734	RU	Geluk (CL clast)	46.1	1.2	10.1	0.3	17.0	0.6	7.4	7.1	2.7	0.5	1.1	4.8	1.00	99.9	461	244	68
2771	RU	Deadwood	44.0	1.0	8.3	0.3	19.4	0.2	5.7	6.7	2.2	0.6	1.1	9.2	1.12	99.9	410	521	301
2787	RU	Transvaal	45.9	1.1	9.2	0.3	17.8	0.4	7.5	6.6	2.3	0.5	1.0	6.3	0.98	99.9	565	294	139
2801	RB	Boesmanskop (matrix)	45.6	1.0	9.5	0.3	17.6	0.4	8.9	5.7	2.4	0.5	1.2	5.6	1.00	99.8	615	350	153
2805	RU	Komati (clast)	44.7	1.1	9.3	0.2	18.7	0.6	8.4	6.1	2.4	0.6	1.2	5.8	0.90	99.9	461	266	229
2834	RU	Amboy 2	45.7	1.0	9.2	0.2	17.8	0.4	9.1	5.9	2.2	0.4	1.1	6.1	0.85	99.9	524	280	96
2920	RU	Amboy 4	46.0	1.1	10.0	0.2	17.1	0.5	7.5	7.5	2.3	0.5	1.1	5.4	0.74	100.0	306	194	103
2940	RU	Amboy 12	44.9	1.1	9.2	0.2	18.1	0.9	7.6	6.7	2.2	0.5	1.1	6.5	0.90	99.9	615	337	110
2995	RB	Grasberg 1	45.1	1.0	7.8	0.3	19.7	0.2	5.3	5.1	2.2	0.7	1.1	8.8	2.54	99.8	365	923	479
3022	RU	MonsCupri	45.3	1.0	8.4	0.3	19.2	0.2	5.7	5.9	2.2	0.7	1.2	8.1	1.71	99.9	470	558	286
3027	RU	Rushall 1	40.8	0.9	7.7	0.2	17.2	0.3	7.0	7.5	2.0	0.5	0.9	13.9	0.95	99.9	379	390	210
3067	RB	Kirkwood 1	49.1	0.8	9.9	0.3	16.7	0.2	8.5	5.0	2.4	0.5	0.7	4.5	1.08	99.9	881	134	112
3085-7	RR	Azilda	51.2	0.9	10.6	0.2	15.4	0.4	7.9	6.0	2.6	0.3	1.5	2.5	0.53	100.0	922	134	48
3096	RB	Chelmsford 3	45.1	0.9	9.0	0.3	16.0	0.5	7.6	7.2	2.4	0.4	1.3	7.6	1.63	99.9	815	331	154
3146	RR	SandCherry (veneer)	44.7	0.9	9.0	0.2	16.3	0.4	8.6	7.1	2.8	0.3	1.3	6.4	1.75	99.9	914	373	332
3158	RU	Onaping 1	47.0	0.9	11.3	0.3	13.6	0.4	8.2	7.0	2.2	0.3	1.0	6.7	1.04	100.0	684	212	62
3171	RU	Vermillion Cliffs 2	45.0	0.8	10.3	0.3	14.2	0.4	8.1	7.2	2.3	0.3	1.0	8.7	1.27	99.9	868	216	312
3192	RU	Ortiz 2 (no veins)	46.5	0.9	9.6	0.2	15.1	0.5	6.6	7.9	2.2	0.3	1.2	7.9	0.92	99.9	723	193	157
3200	RB	Ortiz2B (vein rich)	42.0	0.8	8.6	0.2	13.2	0.5	6.3	10.3	2.1	0.3	1.2	13.5	0.95	100.0	670	144	208
3209	RB	Fullerton 3	50.1	1.0	10.5	0.3	14.7	0.3	8.2	5.8	2.2	0.3	0.9	4.6	0.85	99.9	738	176	159
3214	RB	FecunisLake	46.3	0.9	9.9	0.3	15.9	0.3	8.3	5.9	2.4	0.4	0.9	6.8	1.50	99.9	938	228	108
3224	RB	Maley	43.6	0.9	8.9	0.3	15.5	0.4	8.2	7.0	2.2	0.4	1.0	9.8	1.70	99.9	863	414	85
3253	RR	SturgeonRiver 3 RAT 2	49.5	0.8	9.6	0.4	17.9	0.3	9.3	5.1	2.2	0.4	0.6	3.3	0.47	100.0	1165	132	57
3383	RR	Black Shoulder RAT	36.5	0.8	5.9	0.2	16.5	0.2	8.1	4.3	1.8	0.6	1.0	22.4	1.60	100.0	612	294	40
3396	RU	Tickbush 2	49.8	1.2	14.0	0.1	13.2	1.2	4.9	7.3	3.1	0.5	1.3	2.7	0.67	99.9	985	670	40
3403	RB	Platypus	46.2	1.0	8.2	0.3	19.5	0.2	4.4	5.9	2.1	0.8	1.0	8.6	1.44	99.8	368	764	1004
3434	RB	WallyWombat	45.5	1.0	8.5	0.3	18.5	0.2	4.4	6.3	2.2	0.8	1.1	9.6	1.70	99.9	196	553	293
3445	RB	Callitris	39.4	0.8	6.7	0.2	16.9	0.1	5.5	7.5	1.5	0.5	1.1	18.8	0.84	100.0	275	330	65
3463	RB	Spinifex	45.7	1.0	8.8	0.2	17.6	0.8	8.9	6.2	2.3	0.7	1.2	5.5	0.95	99.9	537	460	706
3542	RB	CapeElizabeth	44.7	1.0	9.1	0.2	16.7	0.3	8.0	5.9	2.5	0.4	0.9	9.2	1.12	100.0	447	121	78
3569	RB	GreenIsland	43.3	1.0	8.9	0.2	16.7	0.3	7.3	6.4	2.5	0.4	1.0	10.5	1.54	100.0	376	152	65
3598	RB	TurnagainArm	44.5	1.0	9.1	0.2	16.4	0.3	8.1	6.0	2.3	0.4	1.0	9.4	1.36	100.0	453	114	167
3671	RB	Sarcobatus Flat 1	44.9	1.0	8.8	0.2	17.6	0.2	7.8	6.4	2.3	0.5	1.2	7.1	1.92	100.0	293	162	98
3741	RU	Cape Fairweather	39.6	0.8	7.1	0.2	16.2	0.2	7.3	6.4	1.9	0.5	1.0	17.9	0.88	100.0	311	276	114
3796	RB	Hoover	42.2	1.0	7.6	0.2	19.2	0.3	6.5	7.7	2.0	0.5	1.2	9.7	1.61	99.9	549	666	44
3812	RB	Margaret Brush	48.4	1.2	12.6	0.2	15.2	0.4	6.2	7.3	2.7	0.4	1.2	3.7	0.42	100.0	289	111	20
NA	Soil	Average Soil	45.3	1.1	9.0	0.4	19.2	0.4	7.4	7.0	2.2	0.5	0.9	5.8	0.60	99.8	420	314	127
NA	Dust	Average Dust	45.5	1.0	9.2	0.4	17.6	0.4	7.6	6.7	2.2	0.5	0.9	7.1	0.80	100.0	536	403	73
NA	MM	EETA 79001 B	49.4	1.2	11.2	0.2	17.4	0.4	6.6	10.8	1.7	0.1	1.3	0.5	0.00	100.7	28	91	0
NA	MM	Zagami	50.5	0.8	6.1	0.3	18.1	0.5	11.3	10.5	1.2	0.1	0.5	0.5	0.01	100.4	48	60	1
NA	MM	NWA 7475/7034	48.3	1.0	10.7	0.3	16.6	0.4	10.9	7.0	2.8	0.5	1.29	0.2		99.9			

*RU: Rock Unbrushed; RB: Rock Brushed; RR: Rock RAT Grind, MM: martian meteorite

In this study, we restrict our assessment to rocks analyzed by Opportunity before reaching Marathon Valley (Arvidson et al., 2017; Fox et al., 2016), focusing our selection on sites examined along the rim of Endeavour crater at Cape York and Cape Tribulation up to sol 3812, a subset of Burns formation sulfate sandstones from the Meridiani Plains, several erratics analyzed along Opportunity's traverse, and a selection of martian meteorites are included to provide a broader context for the Endeavour crater rim rocks (Tables 2.2-2.3). Limiting the study

to these targets allows us to determine how well-studied rock groups cluster and establishes a quantitative metric for comparing compositions. We have limited the selected targets to sites that have been brushed or abraded using the RAT, augmented by a subset of rocks analyzed "as-is," without brushing, in cases where rock surfaces were deemed to be relatively clean of soil or dust coatings through visual inspection. Many of the analyzed samples have very high concentrations of S and Cl; accordingly, we apply the methodology to two sets of compositions, one that includes SO_3 and Cl, and one that considers the SO_3- and Cl-free compositions normalized to 100%.

Table 2.2: Summary of the selected targets general and specific locations for regional context

Sol	Target Name	Type[1]	General Location	Specific Location
36	Guadalupe	RR	Meridiani Plains	Eagle crater
68	BounceRock Case	RR	Meridiani Plains	Outside Eagle crater
108	LionStone Numa	RR	Meridiani Plains	Endurance crater rim
155	Kettlestone	RR	Meridiani Plains	Endurance crater wall
184	MacKenzie	RR	Meridiani Plains	Endurance crater interior
400	Gagarin	RU	Meridiani Plains	Plains between Endurance and Erebus
401	Gagarin	RB	Meridiani Plains	Plains between Endurance and Erebus
403	Gagarin	RR	Meridiani Plains	Plains between Endurance and Erebus
642	Antistasi	CU	Meridiani Plains	North of Erebus crater
1311	Steno	RU	Meridiani Plains	Victoria crater
1313	Steno	RB	Meridiani Plains	Victoria crater
1316	Steno	RR	Meridiani Plains	Victoria crater
2070	Marquette PeckBay1	RB	Meridiani Plains	Plains south of Victoria
2075	Marquette IslingtonBay	RB	Meridiani Plains	Plains south of Victoria
2486	LuisDeTorres	RB	Meridiani Plains	Plains west of Endeavour
2669	Gibraltar	RU	Meridiani Plains	Plains west of Cape York
2696	Tisdale2 Timmins3	RU	Cape York	Shoemaker Ridge
2701	Tisdale2 Shaw2	RU	Cape York	Shoemaker Ridge
2722-6	Salisbury1 (Chester Lake matrix)	RR	Cape York	Shoemaker Ridge
2734	Geluk (Chester Lake clast)	RU	Cape York	Shoemaker Ridge
2771	Deadwood	RU	Cape York	Cape York Bench
2787	Transvaal	RU	Cape York	Shoemaker Ridge

2801	Boesmanskop (matrix)	RB	Cape York	Shoemaker Ridge
2805	Komati (clast)	RU	Cape York	Shoemaker Ridge
2834	Amboy2	RU	Cape York	Shoemaker Ridge
2920	Amboy4	RU	Cape York	Shoemaker Ridge
2940	Amboy12	RU	Cape York	Shoemaker Ridge
2995	Grasberg1	RB	Cape York	Cape York Bench
3022	MonsCupri	RU	Cape York	Cape York Bench
3027	Rushall1	RU	Cape York	Cape York Bench
3067	Kirkwood1	RB	Cape York	Matijevic Hill
3085-7	Azilda Average	RR	Cape York	Matijevic Hill
3096	Chelmsford3	RB	Cape York	Matijevic Hill
3146	Sandcherry (veneer)	RR	Cape York	Matijevic Hill
3158	Onaping	RU	Cape York	Copper Cliff - Matijevic Hill
3171	Vermillion Cliffs2	RU	Cape York	Copper Cliff - Matijevic Hill
3192	Ortiz 2 (vein poor)	RU	Cape York	Matijevic Hill
3200	Ortiz2B (vein rich)	RB	Cape York	Matijevic Hill
3209	Fullerton3 (spherule-poor)	RB	Cape York	Matijevic Hill
3214	FecunisLake	RB	Cape York	Matijevic Hill
3224	Maley	RB	Cape York	Copper Cliff - Matijevic Hill
3253	SturgeonRiver3RAT2 (sphrl-rich)	RR	Cape York	Matijevic Hill
3383	Black Shoulder	RR	Botany Bay	Botany Bay
3396	Tickbush	RU	Cape Tribulation	Solander Point
3403	Platypus	RB	Cape Tribulation	Solander Point, bench
3434	WallyWombat	RB	Cape Tribulation	Solander Point, bench
3445	Callitris	RB	Cape Tribulation	Solander Point, at bench-plains contact
3463	Spinifex	RB	Cape Tribulation	Solander Point, Kangaroo Paw Outcrop
3542	CapeElizabeth	RB	Cape Tribulation	Murray Ridge
3569	GreenIsland	RB	Cape Tribulation	Murray Ridge
3598	TurnagainArm	RB	Cape Tribulation	Murray Ridge
3671	Sarcobatus Flat1	RB	Cape Tribulation	Pillinger Point
3741	Cape Fairweather	RU	Plains beyond bench	West of Cape Tribulation
3796	Hoover	RB	Cape Tribulation	Wdowiak Ridge
3812	Margaret Brush	RB	Cape Tribulation	Wdowiak Ridge
	Average Soil[2]	Soil	Meridiani Plains	various locations
	Average Dust[3]	Dust	Meridiani Plains	various locations
	EETA 79001 B	MM	-	collected on Earth
	Zagami	MM	-	collected on Earth
	NWA 7475/7034	MM	-	collected on Earth

[1]RU: Rock Unbrushed; RB: Rock Brushed; Rock RAT Grind

[2]Average of 9 soil analyses (sols 011, 090, 249, 373, 499, 507, 730, 879, 1918)

[3]Average of 3 bright soil analyses (HemaTrench, sol 025; Mont Blanc - LesHouches, sol 060; McDonnell - HilltopWilson, sol 123) (Yen et al., 2005)

Table 2.3: Summary of the selected targets geologic classification and data source

Sol	Target Name	Type[1]	Description	Classification	Data Sources[4]
36	Guadalupe	RR	Outcrop, Eagle crater	Burns formation	Rieder et al., 2004
68	BounceRock Case	RR	Rock, secondary ejecta	Plains erratic	Rieder et al., 2004
108	LionStone Numa	RR	Rock, Endurance crater	Burns formation	Fleischer et al., 2010
155	Kettlestone	RR	Outcrop pavement	Burns formation	PDS, Dec. 6, 2012
184	MacKenzie	RR	Outcrop pavement	Burns formation	PDS, Dec. 6, 2012
400	Gagarin	RU	Outcrop pavement	Burns formation	PDS, Dec. 6, 2012
401	Gagarin	RB	Outcrop pavement	Burns formation	PDS, Dec. 6, 2012
403	Gagarin	RR	Outcrop pavement	Burns formation	PDS, Dec. 6, 2012
642	Antistasi	CU	Cobble, float	"Arkansas group"	Fleischer et al., 2010
1311	Steno	RU	Outcrop pavement	Burns formation	PDS, Dec. 6, 2012
1313	Steno	RB	Outcrop pavement	Burns formation	PDS, Dec. 6, 2012
1316	Steno	RR	Outcrop pavement	Burns formation	PDS, Dec. 6, 2012
2070	Marquette PeckBay1	RB	Float rock on plains	Plains erratic	PDS, Dec. 6, 2012
2075	Marquette IslingtonBay	RB	Float rock on plains	Plains erratic	PDS, Dec. 6, 2012
2486	LuisDeTorres	RB	Outcrop pavement	Burns formation	PDS, Dec. 6, 2012
2669	Gibraltar	RU	Outcrop pavement	Burns formation	PDS, Dec. 6, 2012
2696	Tisdale2 Timmins3	RU	Rock, ejecta - Odyssey	Shoemaker formation	Squyres et al., 2012
2701	Tisdale2 Shaw2	RU	Rock, ejecta - Odyssey	Shoemaker formation	PDS, Dec. 6, 2012
2722-6	Salisbury1 (matrix)	RR	Outcrop (breccia)	Shoemaker formation	Squyres et al., 2012
2734	Geluk (clast)	RU	Clast in breccia	Shoemaker formation	Squyres et al., 2012
2771	Deadwood	RU	Outcrop pavement	Grasberg formation	PDS, Dec. 6, 2012
2787	Transvaal	RU	Outcrop	Shoemaker formation	PDS, Dec. 6, 2012
2801	Boesmanskop (matrix)	RB	Outcrop (breccia matrix)	Shoemaker formation	Squyres et al., 2012
2805	Komati (clast)	RU	Outcrop (breccia clast)	Shoemaker formation	Squyres et al., 2012
2834	Amboy2	RU	Outcrop	Shoemaker formation	PDS, Dec. 6, 2012
2920	Amboy4	RU	Outcrop	Shoemaker formation	PDS, Dec. 6, 2012
2940	Amboy12	RU	Outcrop	Shoemaker formation	PDS, Dec. 6, 2012
2995	Grasberg1	RB	Outcrop pavement	Grasberg formation	PDS, Dec. 6, 2012
3022	MonsCupri	RU	Outcrop pavement	Grasberg formation	PDS, Dec. 6, 2012
3027	Rushall1	RU	Outcrop pavement	Burns formation	PDS, Dec. 6, 2012
3067	Kirkwood1	RB	Outcrop	Matijevic formation	PDS, Dec. 6, 2012
3085-7	Azilda Average	RR	Outcrop pavement	Matijevic formation	Arvidson et al., 2014
3096	Chelmsford3	RB	Coating/Veneer	Matijevic formation	PDS, Dec. 6, 2012
3146	Sandcherry (veneer)	RR	Coating/Veneer	Matijevic formation	Arvidson et al., 2014
3158	Onaping	RU	Outcrop	Copper Cliff Unit	Arvidson et al., 2014

3171	Vermillion Cliffs2	RU	Outcrop	Copper Cliff Unit	Arvidson et al., 2014
3192	Ortiz 2 (vein poor)	RU	Outcrop pavement	Matijevic formation	PDS, Dec. 6, 2012
3200	Ortiz2B (vein rich)	RB	Outcrop pavement	Matijevic formation	PDS, Dec. 6, 2012
3209	Fullerton3 (sph-poor)	RB	Outcrop pavement	Matijevic formation	PDS, Dec. 6, 2012
3214	FecunisLake	RB	Outcrop pavement	Matijevic formation	PDS, Dec. 6, 2012
3224	Maley	RB	Outcrop pavement	Copper Cliff Unit	Arvidson et al., 2014
3253	SturgeonRiver3RAT2	RR	Outcrop	Matijevic formation	PDS, Dec. 6, 2012
3383	Black Shoulder	RR	Outcrop pavement	Burns formation	PDS, Dec. 6, 2012
3396	Tickbush	RU	Float rock	TBD	PDS, Dec. 6, 2012
3403	Platypus	RB	Outcrop pavement	Grasberg	PDS, Dec. 6, 2012
3434	WallyWombat	RB	Outcrop pavement	Grasberg	PDS, Dec. 6, 2012
3445	Callitris	RB	Outcrop pavement	Burns formation	PDS, Dec. 6, 2012
3463	Spinifex	RB	Outcrop, breccia matrix	Shoemaker Breccia	PDS, Dec. 6, 2012
3542	CapeElizabeth	RB	Outcrop pavement, brc.	Shoemaker Breccia	PDS, Dec. 6, 2012
3569	GreenIsland	RB	Outcrop pavement	Shoemaker Breccia	PDS, Dec. 6, 2012
3598	TurnagainArm	RB	Outcrop (breccia)	Shoemaker Breccia?	PDS, Dec. 6, 2012
3671	Sarcobatus Flat1	RB	Outcrop pavement, brc.	Shoemaker Breccia?	PDS, Dec. 6, 2012
3741	Cape Fairweather	RU	Outcrop	Burns formation	PDS, Dec. 6, 2012
3796	Hoover	RB	Ejecta, Ulysses crater	TBD	PDS, Dec. 6, 2012
3812	Margaret Brush	RB	Ejecta, Ulysses crater	TBD	PDS, Dec. 6, 2012
	Average Soil[2]	Soil			Average: PDS-1 data
	Average Dust[3]	Dust		Meridiani bright soil	Clark et al., 2005b
	EETA 79001 B	MM	Basalt	Shergottite	Lodders, 1998
	Zagami	MM	Basalt	Shergottite	Lodders, 1998
	NWA 7475/7034	MM	Regolith Breccia	Surface Material	Wittmann et al., 2015

[1]RU: Rock Unbrushed; RB: Rock Brushed; Rock RAT Grind

[2]Average of 9 soil analyses (sols 011, 090, 249, 373, 499, 507, 730, 879, 1918)

[3]Average of 3 bright soil analyses (HemaTrench, sol 025; Mont Blanc - LesHouches, sol 060; McDonnell HilltopWilson, sol 123 ; cf. Yen et al. (2005)

[4](Arvidson et al., 2014; Clark, et al., 2005b; Fleischer et al., 2010; Lodders, 1998; Rieder et al., 2004; Squyres et al., 2012; Wittmann et al., 2015; Zipfel et al., 2011)

For the SO_3- and Cl-free dataset, these volatile elements were removed from the data to better evaluate potential relationships between volcanic precursor rocks, which would have much lower indigenous S and Cl contents, judging from the compositions of martian meteorites (S + Cl typically <1 wt.%) (McSween Jr. & Treiman, 1998). However the S and Cl enrichment of the

Burns formation is a fundamental aspect of their chemical composition and the basaltic protolith may not be easily extracted (McLennan et al., 2005). If the sulfate-rich martian sedimentary rocks and impact breccias were mainly affected by isochemical alteration of protoliths (McLennan et al., 2005) coupled with addition of S and Cl, then comparing the S- and Cl-free compositions may provide insights into the compositions of volcanic precursors.

2.2.1 Dust and Soil Contamination

Dust at Meridiani is defined as a globally mixed air fall material that is compositionally consistent across hundreds of meters and can be visually identified by its bright coloration in Pancam images, for this study we use an average of several bright dust targets as reported in Clark et al. (2005b). Soil at Meridiani is defined as loose fine regolith derived from locally eroded sources, for this study we use an average of several APXS measurements of Meridiani soil. The majority of sites of investigation along the traverse of Opportunity across Meridiani Planum have some soil or dust contamination (Rieder et al., 2004). For this reason the RAT has been used whenever possible to remove dust or soil contamination from rock surfaces. The RAT has also been used to attempt to grind through potential alteration rinds (Knoll et al., 2008). In order to characterize the effects of soil and dust or rinds on an APXS analysis we can compare compositions for a target for which we have the as-is or undisturbed rock (RU), RAT-brushed (RB), and RAT-abraded-rock (RR) measurements. We included three "Gagarin" (sols 400-403) and three "Steno" (sols 1311-1316) targets to test the effects that different levels of site preparation have on the clustering and SI values. Comparing the RU, RB, and RR compositions with average soil and dust compositions commonly shows that unbrushed compositions are more or less linear mixtures of the brushed rock and soil or dust compositions. Alteration rinds or coatings can be more complex, but commonly the application of the RAT by brushing or

grinding reveals a different interior rock composition. Generally martian soil compositions measured at different locations are very similar (Yen et al., 2006).

2.2.2 Hierarchical Clustering

The first step of our target compositional comparison uses a clustering analysis to group the selected 60 compositions into clusters. Hierarchical clustering is an iterative and unsupervised statistical method used to organize large data sets into discrete groupings and can be used as a method of exploratory data analysis (Xu & Wunsch II, 2009). The cluster analysis is unsupervised so as not to prejudice the grouping by forcing the data to fit into a preselected number of clusters. The clustering analysis creates Euclidian distance matrices (n×n) of the sum of the squared differences of the attributes (each of the 11 or 13 major oxide weight percentage's) of each case (APXS target) (Xu & Wunsch II, 2009).

Agglomerative clustering may be completed using a nearest-neighbor, farthest-neighbor, or group-average distance function. The nearest and farthest neighbor techniques fuse clusters according to the least and greatest distance between two cases or group of cases, respectively (Xu & Wunsch II, 2009). The group average technique defines the distance between clusters as the distance between a combined average of all of the individual cases in a cluster, reducing the impact of outliers in the data (Xu & Wunsch II, 2009). Each of the techniques is run recursively until all of the cases have been linked and results are displayed in a single dendrogram. For this study the principal data set (APXS) was run as a quantitative data set with Euclidian distances calculated with the space-conserving group-average technique of agglomerative clustering.

The advantage of hierarchical clustering is that it can easily handle hundreds of samples and displays patterns and relationships of multivariate data. However, because the distance between cases is determined by the sum of the squared differences, the clustering is more

responsive to oxides that exhibit the largest absolute variations in one attribute (oxide) such as SO_3 (0.6-28.6 wt%) and SiO_2 (32.6-51.6 wt%). To prevent these elements from controlling the cluster division each oxide is standardized to 0-1 by subtracting the minimum oxide value and then dividing by the range of the oxide values. This standardization technique provides the best recovery of underlying cluster structure across a range of clustering methods and conditions (Milligan & Cooper, 1988). A similar standardization step was adopted when applying multivariate statistics to classify martian provinces on basis of chemistry (Gasnault et al., 2010).

$$X_{std} = \frac{X - \mathrm{Min}(X)}{Max(X) - Min\ (X)}$$

2.2.3 Similarity Index

The hierarchical cluster method is attractive in principle, but in some cases produces complicated or even misleading results, and groupings may not always represent lithologic relationships. We therefore devised a method to interrogate the data using a χ^2 value, an error-weighted sum of the squares of differences in oxide concentrations between two compositions. The equation that represents this calculation is as follows:

$$\chi^2 = \sum_{i=1}^{n} \left[\frac{(A_i - B_i)}{\left(\frac{A_i + B_i}{2} * un\right)} \right]^2$$

This approach compares two cases (rock targets *A* and *B*) by dividing the difference for each attribute (oxide or element weight concentration *i*) by a weight factor (the attribute average) and accounts for the analytical uncertainty (*un*) (Korotev et al., 1995). The weighting factor for each attribute is based on the average analytical uncertainty of each attribute across the range of selected targets as reported with the APXS data in the PDS (SiO_2: 0.02, TiO_2: 0.15, Al_2O_3: 0.03, Cr_2O_3: 0.2, FeO: 0.02, MnO: 0.1, MgO: 0.03, CaO: 0.02, Na_2O: 0.2, K_2O: 0.2, P_2O_5: 0.1). This

approach provides a complementary but more rigorous composition-to-composition comparison method relative to the clustering results. Analytical uncertainty has a positive correlation with the elemental concentration range so there is no need to standardize these data before calculating the SI.

In our analysis we extract information by comparing compositions including the full set of 13 major oxides, and by comparing the SO_3- and Cl-free compositions. In order to better compare SI values for both cases we use a reduced χ^2 value. This value is determined by dividing the χ^2 by number of oxides included in the analysis:

$$\chi^2{}_r = \frac{\chi^2}{n}$$

We refer to the ${\chi_r}^2$ value as a target's similarity index (SI) value. This technique is a comparison method that can also identify which specific attributes contributed most to variations between two cases. Unlike cluster analysis, this approach compares only two cases at a time. By plotting the SI values in a single matrix, however, all combinations of targets can be reported. An exact match would have a SI value of zero, whereas multiple APXS measurements of the same target can have SI variations of ~1-10 (see next section). It is important to note that the SI values represent the similarity between the bulk chemistry of everything within the field of view of the APXS, so MI and Pancam imagery is required to make an informed interpretation these values.

2.2.4 Previous Modeling

Hierarchical clustering has been used previously to assess MER data but in slightly different contexts. Farrand et al. (2014) used this approach to group VNIR data from the Pancam instrument on Opportunity. Their data clusters included similar sub-groupings to the results presented in this paper but showed the Grasberg targets to be more similar to the Matijevic

targets than to Shoemaker breccia. One explanation for this discrepancy is the application of cluster analysis to different data sets, which relate to different aspects of the samples (e.g., inclusion or exclusion of veneers). Another explanation could be the difference in target size. The Farrand study breaks out clusters for both spherules found scattered with in Matijevic Hill formation rocks, "newberries," and the traditional "blueberries" characteristic of the Burns formation sulfate sandstones (Farrand et al., 2014).

Hierarchical clustering was also used by Mittlefehldt et al. (2018) to assess lithologic variations and alteration among rocks of the Endeavour crater rim. They also group the rock types according to the four main named formations, Burns, Shoemaker, Grasberg, and Matijevic. According to their detailed assessment, four episodes of alteration were discerned: (1) pre-Endeavour alteration within Matijevic rocks, (2) alteration along the Matijevic-Shoemaker contact, (3) alteration along radial fracture zones within the Shoemaker formation, and (4) differential mobilization of Fe, Mn, and Ca ($CaSO_4$ vein formation) in the Shoemaker and Grasberg formations (Mittlefehldt et al., 2018).

Error weighted χ^2 deviations have also been used before. For example, McLennan et al. (2005) used this method to evaluate the distribution of spherules in Burns formation rocks (McLennan et al., 2005). Larsen et al. (2000) combined correspondence analysis, a visualization of variance, with a least squares mixing model to create a rapid quantitative method for sorting new data (Larsen et al., 2000). Larson used the two statistical methods on soil and rock compositions from the Viking 1 Lander and Pathfinder missions, and correspondence analysis has since been performed on data from the MER missions (Arvidson et al., 2006, 2008, 2010, 2011). Variations of error weighted deviations have also been used to compare meteorite and terrestrial samples to Gusev crater rocks, including comparing an impact melt clast of NWA

7034 to the picritic Gusev rock Humphrey (Udry et al., 2014), and comparing martian analog basalts at the Crater of the Moon Monument and Preserve to Gusev rocks and martian meteorites (Adcock et al., 2018). This work provides a unique application by adapting and then combining both techniques and applying them in a rigorously validated and image referenced manner to this specific data set.

2.3 Results

In this section we first present the results of the hierarchical cluster analysis as a dendrogram containing all of the targets. Major groupings of targets are evident in the dendrogram, and we refer to these groupings as "super-clusters," containing one or more tighter groupings, referred to as "sub-clusters." We present the hierarchical clustering results in two cases, first for the full data set (including SO_3 and Cl, but excluding trace elements Ni, Zn, and Br), and then with the SO_3 and Cl removed and compositions renormalized to 100%. We then report the similarity index values used to interrogate relationships between targets and groupings, with and without SO_3 and Cl. Finally we use the Pancam and MI imagery for selected rock targets in each of the super-clusters to aid in assessment of groupings.

Throughout the figures in this paper the targets are color coordinated according to the geologic formation of which they are considered to be a member, as follows: the Burns formation targets are represented by blue, the Grasberg formation targets are green, the Shoemaker formation are red, the Matijevic formation are magenta, and members of the Copper Cliff unit, which may be transitional between the Matijevic and Shoemaker formations, is indicated by gray. The erratic targets that have not been previously mapped as, or considered to

be, a member of one of the four established units, are indicated in black, and the Bounce Rock target and selected martian meteorites are represented by purple.

2.3.1 Cluster Grouping with SO_3 and Cl Included

The Hierarchical clustering algorithm establishes groupings of targets based on their chemical similarity by first grouping together the most similar targets, then hierarchically clustering similar groups onto each other. The farther to the right a linkage is, the less similar the constituent targets of each cluster are to each other. These linkage distances show that the Tickbush 2 rock target is the most dissimilar of all the rocks included in the analysis (Fig. 2.3). The next most dissimilar targets is a loosely linked grouping of the erratic Bounce Rock and the martian meteorites EETA 79001 B and Zagami. As reported by Zipfel et al. (2011) the crystalline erratic rock fragment Bounce Rock, discovered near Eagle crater, has similar texture, composition, and mineralogy to basaltic shergottites, especially EETA 79001 lithology B. Bounce Rock's composition is an outlier compared to the rest of the local Meridiani materials. The bulk composition of Zagami was also included to compare the surface materials to another shergottite martian meteorite.

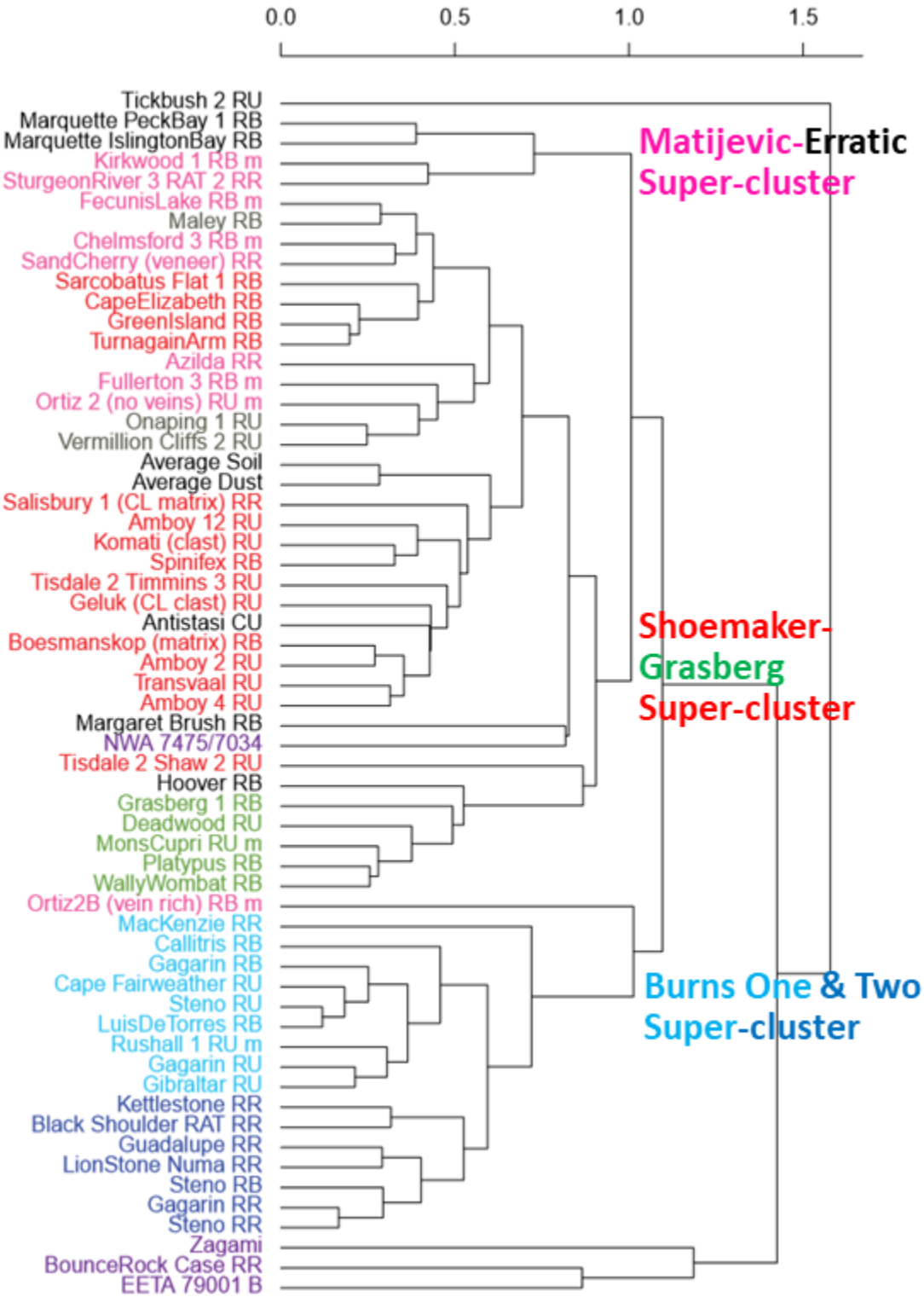

Figure 2.3 Hierarchical cluster dendrogram illustrating compositional relationships of Meridiani rocks and formations with complete oxide weight percentages (including SO_3 and Cl). This cluster was created using the complete oxide weight percentages. The x-axis represents the unitless measure of linkage similarity, with linkages becoming more dissimilar to the right. The cluster analysis breaks the targets into three super-clusters, mostly by geologic formation. Targets labeled with RU have neither been brushed nor ground with the RAT, sites labeled with

RB have been brushed, and RR, ground into by the RAT. The most dissimilar targets are members of the Burns formation (dark and light blue), which form two distinct sub-clusters. The "Burns One" super-cluster is dominated by targets measured on Meridiani Planum, while the "Burns Two" super-cluster includes targets closer to Endeavour crater as well as the targets that were brushed or ground into with the RAT, demonstrating the impact of coatings and soil cover. The Grasberg formation (green) targets form a sub-cluster within the large super-cluster dominated by the Shoemaker formation rocks (red). The Copper Cliff (gray) breccia compositions are also in this super-cluster. The Matijevic formation rocks (magenta) are split between their own distinct super-cluster with erratic Marquette Island (black), and the Shoemaker-Grasberg super-cluster. The Bounce Rock (purple) target is very dissimilar to all the other surface materials and only plots with martian meteorites. The martian meteorite pair NWA 7475/7034 clusters with the erratic Margaret Brush within the Shoemake-Grasberg super-cluster.

The rest of the targets are grouped into three super-clusters containing sub-clusters. The three super-clusters separate partially along the lines of the four lithologies at Endeavour crater. For example, the Burns formation, the clastic sulfate sandstone that rims Endeavour crater in Meridiani Planum, divides into two sub-clusters of one super-cluster. The Burns formation rocks super-cluster is predictably dissimilar to the rest of the Endeavour crater rim rocks. There is a super-cluster composed of the Matijevic formation rocks (the pre-Endeavour impact sedimentary lithology found at Cape York) and an erratic rock. The largest super-cluster for the rocks considered in this work is dominated by the Shoemaker breccia, which is the Endeavor impact-breccia lithology. Notably this super-cluster also includes a sub-cluster of all of the Grasberg targets, which is the lithology of clastic rocks that likely postdate the Shoemaker impact ejecta emplacement, but pre-date the Burns formation (Crumpler et al., 2015). This relationship shows a higher similarity between the Grasberg formation and the Shoemaker formation than any other two main lithologies.

The sulfate sandstones of the Burns formation rocks are expectedly the least similar of the Endeavor crater lithologies owing to their high concentrations of SO_3; however, they do split into two separate sub-clusters.

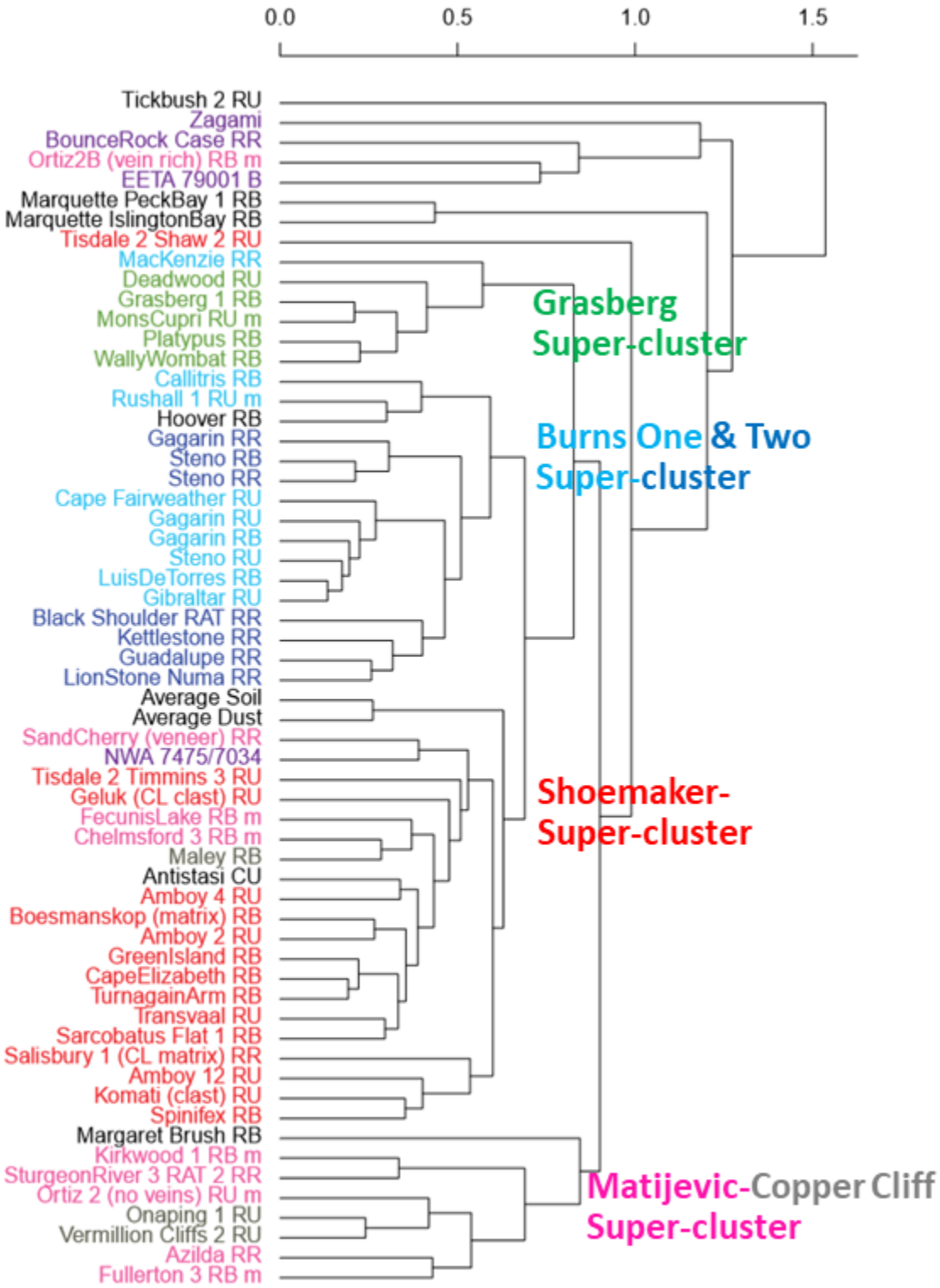

Figure 2.4 Hierarchical cluster dendrogram illustrating compositional relationships of Meridiani rocks and formations, with SO_3 and Cl removed and renormalized to 100%. The x-axis represents the unitless measure of linkage similarity, with linkages becoming more dissimilar to the right. Targets labeled with RU have neither been brushed nor ground with the RAT, sites labeled with RB have been brushed, and RR, ground into by the RAT. The cluster analysis breaks the targets into four super-clusters, mostly by geologic formation. With SO_3 and Cl removed

members of the Burns super-cluster still form distinct sub-clusters. The Copper Cliff (gray) breccia compositions segregate into a super-cluster comprised of Matijevic formation targets. The Grasberg formation (green) is no longer a group within the Shoemaker super-cluster but is now its own super-cluster. The Bounce Rock (purple) target martian meteorites, and a few other erratics are now the most dissimilar compositions, while the martian meteorite pair NWA 7475/7034 groups with the Endeavour rim rocks.

One sub-cluster consists of Burns rocks measured later in the mission, at or close to Endeavour crater, with the single exception noted below. The sub-cluster includes Gagarin (RB, sol 401), Luis De Torres (sol 2486) and Gibraltar (sol 2669) from the plains west of Cape York, Rushall 1 (sol 3027) from the Cape York bench, Callitris (sol 3445) from the bench-plains contact at Solander point, and Cape Fairweather (sol 3741) from west of Cape Tribulation. Also included in this sub-cluster are the unbrushed targets Gagarin (RU, sol 400) and Steno (RU, sol 1311). The Burns super-cluster also includes the Burns target MacKenzie (sol 184) from Endurance crater interior, and the vein-bearing Matijevic target of Ortiz 2B (sol 3200). These Burns targets are labeled as the "Burns One" sub-cluster.

The other Burns sub-cluster includes all of the selected Burns formation rocks measured on the Meridiani Plains at or north of Victoria crater, i.e., Guadalupe (sol 36) from Eagle crater, LionStone Numa (sol 108) and Kettlestone (sol 155) from Endurance crater's rim and wall, Gagarin (RR, sol 403) from the plains between Endurance and Endeavour craters, and Steno (RB, sol 1313) and Steno (RR, 1316) from Victoria crater, with the only exception being Black Shoulder RAT (sol 3383), which occurs along the rim of Endeavour crater in "Botany Bay" between Cape York and Solander Point. These Burns targets are labeled as the "Burns Two" sub-cluster.

The two sub-clusters do not cleanly divide the Burns formation into geographically segregated groupings of targets, i.e., those targets analyzed near Endeavour crater and those targets analyzed in the plains of Meridiani. The Burns formation as a whole contains hematite

spherules, which collect as resistant loose nodules as the surface is deflated by wind (Fig. 2.5). The textures of the Burns lithology vary from massive and fine-grained (Fig. 2.5a, 2.5b) to containing visible laminae and bedding planes (Fig. 2.5c, 2.5d). The segregation of the selected Burns targets into two groupings is also not consistent with this textural difference and is instead representative of chemical differences. The clustering does segregate the unbrushed and "dusty" Steno and Gagarin targets from their brushed and ratted measurements.

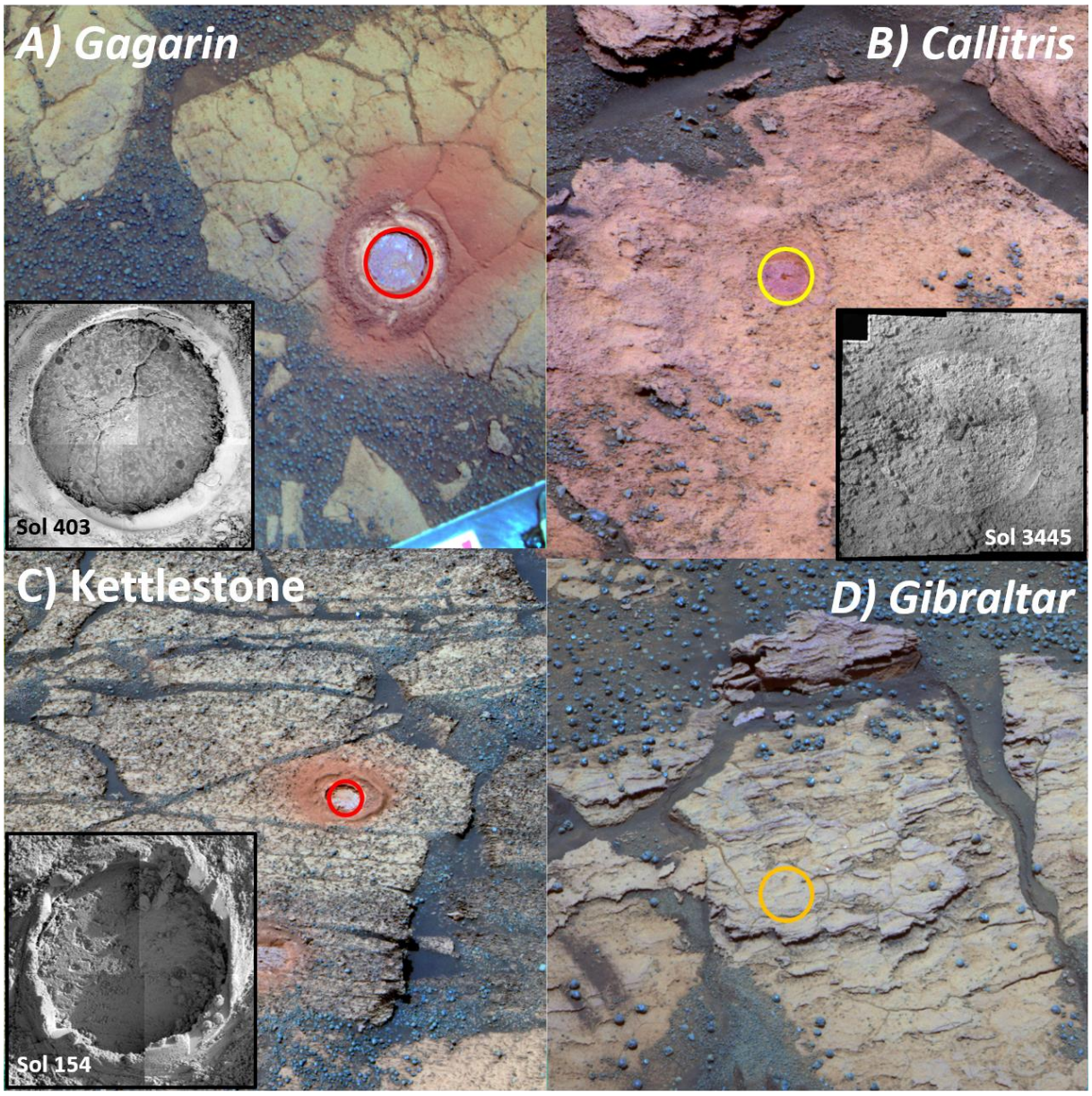

Figure 2.5 False color L257 filter Pancam images, and MI mosaic images of Burns target sites. A and C represent the Burns Two sub-cluster, and B and D represent the Burns One sub-cluster: A) Gagrin RR, obtained on sol 405 (3-14-2005), Burns formation, B) Callitris, obtained on sol 3451 (10-8-2013), Burns formation, C) KettleStone, obtained on sol 157 (7-3-2004), Burns formation, and D) Gibraltar, obtained on sol 2670 (7-29-2011), Burns formation, no MI available. The colored circle represents the RAT activity, either unbrushed (RU = orange), brushed (RB = yellow), or ground into (RR = red), which is ~4.5 cm in diameter. The APXS target area is ~2.5 cm across and has an aproximate location near the RAT site.

The largest super-cluster in the data set contains four sub-clusters and 35 targets. The Shoemaker Breccia, the principal constituent, is the impact lithology created by the impact that formed Endeavour crater (Squyres et al., 2012). The super-cluster also contains members of the Grasberg formation, a post-impact lithology that onlaps the Shoemaker Breccia (Crumpler et al., 2015). The Grasberg rocks are a fine-grained, cohesive unit, which, although softer than terrestrial sandstone, with box-work veins cross cutting the lower most unit, were the most resistant to RAT grinding of all of the units examined at Cape York (Crumpler et al., 2015). Figure 2.6a shows the MI of the fine-grained Grasberg target, and the Pancam image exhibits a characteristic feature of this lithology, a purple false color in the brushed target location. The Grasberg formation has been suggested to be either formed from detritus from the eroding Endeavour crater rim, or as fine-grained air fall from either a distal impact or ash from a volcanic eruption (Crumpler et al., 2015).

All of the Grasberg targets (WallyWombat, Platypus, MonsCupri, Grasberg 1, Deadwood, sols 2771-3434) cluster together in one sub-cluster, making it the most homogenous chemical grouping of the lithologies. The erratic, Hoover and the Shoemaker target Tisdale 2 (Shaw 2) branch off of this cluster. There were no rock-brushed sites available for the two Tisdale targets, but we include them because they are texturally unique, and represent ejecta blocks from the much smaller and younger Odyssey crater at Cape York (Crumpler et al., 2015;

Squyres et al., 2012). The martian meteorite pair NWA 7475/7034 branches off of the two remaining sub-clusters with the erratic Margaret Brush (sol 3812).

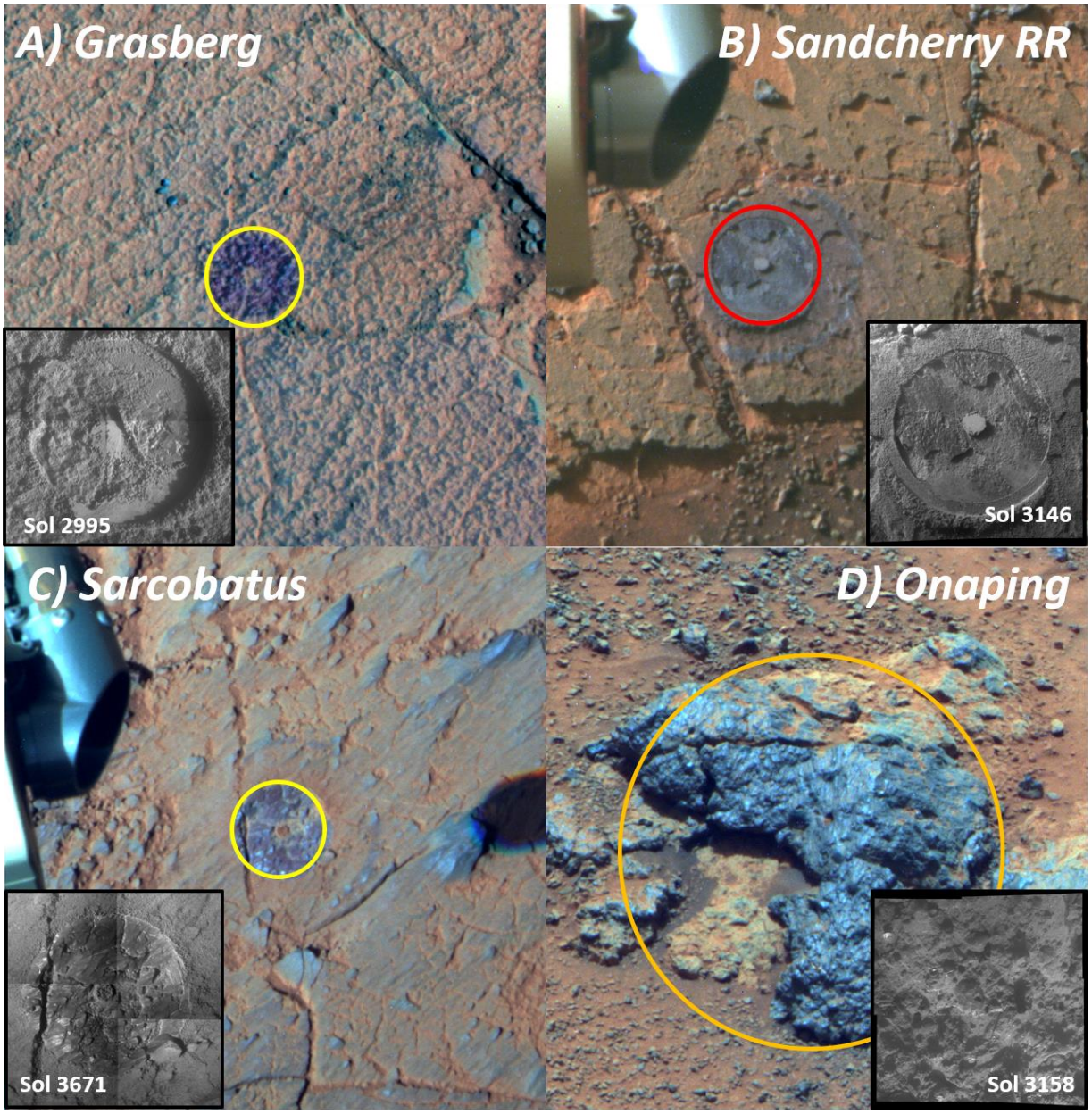

Figure 2.6 False color Pancam images using L257 filters, and MI images of the Shoemaker-Grasberg super-cluster targets: A) Grasberg, obtained on sol 2998 (6-30-2012), Grasberg formation, B) Sandcherry RR, obtained on sol 3146 (11-29-2012), veneer on the Matijevic formation, C) Sarcobatus, obtained on sol 3676 (5-27-2014), Shoemaker formation, and D) Onaping, collected sol 3178 (1-1-2013), Copper Cliff Unit. The colored circle represents the RAT activity, either unbrushed (RU = orange), brushed (RB = yellow), or ground into (RR = red), which is ~4.5 cm in diameter. The APXS target area is ~2.5 cm across and has an aproximate location within the RAT circle.

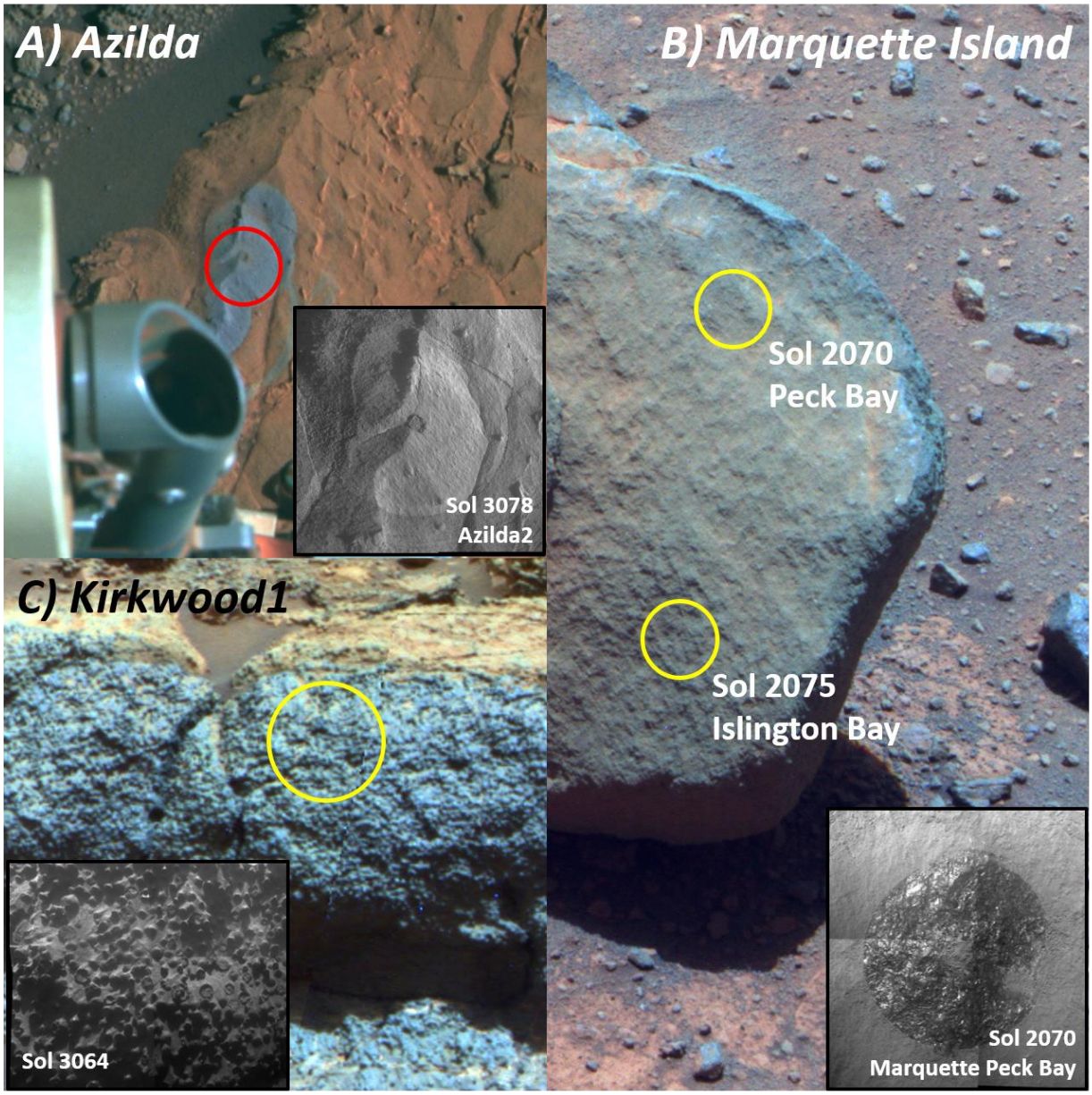

Figure 2.7 False color Pancam images using L257 filters, and MI images of targets from the Matijevic/Erratic super-cluster: A) Azilda targets, obtained on sol 3083 (9-25-2012), Matijevic formation, B) Marquette Island, obtained on sol 2063 (11-12-2009), cobble erratic, and C) Kirkwood 1, obtained on ~sol 3062 (9-2-2012), spherule-rich Matijevic formation. The colored circle represents the RAT activity, either unbrushed (RU = orange), brushed (RB = yellow), or ground into (RR = red), which is ~4.5 cm in diameter. The APXS target area is ~2.5 cm across and is located within the RAT circle.

Some of the first Shoemaker breccias to be investigated are Tisdale 2 (Timmins 3) (sol 2696), Salisbury 1 (sols 2722-6), Geluk (sol 2734), Transvaal (sol 2787), Komati (sol 2805), and Boesmanskop (sol 2801). These Shoemaker targets cluster with other impact breccias in this

sub-cluster: the Amboy 2 (sol 2834), Amboy 4 (sol 2920), and Amboy 12 (sol 2940) targets, Spinifex (sol 3463), and Sarcobatus Flat 1 (sol 3671), and). These targets form the largest Shoemaker sub-cluster and also include the average soil and average dust compositions and the erratic Antistasi (sol 642). The Shoemaker formation is a lithic breccia, characterized by a texture of centimeter-sized and larger, subrounded to angular, dark (blue in false color Pancam) clasts in a light-toned fine-grained matrix, as is visible in figure 2.6c.

Clustered close to, but separate from, this tight cluster are two sub-clusters containing Matijevic formation and Copper Cliff rocks. One contains the Matijevic rocks: Sandcherry (sol 3146), Chelmsford 3 (sol 3096), and Fecunis Lake (sol 3214). These Matijevic targets are unique compared to the other pre-impact clastic rocks in that they are significantly covered by a dark, platy veneer (Fig. 2.6b). This surface feature is both a textural and chemical distinction that differentiates the Matijevic targets. The Copper Cliff rock Maley (sol 3224) is grouped within this sub-cluster. One of the Copper Cliff rocks, Maley (sol 3224), forms a nearby sub-cluster with the Shoemaker targets of the Murray Ridge: Cape Elizabeth (sol 3542), GreenIsland (sol 3569), and TurnagainArm (sol 3598).

A relatively vein-free part of the Matijevic formation rock, Ortiz 2 (sol 3192), clusters with two targets of the Copper Cliff breccia, Vermilion Cliffs 2 (sol 3171) and Onaping 1 (sol 3158). The Copper Cliff breccia marks the transition between the Matijevic and Shoemaker formation. The rocks at Copper Cliff may or may not be part of the overlying Shoemaker formation judging by their compositional and textural differences (Arvidson et al., 2014; Mittlefehldt et al., 2018); however Crumpler et al., (2015) placed Copper Cliff as the lowermost member of Shoemaker formation rocks at Cape York on the basis of the breccia texture and the unconformity between the Shoemaker and Matijevic formations. With SO_3 and Cl included, the

Copper Cliff targets cluster with the Shoemaker super-cluster. Mittlefehldt et al., (2018) pointed out the inclusion of spherules in the Copper Cliff rocks (Fig. 2.5d). These spherules are not a common feature of Shoemaker formation rocks but have been observed in the older Matijevic formation (Fig. 2.7c). The Copper Cliff breccias are compositional more similar to the Shoemaker formation, but their textures imply the inclusion of older Matijevic materials.

The final super-cluster comprises the Matijevic formation rocks (SturgeonRiver 3 RAT 2 and Kirkwood 1, sols 3067-3253), and an erratic rock targets found along Opportunity's traverse (Marquette - Islington Bay, and Marquette - Peck Bay 1). The spherule-poor (Azilda, Fig. 2.7a) and spherule-rich (Kirkwood, Fig. 2.7b) Matijevic targets are not grouped in the same super-cluster with SO_3 and Cl. The Matijevic sites range from sparse (Azilda), to medium (Fullerton), to dense (Kirkwood) concentrations of spherules (Fig. 2.7). The erratic, Tickbush 2, branches off of all of the super-clusters.

2.3.2 Cluster Grouping with SO_3 and Cl Excluded

When SO_3 and Cl are removed and the remaining composition is normalized to 100%, the clustering relationships slightly shift (Fig. 2.4). The new dendrogram also has four super-clusters and a weakly clustered group of outliers, the vein-bearing target of Ortiz 2b groups with Bounce Rock and EETA 79001, and Zagami becomes an outlier relative to this loose grouping of other outliers.

The two Burns sub-clusters without SO_3 and Cl branch off of the Shoemaker clusters, The relationships of the Burns formation targets without SO_3 and Cl should not be over-interpreted because S and Cl are defining components of that suite of rocks; however, with SO_3 and Cl removed, there are still two groupings of Burns formation rocks.

There is still a super-cluster of Matijevic formation rocks and erratics, but while this super-cluster loses the erratic, Antistasi, it gains the Copper Cliff rocks Vermillion Cliffs 2 and Onaping, and the rest of the non-veneer Matijevic formation targets. This grouping shows the chemical similarity between the Copper Cliff unit and the Matijevic formation it overlies, and the chemical difference between the Matijevic formation and the rest of the Endeavour crater rocks. The two Marquette Island targets form a sub-cluster off of the Endeavour rim rocks super-clusters.

The largest super-cluster is still dominated by the Shoemaker targets and still contains the veneer coated Matijevic rocks (Chelmsford 3, Sandcherry, and Fecunis Lakes), and the average soil and dust compositions, and the paired martian meteorite NWA 7475/7034. The five Grasberg formation targets split farther away from the Shoemaker targets in their own super-cluster . The erratic Tickbush remains an outlier of all of the super-clusters.

2.3.3 Similarity Index Values

For clarity only a sub-set of the SI values is presented in matrix form here (Table 2.4). Generally a SI value < 20 is considered highly similar, and is a reasonable score for targets within the same sub-cluster, whereas targets that fall between 20 and 40 are considered moderately similar, and have scores similar to other targets within a super-cluster. Outliers associated with a super-cluster have values that are between 40 and 60 and are considered to be weakly similar, while values above 60 are dissimilar. The data set with SO_3 and Cl removed overall has lower SI values because of the reduction in the number in data vectors (Table 2.5). Removing SO_3 and Cl reduces the number of elements included in the χ^2, but using χ^2_r minimizes the impact this reduction has on the ranges of highly (0-20), moderately (20-40), and

weakly (40-60) similarity index values allowing for the same cutoff ranges to be used across both data sets.

The average of the bright global dust is highly similar (SI: 8) to average of local soils. With SO_3 and Cl included, the average soil composition is highly similar to the average of the Endeavour impact unit of the Shoemaker breccia (SI: 16), moderately similar to the average of the pre-impact Matijevic formation (SI: 22), and weakly similar to the average of the Copper Cliff unit (SI: 48). With SO_3 and Cl the average dust composition is highly similar to the Shoemaker (SI: 6) and Matijevic formations (SI: 19), and the Copper Cliff unit (SI: 20), is weakly similar to the Grasberg average composition (SI: 42).

The closest composition to the erratic Bounce Rock based on the SI scores is the martian meteorite EETA 79001 lithology B, which is consistent with the conclusion of Zipfel et al., (2011). The initial SI score (with SO_3 and Cl included) is a very dissimilar value of 116, but 88% of the variance is due to Cl, which is very low in concentration in EETA 79001. When SO_3 and Cl are removed from the analysis, the SI value decreases to a highly similar score of 14. This similarity was expected due to the comparisons made between these two rocks (Zipfel et al., 2011). Bounce Rock and EETA 79001 are at best only weakly similar to Endeavour crater rim rocks.

The erratic rock, Tickbush, is one of the most dissimilar targets included in the analysis. Tickbush has SI values when compared to the other Endeavour crater rocks that range from 56 (weakly similar) to 362 (dissimilar). It is unlike almost all Endeavour crater rim rocks. On the other hand, the paired martian meteorite and impact breccia NWA 7475/7034 is highly similar to Endeavour crater materials when SO_3 and Cl are removed (SI with the Matijevic average: 7, with

the Copper Cliff average: 8, with the Shoemaker average: 14, and with Marquette Islington Bay: 14).

The Burns formation rocks are separated into two distinct sub-clusters by the clustering algorithm. The SI value (with SO_3 and Cl included) between the two Burns formation sub-clusters is a moderately similar score of 22. The variation comes from SO_3 (responsible for 42% variance with SO_3 and Cl included), Al_2O_3 (16% variance), CaO (15% variance), SiO_2 (12% variance), and MgO (9% variance). When SO_3 and Cl are removed the SI value falls to 8, indicating a high degree of similarity, with the variance coming mainly from MgO (66%) and Al_2O_3 (17%). With SO_3 and Cl included, the Burns formation rocks are dissimilar to all other targets included in the analysis. Both with and without SO_3 and Cl, the average of the Burns Two sub-cluster is more similar to the average soil and dust compositions than the Burns One sub-cluster composition.

With SO_3 and Cl included the average of the clastic Grasberg formation is moderately similar to the Shoemaker formation (SI: 36). When SO_3 and Cl are removed the lithologies remain moderately similar (SI: 24). This similarity places the Grasberg formation within the same range of similarity as the other locally derived Endeavour crater rim rocks.

The average of the three Copper Cliff unit targets is highly similar to the average Shoemaker formation (SI: 20) and moderately similar to the average Matijevic formation (SI: 37). When SO_3 and Cl are removed, the average Copper Cliff unit composition is highly similar to both lithologies but is more similar to the Matijevic formation (SI: 8) than the Shoemaker formation (16). The Copper Cliff represents a potential transition zone between the pre-impact Matijevic formation and the impact breccia of the Shoemaker formation, based on compositional similarities, brecciated textures, and inclusion of Matijevic spherules.

The average of the six non-veneer Matijevic formation targets is highly similar to the average dust composition (SI: 19) and Shoemaker formation averages (SI: 14) when SO_3 and Cl are included, but is dissimilar to both the average Grasberg (71) and both Burns super-clusters (SI 196 and 126). The average Matijevic formation is the only Endeavour crater rim rock group to which the erratic Marquette Islington Bay is moderately similar (SI: 31). When SO_3 and Cl are removed the average Matijevic formation is highly to moderately similar to all the Endeavour crater rim rocks and is highly similar to the Marquette Islington Bay erratic (SI: 12). Most of the erratic rock targets that have not previously been associated with the named rock formations have highly to moderately similar SI values to the Matijevic targets with which they cluster.

Table 2.4: Similarity index (SI) matrix for selected targets and formation average compositions, with SO_3 and Cl included. Values highlighted yellow are highly similar and low enough to be in the same sub-cluster; values highlighted in green are moderately similar, and values highlighted in orange are weakly similar. Most of the highly similar values are between targets and their own geologic formations, or between targets in the same super-clusters. The very high values of Bounce Rock, the martian meteorites and the erratic Tickbush show how dissimilar they are to the other targets.

SI+ Matrix	AvS	AvD	B1 Av	B2 Av	Gs Av	Sh Av	CC	Mt Av	MI	BR	EETA	NWA	Tb
Average Soil	0	8	191	112	64	16	48	22	56	377	414	326	117
Average Dust		0	149	76	42	6	20	19	71	406	436	327	132
Burns 1 Avg			0	22	133	154	138	196	276	580	599	409	362
Burns 2 Avg				0	61	84	69	126	213	505	524	373	271
Grasberg Avg					0	36	49	71	165	491	486	381	198
Shoemaker Avg						0	20	14	72	425	441	325	130
Copper Cliff Avg							0	37	110	416	444	329	150
Matijevic Avg								0	31	394	427	313	91
Marquette Isln.									0	347	404	293	80
BounceRock										0	116	182	292
EETA 79001 B											0	141	352
NWA 7475/7034												0	350
Tickbush 2													0

0 - 20
20 - 40
40 - 60

Table 2.5: Similarity index (SI) matrix for selected targets and formation average compositions on an SO_3 and Cl-free basis and normalized to 100%. Values highlighted yellow are highly similar and low enough to be in the same sub-cluster; values highlighted in green are moderately similar, and values highlighted in orange are weakly similar. Without SO_3 and Cl, the martian surface rocks all appear to be much more similar. The martian meteorite EETA 79001 lithology B is highly similar to Bounce Rock, and NWA 7475/7034 regolith breccia is highly similar to most of the surface materials. Tickbush is still highly dissimilar to nearly every target and formation average.

SI- Matrix	AvS	AvD	B1 Av	B2 Av	Gs Av	Sh Av	CC	Mt Av	MI	BR	EETA	NWA	Tb
Average Soil	0	2	16	4	19	5	20	14	36	91	49	24	87
Average Dust		0	16	4	24	3	12	6	24	87	51	15	76
Burns 1 Avg			0	8	42	12	36	22	40	136	94	21	139
Burns 2 Avg				0	19	4	21	12	36	98	58	20	94
Grasberg Avg					0	24	55	34	63	128	76	60	90
Shoemaker Avg						0	16	5	22	104	63	14	78
Copper Cliff Avg							0	8	22	59	40	8	56
Matijevic Avg								0	12	95	64	7	67
Marquette Isln.									0	138	105	14	87
BounceRock										0	14	98	86
EETA 79001 B											0	71	70
NWA 7475/7034												0	87
Tickbush 2													0

0 – 20
20 – 40
40 – 60

2.4 Discussion

2.4.1 Meridiani Rock Diversity and Model Validation

The surface materials on Mars are primarily volcanic basalts, clastic sedimentary basalt derivatives, and chemical sedimentary rocks. The bulk elemental composition of the selected data set is mafic, and when SO_3 and Cl are removed, the data plot in the basalt and basaltic andesite fields of the Total Alkali-Silica (TAS) diagram (Na_2O+K_2O verses SiO_2 wt%) (Fig. 2.8). As a whole the compositions of Endeavour crater lithologies are more similar to each other than they are to martian meteorites. The Opportunity data does plot near the bulk composition of the NWA 7475/7034 paired martian meteorite. Because this meteorite is a polymict regolith

breccia, the similarity (as indicated by SI and cluster analysis) between its bulk composition and Meridiani surface materials supports the interpretation that these paired meteorites are a better representation of martian surface materials than the other classes of martian meteorites. The average of each of the four geologic formations (Table 2.6) is included in the similarity index matrix.

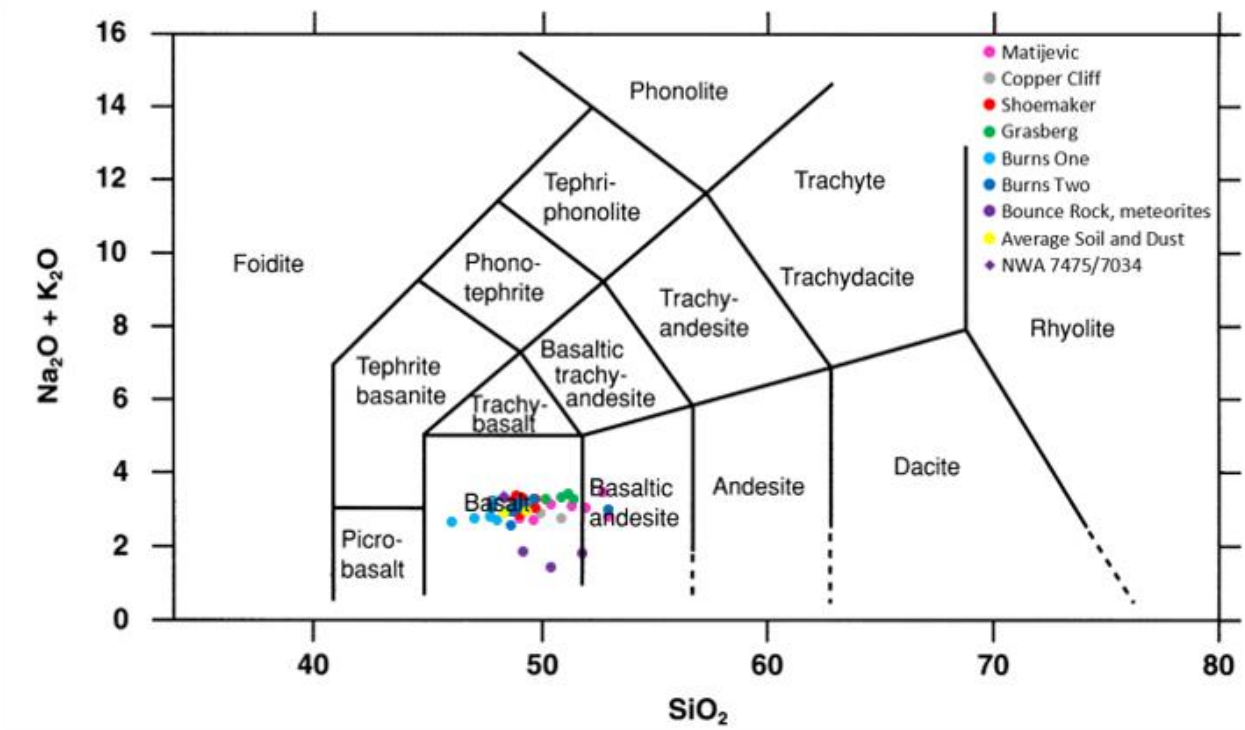

Figure 2.8 Total Alkali-Silica (TAS) diagram for the Endeavour rim data (SO_3 and Cl removed and normalized to 100%) shows compositions to be essentially those of basalt to basaltic andesite.

The hierarchical clustering analysis that includes SO_3 and Cl mostly groups targets with other members of the same geologic formation, which were defined mainly on the basis of geologic relationships. For the most part the clustering algorithm groups members of the same geologic unit together, and where this does not occur co-variant information (from imagery) commonly explains the discrepancies. For example, the separation of three Matijevic

(Sandcherry, Chelmsford 3, and Fecunis Lake) targets from their formation, when SO_3 and Cl are removed, is driven by their Mn-rich veneer.

The SO_3 and Cl-free analysis better reflects relationships between potential volcanic protoliths of the Endeavour crater sedimentary rock units (except for the Burns formation in which sulfate-rich evaporitic materials are a significant component, concentrated by diagenetic processes, and not simply just an isochemical alteration of basalt or an addition of S). The Similarity Index provides a rigorous quantitative and complementary method to interrogate individual target relationships. Finally, variations in imagery provide textural interpretations as well as context for the compositional comparisons.

As an example, we first consider the straightforward case of Bounce Rock. The consistent clustering and low SI values of Bounce Rock with the two reference shergottites, particularly EETA 79001 lithology B, is consistent with the interpretation that Bounce Rock is a piece of shergottite-like crater ejecta, likely from Bopolu crater (Zipfel et al., 2011). The ability of the statistical grouping model to reproduce this type of expected relationship helps to validate both the hierarchal clustering and the SI as appropriate analysis methods for this data set.

Discrepancies between the two methods can appear when trying to comparing two individual targets to a third target. It may not be immediately clear from the clustering dendrograms how similar an outlier is to individual targets within a super-cluster, and key connections may be missed. For this reason, the SI provides a valuable target to target comparison metric that can be used to interrogate the data more thoroughly.

Table 2.6: (A) Average compositions of the Endeavour rim geologic formations, and the Burns formation divided into two groups by hierarchical cluster analysis. (B) Same compositions on a S- and Cl- free basis, renormalized to 100%.

(A)	Matijevic Average n =6	SD	Shoemaker Average n = 15	SD	Grasberg Average n = 5	SD	Burns One Average n = 8	SD	Burns Two Average n = 7	SD
SiO_2	48.8	0.9	45.2	0.7	45.2	0.8	36.0	1.7	40.5	1.5
TiO_2	0.9	0.1	1.1	0.0	1.0	0.0	0.7	0.1	0.8	0.0
Al_2O_3	10.0	0.5	9.2	0.5	8.3	0.3	5.9	0.5	7.2	0.4
Cr_2O_3	0.3	0.1	0.2	0.0	0.3	0.0	0.2	0.0	0.2	0.0
FeO_T	16.0	1.4	17.9	1.2	19.2	0.5	15.5	0.8	16.4	0.5
MnO	0.3	0.1	0.5	0.2	0.2	0.0	0.3	0.0	0.3	0.1
MgO	8.1	0.6	7.8	0.9	5.1	0.7	7.9	0.7	6.8	0.9
CaO	6.0	0.5	6.3	0.6	6.0	0.6	5.1	0.5	5.9	0.9
Na_2O	2.3	0.2	2.4	0.2	2.2	0.0	1.6	0.2	1.9	0.2
K_2O	0.4	0.1	0.5	0.1	0.7	0.1	0.5	0.0	0.6	0.1
P_2O_5	1.0	0.4	1.2	0.3	1.1	0.1	1.0	0.0	1.1	0.0
SO_3	4.9	1.0	6.5	1.9	8.9	0.5	24.1	2.4	17.3	1.9
Cl	0.9	0.3	1.1	0.3	1.7	0.5	1.0	).5	1.0	0.4
SUM	**99.9**		**99.8**		**99.9**		**99.9**		**99.9**	

(B)	Matijevic Average	Shoemaker Average	Grasberg Average	Burns One Average	Burns Two Average
SiO_2	51.9	49.0	50.6	48.1	49.7
TiO_2	0.9	1.1	1.1	1.0	1.0
Al_2O_3	10.7	10.0	9.3	7.8	8.8
Cr_2O_3	0.3	0.2	0.3	0.2	0.2
FeO_T	17.0	19.4	21.6	20.8	20.1
MnO	0.3	0.5	0.2	0.4	0.3
MgO	8.6	8.5	5.7	10.6	8.3
CaO	6.3	6.8	6.7	6.9	7.2
Na_2O	2.5	2.6	2.5	2.1	2.3
K_2O	0.4	0.5	0.8	0.7	0.7
P_2O_5	1.0	1.3	1.2	1.4	1.3
SUM	**100**	**100**	**100**	**100**	**100**

Total Fe reported as FeO (FeO_T)

2.4.2 Endeavour Rim Rock Suite Variation and Interpretations

2.4.2.1 Two Burns Groups:

The Burns formation is the dominate surface lithology of Meridiani Planum and is a sequence of interbedded eolian sulfate-sandstones (Grotzinger et al., 2005), which onlaps the rim of Endeavour crater (Crumpler et al., 2015). The separation of Burns formation rocks into two sub-clusters was unexpected and derives principally from variance in SO_3, Al_2O_3, CaO, SiO_2, and MgO (Fig. 2.5). The difference could be the result of a difference in the clastic source material, regional variation in alteration, or in the level of soil contamination, which affects the unbrushed rock compositions. Different Burns target textures do not match the chemical divisions, and the separation is not simply geographic. The “Burns Two” sub-cluster contains all of the unbrushed Burns targets. The separation of the unbrushed and brushed Steno and Gagarin targets from their brushed and ratted compositions is mainly a reflection of soil and dust contamination, which would make the unbrushed bulk composition appear lower in SO_3 compared to the Burns formation. However, when the unbrushed targets are removed from the analysis there remains a second sub-cluster of Burns formation targets.

When SO_3 and Cl are removed, the Burns rocks become closer to the Shoemaker super-cluster, which also includes the average dust and average soil compositions. Moreover, whereas both average Burns compositions (S- and Cl-free basis) are olivine normative, the “Burns Two” sub-cluster has only 10 weight% olivine compared to 20 weight% of the “Burns One” sub-cluster. This difference could support a variation in clastic components; however, since the S and Cl enrichment is a fundamental part of the Burns formation's composition, simple removal of these components may not accurately represent the basaltic protolith. Although soil contamination plays a part in the segregation of the targets, the Burns formation as a whole contains enough compositional variation to split into two super-clusters.

2.4.2.2 Shoemaker and Grasberg Formations:

The Shoemaker formation, the impact-breccia presumed to have been deposited during the Endeavour impact event, and the Grasberg formation, a bench of fine-grained clastic material surrounding exposures of the Shoemaker formation, were both first characterized at Cape York (Arvidson et al., 2014; Crumpler et al., 2015; Squyres et al., 2012). The inclusion of the average soil and dust targets in the Shoemaker formation clusters indicates that the Shoemaker formation represents a mixture similar to average martian surface materials. The Grasberg rocks are more similar to the Shoemaker formation than any other surface material, with SI values of 36 (SO_3 and Cl included) and 24 (SO_3 and Cl removed) (Fig. 2.6). Crumpler et al. (2015) offered an alternative hypothesis that the Grasberg formation might have originated as fine air fall particles from a distal impact or volcanic eruption; however, the compositional similarities with the Shoemaker formation do not favor that hypothesis.

The two units are separate geologic formations with distinct sedimentary textures; however, because the clastic Grasberg onlaps the Shoemaker formation at Cape York, the chemical similarity and lithochemical groupings suggest that the Grasberg formation derived in part from, and incorporated, eroded Endeavour impact material and ejecta of the Shoemaker formation. Considering normative mineralogy but both the Shoemaker and Grasberg formations are olivine-normative, with 14.5% and 2.5% olivine, respectively. The lower normative olivine content of the Grasberg would be consistent with a reworked sediment derived from the Shoemaker, and possibly including a Matijevic formation component (Table 2.7).

The statistical similarity between the composition of the Grasberg and Shoemaker formations is not proof that the Grasberg derived from the locally eroded Shoemaker material. However, its high similarity to the local rocks as well as the global dust composition does suggest that it was deposited over time, incorporating either the local dust-like material or dust

itself. Such a long duration for the deposition of the Grasberg is less consistent with an airfall event of either volcanic or impact in origin. The existence of two distinct (upper and lower) units of the Grasberg formation (Crumpler et al., 2015) that are not differentiated by the statistical grouping model is also more likely to represent a continuous deposition of the Grasberg through time from the local environment.

2.4.2.3 The Copper Cliff/Matijevic unconformity:

The Copper Cliff unit, located on Cape York, lies at the lower margin of the Shoemaker impact breccia and the upper margin of the pre-impact Matijevic formation (Arvidson et al., 2014; Crumpler et al., 2015). Texturally the Copper Cliff rocks are breccias similar in appearance to the Shoemaker formation. Hierarchical clustering (with SO_3 and Cl) clusters the Copper Cliff rocks within the Shoemaker super-cluster; however, when SO_3 and Cl are removed, the Copper Cliff rocks cluster within the Matijevic formation super-cluster. The compositional difference shown by the clustering and the SI values signifies that there may be a higher fraction of Matijevic formation components incorporated within the Copper Cliff breccia than the typical Shoemaker breccia. This interpretation is supported by the inclusion of Matijevic like spherules in the Copper Cliff breccia (Mittlefehldt et al., 2018). The rocks at Copper Cliff are the lowermost member of the Endeavour impact breccia and mark the transition between the Matijevic and Shoemaker formation. This transition is evidently a diffuse one that involved mixing of the pre-impact materials with the lower most section of the impact ejecta.

2.4.2.4 Matijevic formation and erratic rocks:

Cape York is the only location where the Matijevic formation has been observed to date. The Matijevic formation is a pre-Endeavour impact, light-toned, fine-grained clastic lithology that is chemically distinct from the other units mapped by Opportunity, and clusters with some of

the erratics (Bouchard, et al., 2017). With SO_3 and Cl, this super-cluster includes several rocks from different locations, such as Marquette Island, which lies in the center of a boulder/cobble field on the plains of Meridiani, and Margaret Brush from Wdowiak Ridge without SO_3 and Cl (Fig. 2.7). The coupling of these erratics to the Matijevic formation could indicate that they are both older than the Noachian-Hesperian-boundary-aged rocks and were exhumed by impacts. Tickbush, an Endeavour rim float rock, is an outlier of all super-clusters.

Marquette Island was found lying on top of the Meridiani sedimentary terrane, but the low Ni/Si content and lack of kamacite or troilite discourage a meteoritic origin (Mittlefehldt et al., 2010). The erratic is mafic in composition but does not seem to be part of an igneous sequence with the more basaltic Bounce Rock (Mittlefehldt et al., 2010). The texture in figure 2.7b is difficult to determine and may include highly reflective mm-size angular grains in a fine matrix, yet unlike a breccia the rock is well lithified (Mittlefehldt et al., 2010).The SI values of Tickbush indicated that its composition is dissimilar to most other compositions but weakly similar to the Copper Cliff composition average (SI = 56).

Three of the Matijevic targets (Sandcherry, Fecunis Lake, and Chelmsford 3) cluster apart from the other Matijevic rocks but this is likely due to the inclusion of a dark coating on the surface where the APXS integrated (Fig. 2.6b). The Matijevic veneer rock targets are located near the Azilda outcrop, but group in the Shoemaker super-cluster with and without SO_3 and Cl. The veneers are an alteration coating enriched in K, Ca, and mobile/volatile elements (S, Cl, Zn and Br), formed post-Endeavour impact along the Matijevic-Shoemaker boundary (Mittlefehldt et al., 2018), and likely contain Fe-smectite formed by reactions with mildly acidic water (Arvidson et al., 2014).

Table 2.7: Average compositions (on a S- and Cl- free basis, renormalized to 100%) of the Endeavour rim geologic formations, the Burns formation, and martian meteorite EETA 79001 B. Also included are calculated normative mineralogies expressed as (weight percent) quartz, plagioclase, orthopyroxene, clinopyroxene, and olivine, as established with a CIPW norm.

Oxide wt.%	Matijevic Average	Shoemaker Average	Grasberg Average	Burns Average	EETA[2] 79001 B	Bounce Rock Case
SiO_2	51.9	49.0	50.6	48.1	49.3	51.9
TiO_2	0.9	1.1	1.1	1.0	1.2	0.7
Al_2O_3	10.7	10.0	9.3	7.8	11.2	10.5
Cr_2O_3	0.3	0.2	0.3	0.2	0.2	0.1
FeO_T	17.0	19.4	21.6	20.8	17.4	14.5
MnO	0.3	0.5	0.2	0.4	0.4	0.4
MgO	8.6	8.5	5.7	10.6	6.6	6.9
CaO	6.3	6.8	6.7	6.9	10.8	12.2
Na_2O	2.5	2.6	2.5	2.1	1.7	1.7
K_2O	0.4	0.5	0.8	0.7	0.08	0.1
P_2O_5	1.0	1.3	1.2	1.4	1.3	0.9
SUM	**100**	**100**	**100**	**100**	**100**	**100**
CIPW Norm[1]						
Quartz	0	0	0	0	0.6	3.4
Plagioclase	38.0	36.2	32.9	27.6	37.2	35.1
Orthopyroxene	48.2	31.6	42.9	29.8	37.2	29.0
Clinopyroxene	6.6	9.4	11.6	12.8	19.1	28.5
Olivine	0.0	14.5	2.5	20.3	0	0
Others	7.2	8.4	10.0	9.6	5.8	4.2
SUM	**100**	**100**	**100**	**100**	**100**	**100**

[1]Normative mineralogy, weight percent; total Fe as FeO (FeO_T); "others" include orthoclase, ilmenite, chromite, and apatite; [2]Composition of EETA 79001 Lithology B from Lodders [1998], normalized to 100.0% on a S- and Cl-free basis.

2.4.3 Meridiani Rocks vs Martian Meteorites

Both the cluster analysis and the similarity index show the erratic, Bounce Rock, and the martian meteorite EETA 79001 B to be chemically distinct from the rest of the rocks investigated by Opportunity, while being similar to each other (SI: 14 with SO_3 and Cl removed). Both compositions (minus S and Cl) are slightly quartz normative whereas the average compositions range from having no quartz in the norm to being moderately olivine normative (Table 2.7). Also, in the norms of Bounce Rock and EETA 79001 B, clinopyroxene is significantly more abundant (19% and 29% respectively) compared to the other average

compositions (Matijevic, Grasberg, Shoemaker, and Burns formations, 7-13%). This difference between Bounce Rock and the rest of the surface rocks indicates that igneous rocks like Bounce Rock are not the primary protolith for the sedimentary rocks and Endeavour impact breccias.

From global remote sensing and in-situ rover observations, it has been shown that the martian meteorites do not adequately represent the bulk crust of Mars (e.g., (McSween Jr. et al., 2009). Comparing a suite of martian meteorites to a subset of the rocks analyzed by Opportunity, we find that most of the meteorites do not have compositions similar to the compositions of the sedimentary rocks and impact-breccias from Meridiani and Endeavour rim materials (Bouchard & Jolliff, 2016). Other than EETA 79001 lithology B pairing to Bounce Rock, the only other martian meteorite that groups with the surface rocks is NWA 7475/7034 (Wittmann et al., 2015).

NWA 7475 and 7034 are a recently identified set of paired martian meteorite regolith breccias (Agee et al., 2013; Cannon et al., 2015; Humayun et al., 2013). This new type of meteorite is more similar in bulk composition to the average surface of Mars than any of the other martian meteorites (Cannon et al., 2015; McSween Jr. et al., 2009). The Noachian southern highlands near-surface has been suggested as an origin for the regolith breccia NWA 7533, paired with 7034 (Agee et al., 2013; Beck et al., 2015). NWA 7034 has also been compared to orbital measurements of low albedo (dust poor) regions (Cannon et al., 2015), and igneous lithologies like those at Gusev crater (Udry et al., 2014). NWA 7475/7034 is the only martian meteorite examined in this study that clusters within Endeavour rim rock super-clusters. With SO_3 and Cl in the cluster analysis, NWA 7475/7034 groups with the basaltic erratic, Margaret Brush, and within the Shoemaker formation super-cluster.

Our study supports the interpretation that the polymict regolith breccia NWA 7475/7034 is a better chemical representation of martian surface materials than other classes of martian

meteorites. This meteorite has been proposed to be sourced from the Noachian southern highlands, but our study also highlights its similarity to a Meridiani Planum erratic rock and rocks of the Matijevic and Shoemaker formations of Endeavour crater (SI = 7 and 14 respectively). While such statistical similarity does not imply a petrogenetic link, it does suggest that Noachian-aged regions currently covered by younger terrains such as Meridiani Planum should not be ruled out as a source for such materials (Wittmann et al., 2015).

2.5 Conclusions

We have used a set of statistical approaches to examine potential relationships among rocks analyzed by the MER rover Opportunity, focusing on members that have been mapped according to four major geologic formations, the Burns formation sulfate sandstones of Meridiani Planum, the Shoemaker breccias on the remnant rim of Endeavour crater, the Grasberg formation, an onlapping unit between the Burns formation and Shoemaker breccias, and the Matijevic formation, which may represent pre-Endeavour crater deposits exposed in a window in one of the rim segments. Using well understood relationships among rocks analyzed by Opportunity, based on years of intensive study, we have validated these statistical approaches using a subset of Opportunity's data. The presence of dust and soil can impact the clustering algorithm, but the effect can be reduced by selecting visually “clean” targets and by comparing compositions after removing SO_3 and Cl, and renormalizing to 100%.

Some of the key results from our combined use of clustering analysis, quantitative similarity index, and imagery are as follows:

- The Burns formation contains compositional variation great enough to form two sub-clusters, loosely but not entirely related to soil contamination, and when SO_3 and Cl are removed

some Burns target compositions become very similar to the average Shoemaker formation composition.

- The clastic Grasberg formation is the most chemical homogenous of the Endeavour crater rim lithologies and (with and without SO_3 and Cl) is more similar to the impact breccia of the Shoemaker formation rocks than any other formation. The Grasberg formation likely incorporated eroded Endeavour rim material of the Shoemaker formation as clastic components. These similarities point to a local origin for the unit as opposed to a distal origin.

- The Copper Cliff breccia is the lowermost unit of the Shoemaker impact breccia. It is similar in texture to the Shoemaker formation but similarity in composition and the inclusion of spherules indicates that it contains eroded Matijevic material.

- The pre-impact Matijevic formation is chemically distinct from the other geologic formations at Endeavour crater but exhibits compositional similarities to the Marquette Island and Margaret Brush erratic rocks.

- Bounce Rock is similar to lithology B of the martian meteorite EETA 79001, and is chemically distinctive enough to have a different source from all of the other Endeavour rim and Meridiani Planum rocks investigated by Opportunity.

- The regolith breccia pair NWA 7475/7034 is the only martian meteorite considered in this study other than EETA 79001 B to have a bulk composition that is highly similar to any of the late Noachian and early Hesperian martian materials investigated by Opportunity. Specifically, its composition is similar to the average compositions of the Matijevic and Shoemaker formation rocks, and some of the erratic rocks, which supports the interpretation that this new type of martian meteorite is composed of martian surface materials. The statistical similarity between rocks excavated by Endeavour crater and this meteorite pair does not

necessarily indicate that this region of Mars is the source for these meteorites, but it does suggest that Noachian regions in the northern hemisphere that are thinly mantled by younger terrains should not be ruled out as possible source regions.

This statistical grouping model can be extended to more recent Opportunity data as well as other rovers with similar APXS compositional data sets (Bouchard & Jolliff, 2018; Bouchard, et al., 2017) as well as to bulk-rock compositional data from martian meteorites (Bouchard & Jolliff, 2016). This two-pronged model can also be used to quickly classify future targets, find best matches, identify potential protoliths, assess potential groupings with previously mapped units, and to quantitatively demonstrate the uniqueness of new targets.

Acknowledgements

We thank the MER team (Jet Propulsion Laboratory and participating institutions) for their daily hard work to make the MER mission possible, the APXS, Pancam, and MI teams for the data sets utilized in this study, and NASA for supporting the MER extended mission. The data used are listed in the tables and references, and we are especially grateful to Dr. Ralph Gellert for the provision of processed APXS data to the Planetary Data System. We would also like to thank Cindy Traub PhD, for her consultation on multivariate statistics and R programming. Support for a portion of this work was from JPL subcontract JPL1536058 to B. Jolliff, and NASA Earth and Space Science Fellowship grant number 80NSSC17K0490 to M. Bouchard.

2.6 References

Adcock, C. T., Udry, A., Hausrath, E. M., & Tschauner, O. (2018). Craters of the Moon National Monument basalts as unshocked compositional and weathering analogs for martian rocks and meteorites. American Mineralogist, 103, 502-516. doi:10.2138/am-2018-6193

Agee, C. B., Wilson, N. V., McCubbin, F. M., Ziegler, K., Polyak, V. J., Sharp, Z. D., . . . Elardo, S. M. (2013). Unique meteorite from early Amazonian Mars: Water-rich basaltic breccia Northwest Africa 7034. Science, 339(6121).

Arvidson, R. E., et al., (2011). Opportunity Mars Rover mission: Overview and selected results from Purgatory ripple to traverses to Endeavour crater. Journal of Geophysical Research, 116, E00F15. doi:10.1029/2010JE003746

Arvidson, R. E., Anderson, R. C., Bartlett, P., III, J. F. B., Christensen, P. R., Chu, P., . . . Wilson, J. (2004). Localization and Physical Property Experiments Conducted by Opportunity at Meridiani Planum Science, 306(5702), 1730-1733.

Arvidson, R. E., Anderson, R. C., Haldemann, A. F. C., Landis, G. A., Li, R., Lindemann, R. A., . . . Snider, N. O. (2003). Physical properties and localization investigations associated with the 2003 Mars Exploration rovers. Journal of Geophysical Research, 108(E12). doi:10.1029/2002JE002041

Arvidson, R. E., Bell III, J. F., Bellutta, P., Cabrol, N. A., Catalano, J. G., Cohen, J., . . . Yen, A. S. (2010). Spirit Mars Rover Mission: Overview and selected results from the northern Home Plate Winter Haven to the side of Scamander crater. Journal of Geophysical Research: Planets, 115(E00F03).

Arvidson, R. E., Poulet, F., Morris, R. V., Bibring, J. P., Bell III, J. F., Squyres, S. W., . . . Wolff, M. (2006). Nature and origin of the hematite-bearing plains of Terra Meridiani based on analyses of orbital and Mars Exploration rover data sets. Journal of Geophysical Research: Planets, 111(E12S08).

Arvidson, R. E., Ruff, S. W., Morris, R. V., Ming, D. W., Crumpler, L. S., Yen, A. S., . . . McLennan, S. M. (2008). Spirit Mars Rover Mission to the Columbia Hills, Gusev Crater: Mission overview and selected results from the Cumberland Ridge to Home Plate. Journal of Geophysical Research, 113, E12S33. doi:10.1029/2008JE003183

Arvidson, R. E., Squyres, S. W., Anderson, R. C., Bell, J. F., III, Blaney, D., Brückner, J., . . . Yen, A. (2006). Overview of the Spirit Mars Exploration Rover Mission to Gusev Crater: Landing site to Backstay Rock in the Columbia Hills. Journal of Geophysical Research, 111(E2), 22. doi:10.1029/2005JE002499

Arvidson, R. E., Squyres, S. W., Bell III, J. F., Catalano, J. G., Clark, B. C., Crumpler, L. S., . . . Wolff, M. J. (2014). Ancient aqueous environments at Endeavour crater, Mars. Science, 343, 441-448. doi:DOI: 10.1126/science.1248097

Arvidson, R. E., Squyres, S. W., & Team, A. S. (2017). Recent results from the Opportunity rover's exploration of Endeavour crater, Mars. Lunar and Planetary Science Conference, 48, #1149.

Beck, P., Pommerol, A., Zanda, B., Remusat, L., Göpel, C., Hewins, R., . . . Chevrier, V. F. (2015). A Noachian source region for the "Black Beauty" meteorite, and a source lithology for Mars surface hydrated dust? . Earth and Planetary Science Letters, 427, 104-111. doi:10.1016/j.epsl.2015.06.033

Bibring, J.-P., Langevin, Y., Mustard, J. F., Poulet, F., Arvidson, R., Gendrin, A., . . . Omega Team, T. (2006). Global Mineralogical and Aqueous Mars History Derived from OMEGA/Mars Express Data. Science, 312(5772), 400-404.

Bouchard, M. C., & Jolliff, B. L. (2016). Comparing MER Opportunity rock groups and martian meteorites using hierarchical clustering and a similarity index. Lunar and Planetary Science Conference, 47, #2551.

Bouchard, M. C., & Jolliff, B. L. (2018). Rock suites of Endeavour crater, Mars: comparing Perseverance Valley to the floor of Spirit of St. Louis Crater. Lunar and Planetary Science Conference, 49, 2590.

Bouchard, M. C., Jolliff, B. L., Farrand, W. H., & Mittlefehldt, D. W. (2017). Constraining the origin of basaltic volcanic rocks by Opportunity along the rim of Endeavour crater. Lunar and Planetary Science Conference, 48, #1608.

Cannon, K. M., Mustard, J. F., & Agee, C. B. (2015). Evidence for a widespread basaltic breccia component in the martian low-albedo regions from the reflectance spectrum of Northwest Africa 7034. Icarus, 252, 150-153. doi:10.1016/j.icarus.2015.01.016

Clark, B. C., McLennan, S. M., Morris, R. V., Gellert, R., Jolliff, B. L., Knoll, A. H., . . . Squyres, S. W. (2005). Results and implications of mineralogical models for chemical sediments at Meridiani Planum. Lunar Planetary Science Coneference, 36, #1446.

Clark, B. C., Morris, R. V., McLennan, S. M., Gellert, R., Jolliff, B., Knoll, A., . . . Rieder, R. (2005). Chemistry and mineralogy of outcrops at Meridiani Planum. Earth and Planetary Science Letters, 240, 73-94.

Crumpler, L. S., Arvidson, R. E., Bell, J., Clark, B. C., Cohen, B. A., Farrand, W. H., . . . Yen, A. S. (2015). Context of ancient aqueous environments on Mars from in situ geologic mapping at Endeavour Crater. Journal of Geophysical Research: Planets, 120, 538-569. doi:10.1002/2014JE004699

Farrand, W. H., Bell III, J. F., Johnson, J. R., Rice, M. S., Jolliff, B. L., & Arvidson, R. E. (2014). Observations of rock spectral classes by the Oppotunity rover's Pancam on nothern Cape York and on Matijevic Hill, Endeavour Crater, Mars. Journal of Geophysical Research: Planets, 119, 2349-2369. doi:10.1002/2014JE004641

Fleischer, I., Brückner, J., Schröder, C., Farrand, W., Tréguier, E., Morris, R. V., . . . Cohen, B. A. (2010). Mineralogy and chemistry of cobbles at Meridiani Planum, Mars, investigated

by the Mars Exploration Rover Opportunity. Journal of Geophysical Research: Planets, 115(E7). doi:10.1029/2010JE003621

Fox, V. K., Arvidson, R. E., Guinness, E. A., McLennan, S. M., Catalano, J. G., Murchie, S. L., & Powell, K. E. (2016). Smectite deposits in Marathon Valley, Endeavour Crater, Mars, identified using CRISM hyperspectral reflectance data. Geophysical Research Letters, 43(10), 4885-4892. doi:10.1002/2016gl069108

Gasnault, O., Taylor, G. J., Karunatillake, S., Dohm, J., Newsom, H., Forni, O., . . . Boynton, W. V. (2010). Quantitative geochemical mapping of martian elemental provinces. Icarus, 207, 226-247. doi:10.1016/i.icarus.2009.11.010

Gellert, R., Rieder, R., Brückner, J., Clark, B. C., Dreibus, G., Klingelhöfer, G., . . . Squyres, S. W. (2006). Alpha Particle X-Ray Spectrometer (APXS): Results from Gusev crater and calibration report. Journal of Geophysical Research: Planets, 111(E02S05), 1-32. doi:10.1029/2005JE002555

Grotzinger, J. P., Arvidson, R. E., Bell III, J. F., Calvin, W., Clark, B. C., Fike, D. A., . . . Watters, W. A. (2005). Stratigraphy and sedimentology of a dry to wet eolian depositional system, Burns formation, Meridiani Planum, Mars. Earth and Planetary Science Letters, 240, 11-72.

Humayun, M., Nemchin, A., Zanda, B., Hewins, R. H., Grange, M., Kennedy, A., . . . Deldicque, D. (2013). Origin and age of the earliest Martian crust from meteorite NWA 7533. Nature, 503.

Knoll, A. H., Jolliff B. L., Farrand W. H., Bell III J. F., Clark, B. C., Gellert R, . . . Learner Z. (2008). Veneers, rinds, and fracture fills: Relatively late alteration of sedimentary rocks at Meridiani Planum, Mars, J. Geophys. Res., 113, E06S16, . Journal of Geophysical Research, 113, E06S16. doi:doi:10.1029/2007JE002949

Korotev, R. L., Haskin, L. A., & Jolliff, B. L. (1995). A simulated geochemical rover mission to the Taurus-Littrow valley of the Moon. Journal of Geophysical Research: Planets, 100(E7), 14,403-414,420.

Larsen, K., Arvidson, R. E., Jolliff, B. L., & Clark, B. E. (2000). Correspondence and least squares analyses of soil and rock compositions for the Viking Lander 1 and Pathfinder landing sites. Journal of Geophysical Research, 105(E12), 29207-29221.

Lodders, K. (1998). A survey of shergottite, nakhlite, and chassigny meteorites whole-rock compositions. Meteoritics & Planetary Science, 33, A183-190.

McLennan, S. M., Bell, J. F., III, Calvin, W. M., Christensen, P. R., Clark, B. C., de Souza, P. A., . . . Yen, A. (2005). Provenance and diagenesis of the evaporite-bearing Burns formation, Meridiani Planum, Mars. Earth and Planetary Science Letters, 240, 95-121.

McSween Jr., H. Y., & Treiman, A. H. (1998). Martian Meteorites (Chapter 6). In J. J. Papike (Ed.), Planetary Materials, (Vol. Vol. 36, pp. 6-1-6-53): Mineralogical Society of America.

McSween Jr., H. Y., Taylor, G. J., & Wyatt, M. B. (2009). Elemental Composition of the Martian Crust. Science, 324(736), 736-739. doi:10.1126/science.1165871

Milligan, G. W., & Cooper, M. C. (1988). A study of standardization of variables in cluster analysis. Journal of Classification, 5, 181-204.

Mittlefehldt, D. W., Gellert, R., Herkenhoff, K. E., Morris, R. V., Clark, B. C., Cohen, B. A., . . . Team, t. A. S. (2010). Marquette Island: a distinct mafic lithology discovered by Opportunity. Lunar and Planetary Science Conference, 41, #2109.

Mittlefehldt, D. W., Gellert, R., VanBommel, S. J., Ming, D. W., Yen, A. S., Clark, B. C., . . . Rice, J. W. (2018). Diverse Lithologies and Alteration Events on the Rim of Noachian-Aged Endeavour Crater, Meridiani Planum, Mars: In-Situ Compositional Evidence. Journal of Geophysical Research: Planets(123). doi:10.1002/2017JE005474

Rieder, R., Gellert, R., Anderson, R. C., Brückner, J., Clark, B. C., Dreibus, G., . . . Zipfel, J. (2004). Chemistry of Rocks and Soils at Meridiani Planum from the Alpha Particle X-ray Spectrometer Science, 306(5702), 1746-1749.

Squyres, S. W., Arvidson, R. E., Baumgartner, E. T., Bell, J. F., III, Christensen, P. R., Gorevan, S., . . . Romero, R. A. (2003). Athena Mars rover science investigation. Journal of Geophysical Research, 108(E12). doi:10.1029/2003JE002121

Squyres, S. W., Arvidson, R. E., Bell III, J. F., Clef III, F., Clark, B. C., Cohen, B. A., . . . Zacny, K. (2012). Ancient Impact and Aqueous Processes at Endeavour Crater, Mars. Science, 336, 570-576. doi:10.1126/science.1220476

Squyres, S. W., Arvidson, R. E., Bell, J. F. I., Brückner, J., Cabrol, N. A., Calvin, W., . . . Yen, A. (2004). The Spirit rover's Athena science investigation at Gusev Crater, Mars. Science, 305, 794-799.

Squyres, S. W., & Knoll, A. H. (2005). Sedimentary rocks at Meridiani Planum: Origin, diagenesis, and implications for life on Mars. Earth and Planetary Science Letters, 240(1), 1-10.

Squyres, S. W. A., R. E., Bell III, J. F., Brückner, J., Cabrol, N. A., Calvin, W., Carr, M. H., . . . Yen, A. (2004). The Opportunity Rover's Athena Science Investigation at Meridiani Planum, Mars Science, 306(5702), 1698-1703.

Stein, N. T., Arvidson, R. E., O'Sullivan, J. A., Catalano, J. G., Guinness, E. A., Politte, D. V., . . . VanBommel, S. J. (2018). Retrieval of Compositional End-Members From Mars Exploration Rover Opportunity Observations in a Soil-Filled Fracture in Marathon Valley, Endeavour Crater Rim. Journal of Geophysical Research: Planets, 123(1), 278-290. doi:10.1002/2017JE005339

Udry, A., Lunning, N. G., McSween, H. Y., & Bodnar, R. J. (2014). Petrogenesis of a vitrophyre in the martian meteorite breccia NWA 7034. Geochimica et Cosmochimica Acta, 141, 281-293. doi:10.1016/j.gca.2014.06.026

VanBommel, S. J., Gellert, R., Berger, J. A., Campbell, J. L., Thompson, L. M., Edgett, K. S., . . . Boyd, N. I. (2016). Deconvolution of distinct lithology chemistry through oversampling with the Mars Science Laboratory Alpha Particle X-Ray Spectrometer. X-Ray Spectrometry, 45(3), 155-161. doi:10.1002/xrs.2681

VanBommel, S. J., Gellert, R., Berger, J. A., Thompson, L. M., Edgett, K. S., McBride, M. J., . . . Campbell, J. L. (2017). Modeling and mitigation of sample relief effects applied to chemistry measurements by the Mars Science Laboratory Alpha Particle X-ray Spectrometer. X-Ray Spectrometry, 46(4), 229-236. doi:10.1002/xrs.2755

Wittmann, A., Korotev, R. L., Jolliff, B. L., Irving, A. J., Moser, D. E., Barker, I., & Rumble III, D. (2015). Petrography and composition of Martian regolith breccia meteorite Northwest Africa 7475. The Meteoritical Society, 50(2), 326-352.

Xu, R., & Wunsch II, D. C. (2009). Clustering: Institute of Electrical and Electronics Engineers.

Yen, A. S., Gellert, R., Schröder, C., Morris, R. V., Bell, J. F., III, Knudson, A. T., . . . Zipfel, J. (2005). An integrated view of the chemistry and mineralogy of martian soils Nature, 436, 49-54.

Yen, A. S., Mittlefehldt, D. W., McLennan, S. M., Gellert, R., Bell, J. F. I., McSween, H. Y., . . . Squyres, S. W. (2006). Nickel on Mars: Constraints on meteoritic material at the surface. Journal of Geophysical Research, 111, E12S11. doi:doi:10.1029/2006JE002797

Zipfel, J., Schröder, C., Jollif, B. L., Gellert, R., Herkenhoff, K. E., Rieder, R., . . . Yen, A. S. (2011). Bounce Rock—A shergottite-like basalt encountered at Meridiani Planum, Mars. Meteoritics & Planetary Science, 46(Nr 1), 1–20. doi:10.1111/j.1945-5100.2010.01127.

Chapter 3: Rock Suites of Endeavour Crater, Mars: Comparing Perseverance Valley, Spirit of St. Louis, and Marathon Valley

Abstract

Perseverance Valley is an erosional feature with the appearance of an eroded gully, located in the western wall of the Noachian aged Endeavour crater in Meridiani Planum, Mars. It is the most lithologically diverse location investigated by the Opportunity rover other than Cape York, where the rover first characterized the pre-, post-, and syn-depositional lithologies of Endeavour crater. We use hierarchical clustering and a similarity index combined with examination of Panoramic camera and Microscopic Imager images to classify these rock suites in Perseverance Valley, and contextualize them with comparison to rocks examined previously along the rim of Endeavour crater. The Perseverance Valley lithologies are classified into four rock suites, a clast-poor impact breccia that forms the "walls" of the valley, a competent basaltic outcrop of rocks that appear "blue" in false color Panoramic camera imagery, an outcrop of pitted rocks that has among the highest silica concentrations investigated by Opportunity, and a loose regolith mixture of martian soil, impact breccia, and local "blue" rocks that makes up the valley floor. Macro and micro textures indicate that the valley is currently being eroded by wind exiting the crater basin from west to east. Units that are offset both within and across Perseverance Valley indicate that the valley location and structure is likely influenced by a

system of radial impact faults. Lithologies such as the collocated “blue” and silica-rich pitted rocks, and observations of aqueous alteration such as “red” zones, show similarities between Perseverance Valley and both Marathon Valley and the Spirit of St. Louis feature. We explore multiple working hypotheses to explain the formation mechanisms of Perseverance Valley, but can now say: the valley is likely structurally controlled including an ~80 meter vertical offset by a graben; the valley hosted local aqueous alteration; the floor material of valley consists of mass-wasted local materials; and the current topographic expression was overprinted by modern aeolian erosion.

3.1 Introduction

The Mars Exploration Rover (MER) Opportunity (Arvidson et al., 2004; Arvidson et al., 2003; Squyres et al., 2003; Squyres et al., 2004) began the first exoplanetary traverse of a complex impact crater rim (Crumpler et al., 2015) when it arrived at Endeavour crater in August of 2011 (sol 2681) (Arvidson et al., 2014; Squyres et al., 2012) (Fig. 3.1). Endeavour crater is a 22km diameter, Noachian-aged impact structure in Meridiani Planum (Grant et al., 2016; Hynek, Arvidson, & Phillips, 2002; Squyres et al., 2012). Craters are the road cuts of planetary science, and Endeavour crater is older than the late-Noachian to early-Hesperian sulfate-sandstone Burns formation that dominates Meridiani and represents the Noachian basement rocks (Clark et al., 2005; Grotzinger et al., 2005; McLennan et al., 2005; Squyres & Knoll, 2005). The Endeavour crater rim materials have been characterized in detail in other works and include the impact breccia of the Shoemaker formation that makes up the bulk of the remnant crater rim, the pre-impact Matijevic formation, and the post-impact clastic Grasberg formation, all of which were first identified at Cape York (Crumpler et al., 2015; Mittlefehldt, Gellert, et al., 2018; Squyres et

al., 2012). The crater rim is heavily degraded (Grant et al., 2016; Hughes, Arvidson, Grant, Purdy, & Howard, 2018) and younger morphologic features such as Perseverance Valley (section 1.1), Marathon Valley (section 1.2), and the Spirit of St. Louis feature (section 1.2) overprint the remnant crater rim.

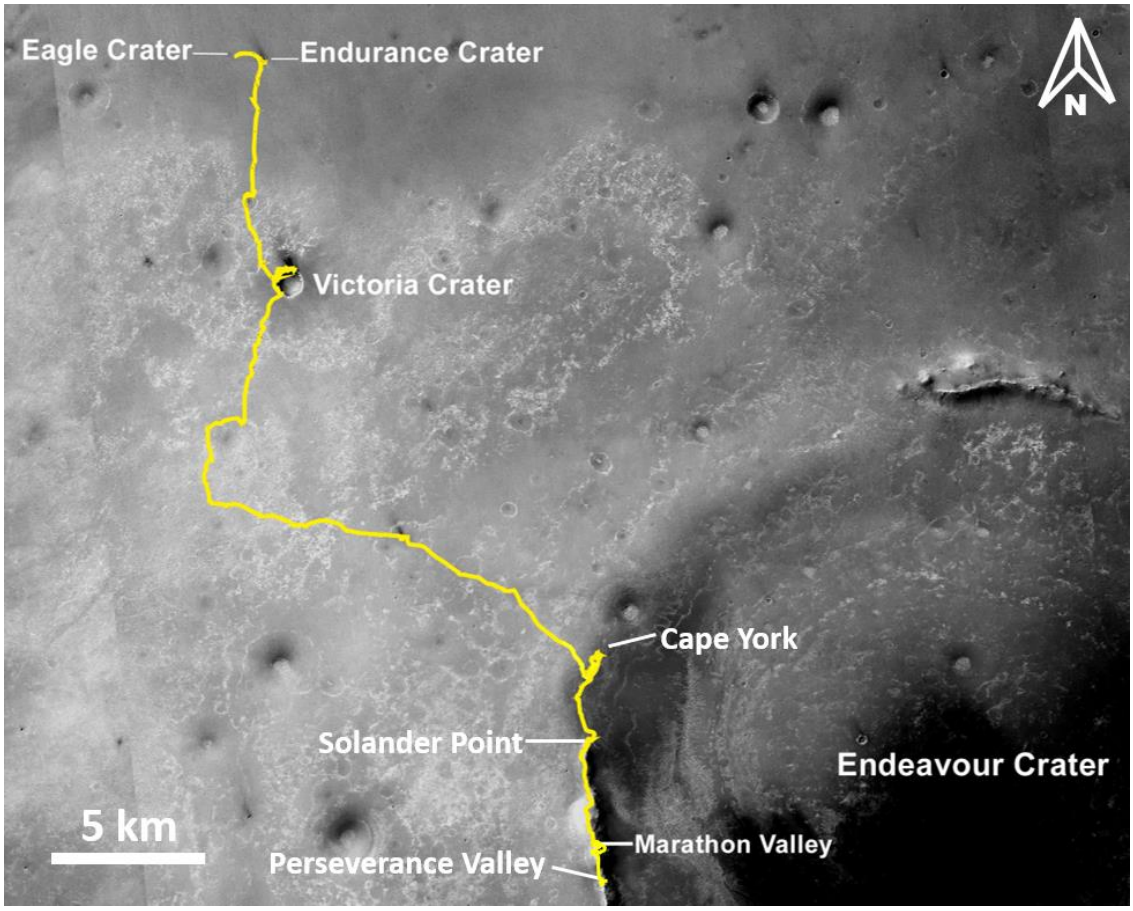

Figure 3.1 The Opportunity rover traverse (yellow) from landing in Eagle Crater to the exploration of the rim of Endeavour Crater. Exploration of the crater rim lithologies began at Cape York and continued along remnant rim segments such as those exposed at Solander point. Opportunity descended into both Marathon and Perseverance Valleys, features that cut across the crater rim. The rover traverse is plotted on a CTX image from the Mars Reconnaissance Orbiter, and Endeavour crater is ~22 km in diameter. Modified from: NASA/JPL-Caltech/MSSS/NMMNHS.

3.1.1 Perseverance Valley

About sol 4730 Opportunity began its campaign to explore Perseverance Valley (Fig. 3.1) (Bouchard, Jollif, & Farrand, 2019; Bouchard & Jolliff, 2018a; Crumpler, Arvidson, Farrand, Grant, & Mittlefehldt, 2018; Crumpler & Team, 2018; Farrand et al., 2019; Mittlefehldt, Crumpler, Grant, Arvidson, & Farrand, 2018; Parker & Golombek, 2018; Squyres et al., 2018; Sullivan et al., 2019; Sullivan, Golombek, Herkenhoff, & Team, 2018; Tait et al., 2019). Perseverance Valley is a 250-meter long and 30-meter wide valley that cuts west to east across the remnant rim of Endeavour crater at a slope of ~18°. The valley is younger than Endeavour crater according to superposition, but is thought to be the present-day erosional manifestation of an ancient feature. Much of the Endeavour crater rim degradation likely preceded deposition of the Burns formation (Grant et al., 2016) when fluvial processes were still active. Thus, it is possible that ancient fluvial activity or some other manifestation of aqueous alteration played a role in the formation of Marathon and Perseverance Valleys. A more specific age cannot be assigned using crater counting methods owing to the small total surface area (~7.5 km^2) and the valley's occurrence on a slope, which intensifies aeolian erosion and mass wasting degradation of smaller craters. Perseverance Valley was targeted for in-situ exploration based on orbital HiRISE imagery such as figure 3.2, in which it appears to show an anastomosing gully-like feature.

Hypotheses for the valley's formation include: 1) wind abrasion, 2a) flowing water from a catchment basin outside the Endeavour crater rim, or 2b) another water source such as ground water swell, 3) mass wasting along radial crater fractures, or some combination of these mechanisms (Bouchard & Jolliff, 2018a; Crumpler & Team, 2018; Parker & Golombek, 2018; Squyres et al., 2018; Sullivan et al., 2018). The Microscopic Imager (MI) and Panoramic Camera (Pancam) show evidence of modern wind erosion, see figures 3.10 and 3.12, wind tails and

scouring from wind moving in an up-valley direction (east to west), indicating that eolian process are currently active in valley erosion (Squyres et al., 2018; Sullivan et al., 2018).

Because Perseverance Valley contains the highest diversity of new lithologies encountered by Opportunity since the rover left Cape York, this work characterizes these rock suites and contextualizes them by comparisons to rocks previously observed along the rim of Endeavour crater (Bouchard et al., 2019).

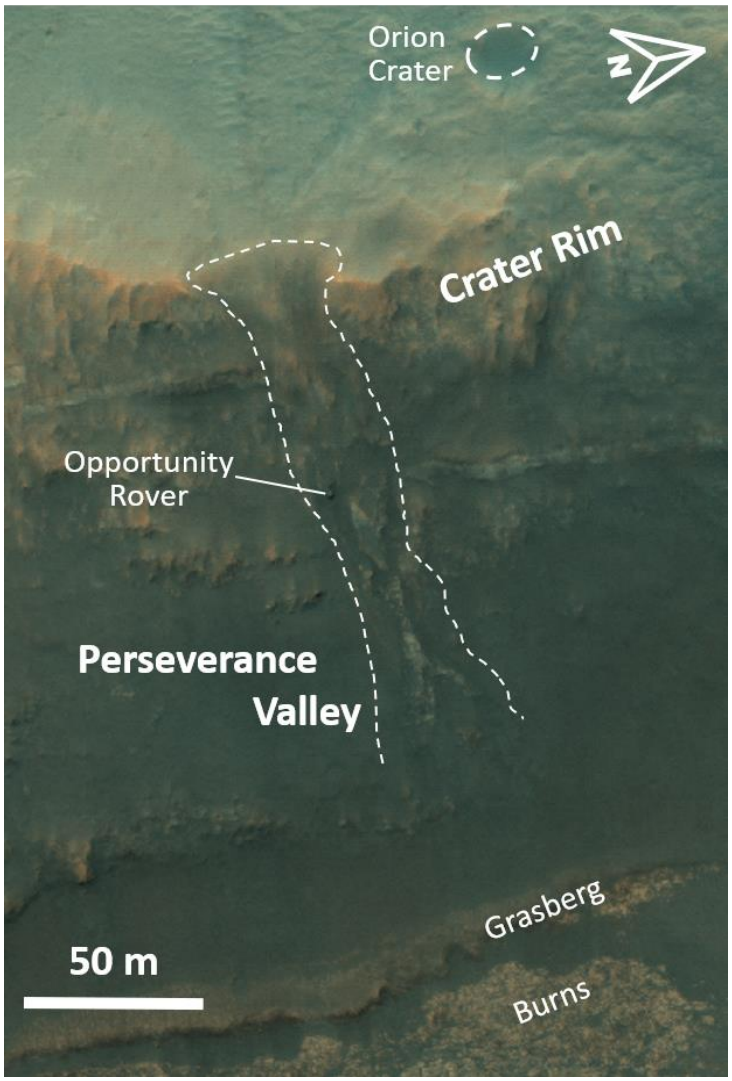

Figure 3.2 HiRise (Mars Reconnaissance Orbiter) image of Perseverance Valley (ESP_058208_1775_RGBcolor, NASA/JPL/University of Arizona). The top of the image is West and the outer rim of the crater, and the valley cuts towards the East, descending into the crater at a slope of ~18 degrees to the benches that may represent the Grasberg and Burns formations inside of the crater. The Ysleta Del Sur location (Figure 3.14) is the trough "nose" just east of the Opportunity rover.

3.1.2 Spirit of St. Louis & Marathon Valley

On ~sol 3973 Opportunity encountered the Spirit of St. Louis feature (Arvidson, Squyres, & Team, 2017; Bouchard, Jolliff, Farrand, & Mittlefehldt, 2017; Farrand, Johnson, Bell, & Mittlefehldt, 2016; Mittlefehldt, Gellert, VanBommel, Arvidson, Clark, Ming, et al., 2016). The Spirit of St. Louis (SoSL) feature is a 25-35 m ovoid surface feature situated near the entrance of Marathon Valley that is readily observed in HiRISE images such as figure 3.3 by a darker tone, clear elliptical shape, and a small mound of "blue" (bluish color in the Pancam L257 false color scheme, (Bell et al., 2003; Bell et al., 2006) rock at one end (Bouchard et al., 2017; Mittlefehldt, Gellert, VanBommel, Arvidson, Clark, Ming, et al., 2016).

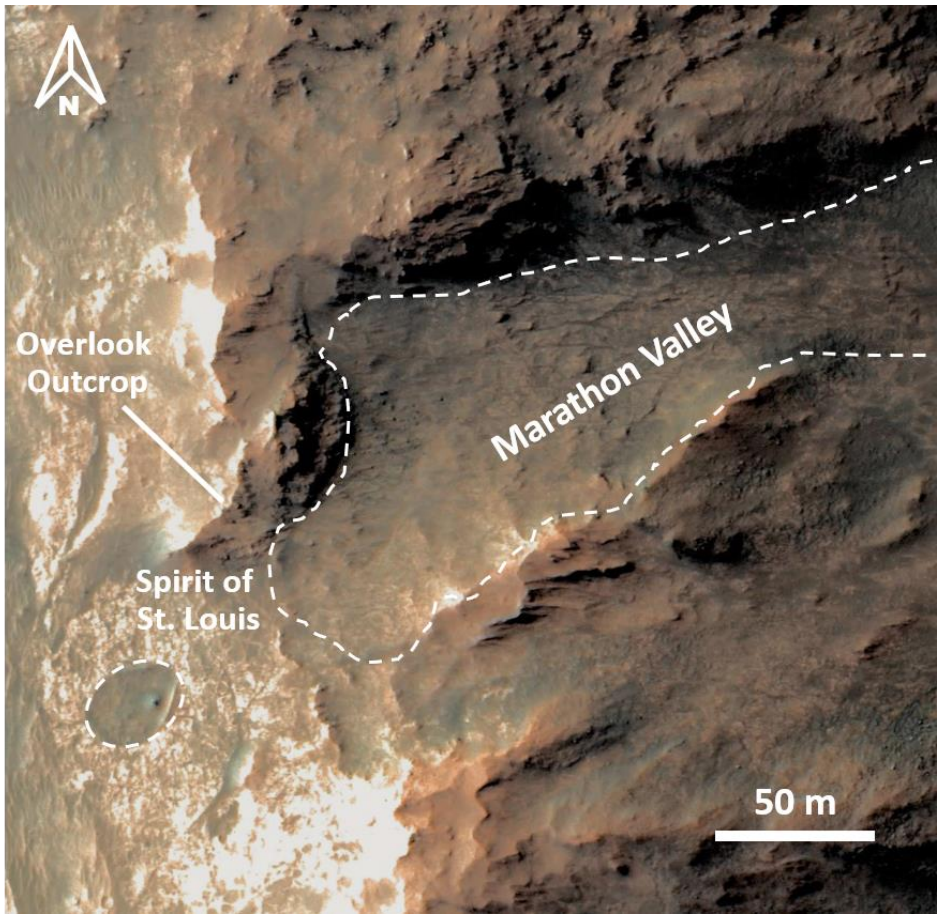

Figure 3.3 HiRise image (Mars Reconnaissance Orbiter) of Opportunity's traverse (yellow) approaching and into Marathon Valley. The top of the image is North, and Marathon Valley cuts West to East across the crater rim. The Spirit of St. Louis feature (25x35 meters in diameter) is visible at the entrance of Marathon Valley, as is rim overlooking the valley entrance where the "blue" and "purple" rock outcrops in Figure 3.6 were investigated.

SoSL has been eroded down to the level of local topography of the entrance of Marathon Valley (Fig. 3.4), and is rimmed by a "red" zone, so named for its appearance in Pancam false color L257 imagery (Bell et al., 2006; Bell et al., 2003) (Fig. 3.5b). These "red" zones have ferric oxide minerals and possible hydration signatures in Pancam spectra that are consistent with aqueous alteration (Farrand et al., 2016). The composition of the loose interior material of SoSL is broadly similar to the surrounding breccia, but the 3-meter-tall rock mound at the eastern end, named Lindberg mound, consists of rocks of basaltic composition. Notably, the APXS detected elevated concentrations of Ge around SoSL (Mittlefehldt, Gellert, VanBommel, Arvidson, Clark, Cohen, et al., 2016; Mittlefehldt, Gellert, VanBommel, Arvidson, Clark, Ming, et al., 2016). Hypotheses for the formation of SoSL include (1) it represents the base of a crater, possibly formed as a secondary impact, that has been eroded down to the level of local topography, removing all crater rim morphologies; (2) a volcanic pipe surrounded by an alteration halo, or (3) an impact-induced hydrothermal pipe (Bouchard et al., 2017). Each hypothesis rests on a different interpretation of the "blue rocks" of Lindberg mound. If the blue rocks are impact melt rocks, then SoSL is likely a small eroded crater basin, but if the "blue" rocks are in fact basaltic, then SoSL is likely an eroded volcanic pipe where the resistant basaltic rocks stand in relief and the original Endeavour rim rocks that were intruded have eroded to the same level as surrounding rocks.

Marathon Valley is another gully-like feature that cuts west to east through the remnant Endeavour crater rim and was targeted for investigation by the Opportunity rover after detections of smectite were made with the CRISM instrument onboard the Mars Reconnaissance Orbiter (Fox et al., 2016). Evidence in Marathon Valley for aqueous alteration include: the source of the CRISM smectite signature found along valley fractures, pebbles enriched in Al and Si by

leaching, ferric oxides and evaporative sulfate salts, and ubiquitous gypsum veins across the lower crater rim materials (Arvidson, Squyres, Gellert, & Team, 2015; Arvidson et al., 2017; Fraeman, 2018; Mittlefehldt, Gellert, VanBommel, Arvidson, Clark, Cohen, et al., 2016; Mittlefehldt, Gellert, VanBommel, Arvidson, Clark, Ming, et al., 2016; Stein et al., 2018).

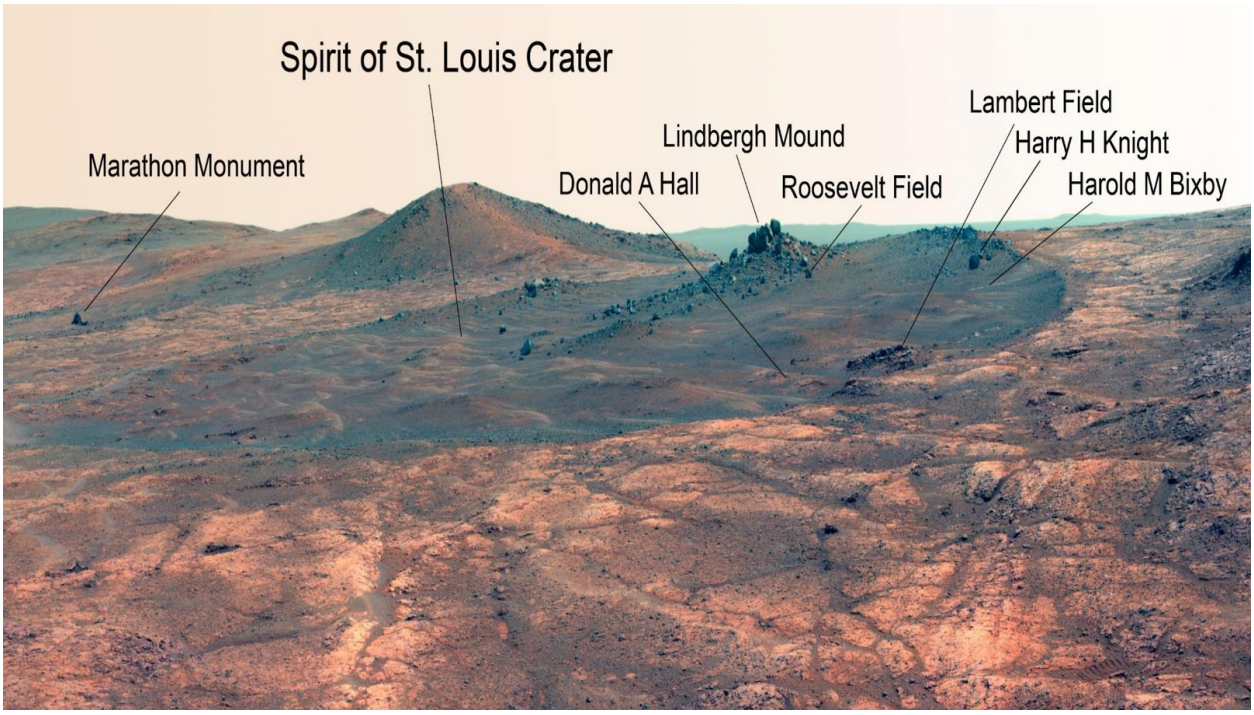

Figure 3.4: A false color Pancam image taken by Opportunity looking South at the Spirit of St. Louis feature. The oval feature is 25x35 meters across, and the Lindberg Mound of blue rocks within the feature was sampled with the APXS at the target Roosevelt Field. Opportunity analyzed "bedrock" at the Donald A. Hall, Lambert Field, and Harold M. Bixby locations with the APXS. Figure 3.5b was taken along the rim of this feature. Image credits: NASA/JPL-Caltech/Cornell Univ./Arizona State Univ (Bell 2003, 2006).

3.1.3 Pre-Endeavour Impact Lithology

The Matijevic formation was identified in a window through the Shoemaker formation at Cape York (Crumpler et al., 2015). It is a clastic, soft rock with a generally basaltic composition, with some locations that contain concretions (Arvidson et al., 2014). The Matijevic formation has been determined to be a pre-Endeavour-impact lithology (Crumpler et al., 2015). Similarities in composition and the inclusion of spherules in the lowest member of the Shoemaker formation, the Copper Cliffs breccia, have been interpreted as the inclusion of Matijevic material in this

portion of the Shoemaker breccia (Bouchard & Jolliff, 2018b; Mittlefehldt, Gellert, et al., 2018). The Matijevic formation is also similar in bulk composition to the basaltic erratic Marquette Island (Bouchard & Jolliff, 2018b). Cape York is the only location were the Matijevic formation has been identified to date.

Figure 3.5 Comparable "red zones" in false color Pancam imager. 4a is the red zone that rims the Spirit of St. Louis feature and was analyzed at the Pvt. William Bratton APXS target location. This red zone has elevated silica and is an alteration rind. 4b is an image taken of the red zone along the Tao fracture in Perseverance Valley which is juxtaposed to similarly trending trace of "blue" rubble. Image credits: D. Savransky and J. Bell/JPL/NASA/Cornell/ASU (Bell 2003, 2006).

3.1.4 Occurrence of "Blue" Rocks

Throughout its traverse through Meridiani Planum and along Endeavour crater, Opportunity encountered rocks that appear "blue" in false color L257 Pancam imagery, see figure 3.6. Alpha Particle X-Ray Spectrometer (APXS) measurements of several of these "blue" rocks show a broadly basaltic and tholeiitic composition (Fig. 3.7) (Bouchard et al., 2017; McSween Jr., Taylor, & Wyatt, 2009). Prior to arriving at Endeavour crater these "blue" rocks were observed as erratics of uncertain origin, such as the basalt, Marquette Island (sols 2070-2120), (Fleischer et al., 2010; Mittlefehldt et al., 2010) (Fig. 3.6b).

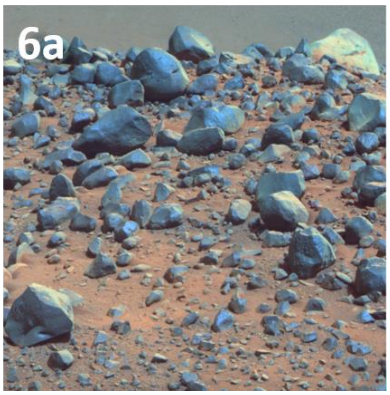
6a

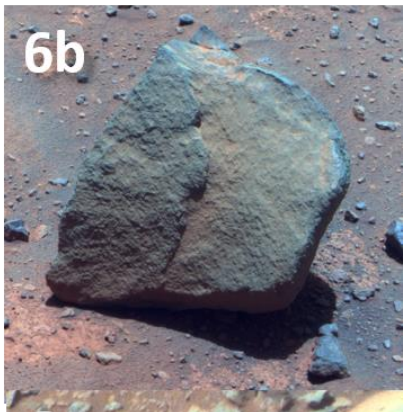
6b


6e

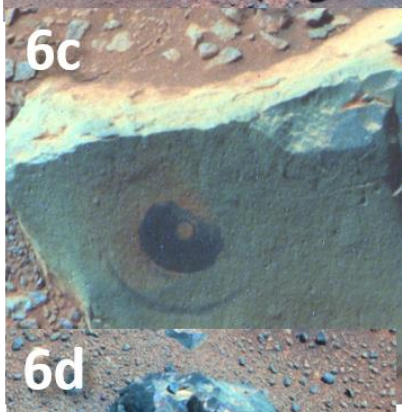
6c


6f


6d

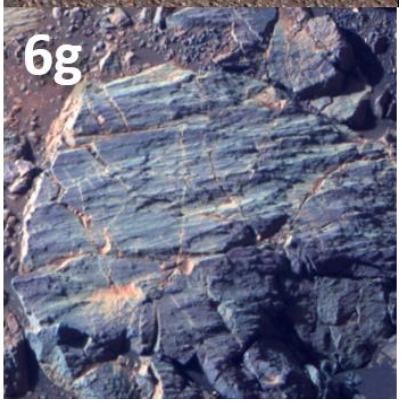
6g

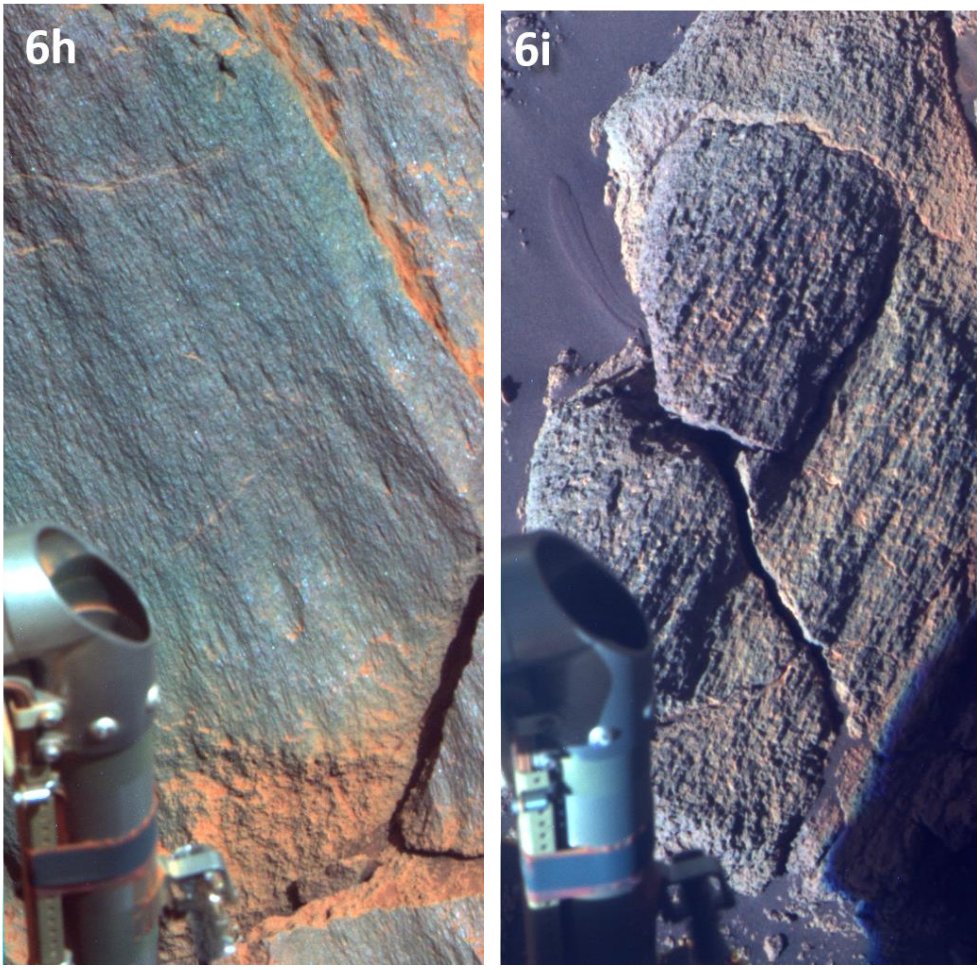

Figure 3.6 False color Pancam images of the crystalline, basaltic, "blue" rocks of Endeavour crater and Meridiani Planum. (6a) Spirit Mound, a collection of blue rock cobbles and boulders collected inside of Endeavour crater. (6b) Marquette Island, an erratic float rock found out on Burns plains of Meridiani Planum. (6c) Margaret Brush, a blue rock analyzed near Wdowiak Ridge. (6d) Roosevelt Field, the blue rock from Lindberg Mound within the Spirit of St. Louis feature. (6e-f) are the APXS targets Inde and La Joya, the tabular "blue" rocks of the linear outcrop of in Perseverance Valley. (6g) Nueva Vizcaya, another "blue" rock outcrop within Perseverance Valley. (6h) Sergeant Charles Floyd, the APXS target of the "blue" rock out crop sampled on the rim overlooking the entrance to Marathon Valley (Figure 3.8). (6i) Jornada Del Muerto, the APXS target on San Miguel, the type outcrop of "blue" rocks within Perseverance Valley. Image credits: D. Savransky and J. Bell/JPL/NASA/Cornell/ASU (Bell 2003, 2006).

Along the Endeavour crater rim the Shoemaker breccias contain prominent "blue" rock clasts that are notably harder and more resistant to weathering and abrasion than the breccia matrix, such as Sarcobatus Clast (sols 3675-3676) (Arvidson et al., 2016). Opportunity explored Wdowiak ridge, a morphologic ridge of rocks that trends sub-parallel to the Endeavour crater

rim, and took MI and APXS measurements of the "blue" rock Margaret Brush (sol 3812) (Fig. 3.6c).

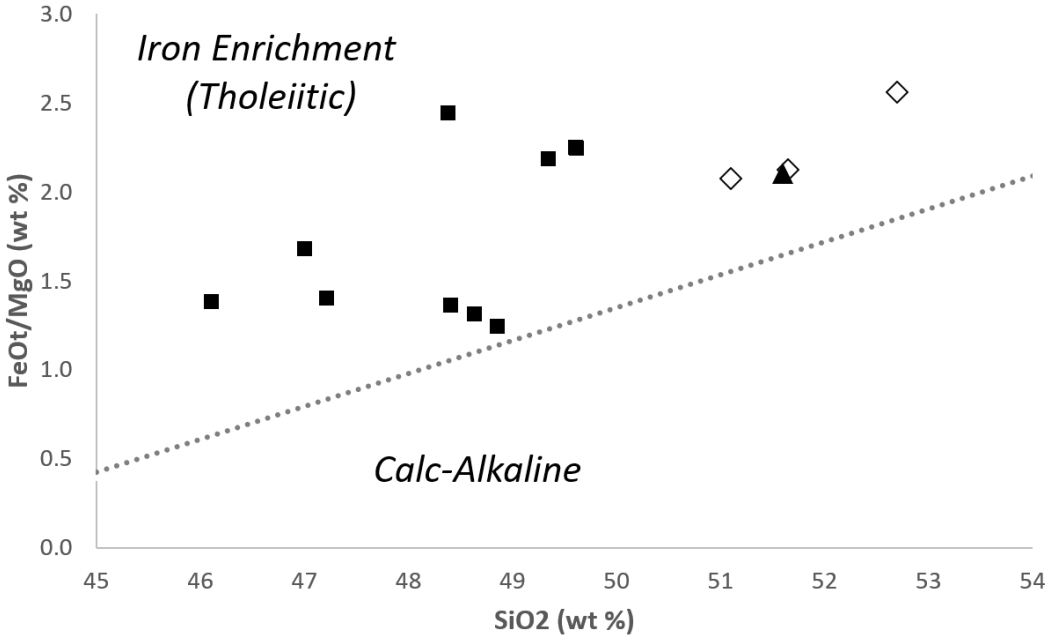

Figure 3.7 The crystalline rocks of Endeavour crater (squares: "blue" rocks, diamonds: pitted rocks, triangle: Bounce Rock erratic) all plot above the line separating dry Tholeiitic (above line) from wet calc-alkaline (below line) provenances (McSween 2009).

Upon Opportunity's arrival at the ridge overlooking the entrance to Marathon Valley, the "blue" rocks became a more prominent component of the surface debris, forming cobble- to boulder-sized rocks (Fig. 3.6d and 3.6h), as well a continuous unit along the rim of the crater. On sol 3953 one of the "blue" rocks that occurs along the ridge, Sergeant Charles Floyd, was brushed with the Rock Abrasion Tool (RAT), imaged with the MI, and analyzed with the APXS (Fig. 3.8). The collocated "blue" and pitted "purple" rock outcrops are clearly distinguishable in figure 3.8. Just below this portion of the rim lies the entrance to Marathon valley and SoSL. On sol 4009 the Lindbergh Mound "blue" rock, Roosevelt Field, was analyzed, unbrushed, with the MI and APXS (Bouchard et al., 2017; Farrand et al., 2016). After descending into Marathon Valley, cobble- to boulder-sized "blue" rocks were seen as dense concentrations in lag deposits along the interior of the Endeavour crater rim, in some cases occurring in piles such as Spirit

Mound (sol 4506), found below Marathon Valley (Fig. 3.6a) (Arvidson et al., 2017; Bouchard et al., 2017). These deposits appear to be colluvium from the erosion and collapse of the interior of the Endeavour crater rim (Crumpler et al., 2017).

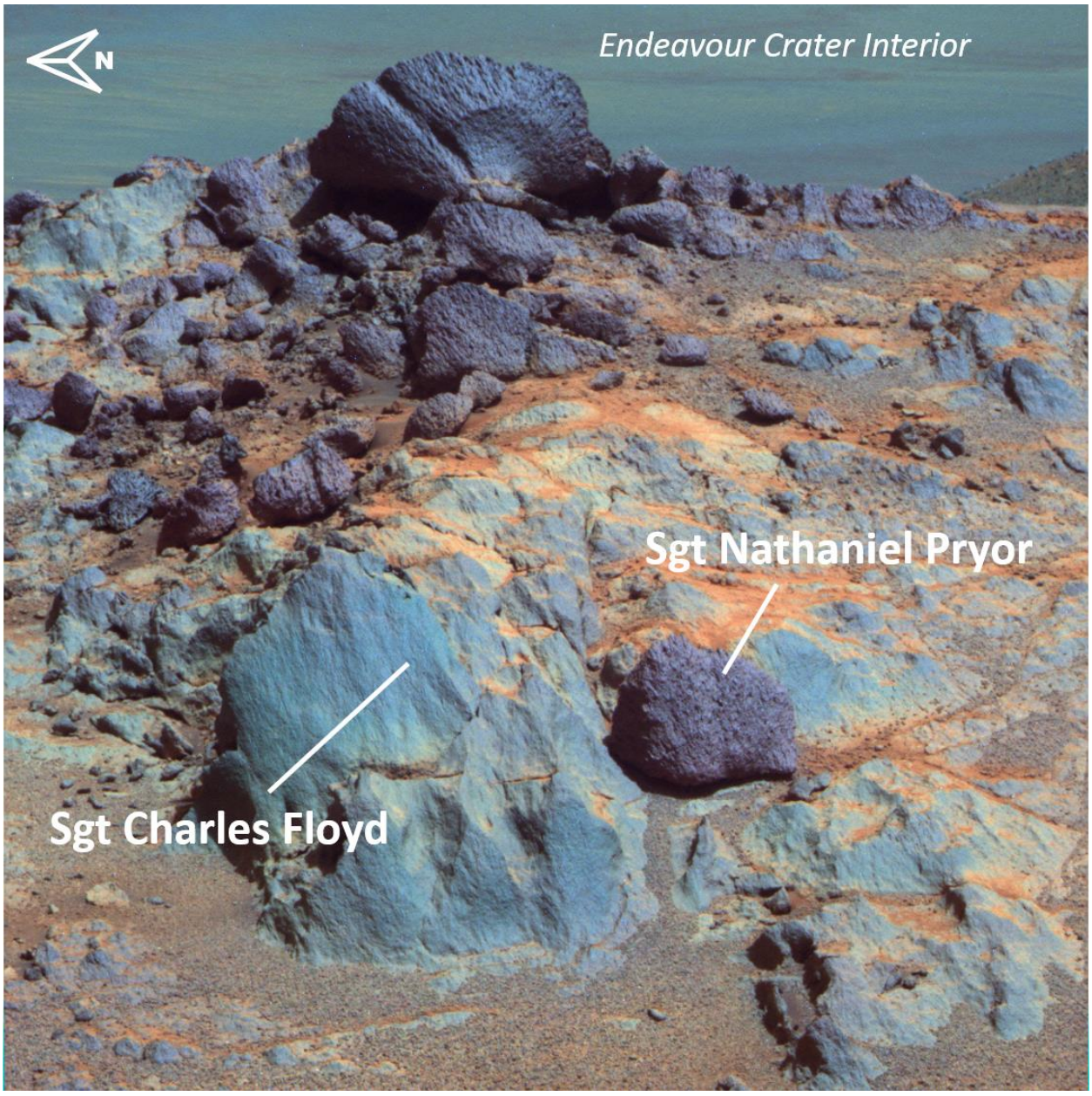

Figure 3.8 A false color Pancam image of the outcrop of "blue" and "purple" capping rocks on the rim of Endeavour crater overlooking Marathon Valley. These two rock types were sampled at the Sergeant Charles Floyd and Sergeant Nathaniel Pryor APXS target locations. Pancam image: Sol3948B_P2588_1_False_L257, image credits: D. Savransky and J. Bell/JPL/NASA/Cornell/ASU (Bell 2003, 2006).

Owing to its ubiquitous nature and crystalline texture, an impact melt origin for these "blue" rocks has been suggested (Crumpler et al., 2015; Mittlefehldt, Gellert, et al., 2018); however, their distinctive compositions compared to the Shoemaker formation, low Ni content, and occurrence in features younger than Endeavour crater such as SoSL, may point to a volcanic origin that both pre-and post-dates the Endeavour crater impact (Bouchard et al., 2017). Rocks of the Matijevic formation also appear "blue" in false color L257 Pancam imagery and have compositions that overlap those of the "blue" rocks (Bouchard et al., 2017).

3.2 Data & Methods

The Athena science payload of the Opportunity rover comprised a suite of tools to investigate the lithologies of Endeavour crater (Squyres et al., 2003). The Instrument Deployment Device (IDD), or arm of the rover, contains the Alpha Particle X-Ray Spectrometer (APXS), the Microscopic Imager (MI), and Panoramic Camera (Pancam). The APXS spectrum is translated into bulk elemental composition of rocks and soils, represented here as oxide weight percentages (Gellert et al., 2006), and the MI provides hand-lens scale images to evaluate rock textures (Herkenhoff et al., 2003). Opportunity's mast hosts the Panoramic Camera (Pancam) (Bell et al., 2003; Bell et al., 2006), which is a multispectral imager that provides context imagery for geologic investigation and also some spectral information about rocks, including many that were not analyzed with the IDD (Squyres et al., 2003). The false-color filter combination of L257 (753, 535, and 432 nm composite) is used throughout this paper because it discriminates different rock types based on composition and mineralogy. These instruments provide the data sets used to make comparisons between the rock suites of Endeavour crater.

To classify the rock targets and quantify their similarities we use a two-prong statistical grouping model that was validated using Endeavour crater rim targets (Bouchard & Jolliff, 2016, 2018b). The APXS elemental data is standardized for variance across each element by subtracting by the minimum and dividing by the range. Then the data is passed through an agglomerative, group average, hierarchical clustering algorithm to provide a rapid first categorization of the rock targets. We also use the APXS data to generate an error-weighted, reduced-χ^2 similarity index (SI) based on the sum of squared differences between oxide components (Bouchard & Jolliff, 2016, 2018b). Both methods are applied to selected APXS targets, and then applied to the same targets after SO_3 and Cl have been removed and the data is normalized to 100%. Most alteration occurring at Meridiani Planum is essentially isochemical with the addition of some S and Cl (McLennan, 2012; McLennan & Grotzinger, 2008; Ming, Morris, & Clark, 2008; Morris & Klingelhöfer, 2008), so removing these elements (which exist in much higher concentrations than in martian meteorites) allows us to interrogate the relationships between pre-alteration rock compositions (Bouchard & Jolliff, 2016, 2018b). Clusters and similarity indices are compared to imagery from the MI and Pancam to evaluate other effects on similarity such as dust coatings, veneers, and clast components within the APXS integration field of view (Bouchard & Jolliff, 2018b; Stein et al., 2018). To further interrogate targets that may represent physical mixtures, such as breccias and soil or valley floor targets, a multi-component mixing model is used to determine endmember proportions and assess goodness of fit of multiple end-member components within the APXS integration field of view.

3.3 Lithochemical Rock Suites of Perseverance Valley

Prior its loss in the global dust storm of 2018 (Mars year 34), Opportunity explored the upper half of Perseverance Valley. In this traverse the team performed IDD science, including APXS analysis, on 16 discrete targets (Table 3.1, Fig 3.9). Some of these targets were brushed (RB) and others ground into (RR) by the RAT, and still other targets were analyzed without any surface preparation (RU) owing to difficult approach angles or loose debris. The statistical grouping model, informed by imagery comparisons, was used to divide these targets into four distinct lithochemical groupings, described in Table 3.2 (Bouchard et al., 2019). Distinguishing characteristics (occurrence, textures, composition) of each of the groups and their members are described below, and similarities to previously explored Endeavour crater lithologies are noted.

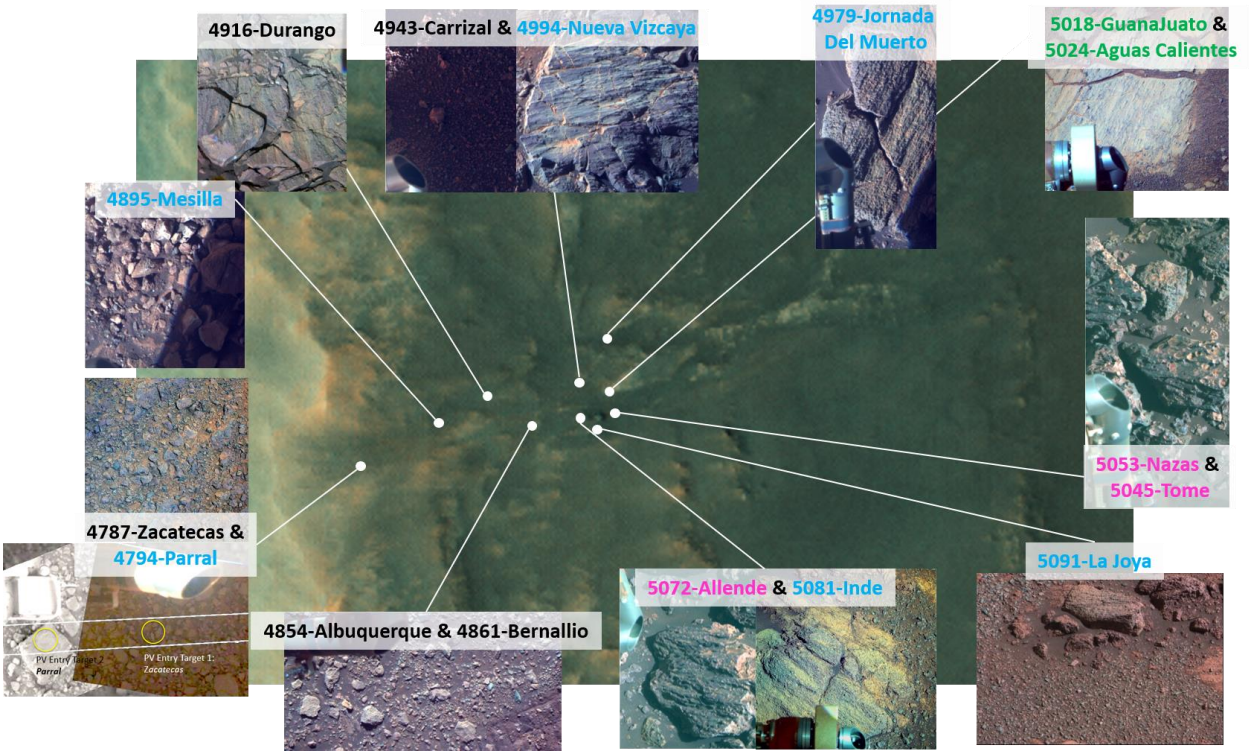

Figure 3.9 HiRISE (Mars Reconnaissance Orbiter) image of Perseverance Valley (ESP_058208_1775_RGBcolor, NASA/JPL/University of Arizona). The top of the image is North and the valley trends West to East across the remnant crater rim and into the crater basin. The Opportunity rover is visible at its final resting site between the Allende/Inde, La Joya, and Nazas/Tome sites. The locations of each APXS analysis taken within the valley are

notated with the corresponding false color Pancam image of the target. APXS labels: black - members of the Perseverance Valley Trough Fill unit; green - Ysleta Del Sur breccia; blue - the San Miguel blue rock members; pink - members of the pitted rock lithology. Pancam image credits: D. Savransky and J. Bell/JPL/NASA/Cornell/ASU (Bell 2003, 2006).

Table 3.1: APXS target names, Sol and location of analysis, lithology, 13 major elemental oxides in weight percentages, and target pre-integration preparation by the Rock Abrasion Tool (RU = untreated, RB = brushed by the RAT, RR = first few mm's ground into by the RAT). (MV) Marathon Valley, (SoSL) Spirit of St. Louis, (PV) Perseverance Valley.

Location	Sol	Prep	Target Name	Lithology
Marathon Valley Overlook	B3935	RU	JeanBaptisteCharbonneau	purple rock above MV
Marathon Valley Overlook	B3951	RB	SgtCFloyd	blue rock above MV
Marathon Valley Overlook	B3952	RB	SgtCFloyd2	blue rock above MV
Marathon Valley Overlook	B3953	RB	SgtCFloyd3	blue rock above MV
Marathon Valley Overlook	B3959	RU	SgtNathanielPryor	purple rock above MV
Marathon Valley Overlook	B3961	RU	SgtNathanielPryor2	purple rock above MV
Spirit of St. Louis Crater	B4003	RU	Lambert_Field	SoSL "purplish" fill
Spirit of St. Louis Crater	B4009	RU	Roosevelt_Field	SoSL Lindberg mound blue rock
Spirit of St. Louis Crater	B4013	RU	Harold+M_Bixby	SoSL fill
Spirit of St. Louis Crater	B4023	RB	Donald_A_Hall	SoSL fill
Spirit of St. Louis Crater	B4035	RU	Pvt. Wm. Bratton	SoSL red zone
Spirit of St. Louis Crater	B4054	RU	Pvt. Wm. Bratton 2	SoSL red zone
Spirit of St. Louis Crater	B4064	RB	Ryan_NYP	SoSL next to red zone
Spirit of St. Louis Crater	B4066	RU	Ryan_NYP2	SoSL next to red zone
Cape Tribulation-Cape Byron	B4697	RU	Julesburg	Burns or Grasberg rock between Capes
Cape Tribulation-Cape Byron	B4701	RB	Ogallala	Grasberg rock between Capes
Cape Tribulation-Cape Byron	B4704	RR	Ogallala	Grasberg rock between Capes
Perseverance Valley	B4787	RU	Zacatecas	PV floor fill
Perseverance Valley	B4794	RU	Parral	PV blue rock cobble
Perseverance Valley	B4854	RU	Albuquerque	PV floor fill
Perseverance Valley	B4861	RU	Bernallilo	PV cobble "shoemaker like"
Perseverance Valley	B4865	RU	Bernallilo_Offset	PV cobble "shoemaker like"
Perseverance Valley	B4895	RU	Mesilla	PV cobble "shoemaker like"
Perseverance Valley	B4916	RU	Durango	PV floor fill
Perseverance Valley	B4943	RU	Carrizal	PV floor fill
Perseverance Valley	B4979	RU	JornadaDelMuerto	PV blue rock "San Miguel" outcrop
Perseverance Valley	B4984	RU	JornadaDelMuerto2	PV blue rock "San Miguel" outcrop
Perseverance Valley	B4986	RU	JornadaDelMuerto3	PV blue rock "San Miguel" outcrop
Perseverance Valley	B4994	RU	Nueva Vizcaya	PV

Perseverance Valley	B4995	RU	Nueva Vizcaya Offset	PV
Perseverance Valley	B5018	RU	GuanaJuato	PV Ysleta del Sur, PV wall
Perseverance Valley	B5024	RU	AguasCalientes	PV Ysleta del Sur, PV wall
Perseverance Valley	B5025	RB	AguasCalientes	PV Ysleta del Sur, PV wall
Perseverance Valley	B5027	RR	AguasCalientes1 RAT1	PV Ysleta del Sur, PV wall
Perseverance Valley	B5028	RR	AguasCalientes2 RAT1	PV Ysleta del Sur, PV wall
Perseverance Valley	B5033	RR	AguasCalientes1 RAT2	PV Ysleta del Sur, PV wall
Perseverance Valley	B5036	RR	AguasCalientes2 RAT2	PV Ysleta del Sur, PV wall
Perseverance Valley	B5045	RU	Tome	PV Vesicular rocks, radial strike
Perseverance Valley	B5047	RR	Tome2	PV Vesicular rocks, radial strike
Perseverance Valley	B5053	RU	Nazas	PV Vesicular rocks, radial strike
Perseverance Valley	B5072	RU	Allende	PV Vesicular
Perseverance Valley	B5073	RU	Allende2	PV Vesicular
Perseverance Valley	B5079	RU	Inde	PV Tabular rocks, San Miguel
Perseverance Valley	B5081	RU	Inde2	PV Tabular rocks, San Miguel
Perseverance Valley	B5091	RU	LaJoya1	PV Tabular/Tan rocks
Perseverance Valley	B5092	RU	LaJoya1b	PV Tabular/Tan rocks
Perseverance Valley	B5093	RU	LaJoya2	PV Tabular/Tan rocks
Cape York	-	avg	Matijevic Average No Veneer n=6	Pre-impact clastic
Endeavour Crater	-	avg	Shoemaker Average n=15	Impact breccia
Cape York	-	avg	Grasberg Average n=5	Post-impact clastic
Meridiani Planum and Endeavour Crater	-	avg	Burns Average n=15	Meridiani Plains unit
Meridiani Planum and Endeavour Crater	-	avg	Average Soil n=9	Meridiani soil

Target Name	**SiO_2**	**TiO_2**	**Al_2O_3**	**Cr_2O_3**	**FeO**	**MnO**	**MgO**	**CaO**	**Na_2O**	**K_2O**	**P_2O_5**	**SO_3**	**Cl**	**SUM**
JeanBaptisteCharbonneau	52.70	0.91	16.16	0.01	10.35	0.18	4.04	7.25	3.27	0.44	0.92	3.19	0.51	99.94
SgtCFloyd	48.85	0.73	12.55	0.27	13.65	0.28	10.96	5.71	2.39	0.28	0.97	2.80	0.53	99.97
SgtCFloyd2	48.63	0.67	12.26	0.26	14.04	0.25	10.65	5.77	2.52	0.29	1.01	3.04	0.57	99.96
SgtCFloyd3	48.40	0.58	12.53	0.27	14.27	0.29	10.46	5.81	2.43	0.30	1.01	3.09	0.52	99.96
SgtNathanielPryor	51.65	0.63	18.39	0.03	9.07	0.16	4.27	8.47	2.74	0.29	0.85	2.88	0.48	99.92
SgtNathanielPryor2	51.10	0.53	18.22	0.05	9.57	0.17	4.61	8.43	2.88	0.25	0.81	2.81	0.47	99.93
Lambert_Field	43.86	0.81	9.94	0.19	15.57	0.27	7.16	6.55	2.22	0.31	0.95	11.16	0.56	99.62
Roosevelt_Field	49.34	0.89	12.62	0.16	14.01	0.32	6.40	6.88	2.87	0.45	1.17	3.10	0.38	98.60
Harold+M_Bixby	44.17	0.82	9.84	0.20	16.30	0.30	7.01	6.33	2.36	0.34	1.17	10.24	0.69	99.83
Donald_A_Hall	45.18	0.74	9.84	0.23	16.40	0.30	7.01	6.33	2.29	0.26	1.06	9.09	0.72	99.51
Pvt. Wm. Bratton	55.64	0.79	10.74	0.28	9.45	0.16	5.49	5.00	2.07	0.37	0.85	7.36	1.02	99.24
Pvt. Wm. Bratton 2	54.32	0.71	10.54	0.27	11.11	0.20	5.80	5.55	2.22	0.34	0.85	6.78	0.90	99.61
Ryan_NYP	43.05	0.80	8.65	0.20	15.78	0.30	7.54	5.55	2.51	0.38	0.95	12.31	1.56	99.59
Ryan_NYP2	42.85	0.81	8.46	0.19	16.40	0.30	7.32	5.66	2.22	0.36	0.85	12.54	1.61	99.63

Julesburg	43.25	0.63	8.26	0.19	17.75	0.24	5.80	7.88	1.71	0.38	0.85	13.46	0.63	101.12
Ogallala RB	47.62	0.84	8.26	0.23	19.92	0.25	4.35	5.77	1.93	0.55	1.06	8.86	0.79	100.55
Ogallala RAT	48.23	0.88	8.06	0.23	20.55	0.24	3.97	5.77	1.64	0.60	1.06	8.51	0.71	100.56
Zacatecas	46.30	0.69	9.94	0.39	17.75	0.36	7.39	7.10	2.00	0.36	0.85	5.40	0.69	99.30
Parral	48.02	0.68	10.94	0.23	13.70	0.18	9.06	5.77	2.29	0.24	0.95	5.40	0.75	98.26
Albuquerque	46.50	0.71	9.94	0.32	17.02	0.21	7.54	6.44	2.58	0.35	0.85	5.63	0.85	98.98
Bernallilo	45.69	0.73	9.94	0.30	15.67	0.31	7.54	6.77	2.51	0.41	0.85	7.36	1.01	99.15
Bernallilo_Offset	45.38	0.78	9.84	0.18	15.05	0.17	7.39	6.33	2.29	0.36	0.95	9.43	1.32	99.55
Mesilla	45.69	0.66	10.14	0.24	13.91	0.21	7.92	5.33	2.29	0.39	1.17	10.59	0.68	99.34
Durango	47.21	0.63	10.74	0.27	15.98	0.23	7.16	6.33	2.36	0.29	0.74	6.21	0.94	99.15
Carrizal	46.30	0.78	9.94	0.39	17.12	0.45	7.54	7.10	2.29	0.36	0.85	5.06	0.63	98.83
JornadaDelMuerto	47.21	0.63	12.03	0.25	13.29	0.48	9.44	5.55	2.51	0.24	1.06	4.25	0.97	97.92
JornadaDelMuerto2	47.41	0.63	12.03	0.27	13.50	0.36	9.29	5.66	2.58	0.24	1.06	4.25	1.03	98.31
JornadaDelMuerto3	46.30	0.63	11.33	0.28	14.22	0.59	9.52	5.66	2.80	0.24	1.06	4.48	1.10	98.22
Nueva Vizcaya	46.70	0.63	11.63	0.20	14.33	0.18	7.77	5.66	2.51	0.24	0.85	6.78	1.08	98.64
Nueva Vizcaya Offset	46.70	0.63	11.53	0.26	14.74	0.18	7.77	5.55	2.51	0.26	0.95	6.78	1.10	99.05
GuanaJuato	45.89	0.73	10.34	0.24	15.57	0.14	8.15	5.66	2.51	0.36	0.63	7.36	1.30	98.94
AguasCalientes	46.30	0.77	10.34	0.24	15.05	0.18	8.30	5.99	2.51	0.32	0.63	7.13	1.24	99.06
AguasCalientesRB	46.50	0.69	10.54	0.20	14.74	0.16	8.68	5.99	2.07	0.29	0.41	6.78	1.60	98.74
AguasCalientes1 RAT1	46.30	0.67	10.34	0.22	13.91	0.14	11.19	5.33	2.36	0.24	0.08	5.63	0.99	97.47
AguasCalientes2 RAT1	46.50	0.63	10.54	0.20	14.22	0.13	11.04	5.33	2.36	0.24	0.08	5.40	0.96	97.71
AguasCalientes1 RAT2	46.91	0.63	10.54	0.19	14.53	0.13	11.04	5.22	2.07	0.24	0.08	5.06	0.68	97.38
AguasCalientes2 RAT2	46.70	0.63	10.34	0.19	14.64	0.13	11.19	5.22	2.00	0.24	0.08	5.40	0.67	97.49
Tome	61.93	0.80	11.53	0.04	7.38	0.25	3.97	4.89	2.58	0.27	1.50	3.33	0.79	99.27
Tome2	62.84	0.84	10.34	0.06	7.69	0.26	3.97	4.77	2.29	0.27	1.61	3.67	0.84	99.47
Nazas	57.97	0.63	15.60	0.02	8.42	0.21	3.97	4.55	2.58	0.26	1.28	3.10	0.69	99.29
Allende	53.20	0.63	15.60	0.06	8.83	0.19	4.73	7.32	3.45	0.24	1.28	2.75	0.55	98.83
Allende2	53.00	0.63	15.60	0.07	8.83	0.17	4.73	7.21	3.59	0.24	1.28	2.75	0.56	98.66
Inde	47.62	0.66	12.62	0.25	12.56	0.52	7.92	6.44	2.36	0.25	0.95	5.63	1.02	98.83
Inde2	47.21	0.63	12.23	0.25	12.98	0.72	8.53	5.99	2.36	0.24	0.95	5.63	1.03	98.77
LaJoya1	46.09	0.65	10.74	0.28	15.05	0.26	9.44	5.33	2.07	0.24	0.74	6.21	1.18	98.32
LaJoya1b	46.30	0.64	10.54	0.28	14.95	0.25	9.44	5.55	2.00	0.26	0.85	6.21	1.23	98.51
LaJoya2	47.21	0.63	12.03	0.27	13.60	0.32	9.67	5.66	1.71	0.24	0.85	5.06	1.06	98.31
Matijevic Average No Veneer n=6	48.80	0.87	10.02	0.28	15.96	0.33	8.13	5.96	2.34	0.36	0.98	4.93	0.89	99.95
Shoemaker Average n=15	45.20	1.05	9.24	0.22	17.91	0.46	7.83	6.29	2.39	0.48	1.16	6.51	1.09	99.90
Grasberg Average n=5	45.22	0.98	8.26	0.27	19.24	0.20	5.11	5.98	2.20	0.72	1.11	8.85	1.70	99.87
Burns Average n=15	38.08	0.78	6.48	0.19	15.94	0.29	7.38	5.48	1.74	0.55	1.03	20.94	1.00	99.94
Average Soil n=9	45.30	1.10	9.00	0.40	19.20	0.40	7.40	7.00	2.20	0.50	0.90	5.80	0.60	99.84

Table 3.2: Rock suites of Perseverance Valley.

	APXS Targets	Characteristic Composition	Pancam Color	MI Textures	Occurrence	Related Endeavour Rock Suites	Related to Mapped Units
Perseverance Valley Trough Floor Fill	Zacatecas, Albuquerque, Durango cobble, Carrizal, Bernallio cobble	Relatively tight SiO_2 (45.4-47.2 wt%) and Al_2O_3 ranges (9.8-10.7 wt%); minor MnO enrichment compared to other PV materials (0.2-0.5 wt%)	Mixtures	Few cm sized cobbles and a mix of sub cm pebbles and fine regolith	The loose material that fills in the putative valley depression	3 component mixture of: -San Miguel type blue rocks -Shoemaker -Average Endeavour Crater Soil	Shoemaker impact breccia (lower unit?)
San Miguel type "Blue" Rocks	Jornada Del Muerto, Parral Cobble, Inde, La Joya, Mesilla, Nueva Vizcaya	Relatively tight SiO_2 (46.1-48.0 wt%) and FeO, MgO ranges (12.6-15.1 wt%, 7.8-9.7 wt%); relative MnO enrichment compared to other PV materials (0.2-0.7 wt%)	Blue to Tan	Massive, fine grained, crystalline. Lineations, (secondary?), wind scours /fluting	Linear outcrop running along the valley strike in the South fork, outcrop in North fork, and cobbles found up hill near valley mouth	Similar to Endeavour crater "blue rocks," but especially the blue rock outcrop found on rim above Marathon Valley (Srgt Charles Floyd)	Db, dark "cap" rocks, blue basaltic rock.
Ysleta Del Sur breccia, Trough Wall	Aguas Calientes, GuanJuato	Generally overlapping composition with most PV materials except lower MnO (0.1-0.2 wt%); and the much higher MgO in RATed targets (8.2-11.2 wt%)	Blueish clasts in tanish matrix	Sub cm-cm sized angular clasts in fine grained matrix = breccia. Also exhibits wind scour/fluting.	The "nose" of valley wall separating the North and South forks	Similar to the San Miguel blue rocks in bulk composition, but has a distinct texture.	Shoemaker impact breccia (upper-lower unit?)
Pitted, Silica-Rich Rocks	Tome, Nazas, Allende	Extremely high SiO_2 (53.0-62.8 wt%); low FeO and MgO (7.4-8.8 wt%, 4.0-4.7 wt %) and high Al_2O_3 (10.3-15.6 wt%) relative to Shoemaker	Purple to Tan	Cm sized surface vugs in a fine grained rock	Linear outcrop running along the valley strike, near the San Miguel outcrop	The highest silica rock outcrop encountered by Opportunity, most similar to Endeavour crater "purple rocks" such as those found near Marathon Valley (XXX)	Dp, dark "cap" rocks, purple high silica basalt.

3.3.1 Perseverance Valley Floor Fill Material

As the rover descended into the valley the team made an initial examination of the valley floor material (Zacatecas, sol 4787). The floor can be characterized as a loose collection of regolith and sub-cm to several-cm large cobbles (Fig. 3.10a-e). The RAT could not be used on this material owing to its unconsolidated nature. The floor material likely includes a significant proportion of locally derived soil (no organics implied). This material was analyzed at two additional sites in the upper third of Perseverance Valley (Albuquerque, sol 4854, and Carrizal, sol 4943). The APXS integration field of view for these Perseverance Valley floor targets is

filled by loose bedrock material, soil grains, and rock cobbles (confirmed by Pancam and MI imagery), whereas the field of view of the Bernalillo (sol 4861) and Bernalillo Offset (sol 4865) targets are dominated by a single ~1.25 x 2 cm sized cobble. The final target of this rock suite is a ~1.5 x 3 cm sized cobble (Durango, sol 4916).

This group is roughly similar to the Shoemaker formation in composition (Fig. 3.11), but has a relatively tight SiO_2 (45.4-47.2 wt%) and Al_2O_3 distribution (9.8-10.7 wt%) with minor MnO enrichment compared to other PV materials (0.2-0.5 wt%). Collectively these targets are a representative sample of the floor material of the upper half of Perseverance Valley, which appears to be loose material that has filled in troughs in the valley. We used a multi-component mixing model to estimate the end-member components and their proportions within the APXS integration field of view. An average of the Perseverance Valley floor fill target compositions is best modeled as a three-component mixture of: Meridiani soil (~13-28 wt%), a material similar in composition to the floor of the SoSL feature (~47-55 wt%), and a significant component (~21-31 wt%) of cobbles of the San Miguel type "blue" rock as shown in table 3.3.

3.3.2 Ysleta Del Sur Type Outcrop

In HiRISE imagery Perseverance Valley appears to bifurcate in several places in the downhill direction (Fig. 3.2, 3.12). The first distinctive fork reached by Opportunity was a location named Ysleta Del Sur, separating the trough into a North and South fork. While the "noses and troughs" appear striking in HiRISE imagery, at the surface they are topographically subtle, represented by only a few centimeters of relief. The outcrop appears to be a breccia with sub-cm sized angular "blue" clasts visible in figures 3.10k-p and a fine-grained homogeneous "tan" matrix.

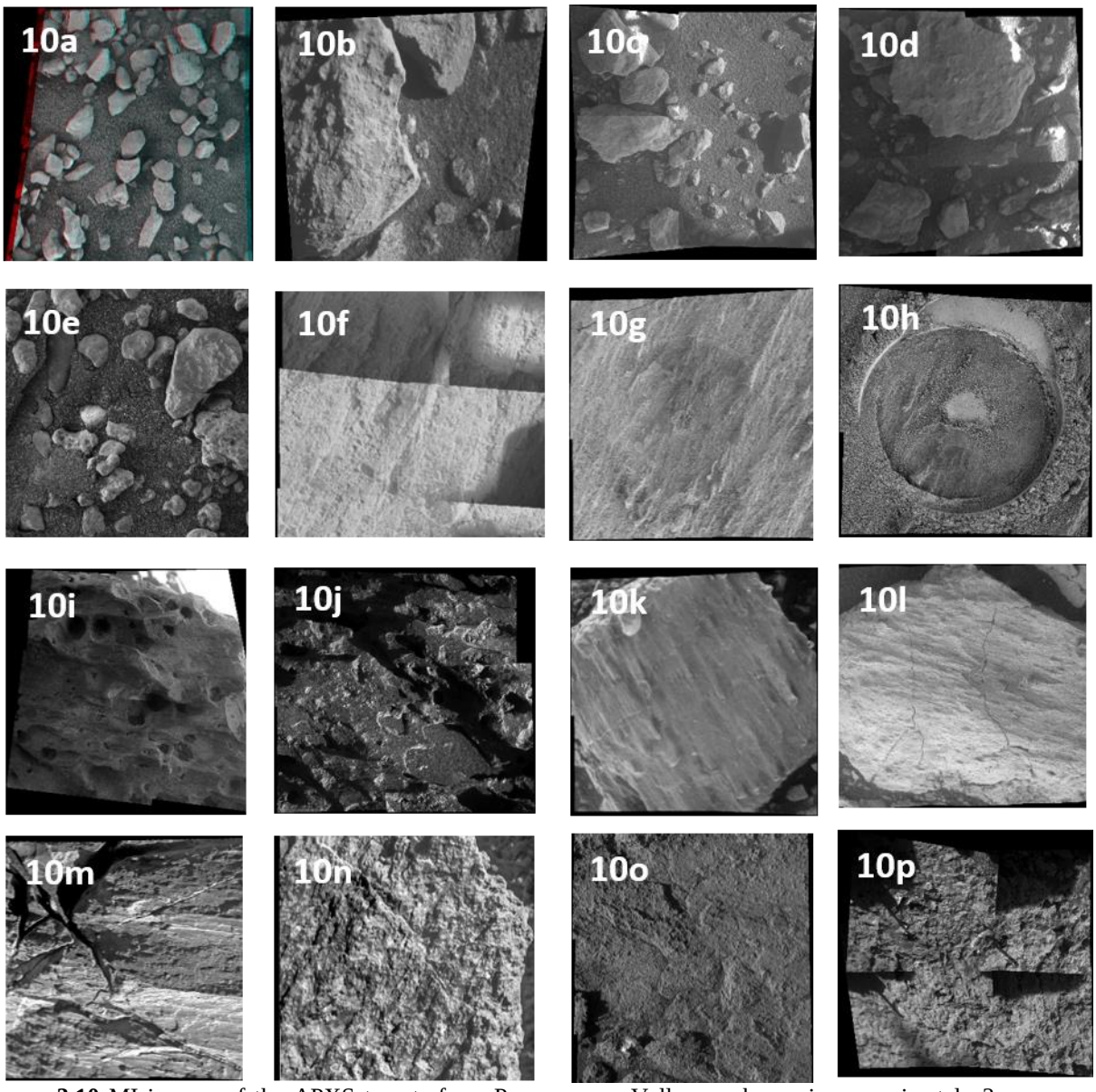

Figure 3.10 MI images of the APXS targets from Perseverance Valley, each one is approximately 3 cm across. (10a-e) Perseverance Valley Trough Floor Fill materials (Zacatecas, Durango, Albuquerque, Bernallio, Carrizal). (10f-h) Ysleta Del Sur breccia (GuanaJuato and Aguas Calientes pre- and post-RAT). (10i-j) Pitted Rocks. (10k-p) San Miguel type "blue" rocks.

Table 3.3: Summary of the three-component mixing model of the average of the Perseverance Valley Trough Floor Fill materials. The rubble that fills the valley is broadly Shoemaker in composition, and is best represented (reduced χ^2 of 2) as a mixture of Spirit of St. Louis type Shoemaker material (51%), San Miguel type "blue" rocks (26%), and a soil component (23%).

	Parral	**Average Soil**	**Average PV Shoemaker Cobbles**	**Average PV Floor**	**Modeled**	**Weights**
SiO_2	48.02	45.30	46.09	46.20	46.03	2
TiO_2	0.68	1.10	0.71	0.71	0.86	10
Al_2O_3	10.94	9.00	10.17	9.99	9.84	2
Cr_2O_3	0.23	0.40	0.25	0.33	0.30	20
FeO	13.70	19.20	15.57	16.45	16.57	2
MnO	0.18	0.40	0.23	0.31	0.29	10
MgO	9.06	7.40	7.37	7.60	7.70	3
CaO	5.77	7.00	6.47	6.49	6.52	2
Na_2O	2.29	2.20	2.39	2.29	2.29	20
K_2O	0.24	0.50	0.36	0.36	0.39	20
P_2O_5	0.95	0.90	0.85	0.93	0.89	20
SO_3	5.40	5.80	7.67	6.67	6.46	2
Cl	0.75	0.60	1.09	0.72	0.83	5
NiO	0.03	0.04	0.07	0.06	0.05	15
SUM	98.26	99.84	99.28	99.11	99.00	

	%	±
Average PV Floor		
Parral	20.2%	7.2%
Average Soil	39.2%	6.0%
Average PV Shoemaker Cobbles	40.4%	7.0%
SUM	99.7%	
χ^2	**20.24**	
χ^2 /n	1.84	

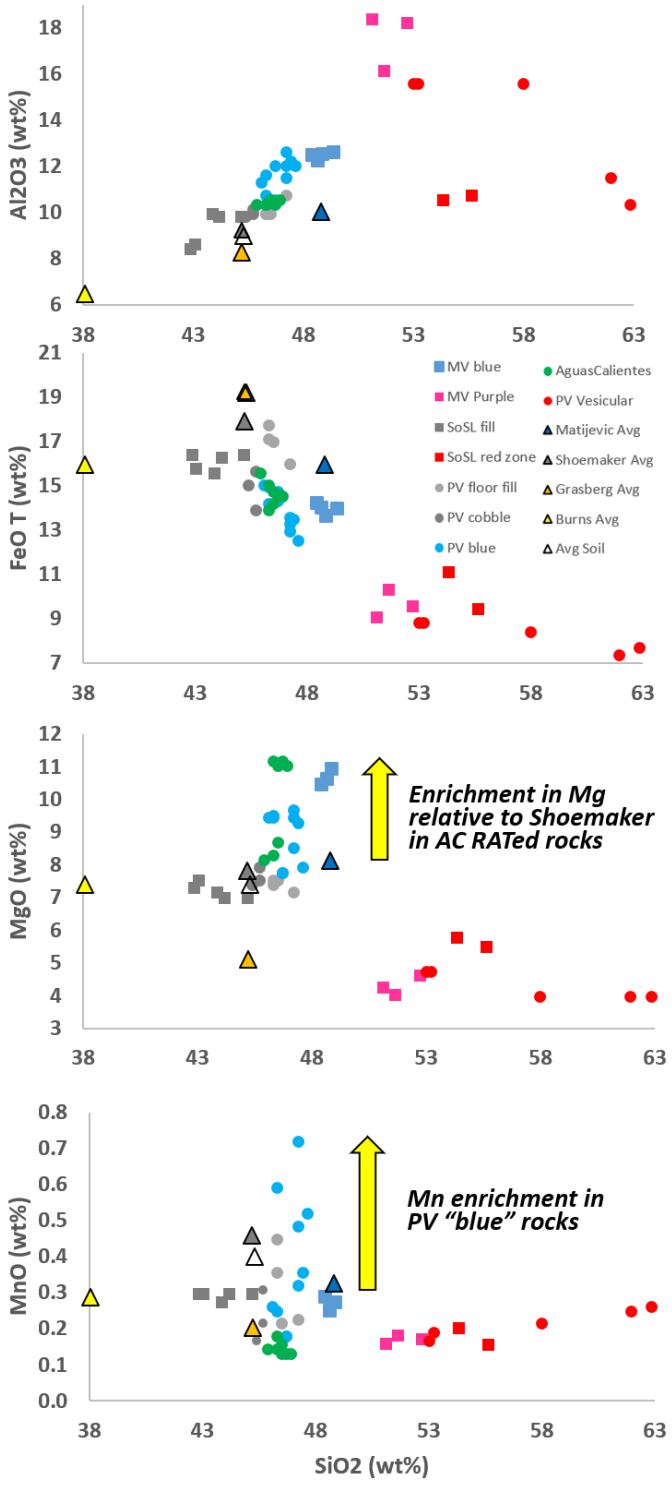

Figure 3.11 Composition plots of different oxide weight percentages vs SiO2 wt percentage of the targets included in Table 3.1. There is a general enrichment in MgO in the Perseverance Valley rocks relative to the other Endeavour rim rock averages potentially indicating the presence of aqueous alteration in the valley. There is also an enrichment in MnO in the Perseverance Valley "blue" rocks. These are weight percentages based on data that includes SO3 and Cl.

The Ysleta Del Sur outcrop was analyzed in two locations (GuanaJuato, sol 5018 and Aguas Calientes, sol 5024). Generally, the composition overlaps that of most PV materials except with lower MnO (0.1-0.2 wt%) and much higher MgO in RATed targets (8.2-11.2 wt% compared to 8 wt% average for PV materials). This outcrop is similar in bulk composition to the San Miguel "blue" rocks, but is classified as a different rock suite on the basis its breccia texture (Bouchard et al., 2019). The outcrop exhibits lineations in the matrix that are essentially wind tails of less resistant matrix behind the more resistant clasts in the up-valley direction, hence this feature is interpreted as a secondary wind erosion feature and not a primary lineation in the rock fabric.

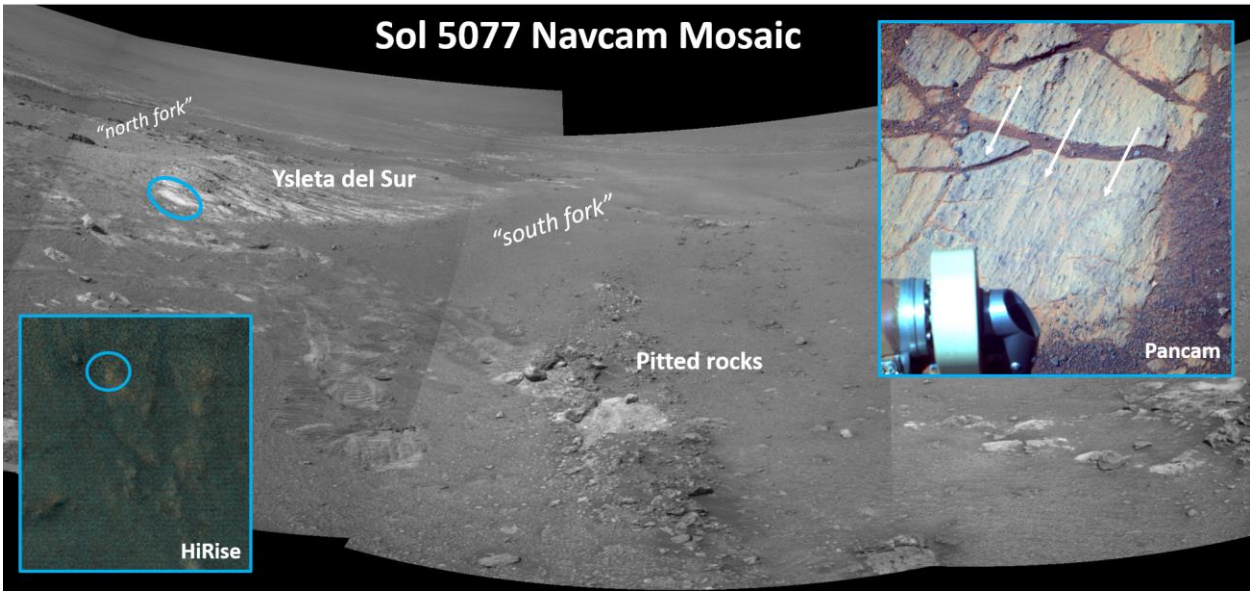

Figure 3.12 A Navcam mosaic taken by the rover looking east down Perseverance Valley. Ysleta Del Sur, the trough "nose," is noted by the blue circles in the Navcam mosaic and HiRISE image inset. The Navcam mosaic also captures the south fork of the trough where the pitted rocks and a tabular outcrop of "blue" rocks are located. Pancam inset is a false color image of the Ysleta Del Sur (GuanaJuato and Aguas Calientes) breccia with wind tails indicative of up-valley wind erosion (arrows).

3.3.3 San Miguel Type "Blue" Rocks (Cobbles & Outcrops)

The lowest point in Perseverance Valley reached by Opportunity was in the "North fork" past Ysleta Del Sur, and this was the site of the investigation of the San Miguel outcrop. San Miguel is a fine-grained, competent outcrop of crystalline rock, as visible in MI images in

figures 3.10k-p, with a distinctive “blue” color in false color Pancam imagery that was analyzed several times with the APXS (Jornada Del Muerto, sol 4979). The lithology and composition of San Miguel is similar enough to classify it as another location of “blue” rocks within Endeavour crater (Fig. 3.11, and 3.14-3.16) (Bouchard et al., 2019). The San Miguel outcrop was analyzed at another exposure (Nueva Vizcaya, sol 4994) by backtracking up the valley ~16 meters.

After characterizing this outcrop, it became clear that several-cm-sized cobbles of the same composition were encountered up-valley from this site (Parral, sol 4794, and Mesilla, sol 4895). These cobbles have a similar “blue” color in L257 Pancam imagery and their characteristics match the lithochemical and textural classification of this rock suite. Two more “blue” rock outcrops were analyzed in Perseverance Valley. Just south of the Nueva Vizcaya outcrop there is a linear expression of rock outcrops that trends down-valley in the “south fork” (Fig. 3.6e-g, 3.6i). This feature includes both tabular “blue” and “purple” silica-rich rocks. The “blue” rocks in this outcrop were analyzed at two locations (Inde, sol 5081 and La Joya, sol 5091).

Compositionally, the “blue” rocks in Perseverance Valley have relatively tight (standard deviation in elements ranges from 0.02-1.84). The San Miguel type “blue” rocks also have a relative MnO enrichment compared to other PV materials (0.2-0.7 wt%). All of these Perseverance Valley “blue” rocks exhibit similar lineations. These lineations strike along the valley trend and are likely a secondary alteration product resulting from wind scouring similar to those observed on the Ysleta Del Sur outcrop, visible in figures 3.10f-h.

The lithology and composition of San Miguel is the most similar to an outcrop of “blue” rocks that was investigated on the rim of Endeavour crater on a topographic high overlooking SoSL and the entrance to Marathon Valley. APXS analyses were done on this outcrop of rocks

along the ridge overlooking Marathon Valley (Sergeant Charles Floyd, sol 3951). Specifically, on a sulfur- and chlorine-free basis, the Jornada Del Muerto (San Miguel) target is highly similar in composition to Sergeant Charles Floyd, with a highly similar SI value of 23. SI values this low are within the range of possible SI variation between several APXS measurements on the same rock target, demonstrated by the SI variation between APXS analysis on the same Ysleta Del Sur Outcrop (SI: 40) (Table 3.4).

Table 3.4: Similarity index matricies for selected targets, with SO_3 and Cl included (SI+) and removed (SI-). Values highlighted yellow are highly similar and low enough to be in the same sub-cluster; values highlighted in orange are moderately similar. (Blue) "blue" rocks, without SO_3 and Cl the Marathon Valley "blue" rocks (SCF) are highly similar to the Perseverance Valley tabular "blue" rocks (JDM). (Pink) the silica-rich targets are not similar to any other targets, but the Marathon Valley (SNP) targets are more similar to the Perseverance Valley silica-rich targets than any other targets (Tme, Ald). (Gray) the floor of Spirit of St. Louis (DAH) is as similar to the floor of Perseverance Valley as the they are to each other (Albq, Brn). (Green) the Ysleta Del Sur floor breccia targets (GuJu, AgCl).

SI +	SCF	SNP	DAH	Prl	Albq	Brn	JDM	NuVz	GuJu	AgCl	Tme	Ald
Sgt Charles Floyd RB	0	860	469	350	459	489	344	403	430	413	1609	1014
Sgt Nathaniel Pryor RU		0	1121	1077	1098	1069	1097	1148	1240	1146	1832	451
Donald A Hall RB			0	150	62	32	272	101	92	61	1772	1000
Parral RU				0	89	133	53	35	74	60	1531	982
Albuquerque RU					0	33	183	93	87	49	1682	1016
Bernalillo RU						0	243	104	96	47	1799	982
Jornada Del Muerto RU		0-40	*highly similar*				0	104	158	154	1425	1037
Nueva Vizcaya RU		40-80	*moderately similar*					0	26	29	1584	1017
GuanaJuato RU									0	16	1625	1124
Aguas Calientes RB										0	1671	1043
Tome RU											0	1921
Allende RU												0

SI -	SCF	SNP	DAH	Prl	Albq	Brn	JDM	NuVz	GuJu	AgCl	Tme	Ald
Sgt Charles Floyd RB	0	1197	233	116	231	252	23	76	118	145	2109	1116
Sgt Nathaniel Pryor RU		0	1218	1021	1262	1175	1137	1050	1217	1114	2233	184
Donald A Hall RB			0	208	12	15	211	150	97	114	2372	1132
Parral RU				0	211	228	77	26	87	42	2024	884
Albuquerque RU					0	20	225	148	83	109	2386	1179
Bernalillo RU						0	233	181	120	123	2435	1119
Jornada Del Muerto RU		0-40	*highly similar*				0	57	103	119	2095	1035
Nueva Vizcaya RU		40-80	*moderately similar*					0	55	40	2087	923
GuanaJuato RU									0	40	2192	1127
Aguas Calientes RB										0	2181	968
Tome RU											0	2036
Allende RU												0

3.3.4 Pitted, Silica-Rich Outcrop

In a ~15 m x ~1 m linear outcrop that trends down-valley adjacent to the tabular "blue" rocks (Inde and LaJoya) lies a suite of rocks with a distinct pitted texture (Fig. 3.10i-j) (Bouchard et al., 2019; Farrand et al., 2019; Tait et al., 2019). These rocks are fine grained and have surficial pits that are several centimeters across. The pitted rocks range from "dark blue" to "purple" to "tan" in false color Pancam imagery (Farrand et al., 2019) but are clearly distinct from previous rocks examined by Opportunity according to their texture (Fig. 3.13a). These rocks were analyzed by APXS in two locations (Tome/Nazas sol 5045-53, and Allende, sol 5072); these sites have a roughly aligned planar fabric, implying that they are members of the same outcrop (Tait et al., 2019).

The pitted rocks have relatively high SiO_2 (53.0-62.8 wt%), low FeO and MgO (7.4-8.8 wt%, 4.0-4.7 wt%), and high Al_2O_3 (10.3-15.6 wt%) relative to typical Shoemaker formation rocks. These rocks have among the highest-silica compositions of rocks analyzed by Opportunity; using the total-alkali - silica (TAS) compositional classification, these rocks lie in the andesite field, however, the silica enrichment may represent the addition of a secondary cement not a primary igneous composition, although there does not appear to be a Si-addition trend (Fig. 3.11). The compositions of these rocks are similar to that of Sergeant Nathanial Pryor (51-52 wt.% SiO_2 on a relatively clean, unbrushed surface) analyzed on sol 3959 along the ridge overlooking Marathon Valley and adjacent to "blue" rock Sergeant Charles Floyd.

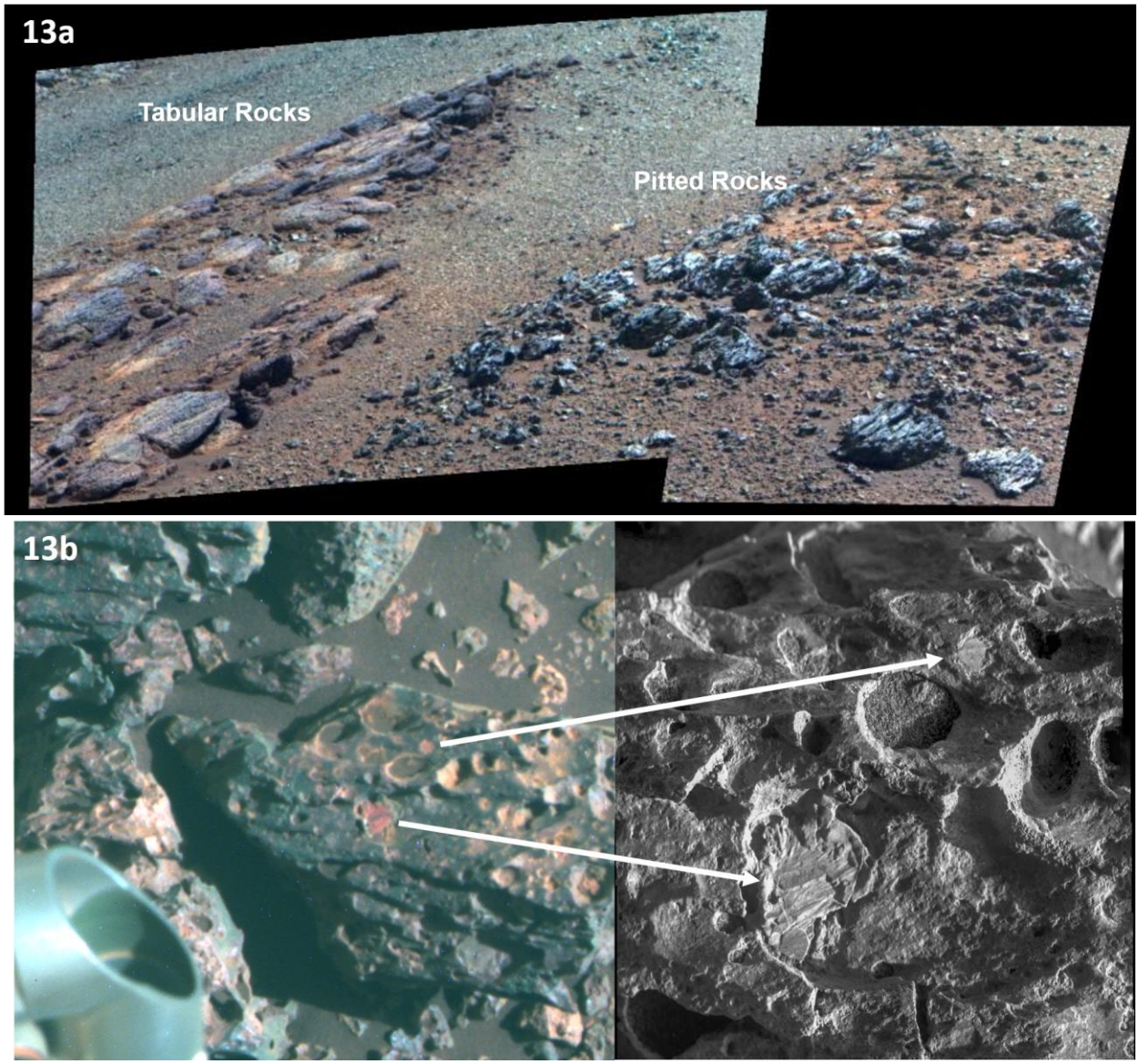

Figure 3.13 (13a) Pitted rocks of Perseverance Valley. 10a shows a false color Pancam image of the linear outcrop of tabular "blue" and pitted high-silica rocks that trend down the valley (left side of image). Image credits: D. Savransky and J. Bell/JPL/NASA/Cornell/ASU (Bell 2003, 2006). (13b) False color Pancam image of the pitted rock APXS target, Nazas with "orange" infill material that may be a zeolite filling a pit, and MI mosaic (~3 cm across, Sol 5053, MI mosaic: Robert Burnham). Pancam image credits: D. Savransky and J. Bell/JPL/NASA/Cornell/ASU (Bell 2003, 2006).

The pitted rocks are genetically confounding. They could be vesicular volcanic evolved basalt, a coarsely vesicular impact melt, or even a pseudotachylite (Tait et al., 2019). A faint lineation is visible in the outcrop, but this may just be the result of wind etching and not a primary pattern in the pits. Spectra extracted from Pancam imagery indicate that the pitted rocks

have a dark coating with a red near-Infrared slope feature consistent with effects of aqueous alteration (Farrand et al., 2019; Tait et al., 2019).

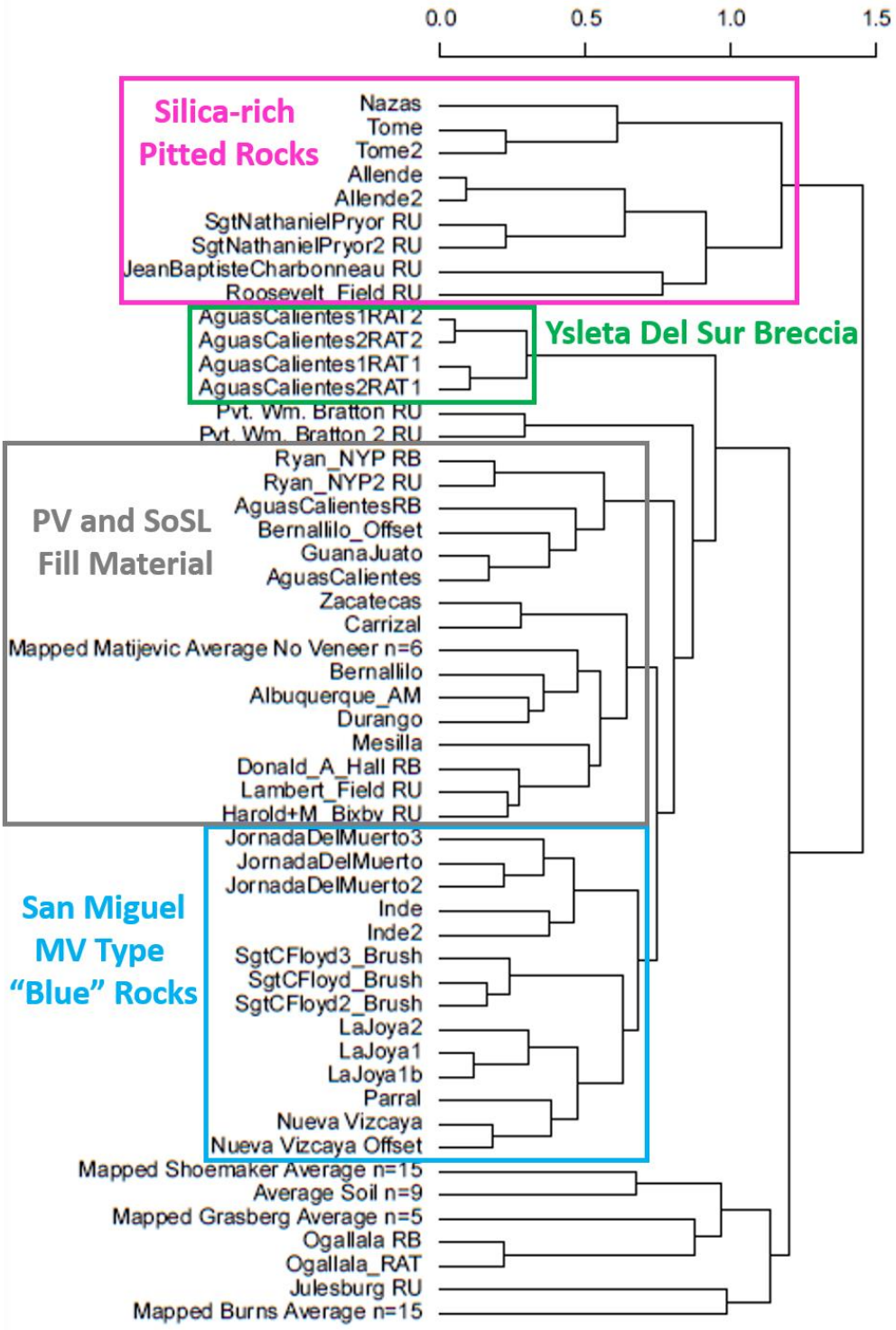

Figure 3.14 Hierarchical cluster of targets in Table 3.1. The silica-rich pitted rocks are the most distinct rock group (pink). The Ysleta Del Sur RATed targets form their own unique sub-cluster (green). The San Miguel Perseverance Valley rocks cluster with the "blue" rock Sgt Charles Floyd (blue), and the Perseverance Valley Trough Floor Fill material clusters with the APXS targets form the interior of the Spirit of St. Louis feature (gray). The Ogallala target clusters with the Grasberg formation average and Julesburg target with the Burns formation average.

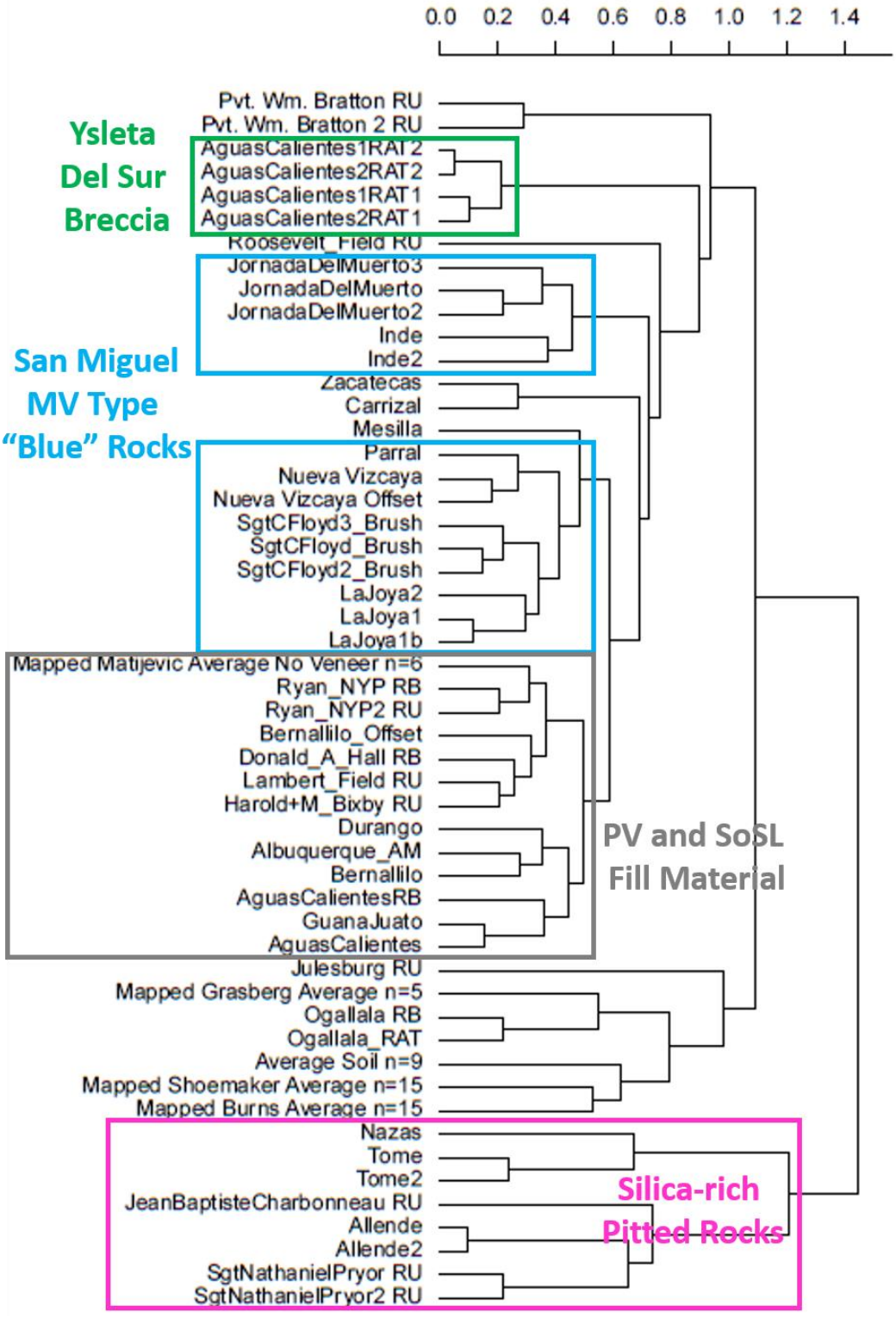

Figure 3.15 Hierarchical cluster of targets in Table 3.1 after SO_3 and Cl have been removed and renormalized. The silica-rich pitted rocks are the most distinct rock group (pink). The Ysleta Del Sur RATed targets form their own unique sub-cluster (green). The San Miguel Perseverance Valley "blue" rocks form two subclusters (blue), and the Perseverance Valley Trough Floor Fill material clusters with the APXS targets form the interior of the Spirit of St. Louis feature (gray). The Ogallala target clusters with the Grasberg formation average and Julesburg target clusters off of a supercluster with the Burns formation average.

There appears to be some form of rind, or filling within some of the vesicles (Fig. 3.13b). In one occurrence, the filling appears "orange" in false color Pancam imagery. The "Nazas" target was an attempt to fill a larger fraction of the APXS integration field-of-view with the features (Tait et al., 2019). The "orange" pit-filling material displays a strong 535 nm band depth indicative of crystalline ferric oxides in Pancam spectra (Tait et al., 2019). These fillings could be a secondary mineral coating, dissolution of lithic clasts, devitrification, or fluid-induced zeolite alteration (Tait et al., 2019). Contact with Opportunity was lost during investigation of this outcrop.

3.4 Discussion

3.4.1 Relationships to Suites Outside of Perseverance Valley

Perseverance Valley shares several similarities with the Spirit of St. Louis feature. The bulk composition of the PV floor fill is more similar to the fill material within SoSL than any other Endeavour crater rim lithology, as shown in the cluster dendrograms in figures 3.14-3.16, both including and excluding sulfur and chlorine. The SI values comparing Marathon Valley floor fill material and Perseverance Valley floor material are highly similar (SI values of 12 and 15, respectively), which are as highly similar as the variation between Perseverance Valley floor targets (SI: 20) (Table 3.4).

Another similarity between the rock suites within Perseverance Valley and the rocks at the Marathon Valley overlook above SoSL are the adjacent occurrences of "blue" and "purple"

rocks. The outcrop overlooking the entrance to Marathon Valley hosts an outcrop of massive "blue" rocks (analyzed at Sergeant Charles Floyd), which lie stratigraphically beneath a pitted "purple" rock unit (analyzed at Sergeant Nathaniel Pryor). On a sulfur- and chlorine-free basis, Sergeant Charles Floyd is compositionally more similar to the San Miguel type "blue" rocks than any other rock lithology at Endeavour crater (Fig. 3.14-3.16). The Sergeant Charles Floyd and Jornada Del Muerto compositions have an SI value of 23, a value that is so low that it falls within the range of SI values that could reflect differences in analyses of the same rock (Table 3.4). The rock units also have similar massive crystalline textures, and while Sergeant Charles Floyd does have minor surface lineations, they are not as defined as those of San Miguel.

Sergeant Nathaniel Pryor is relatively high in silica (51-52 wt.%, RU), but not quite as high as the pitted rocks in Perseverance Valley (52-62 wt.%, RU). The pitted rocks of Marathon Valley and Perseverance Valley differ in composition in Ca, Al, and Si contents, but these differences could be the result of alteration minerals in pits. Sergeant Nathaniel Pryor has a rough, relatively pitted texture, but its pits are smaller than Allende and Tome. Pitting as a result of alteration would support a hypothesis of different erosional and alteration environments. Both sets of pitted rocks are different enough from the rest of the Endeavour crater rim rocks that they cluster together (Fig. 3.14-3.16), and while they have SI values of well over 1,000 compared to other Endeavour crater rim rocks, the most similar SI value is between the Marathon Valley pitted rock Sergeant Nathaniel Pryor and the Perseverance Valley pitted rock Allende (SI: 184) (Table 3.4).

The compositional similarity between the "blue" rocks at these locations and the colocation with the silica-rich pitted rocks could be interpreted as exposure of a block of the same unit as occurs on the overlook that was dropped down by a graben activated along radial

faults. The difference in erosional patterns and alteration minerals could be the result of greater wind- and/or water-related erosion within Perseverance Valley.

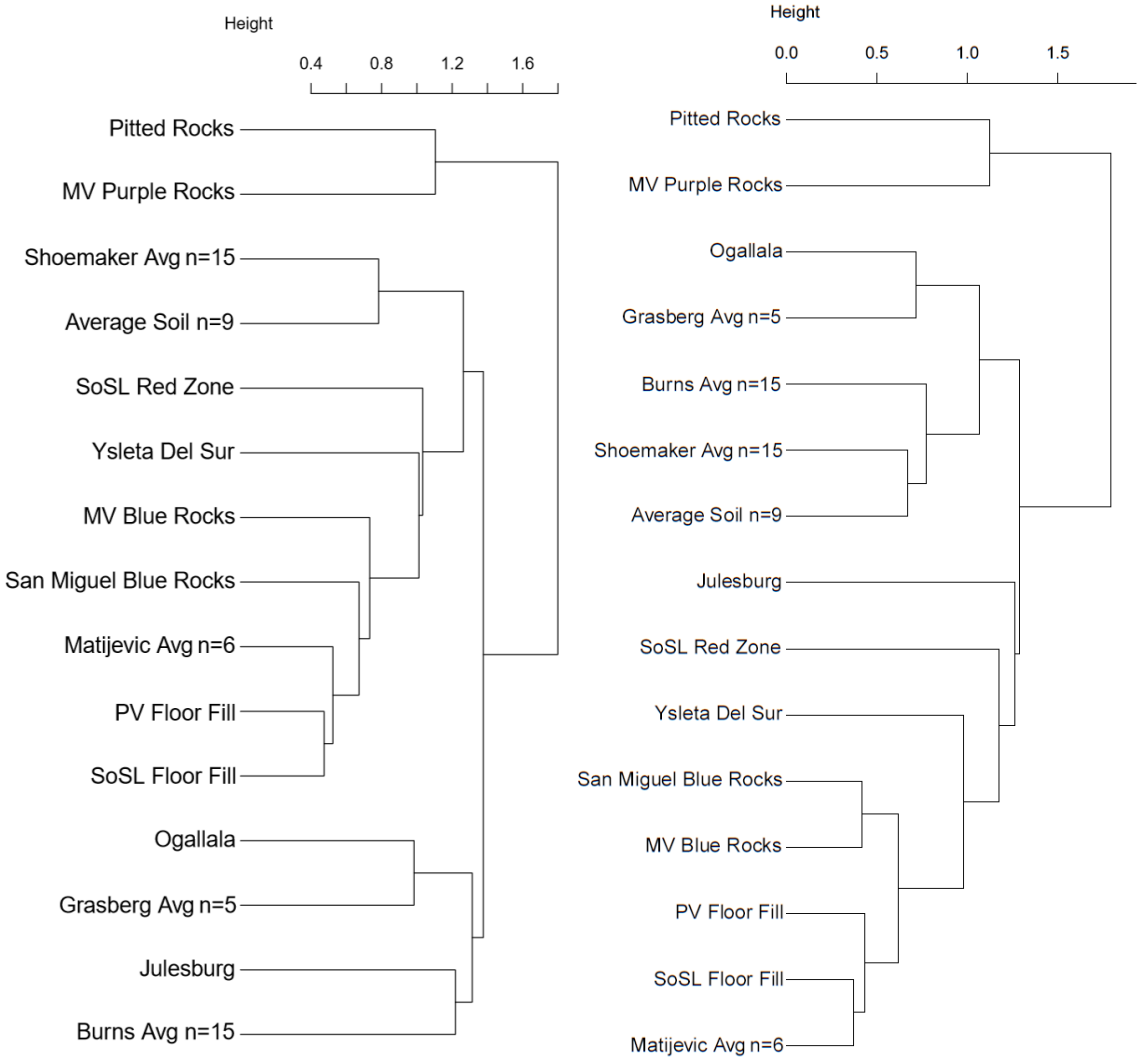

Figure 3.16 Hierarchical cluster of the targets in Table 3.1 averaged into representative groups, with the cluster on the right representing targets after SO_3 and Cl have been removed and renormalized. The silica-rich Perseverance Valley (PV) pitted rocks and Marathon Valley (MV) "purple" rocks are the most dissimilar rock groups in both cases. The San Miguel PV "blue" rocks subclusters with MV "blue" rocks both with and without SO_3 and Cl. The PV floor fill material clusters the Spirit of St. Louis floor fill material in both cases. The Ogallala target clusters with the Grasberg formation in both cases.

Based on cross-cutting relationships we interpret the Spirit of St. Louis feature to be younger than Endeavour crater. It has a smooth elliptical outline marked by an alteration zone (red rocks); such a feature would likely not survive the Endeavour-forming impact event if it existed in these rocks prior to the impact. Thus, according to cross-cutting relationships, we take

both SoSL and Perseverance Valley to be younger than the Endeavour impact event. Moreover, both have "red" alteration zones (Fig. 3.5), indicating fluid-related oxidative alteration post-dating Endeavour crater formation. There are also occurrences of "blue" rocks within both features. These general similarities suggest the possibility that fluid alteration occurred along the fractures in PV and around SoSL, both post-Endeavour, and either post- or syn-formation of the PV and SoSL features.

One working hypothesis is that the SoSL feature is an impact-induced hydrothermal vent. A similarly sized (27 m diameter) circular feature occurs 30-40 meters from the rim of Perseverance Valley named Orion crater (Fig. 3.2). Hydrothermal impact vents are a common occurrence among large impact craters on Earth. Taking Haughton Crater, a 23 km diameter impact crater in the Canadian Artic, as an analog, we might expect there to have been multiple such hydrothermal vents along the rim of Endeavour crater (Abramov & Kring, 2005; Osinski, Lee, Parnell, Spray, & Baron, 2005; Osinski, Spray, & Pascal, 2001). Alternatively, the SoSL feature might represent an alteration zone that formed in association with a thermal pulse surrounding a volcanic pipe (Roosevelt-Field-class blue rock) that passed though the volatile-rich Endeavour ejecta deposits. Either hypothesis, hydrothermal vent or volcanic pipe, cross-cuts the rim and could have acted as a conduit to deliver hot waters to Endeavour's rim, water that could have helped to carve Marathon and Perseverance Valleys.

3.4.2 Perseverance Valley Formation Mechanisms

While the exact formation mechanism for Perseverance Valley is still an open question, observations have been made that can constrain and test the possible mechanisms mentioned in the introduction, as follows.

1) Wind Abrasion: On the basis of HiRise imagery and pre-dust storm solar-panel dust cleaning, Perseverance Valley is subject to active wind erosion. This erosional regime has been active long enough to scour or excavate and form the current valley surface expression. The textures evident on the San Miguel and Ysleta Del Sur outcrops and the Parral cobble all exhibit a uniform up-valley (east to west) wind erosion direction. Elevation modeling shows no slope break where the Grasberg and Burns formations onlap the interior of the crater rim, which would indicate that the current surface has been eroded down to a common level. This erosion also explains the muted topographic difference between the valley trough "walls" and "fill." Whatever formed Perseverance Valley initially, the modern valley is overprinted and dominated by aeolian processes.

2) Aqueous Alteration: Several lines of evidence for aqueous alteration within the neighboring Marathon Valley include; orbital CRISM detections of Fe^{3+}/Mg^{2+} smectites (Fox et al., 2016); Al, Si, and Ge enrichment in "red" zones, indicating local alteration (Mittlefehldt, Gellert, VanBommel, Arvidson, Clark, Ming, et al., 2016), sulfate phases in soil-filled fractures, an enriched vein of Ca and S at the Gasconade target (sol 4509), and enriched Mg and S relative to the average Shoemaker rock, indicating leaching by aqueous alteration (Arvidson et al., 2017).

Orbital evidence for alteration in the form of CRISM detection of smectites, such as observed for Marathon Valley, is lacking for Perseverance Valley, in part owing to its small size compared to CRISM resolution. However, the morphology of Perseverance Valley as seen in HiRISE is distinctly anastomosing and there are in-situ observations that point to local aqueous alteration including (1) a general enrichment in Mg and S relative to the average Shoemaker formation rocks (Fig. 3.11), (2) possible ferric and hydrated materials associated with the pitted rocks by Pancam spectra and potential zeolite minerals filling the pits, and (3) an observed "red"

alteration zone that occurs in association with a fracture that trends parallel to Perseverance Valley as seen in Fig 3.5a. Although not investigated in-situ with the rover, this alteration zone appears very similar in false-color Pancam imagery to the "red" alteration zone examined at the perimeter of the SoSL feature where an enrichment in Si (54-55 wt% SiO_2 compared to adjacent materials with 43-45 wt % SiO_2) and Ge was detected at the Private William Bratton target (sols 4035, 4047, Fig. 3.5b).

There is no direct evidence for a catchment basin west of the remnant crater rim, and the western slope cannot be realistically tilted to accommodate such a basin (Hughes, Arvidson, Grant, Howard, & Wilson, 2017). Since the valley was likely not formed by a basin of water breaching the crater rim, another mechanism must be invoked to supply liquid water to the rim. Possibilities include the following: precipitation, melting of ice collected at the rim, an impact induced hydrothermal system, or a general groundwater seep.

3) Mass Wasting: East-West fractures appear to truncate crater units within the valley, and act as conduits for fluid flow. Structures visible with both satellite and rover imagery support the interpretation that there is a lateral offset across Perseverance Valley, and a radial fault system (Crumpler et al., 2018) (Fig. 3.17). Mass wasting erosion is likely to have occurred, enhanced by aeolian weathering, to cause a leveling of the valley walls and a filling of any troughs in the valley. It is possible that such a radial fault system created a graben, which lowered a segment of the "blue and purple" units of the Marathon Valley overlook to their current location, thus protecting them from erosion (Fig. 3.18). Vertical offset of units is expected along the interior of a complex crater such as Endeavour parallel to the rim strike (Crumpler, Arvidson, Mittlefehldt, Grant, & Farrand, 2019), which would provide another

mechanism to juxtapose a stratigraphically higher set of units with the clast-poor lower Shoemaker member.

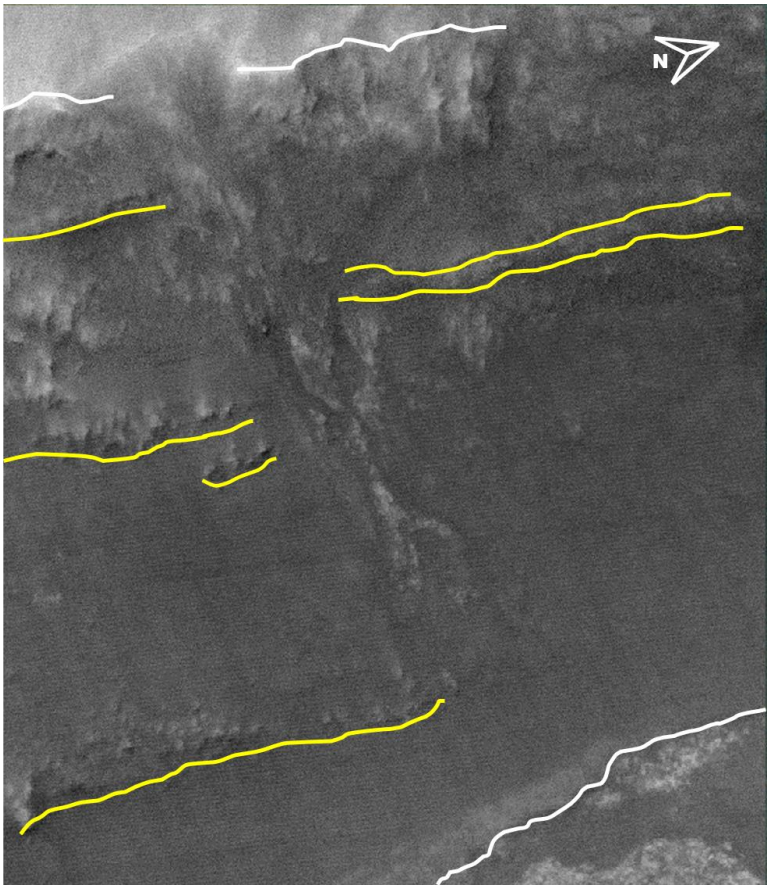

Figure 3.17 HiRISE (Mars Reconnaissance Orbiter) image of Perseverance Valley (ESP_058208_1775_RGBcolor, NASA/JPL/University of Arizona). The approximate remnant Endeavour crater rim (top, white) is broken by the entrance of the valley. Units exposed in the crater wall (yellow) are laterally offset across the valley. The Grasberg bench (bottom, white) appears to be overlying, and thus is younger than the valley.

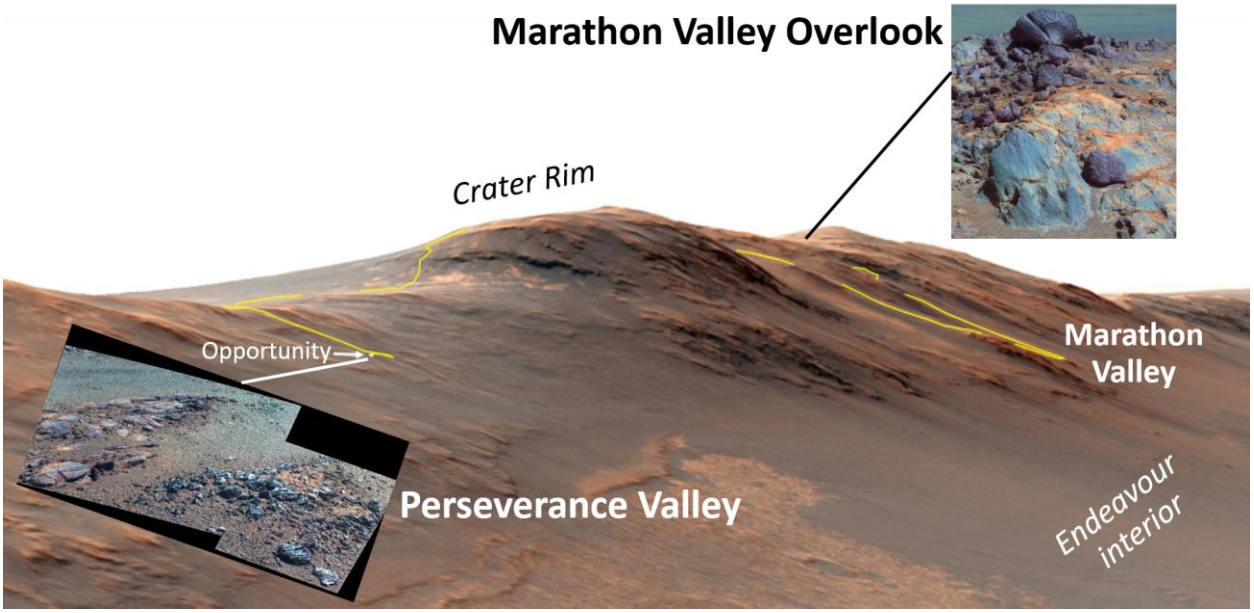

Figure 3.18 Oblique view of western Endeavour crater rim looking ~north-west from within the crater. The yellow line is the traverse path of the Opportunity rover as plotted by Larry Crumpler. There is an outcrop of false color "blue" rocks collocated with pitted silica-rich rocks at both the Marathon Valley overlook, and third the way down Perseverance Valley. The "blue" rock outcrop's compositions are highly similar to each other, and the pitted rock outcrops are both some of the most silica-rich materials examined by Opportunity. The vertical offset between these two locations is ~80 meters. Pancam image credits: D. Savransky and J. Bell/JPL/NASA/Cornell/ASU (Bell 2003, 2006).

3.4.3 Perseverance Valley Formation Model

One possible model for the formation of Perseverance Valley that explains the above observables is as follows: 1) after the Endeavour impact a structurally controlled graben formed along a radial impact fracture, and dropped a segment of "blue" and pitted rocks similar to the layers observed above Marathon Valley (at Sergeant Charles Floyd and Sergeant Nathanial Pryor) ~80 meters down, juxtaposing those units with lower-Shoemaker and Ysleta Del Sur impact breccias; 2) water (potentially from an impact induced hydrothermal system, ice melt, rain fall, or a ground water seep) flowed along the fractured conduits, expanded the vugs of the pitted rocks and depositing vug-filling materials, and formed the "red" oxidative alteration zones along the radial fractures. Perhaps such waters breached the surface episodically, forming surface flow or seeps that carved – or led to weakening of rock – along anastomosing troughs; 3) over time these troughs filled with mass-wasted debris of the "blue" San Miguel rocks, soil, and

Shoemaker breccia; 4) the Grasberg formation formed by further erosion of the Endeavour crater rim, the crater rim further degraded, and the Burns formation embayed the rim and filled in the crater; 5) modern Aeolian erosion has excavated the valley, leveled the slope breaks between units, eroded the breccia walls and trough fill at about the same rate, and etched the more resistant rock units (Ysleta Del Sur, San Miguel, and the pitted rocks) with wind scour features.

These steps occur represent a significant stretch of geologic time, with the initial impact likely occurring over 3.5 billion years ago, but the sequence can be establish by their relative ages and cross cutting and stratigraphic relationships. At some point between 3 and 5 hundreds of meters of the Burns formation are deposited. Volcanic activity could also have occurred in the region across this time frame, including the possible emplacement of the post-Endeavor crater "blue" basalts such as Lindberg mound in Spirit of St. Louis.

3.5 Conclusion

The Opportunity rover explored the upper third of Perseverance Valley, a morphologically intriguing feature that cuts across the rim of the degraded, late-Noachian to early-Hesperian aged, Endeavour crater. Perseverance Valley exhibits the greatest localized lithological diversity of any location examined during the mission since Cape York. The valley has both upper and lower members of the Shoemaker impact breccia formation, a "blue" crystalline basaltic rock, an aggregated valley fill material derived from these lithologies and additional soil, and a relatively silica-rich rock characterized by rough to pitted textures that appears to crop out in within the Valley. Perseverance Valley shares several similarities to the Spirit of St. Louis feature including compositions similar to the Perseverance Valley floor material, "red" alteration zones, and evidence of secondary aqueous alteration. The San-Miguel-

type rocks of the valley are particularly similar to the "blue" rocks examined on the ridge overlooking the entrance to Marathon Valley, an outcrop that was also co-located with a pitted, silica-rich rock. The formation of Perseverance Valley is likely the result of radial impact fractures (that possibly lowered "blue" and pitted rock outcrops to become adjacent to lower shoemaker formation), which served as conduits for fluid flow that led to the alteration of local lithologies and may have helped to create zones of weakness that were easily eroded and subsequently filled by local mass wasting and ultimately excavated by the modern aeolian environment.

Acknowledgements

This investigation would not be possible without the continued work and professionalism of the MER science, engineering, and operations teams (Jet Propulsion Laboratory and participating institutions), especially the APXS, Pancam, and MI teams whose data sets were used in this study, and NASA for their continued support of the MER extended mission. Data utilized in this study are listed in tables with references and we are especially grateful to Dr. Ralf Gellert for providing initial APXS compositions used in this analysis. This work was supported by a NASA Earth and Space Science Fellowship grant number 80NSSC17K0490 (MCB) and subcontract 1536058 through Cornell University and the Jet Propulsion Lab (BLJ).

3.6 References

Abramov, O., & Kring, D. A. (2005). Impact-induced hydrothermal activity on early Mars. *Journal of Geophysical Research, 110*. doi:10.1029/2005JE002453

Arvidson, R. E., Anderson, R. C., Bartlett, P., III, J. F. B., Christensen, P. R., Chu, P., . . . Wilson, J. (2004). Localization and Physical Property Experiments Conducted by Opportunity at Meridiani Planum *Science, 306*(5702), 1730-1733.

Arvidson, R. E., Anderson, R. C., Haldemann, A. F. C., Landis, G. A., Li, R., Lindemann, R. A., . . . Snider, N. O. (2003). Physical properties and localization investigations associated with the 2003 Mars Exploration rovers. *Journal of Geophysical Research, 108*(E12). doi:10.1029/2002JE002041

Arvidson, R. E., Squyres, S. W., Bell III, J. F., Catalano, J. G., Clark, B. C., Crumpler, L. S., . . . Wolff, M. J. (2014). Ancient aqueous environments at Endeavour crater, Mars. *Science, 343*, 441-448. doi:DOI: 10.1126/science.1248097

Arvidson, R. E., Squyres, S. W., Gellert, R., & Team, A. S. (2015). Recent results from the Opportunity rover's exploration of Endeavour crater, Mars. *Lunar and Planetary Science Conference, 46*, 1118.

Arvidson, R. E., Squyres, S. W., Morris, R. V., Knoll, A. H., Gellert, R., Clark, B. C., . . . de Souza, P. A. (2016). High concentrations of manganese and sulfur in deposits on Murray Rodge, Endeavour Crater, Mars. *American Mineralogist, 101*, 1389-1405. doi:10.2138/am-2016-5599

Arvidson, R. E., Squyres, S. W., & Team, A. S. (2017). Recent results from the Opportunity rover's exploration of Endeavour crater, Mars. *Lunar and Planetary Science Conference, 48*, #1149.

Bell, J. F., III, Joseph, J., Sohl-Dickstein, J. N., Arneson, H. M., Johnson, M. J., Lemmon, M. T., & Savransky, D. (2006). In-flight calibration and performance of the Mars Exploration Rover Panoramic Camera (Pancam) instruments. *J. Geophys. Res., 111*(E2), 38. doi:10.1029/2005JE002444

Bell, J. F., III, Squyres, S. W., Herkenhoff, K. E., Maki, J. N., Arneson, H. M., Brown, D., . . . Wadsworth, M. (2003). Mars Exploration Rover Athena Panoramic Camera (Pancam) investigation. *J. Geophys. Res., 108*(E12). doi:10.1029/2003JE002070

Bouchard, M. C., Jollif, B. L., & Farrand, W. H. (2019). Lithochemical Rock Suites of Perseverance Valley, Endeavour Crater, Mars. *Lunar and Planetary Science, 50*.

Bouchard, M. C., & Jolliff, B. L. (2016). Comparing MER Opportunity rock groups and martian meteorites using hierarchical clustering and a similarity index. *Lunar and Planetary Science Conference, 47*, #2551.

Bouchard, M. C., & Jolliff, B. L. (2018a). Rock suites of Endeavour crater, Mars: comparing Perseverance Valley to the floor of Spirit of St. Louis Crater. *Lunar and Planetary Science Conference, 49*, #2590.

Bouchard, M. C., & Jolliff, B. L. (2018b). A systematic method for classifying and grouping late Noachian and early Hesperian rock targets analyzed by the Mars Exploration Rover

Opportunity at Endeavour crater, Mars. *Journal of Geophysical Research: Planets, 123*. doi:10.1029/2018JE005631

Bouchard, M. C., Jolliff, B. L., Farrand, W. H., & Mittlefehldt, D. W. (2017). Constraining the origin of basaltic volcanic rocks by Opportunity along the rim of Endeavour crater. *Lunar and Planetary Science Conference, 48*, #1608.

Clark, B. C., Morris, R. V., McLennan, S. M., Gellert, R., Jolliff, B., Knoll, A., . . . Rieder, R. (2005). Chemistry and mineralogy of outcrops at Meridiani Planum. *Earth and Planetary Science Letters, 240*, 73-94.

Crumpler, L. S., Arvidson, R. E., Bell, J., Clark, B. C., Cohen, B. A., Farrand, W. H., . . . Yen, A. S. (2015). Context of ancient aqueous environments on Mars from in situ geologic mapping at Endeavour Crater. *Journal of Geophysical Research: Planets, 120*, 538-569. doi:10.1002/2014JE004699

Crumpler, L. S., Arvidson, R. E., Farrand, W. H., Grant, J. A., & Mittlefehldt, D. W. (2018). First field examination of the near-surface rim structure on a large impact crater, Opportunity rover, Enveadour crater, Mars. *Geological Society of America Abstracts with Programs, 50*(6). doi:10.1130/abs/2018AM-318088

Crumpler, L. S., Arvidson, R. E., Golombek, M., Grant, J. A., Jollif, B. L., Mittlefehldt, D. W., & Team, A. S. (2017). Rim structure, stratigraphy, and aqueous alteration exposures along Opportunity rover's traverse of the Noachian Endeavour crater. *Lunar and Planetary Science Conference, 48*, 2276.

Crumpler, L. S., Arvidson, R. E., Mittlefehldt, D. W., Grant, J. A., & Farrand, W. H. (2019). In Situ Mapping of the Structural and Stratigraphic Complexities of Endeavour Crater's Rim. *Lunar and Planetary Science, 50*.

Crumpler, L. S., & Team, M. A. S. (2018). In situ mapping of fault-control and regolith diversity at the head of Perseverance Valley, Endeavour Crater, Mars. *Lunar and Planetary Science, 49*, 2205.

Farrand, W. H., Johnson, J. R., Bell III, J. F., Mittlefehldt, D. W., Schröder, C., Tait, A. W., . . . Crumpler, L. S. (2019). Spectral Variability Among Rocks and Soils in Perseverance Valley, Mars as Observed by the Opportunity Pancam. *Lunar and Planetary Science, 50*.

Farrand, W. H., Johnson, J. R., Bell, I. J. F., & Mittlefehldt, D. W. (2016). VNIR multispectral observations of rocks at Spirit of St. Louis crater and Marathon Valley on the rim of Endeavour crater made by the Opportunity rover Pancam. *Lunar and Planetary Science, 47*, #1983.

Fleischer, I., Brückner, J., Schröder, C., Farrand, W., Tréguier, E., Morris, R. V., . . . Cohen, B. A. (2010). Mineralogy and chemistry of cobbles at Meridiani Planum, Mars, investigated by the Mars Exploration Rover Opportunity. *Journal of Geophysical Research: Planets, 115*(E7). doi:10.1029/2010JE003621

Fox, V. K., Arvidson, R. E., Guinness, E. A., McLennan, S. M., Catalano, J. G., Murchie, S. L., & Powell, K. E. (2016). Smectite deposits in Marathon Valley, Endeavour Crater, Mars, identified using CRISM hyperspectral reflectance data. *Geophysical Research Letters, 43*(10), 4885-4892. doi:10.1002/2016gl069108

Fraeman, A. A. (2018). Unraveling the history of Meridiani Planum, Mars: New chemical clues from the rim of Endeavour crater. *Journal of Geophysical Research: Planets, 123*. doi:10.1002/2018JE005535

Gellert, R., Rieder, R., Brückner, J., Clark, B. C., Dreibus, G., Klingelhöfer, G., . . . Squyres, S. W. (2006). Alpha Particle X-Ray Spectrometer (APXS): Results from Gusev crater and calibration report. *Journal of Geophysical Research: Planets, 111*(E02S05), 1-32. doi:10.1029/2005JE002555

Grant, J. A., Parker, T. J., Crumpler, L. S., Wilson, S. A., Golombek, M. P., & Mittlefehldt, D. W. (2016). The degradational history of Endeavour crater, Mars. *Icarus, 280*, 22-36.

Grotzinger, J. P., Arvidson, R. E., Bell III, J. F., Calvin, W., Clark, B. C., Fike, D. A., . . . Watters, W. A. (2005). Stratigraphy and sedimentology of a dry to wet eolian depositional system, Burns formation, Meridiani Planum, Mars. *Earth and Planetary Science Letters, 240*, 11-72.

Herkenhoff, K. E., Squyres, S. W., Bell III, J. F., Maki, J. N., Arneson, H. M., Bertelsen, P., . . . Wadsworth, M. V. (2003). Athena Microscopic Imager investigation. *Journal of Geophysical Research: Planets, 108*(E12), ROV 6-1 - ROV 6-23. doi:10.1029/2003JE002076

Hughes, M. N., Arvidson, R. E., Grant, J. A., Howard, A. D., & Wilson, S. A. (2017). Degradation of Endeavour Crater Based on Orbital and Rover-Observations. *Geological Society of America Abstracts with Programs*, 319-315. doi:10.1130/abs/2017AM-302995

Hughes, M. N., Arvidson, R. E., Grant, J. A., Purdy, S. W., & Howard, A. D. (2018). Degradation of Endeavour Crater based on orbital and rover-based observations in combination with landscape evolution modeling. *Geological Society of America Abstracts with Programs*, 320733. doi:10.1130/abs/2018AM-320733

Hynek, B. M., Arvidson, R. E., & Phillips, R. J. (2002). Geologic setting and origin of Terra Meridiani hematite deposit on Mars. *J. Geophys. Res., 107*(E10), 10.1029/2002JE001891.

McLennan, S. M. (2012). Geochemistry of Sedimentary Processes on Mars. In J. P. Grotzinger & R. E. Milliken (Eds.), *Sedimentary Geology of Mars* (Vol. 102, pp. 119-138): SEPM Spec.

McLennan, S. M., Bell, J. F., III, Calvin, W. M., Christensen, P. R., Clark, B. C., de Souza, P. A., . . . Yen, A. (2005). Provenance and diagenesis of the evaporite-bearing Burns formation, Meridiani Planum, Mars. *Earth and Planetary Science Letters, 240*, 95-121.

McLennan, S. M., & Grotzinger, J. P. (2008). The sedimentary rock cycle of Mars. In J. Bell (Ed.), *The Martian Surface: Composition, Mineralogy and Physical Properties* (pp. 541-577). Cambridge: Cambridge University Press.

McSween Jr., H. Y., Taylor, G. J., & Wyatt, M. B. (2009). Elemental Composition of the Martian Crust. *Science, 324*(736), 736-739. doi:10.1126/science.1165871

Ming, D. W., Morris, R. V., & Clark, B. C. (2008). Aqueous alteration on Mars. In J. Bell (Ed.), *The Martian Surface: Composition, Mineralogy and Physical Properties* (pp. 519-540). Cambridge: Cambridge University Press.

Mittlefehldt, D. W., Crumpler, L. S., Grant, J. A., Arvidson, R. E., & Farrand, W. H. (2018). Noachian-aged pre-impact lithology exposed in Endeavour crater rim: Mars Exploration Rover Opportunity observations. *Geological Society of America Abstracts with Programs, 50*(6). doi:10.1130/abs/2018AM-318037

Mittlefehldt, D. W., Gellert, R., Herkenhoff, K. E., Morris, R. V., Clark, B. C., Cohen, B. A., . . . Team, t. A. S. (2010). Marquette Island: a distinct mafic lithology discovered by Opportunity. *Lunar and Planetary Science Conference, 41*, #2109.

Mittlefehldt, D. W., Gellert, R., VanBommel, S. J., Arvidson, R. E., Clark, B. C., Cohen, B. A., . . . Jollif, B. L. (2016). Localized and areally extensive alteraions in Marathon Valley, Endeavour crater rim, Mars. *Geological Society of America Abstracts with Programs*. doi:10.1130/abs/2016AM-283470

Mittlefehldt, D. W., Gellert, R., VanBommel, S. J., Arvidson, R. E., Clark, B. C., Ming, D. W., . . . Team, A. S. (2016). Alumina+Silica+Germanium alteration in smectite-bearing Marathon Valley, Endeavour crater rim, Mars. *Lunar and Planetary Science Conference, 47*, 2086.

Mittlefehldt, D. W., Gellert, R., VanBommel, S. J., Ming, D. W., Yen, A. S., Clark, B. C., . . . Rice, J. W. (2018). Diverse Lithologies and Alteration Events on the Rim of Noachian-Aged Endeavour Crater, Meridiani Planum, Mars: In-Situ Compositional Evidence. *Journal of Geophysical Research: Planets*(123). doi:10.1002/2017JE005474

Morris, R. V., & Klingelhöfer, G. (2008). Iron mineralogy and aqueous alteration on Mars from the MER Mössbauer spectrometers. In J. Bell (Ed.), *The Martian Surface: Composition, Mineralogy and Physical Properties* (pp. 339-365). Cambridge: Cambridge University Press.

Osinski, G. R., Lee, P., Parnell, J., Spray, J. G., & Baron, M. (2005). A case study of impact-induced hydrothermal activity: The Haughton impact structure, Devon Island, Canadian High Arctic. *Meteoritics & Planetary Science, 40*(12), 1859-1877.

Osinski, G. R., Spray, J. G., & Pascal, L. (2001). Impact-induced hydrothermal activity within the Haughton impact structure, arctic Canada: Generation of a transient, warm, wet oasis. *Meteoritics & Planetary Science, 36*, 731-745.

Parker, T. J., & Golombek, M. P. (2018). Origin of Perseverance Valley by spillover of a small lake. *Lunar and Planetary Science Conference, 49*, 2623.

Squyres, S. W., Arvidson, R. E., Baumgartner, E. T., Bell, J. F., III, Christensen, P. R., Gorevan, S., . . . Romero, R. A. (2003). Athena Mars rover science investigation. *Journal of Geophysical Research, 108*(E12). doi:10.1029/2003JE002121

Squyres, S. W., Arvidson, R. E., Bell III, J. F., Brückner, J., Cabrol, N. A., Calvin, W., . . . Yen, A. (2004). The Opportunity Rover's Athena Science Investigation at Meridiani Planum, Mars *Science, 306*(5702), 1698-1703.

Squyres, S. W., Arvidson, R. E., Bell III, J. F., Clef III, F., Clark, B. C., Cohen, B. A., . . . Zacny, K. (2012). Ancient Impact and Aqueous Processes at Endeavour Crater, Mars. *Science, 336*, 570-576. doi:10.1126/science.1220476

Squyres, S. W., Arvidson, R. E., Golombek, M., Fraeman, A., Lamb, M., Palucis, M., . . . Team, A. S. (2018). Opportunity's exploration of Perseverance Valley. *Lunar and Planetary Science Conference, 49*, 1758.

Squyres, S. W., & Knoll, A. H. (2005). Sedimentary rocks at Meridiani Planum: Origin, diagenesis, and implications for life on Mars. *Earth and Planetary Science Letters, 240*(1), 1-10.

Stein, N. T., Arvidson, R. E., O'Sullivan, J. A., Catalano, J. G., Guinness, E. A., Politte, D. V., . . . VanBommel, S. J. (2018). Retrieval of Compositional End-Members From Mars Exploration Rover Opportunity Observations in a Soil-Filled Fracture in Marathon Valley, Endeavour Crater Rim. *Journal of Geophysical Research: Planets, 123*(1), 278-290. doi:10.1002/2017JE005339

Sullivan, R., Arvidson, R. E., Crumpler, L. S., Herkenhoff, K. E., Hughes, M. N., Golombek, M., . . . Team, A. S. (2019). MER Opportubnity at Perseverance Valley: Evaluation of Multiple Working Hypotheses for Valley Formation. *Lunar and Planetary Science, 50*.

Sullivan, R., Golombek, M., Herkenhoff, K. E., & Team, A. S. (2018). Multiple working hypotheses at Perseverance Valley: Fracture and aeolian abrasion. *Lunar and Planetary Science Conference, 49*, 2516.

Tait, A. W., Schröder, C., Farrand, W. H., Ashley, J. W., Cohen, B. A., Gellert, R., . . . Jollif, B. L. (2019). Exploring Origins of Pitted/Vesicular Rocks in Perseverance Valley, Endeavour Crater. *Lunar and Planetary Science, 50*.

Chapter 4: Lithochemical Diversity of Martian Crustal Materials as Represented by Rover APXS and Martian Meteorite Bulk Chemistry

Abstract

In this study we apply a statistical grouping model to quantify and study the diversity of martian meteorites and rock suites across three discrete landing sites as supplied by in-situ analyses with the Alpha Particle X-Ray Spectrometers of the Spirit, Opportunity, and Curiosity rovers. The statistical model consists of a hierarchical cluster analysis and a multi-element similarity index for comparing compositions. Representative APXS analyses from those missions were selected and averaged to capture the diversity of rock lithologies and erratics at Meridiani Planum, and Endeavour, Gusev, and Gale craters. Published bulk elemental compositions are also averaged to represent the current diversity of martian meteorites.

With the exception of the regolith breccia class, martian meteorites are not representative of significant surface lithologies as analyzed by the rovers. The Gusev crater igneous lithologies form discrete compositional groupings based on geography, pointing to limited weathering and mixing by erosion of local materials. The Gusev basaltic plains are more similar to Endeavor crater than Gale crater protolith materials, and Endeavour and Gusev basalts represent a distinctive mantle trend compared to that of the shergottites. Unlike Gusev, most of the Gale

crater materials do not discriminate along geographic lines, however, the few that do point to a similar sediment source material. Gale crater exhibits at least three discrete primary igneous protolith lithologies, two of which are especially alkaline and unlike Gusev and Endeavour igneous materials. Of the Gale rock classes in this study, the Ronan and Mt. Bastion classes are the most similar to the other rover sites. The Grasberg formation at Endeavour crater is more likely to have been formed from degradation of local Endeavour materials than a distal ash deposit, and the geochemical similarities between a pre-Endeavour, possibly igneous rock type observed as false color "blue" rocks and the pre-Endeavour sedimentary Matijevic formation points to a possible protolith relationships. This class of pre-Endeavour "blue" rocks includes the Meridiani plains float rock, Marquette Island, which was likely a projectile from another large crater younger than the Burns formation. These pre-Endeavour "blue" rocks could be volcanic members of the Noachian cratered terrain underlying the Burns sulfate sandstone plains of Meridiani.

All three sites, at Endeavour, Gusev, and Gale craters, include relatively silica-rich rock units that are the most dissimilar units within each site. The silica-enrichment of these units are a mixture of primary (Gale Buckskin class and Clinton erratic, and the orthopyroxenite and some olivine-phyric shergottite martian meteorites) and secondary enrichments (the Gale Greenhorn class and possibly the Endeavour pitted rocks). Using a SiO_2 vs FeO/MgO compositional classification ratio, these silica-rich materials point to a wet and calc-alkaline igneous source chemistry, and for the rocks with a primary Si enrichment, this ratio could indicate an underrepresented martian magma source.

4.1 Introduction

Since the arrival the Mars Pathfinder lander and Sojourner rover on July 4th 1997, there has been a continual robotic presence at Mars in the form of orbiters, landers, and rovers. These remote robotic explorers have provided one of the most complete data sets about another planet beyond Earth. Mars is considered to be a one-plate, one-rock-type planet, with its surface being dominated by primary volcanic rocks of varying basaltic composition and sedimentary and impact derivatives of basaltic precursor compositions (Bell, 2008; McSween, et al., 2009). One of the best studied populations of martian materials are the meteorites delivered to Earth by impact spallation. These meteorites have been used to extrapolate models of martian mantle and crustal compositions (Balta & McSween, 2013; Balta & McSween, 2013; Liu, et al., 2012; McSween et al., 2009; Udry, et al., 2014). However, it has become increasingly clear that, with the exception of the regolith breccia class, martian meteorites are not representative of the bulk composition of Mars' surface as represented by the robotic data sets (Bouchard & Jolliff, 2018b; McSween et al., 2009).

The Alpha Particle X-Ray Spectrometer (APXS), as carried on the Spirit, Opportunity, and Curiosity rovers, provides a large, diverse data set of bulk elemental compositions across a range of geologic units. This paper considers 153 APXS analyses representing the lithologic diversity of Meridiani Planum, Endeavour, Gusev, and Gale craters, as well as 19 martian meteorite compositions representing the diversity of the martian meteorite population brought together from over 50 published sources (Table 4.1). This dataset was analyzed through a statistical grouping model specifically designed for the APXS instrument precision, which was used to classify rock suites and quantify their similarities (Bouchard & Jolliff, 2018b). Using this model, rock suites and target groupings that are highly similar to each other are averaged into 31

APXS and 8 martian meteorite compositions representative of the lithologic diversity in the preliminary data selection (Tables 4.2 and 4.3, Appendix Figure A4.1 and A4.2). This subset of 38 compositions was again analyzed using the statistical grouping model whose results are presented here. This study seeks to update our description of the diversity of the martian crust, compare primitive and evolved igneous rocks across the martian surface and meteorite populations, compare rock lithologies from three discrete locations on the surface of Mars, and refine our understanding of the martian meteorites as representative samples of the martian crust.

Table 4.1: List of all APXS targets and martian meteorites include in this study, the Sol and location of their analysis, the rock suite they are combined into for cluster figures and similarity index charts, and published sources for compositions. Type denotes rock preparation, either unbrushed (RU), brushed by the RAT/DRT (RB), or ground into by the RAT/DRT (RR).

Rover - Location	Site	Sol / Isotope	Target	Rock Suite	Composition Sources
Martian meteorite	-	-	Chassigny	Chassigny n=2	D'yako 1960, Jeremine 1962, Jerome 1970, McCarthy 1974, Boynton 1976, Burghele 1983, Warren 1987
Martian meteorite	-	-	NWA 2737	Chassigny n=2	Beck 2006
Martian meteorite	-	enriched	ALH 84001	Orthopyroxenite	Gleason 1997, Warren 1997a, Warren 1997b, Warren 1996, Dreibus 1994, Warren 1999, Kong 1999
Martian meteorite	-	-	Nakhla	Nahklite n=2	Dreibus 1982, McCarthy 1974, Prior 1912, Kong 1999
Martian meteorite	-	-	Lafayette	Nahklite n=2	Lodders 1998
Martian meteorite	-	-	NWA 5790/6148	NWA 5790/6148	Janborn 10
Martian meteorite	-	intermediate	EETA 79001 – B	Shergottite basalt n=3	McSween 1983, Burghele 1983, Smith 1984, Laul 1986, Ma 1982, Warren 1997, Warren 1997, Warren 1999
Martian meteorite	-	enriched	Zagami	Shergottite basalt n=3	Easton 1977, Smith 1984, Ma 1982, Haramura 1995, Stolper 1979, McCoy 1992, Barrat 2001
Martian meteorite	-	enriched	Dhofar 378	Shergottite basalt n=3	Ikeda 2006
Martian meteorite	-	enriched	Shergotty	Shergottite cumulate n=3	Dreibus 1982, McCarthy 1974, Jerome 1970, Duke 1968, Laul 1986, Stolper 1979
Martian meteorite	-	enriched	Los Angeles	Shergottite cumulate n=3	Rubin 2000, Jambon 2002
Martian meteorite	-	depleted	Queen Alexandra Range 94201	Shergottite cumulate n=3	Warren 1996, Dreibus 1996, Warren 1997, Warren 1999, Kring 2003
Martian meteorite	-	intermediate	EETA 79001 – A	Shergottite olv phyric n=3	McSween 1983, Burghele 1983, Smith 1984, Laul 1986, Ma 1982, Warren 1997, Kong 1999, Warren 1999, Neal 2001
Martian meteorite	-	enriched	Larkman Nunatak 06319/12011	Shergottite olv phyric n=3	Basu 2009
Martian meteorite	-	depleted	Yamato 980459/980497	Shergottite olv phyric n=3	Haramura (d), Dreibus 2003, Shirai 2004, Greshake 2004

Martian meteorite	-	-	NWA 7475/7034	Regolith Breccia	Wittmann 2015
Martian meteorite	-	intermediate	LEW 88516	Shergottite poikilitic n=3	Dreibus 1992, Warren 1996, Gleason 1997
Martian meteorite	-	intermediate	ALH 77005	Shergottite poikilitic n=3	Dreibus 1992, Jarosewich 1990, Burghele 1983, Haramura 1995, Warren 1999, Kong 1999
Martian meteorite	-	enriched	Roberts Massif 04261/04262	Shergottite poikilitic n=3	Anand 2008
MERA - Guesev Crater	Plains, float near lander	A018 - RU	Adirondack_asis	Plains Basalts n=9	PDS, context in McSween 2004
MERA - Guesev Crater	Plains, float near lander	A033 - RB	Adirondack_brush	Plains Basalts n=9	PDS, context in McSween 2004
MERA - Guesev Crater	Plains, float near lander	A034 - RR	Adirondack_RAT	Plains Basalts n=9	PDS, context in McSween 2004
MERA - Guesev Crater	Plains, float near lander	A055 - RU	Humphrey_Ashley_asis	Plains Basalts n=9	PDS, context in McSween 2004
MERA - Guesev Crater	Plains, float on rim of hollow	A057 - RU	Humphrey_Heyworth_asis	Plains Basalts n=9	PDS, context in McSween 2004
MERA - Guesev Crater	Plains, float on rim of hollow	A058 - RB	Humphrey_brush	Plains Basalts n=9	PDS, context in McSween 2004
MERA - Guesev Crater	Plains, float on rim of hollow	A059 - RR1	Humphrey_RAT1	Plains Basalts n=9	PDS, context in McSween 2004
MERA - Guesev Crater	Plains, float on rim of hollow	A060 - RR2	Humphrey_RAT2	Plains Basalts n=9	PDS, context in McSween 2004
MERA - Guesev Crater	Plains, float on Bonneville crater ejecta	A081 - RB	Mazatzal_NewYork_Brush	Mazatzal n=5	PDS, context in McSween 2004
MERA - Guesev Crater	Plains, float on Bonneville crater ejecta	A081 - RU	Mazatzal_Texas_asisRAT1	Mazatzal n=5	PDS, context in McSween 2004
MERA - Guesev Crater	Plains, float on Bonneville crater ejecta	A082 - RU	Mazatzal_NewYork_RAT1Oregon_ Asis	Mazatzal n=5	PDS, context in McSween 2004
MERA - Guesev Crater	Plains, float on Bonneville crater ejecta	A083 - RU	Mazatzal_Oregon_Asis	Mazatzal n=5	PDS, context in McSween 2004
MERA - Guesev Crater	Plains, float on Bonneville crater ejecta	A086 - RR	Mazatzal_Brooklyn_RAT2	Mazatzal n=5	PDS, context in McSween 2004
MERA - Guesev Crater	Plains	A100 - RB	Route 66	Plains Basalts n=9	PDS, context in Arvidson 2006
MERA - Guesev Crater	West Spur	A172 - RR	Pot of Gold	West Spur n=18	PDS, context in Arvidson 2006
MERA - Guesev Crater	West Spur	A195 - RU	WoolyPatch_Sabre_asis	West Spur n=18	PDS, context in Arvidson 2006
MERA -	West Spur	A197 - RR	WoolyPatch_Sabre_RAT	West Spur	PDS, context in Arvidson 2006

Guesev Crater				n=18	
MERA - Guesev Crater	West Spur	A199 - RR	Woolypatch_Mastodon_RAT	West Spur n=18	PDS, context in Arvidson 2006
MERA - Guesev Crater	West Spur	A214 - RU	Clovis_Plano_asis	West Spur n=18	PDS, context in Arvidson 2006
MERA - Guesev Crater	West Spur	A216 - RB	Clovis_Plano_Brush	West Spur n=18	PDS, context in Arvidson 2006
MERA - Guesev Crater	West Spur	A218 - RR	Clovis_Plano_RAT	West Spur n=18	PDS, context in Arvidson 2006
MERA - Guesev Crater	West Spur	A225 - RB	Clovis_BrushMosaic	West Spur n=18	PDS, context in Arvidson 2006
MERA - Guesev Crater	West Spur	A228 - RU	Ebenezer_TinyTim	West Spur n=18	PDS, context in Arvidson 2006
MERA - Guesev Crater	West Spur	A229 - RU	Ebenezer_Cratchit_asis	West Spur n=18	PDS, context in Arvidson 2006
MERA - Guesev Crater	West Spur	A231 - RB	Ebenezer_brushed	West Spur n=18	PDS, context in Arvidson 2006
MERA - Guesev Crater	West Spur	A232 - RR	Ebenezer_RAT	West Spur n=18	PDS, context in Arvidson 2006
MERA - Guesev Crater	West Spur	A235 - RF	Ebenezer_Fritz_RATgrindings	West Spur n=18	PDS, context in Arvidson 2006
MERA - Guesev Crater	West Spur	A284 - RU	Uchban_Koolik_asis	West Spur n=18	PDS, context in Arvidson 2006
MERA - Guesev Crater	West Spur	A287 - RR	Uchben_Koolik_RAT	West Spur n=18	PDS, context in Arvidson 2006
MERA - Guesev Crater	West Spur	A291 - RB	Uchben_Chiikbes_brush	West Spur n=18	PDS, context in Arvidson 2006
MERA - Guesev Crater	West Spur	A300 - RB	Lutefisk_flatfish_Brushed	West Spur n=18	PDS, context in Arvidson 2006
MERA - Guesev Crater	West Spur	A304 - RB	Lutefisk_RATRoe_brushed	West Spur n=18	PDS, context in Arvidson 2006
MERA - Guesev Crater	Husband Hill	A334 - RB	Wishstone_chisel_brush	Husband Hill n=16	PDS, context in Arvidson 2006
MERA - Guesev Crater	Husband Hill	A335 - RR	Wishstone_chisel_RAT	Husband Hill n=16	PDS, context in Arvidson 2006
MERA - Guesev Crater	Husband Hill	A353 - RU	champagne_asis	Husband Hill n=16	PDS, context in Arvidson 2006
MERA - Guesev Crater	Husband Hill	A355 - RB	champagne_brush	Husband Hill n=16	PDS, context in Arvidson 2006
MERA - Guesev Crater	Husband Hill	A356 - RR1	champagne_RAT1	Husband Hill n=16	PDS, context in Arvidson 2006
MERA - Guesev Crater	Husband Hill	A357 - RR2	champagne_RAT2	Husband Hill n=16	PDS, context in Arvidson 2006
MERA - Guesev Crater	Husband Hill	A377 - RR1	Peace_RAT1	Peace n=2	PDS, context in Arvidson 2006

MERA - Guesev Crater	Husband Hill	A380 - RR2	Peace_RAT2	Peace n=2	PDS, context in Arvidson 2006
MERA - Guesev Crater	Husband Hill	A416 - RB	Watchtower_Joker_Brush	Husband Hill n=16	PDS, context in Arvidson 2006
MERA - Guesev Crater	Husband Hill	A417 - RR	Watchtower_Joker_RAT	Husband Hill n=16	PDS, context in Arvidson 2006
MERA - Guesev Crater	Husband Hill	A469 - RU	Methuselah_Keystone	Husband Hill n=16	PDS, context in Arvidson 2006
MERA - Guesev Crater	Husband Hill	A475 - RB	Methuselah_Pittsburg	Husband Hill n=16	PDS, context in Arvidson 2006
MERA - Guesev Crater	Husband Hill	A484 - RB	Keel/Jibsheet	Husband Hill n=16	PDS, context in Arvidson 2006
MERA - Guesev Crater	Husband Hill	A491 - RU	Paros	Husband Hill n=16	PDS, context in Arvidson 2006
MERA - Guesev Crater	Husband Hill	A495 - RU	Pequod_Ahab	Husband Hill n=16	PDS, context in Arvidson 2006
MERA - Guesev Crater	Husband Hill	A496 - RB	Pequod_Ahab_brushed	Husband Hill n=16	PDS, context in Arvidson 2006
MERA - Guesev Crater	Husband Hill	A502 - SU	Pequod_Doubloon_TG	Husband Hill n=16	PDS, context in Arvidson 2006
MERA - Guesev Crater	Husband Hill	A499 - RB	Pequod_MobyDick	Husband Hill n=16	PDS, context in Arvidson 2006
MERB - Meridiani Plains	Meridiani Planum and Endeavour Crater	- - avg	Average Soil n=9	Average Soil n=9	Average of 9 soil analyses (sols 011, 090, 249, 373, 499, 507, 730, 879, 1918)
MERB - Meridiani Plains	Eagle crater	B36 - RR	Guadalupe	Mapped Burns Average n=15	Rieder et al., 2004, Bouchard and Jolliff 2018
MERB - Meridiani Plains	Outside Eagle crater	B68 - RR	BounceRock Case	Bounce Rock	Rieder et al., 2004
MERB - Meridiani Plains	Endurance crater rim	B108 - RR	LionStone Numa	Mapped Burns Average n=15	Rieder et al., 2004, Bouchard and Jolliff 2018
MERB - Meridiani Plains	Endurance crater wall	B155 - RR	Kettlestone	Mapped Burns Average n=15	Bouchard and Jolliff 2018
MERB - Meridiani Plains	Endurance crater interior	B184 - RR	MacKenzie	Mapped Burns Average n=15	Bouchard and Jolliff 2018
MERB - Meridiani Plains	Plains between Endurance and Erebus	B401 - RB	Gagarin RB	Mapped Burns Average n=15	Bouchard and Jolliff 2018
MERB - Meridiani Plains	Plains between Endurance and Erebus	B403 - RR	Gagarin RR	Mapped Burns Average n=15	Bouchard and Jolliff 2018
MERB - Meridiani Plains	Plains between Endurance and Erebus	B400 - RU	Gagarin RU	Mapped Burns Average n=15	Bouchard and Jolliff 2018
MERB - Meridiani Plains	North of Erebus crater	B642 - CU	Antistasi	Post-E “Blue” n=3	Fleischer et al., 2010

MERB - Meridiani Plains	Victoria crater	B1313 - RB	Steno RB	Mapped Burns Average n=15	Bouchard and Jolliff 2018
MERB - Meridiani Plains	Victoria crater	B1316 - RR	Steno RR	Mapped Burns Average n=15	Bouchard and Jolliff 2018
MERB - Meridiani Plains	Victoria crater	B1311 - RU	Steno RU	Mapped Burns Average n=15	Bouchard and Jolliff 2018
MERB - Meridiani Plains	Plains south of Victoria	B2070 - RB	Marquette PeckBay 1	Marquette n=2	Bouchard and Jolliff 2018
MERB - Meridiani Plains	Plains south of Victoria	B2075 - RB	Marquette IslingtonBay	Marquette n=2	Bouchard and Jolliff 2018
MERB - Meridiani Plains	Plains west of Endeavour crater	B2486 - RB	LuisDeTorres	Mapped Burns Average n=15	Bouchard and Jolliff 2018
MERB - Meridiani Plains	Plains west of Endeavour crater	B2669 - RU	Gibraltar	Mapped Burns Average n=15	Bouchard and Jolliff 2018
MERB - Endeavour crater	Shoemaker ridge	B2696 - RU	Tisdale 2 Timmins 3	Mapped Shoemaker Average n=15	Squyres et al., 2012
MERB - Endeavour crater	Shoemaker ridge	B2701 - RU	Tisdale 2 Shaw 2	Mapped Shoemaker Average n=15	Bouchard and Jolliff 2018
MERB - Endeavour crater	Shoemaker ridge	B2722-2726 - RR	Salisbury 1 (Chester Lake matrix)	Mapped Shoemaker Average n=15	Squyres et al., 2012
MERB - Endeavour crater	Shoemaker ridge	B2734 - RU	Geluk (Chester Lake clast)	Mapped Shoemaker Average n=15	Squyres et al., 2012
MERB - Endeavour crater	Cape York bench	B2771 - RU	Deadwood	Mapped Grasberg Average n=5	Bouchard and Jolliff 2018
MERB - Endeavour crater	Shoemaker ridge	B2787 - RU	Transvaal	Mapped Shoemaker Average n=15	Squyres et al., 2012
MERB - Endeavour crater	Shoemaker ridge	B2801 - RB	Boesmanskop (matrix)	Mapped Shoemaker Average n=15	Squyres et al., 2012
MERB - Endeavour crater	Shoemaker ridge	B2805 - RU	Komati (clast)	Mapped Shoemaker Average n=15	Squyres et al., 2012
MERB - Endeavour crater	Shoemaker ridge	B2834 - RU	Amboy 2	Mapped Shoemaker Average n=15	Bouchard and Jolliff 2018
MERB - Endeavour crater	Shoemaker ridge	B2920 - RU	Amboy 4	Mapped Shoemaker Average n=15	Bouchard and Jolliff 2018
MERB - Endeavour crater	Shoemaker ridge	B2940 - RU	Amboy 12	Mapped Shoemaker Average n=15	Bouchard and Jolliff 2018
MERB - Endeavour crater	Cape York bench	B2995 - RB	Grasberg1	Mapped Grasberg Average n=5	Bouchard and Jolliff 2018
MERB - Endeavour crater	Cape York bench	B3022 - RU	MonsCupri	Mapped Grasberg Average n=5	Bouchard and Jolliff 2018
MERB - Endeavour crater	Cape York-Matijevic Hill	B3067 - RB	Kirkwood 1	Mapped Matijevic Average No Veneer n=6	Bouchard and Jolliff 2018
MERB - Endeavo	Cape York-Matijevic	B3085-87 - RR	Azilda average	Mapped Matijevic	Arvidson et al., 2014

ur crater	Hill			Average No Veneer n=6	
MERB - Endeavour crater	Cape York	B3192 - RU	Ortiz 2 (no veins)	Mapped Matijevic Average No Veneer n=6	Bouchard and Jolliff 2018
MERB - Endeavour crater	Cape York-Matijevic Hill	B3209 - RB	Fullerton 3	Mapped Matijevic Average No Veneer n=6	Bouchard and Jolliff 2018
MERB - Endeavour crater	Cape York-Matijevic Hill	B3214 - RB	Fecunis Lake	Mapped Matijevic Average No Veneer n=6	Bouchard and Jolliff 2018
MERB - Endeavour crater	Cape York-Matijevic Hill	B3253 - RR	Sturgeon River 3 RAT2	Mapped Matijevic Average No Veneer n=6	Bouchard and Jolliff 2018
MERB - Endeavour crater	Botany Bay	B3383 - RR	Black Shoulder RAT	Mapped Burns Average n=15	Bouchard and Jolliff 2018
MERB - Endeavour crater	Cape Tribulation-Solander Point	B3396 - RU	Tickbush 2	Tickbush	Bouchard and Jolliff 2018
MERB - Endeavour crater	Cape Tribulation, Solander Point bench	B3403 - RB	Platypus	Mapped Grasberg Average n=5	Bouchard and Jolliff 2018
MERB - Endeavour crater	Cape Tribulation, Solander Point bench	B3434 - RB	WallyWombat	Mapped Grasberg Average n=5	Bouchard and Jolliff 2018
MERB - Endeavour crater	Cape Tribulation	B3445 - RB	Callitris	Mapped Burns Average n=15	Bouchard and Jolliff 2018
MERB - Endeavour crater	Cape Tribulation, Solander Point, Kangaroo Paw outcrop	B3463 - RB	Spinifex	Mapped Shoemaker Average n=15	Bouchard and Jolliff 2018
MERB - Endeavour crater	Cape Tribulation, Murray ridge	B3542 - RB	CapeElizabeth	Mapped Shoemaker Average n=15	Bouchard and Jolliff 2018
MERB - Endeavour crater	Cape Tribulation, Murray ridge	B3569 - RB	GreenIsland	Mapped Shoemaker Average n=15	Bouchard and Jolliff 2018
MERB - Endeavour crater	Cape Tribulation, Murray ridge	B3598 - RB	TurnagainArm	Mapped Shoemaker Average n=15	Bouchard and Jolliff 2018
MERB - Endeavour crater	Cape Trobulation, Pillinger Point	B3671 - RB	Sarcobatus Flat 1	Mapped Shoemaker Average n=15	Bouchard and Jolliff 2018
MERB - Endeavour crater	West of Cape Tribulation	B3741 - RU	Cape Fairweather	Mapped Burns Average n=15	Bouchard and Jolliff 2018
MERB - Endeavour crater	Cape Tribulation-Wdowiak Ridge	B3796 - RB	Hoover	Hoover	Bouchard and Jolliff 2018
MERB - Endeavo	Cape Tribulation-	B3812 - RB	Margaret Brush	Post-E “Blue” n=3	Bouchard and Jolliff 2018

ur crater	Wdowiak Ridge				
MERB - Endeavour crater	Marathon Valley Overlook	B3951 - RB	SgtCFloyd_Brush	Pre-E “Blue” n=6	MERB Quill, corrected by RG
MERB - Endeavour crater	Marathon Valley Overlook	B3952 - RB	SgtCFloyd2_Brush	Pre-E “Blue” n=6	MERB Quill, corrected by RG
MERB - Endeavour crater	Marathon Valley Overlook	B3953 - RB	SgtCFloyd3_Brush	Pre-E “Blue” n=6	MERB Quill, corrected by RG
MERB - Endeavour crater	Marathon Valley Overlook	B3959 - RU	SgtNathanielPryor RU	Pitted n=7	MERB Quill, corrected by RG
MERB - Endeavour crater	Marathon Valley Overlook	B3961 - RU	SgtNathanielPryor2 RU	Pitted n=7	MERB Quill, corrected by RG
MERB - Endeavour crater	Spirit of St. Louis Crater	B4009 - RU	Roosevelt_Field RU	Post-E “Blue” n=3	MERB Quill, corrected by BLJ
MERB - Endeavour crater	Perseverance Valley	B4979 - RU	JornadaDelMuerto	Pre-E “Blue” n=6	MERB Quill, corrected by MCB
MERB - Endeavour crater	Perseverance Valley	B4984 - RU	JornadaDelMuerto2	Pre-E “Blue” n=6	MERB Quill, corrected by MCB
MERB - Endeavour crater	Perseverance Valley	B4986 - RU	JornadaDelMuerto3	Pre-E “Blue” n=6	MERB Quill, corrected by MCB
MERB - Endeavour crater	Perseverance Valley	B5045 - RU	Tome	Pitted n=7	MERB Quill, corrected by MCB
MERB - Endeavour crater	Perseverance Valley	B5047 - RR	Tome2	Pitted n=7	MERB Quill, corrected by MCB
MERB - Endeavour crater	Perseverance Valley	B5053 - RU	Nazas	Pitted n=7	MERB Quill, corrected by MCB
MERB - Endeavour crater	Perseverance Valley	B5072 - RU	Allende	Pitted n=7	MERB Quill, corrected by MCB
MERB - Endeavour crater	Perseverance Valley	B5073 - RU	Allende2	Pitted n=7	MERB Quill, corrected by MCB
MSL - Gale Crater	Bradbury Group, Yellowknife Bay	C169 - RB	Wernecke (John Klein class)	Wernecke	Tompson et al., 2016
MSL - Gale Crater	Bradbury Group	C323 -	Eqalulik (Bell Island class)	Eqalulik	Tompson et al., 2016
MSL - Gale Crater	Bradbury Group	C399 -	Heimdall (Mt. Bastion class)	Heimdall	Tompson et al., 2016
MSL - Gale Crater	Bradbury Group, Kimberley	C472 -	Oswego (Bathurst class)	Oswego	Tompson et al., 2016
MSL - Gale Crater	Igneous Float	C512 - RP	Clinton (erratic)	Clinton	Tompson et al., 2016
MSL - Gale Crater	Bradbury Group, Kimberley	C550 - RP	Jum Jum (erratic)	Jum Jum	Tompson et al., 2016
MSL - Gale Crater	Bradbury Group	C560 -	Secure (Et Then class)	Secure	Tompson et al., 2016
MSL - Gale	Bradbury Group	C570 - RP	Lowerre (Jake M class)	Lowerre	Tompson et al., 2016

Crater					
MSL - Gale Crater	Bradbury Group	C706 -	Thimble (Rocknest class)	Thimble	Tompson et al., 2016
MSL - Gale Crater	Lower Mount Sharp, Murray? Pahrump Hills?	C809 - RB	Mojave (Confidence Hills class)	Mojave	Tompson et al., 2016
MSL - Gale Crater	Lower Mount Sharp, Murray	C1057 - RB	Buckskin (Buckskin class)	Buckskin	Tompson et al., 2016
MSL - Gale Crater	Lower Mount Sharp, Murray	C1114 - RB	Big Sky (Ronan class)	Big Sky	Tompson et al., 2016
MSL - Gale Crater	Lower Mount Sharp, Murray	C1130 - RB	Greenhorn (Greenhorn class)	Greenhorn	Tompson et al., 2016

Table 4.2: The compositions in oxide weight percentages of the 38 representative targets and averages (representing 149 target compositions) included in this analysis with S and Cl.

Rover	Target/Group Name	SiO_2	TiO_2	Al_2O_3	Cr_2O_3	FeO	MnO	MgO	CaO	Na_2O	K_2O	P_2O_5	SO_3	Cl	SUM
MM	Chassigny n=2	37.19	0.12	0.79	0.84	24.36	0.46	34.50	0.85	0.23	0.06	0.09	0.01	0.00	99.48
MM	Orthopyroxenite	52.42	0.21	1.25	0.78	17.63	0.47	24.80	1.84	0.15	0.02	0.00	0.03	0.00	99.60
MM	Nakhlite n=2	50.12	0.53	6.17	0.12	19.63	0.40	8.47	11.22	2.09	0.45	0.51	0.03	0.00	99.73
MM	NWA 5790/6148	54.60	0.81	14.33	0.00	17.13	0.26	0.44	4.25	5.40	1.10	0.96	0.00	0.00	99.28
MM	Regolith Breccia	48.30	1.00	10.70	0.30	16.60	0.40	10.90	7.00	2.80	0.50	1.29	0.50	0.00	100.29
MM	Shergottite basalt n=3	49.77	1.03	8.94	0.10	18.83	0.48	7.84	10.31	1.63	0.12	0.86	0.17	0.00	100.09
MM	Shergottite cumulate n=3	49.01	1.31	9.69	0.11	19.60	0.48	6.32	10.25	1.75	0.17	1.62	0.12	0.01	100.43
MM	Shergottite olv phyric n=3	48.74	0.67	5.89	0.42	18.87	0.48	16.69	6.85	0.89	0.07	0.51	0.14	0.00	100.22
MM	Shergottite poikilitic n=3	45.58	0.41	2.94	0.69	19.84	0.49	24.66	4.47	0.50	0.08	0.38	0.27	0.00	100.31
MERA	Husband Hill n=16	45.19	2.17	13.49	0.04	12.21	0.22	7.13	7.17	3.85	0.51	3.07	4.03	0.85	99.92
MERA	Plains Basalts n=9	45.74	0.55	10.93	0.61	18.16	0.40	9.36	7.76	2.73	0.15	0.62	2.54	0.41	99.96
MERA	Mazatzal n=5	44.84	0.74	9.44	0.36	18.13	0.36	8.55	6.96	2.80	0.39	0.93	5.56	0.83	99.90
MERA	West Spur n=18	45.35	0.83	9.99	0.18	15.45	0.21	11.81	4.75	2.99	0.31	1.02	5.45	1.51	99.85
MERA	Peace n=2	37.19	0.43	2.52	0.67	19.54	0.44	20.64	5.17	0.19	0.00	0.54	11.76	0.80	99.89
MERB	Average Soil n=9_avg	45.30	1.10	9.00	0.40	19.20	0.40	7.40	7.00	2.20	0.50	0.90	5.80	0.60	99.80
MERB	Matijevic Frm Average n=6	48.80	0.87	10.02	0.28	15.96	0.33	8.13	5.96	2.34	0.36	0.98	4.93	0.89	99.86
MERB	Shoemaker Frm Average n=15	45.20	1.05	9.24	0.22	17.91	0.46	7.83	6.29	2.39	0.48	1.16	6.51	1.09	99.84
MERB	Grasberg Frm Average n=5	45.22	0.98	8.26	0.27	19.24	0.20	5.11	5.98	2.20	0.72	1.11	8.85	1.70	99.84
MERB	Burns Frm Average n=15	38.08	0.78	6.48	0.19	15.94	0.29	7.38	5.48	1.74	0.55	1.03	20.94	1.00	99.89

MERB	Pre-Endv "Blue" n=6	47.80	0.64	12.12	0.27	13.83	0.37	10.05	5.69	2.54	0.27	1.03	3.65	0.79	99.05
MERB	Post-Endv "Blue" n=3	48.37	1.06	12.20	0.19	15.25	0.33	6.75	7.05	2.71	0.42	1.15	3.52	0.44	99.45
MERB	Pitted n=7	55.96	0.67	15.04	0.05	8.54	0.20	4.32	6.52	2.87	0.26	1.23	3.04	0.63	99.33
MERB	Bounce Rock	51.60	0.74	10.48	0.11	14.40	0.40	6.84	12.09	1.66	0.11	0.92	0.56	0.10	100.01
MERB	Tickbush	49.80	1.17	13.97	0.10	13.17	1.20	4.90	7.29	3.10	0.49	1.27	2.67	0.67	99.78
MERB	Hoover	42.20	0.97	7.56	0.22	19.20	0.34	6.54	7.72	2.04	0.54	1.19	9.71	1.61	99.86
MERB	Marquette Island n=2	46.55	0.60	11.88	0.49	16.45	0.36	10.83	5.73	2.47	0.41	0.90	2.81	0.47	99.91
MSL	Lowerre (Jake M)	51.20	0.54	16.20	0.07	11.50	0.20	3.08	5.71	5.40	2.23	0.60	2.10	0.89	99.72
MSL	Oswego (Bathurst)	43.00	0.89	8.00	0.54	22.40	0.50	8.71	6.13	2.70	1.96	0.80	3.30	0.95	99.88
MSL	Jum Jum	46.36	0.81	12.63	0.28	15.53	0.25	4.92	5.14	4.09	3.58	0.62	4.26	1.35	99.82
MSL	Thimble (Rocknest)	47.30	0.66	12.00	0.21	16.90	0.10	6.37	5.23	5.00	2.16	0.70	2.20	0.71	99.54
MSL	Secure (Et Then)	45.40	0.67	8.60	0.05	27.20	0.30	4.03	3.67	4.10	1.47	0.70	3.20	0.64	100.03
MSL	Wernecke (John Klein)	46.90	0.91	8.90	0.41	20.50	0.30	9.80	5.40	3.00	0.62	1.00	0.90	1.13	99.77
MSL	Eqalulik (Bell Island)	42.00	0.85	8.80	0.65	20.60	0.40	8.26	6.54	3.00	0.78	0.80	6.10	1.15	99.93
MSL	Heimdall (Mt. Bastion)	45.80	0.94	10.80	0.19	13.20	0.30	7.17	7.46	3.30	0.97	0.90	7.80	0.97	99.80
MSL	Mojave (Confidence Hills)	51.80	1.07	12.40	0.39	13.50	0.30	4.47	4.29	2.80	0.65	1.40	5.80	0.52	99.39
MSL	Buckskin (Buckskin)	68.10	1.51	6.10	0.10	4.40	0.10	3.45	3.87	2.20	0.82	1.30	7.20	0.71	99.86
MSL	Big Sky (Ronan)	43.40	0.93	9.70	0.42	17.40	0.40	8.52	6.87	2.80	0.47	0.90	6.90	1.27	99.98
MSL	Greenhorn (Greenhorn)	56.20	1.00	5.50	0.34	9.40	0.10	4.77	5.98	2.50	0.44	1.20	10.80	1.54	99.77
MSL	Clinton	53.98	0.35	16.80	0.06	5.73	0.12	3.41	7.16	5.19	1.36	0.61	4.43	0.69	99.89

Table 4.3: The compositions in oxide weight percentages of the 38 representative targets and averages (representing 149 target compositions) included in this analysis with S and Cl removed.

Rover	Target/Group Name	SiO_2	TiO_2	Al_2O_3	Cr_2O_3	FeO	MnO	MgO	CaO	Na_2O	K_2O	P_2O_5	SUM
MM	Chassigny n=2	37.39	0.12	0.79	0.84	24.49	0.46	34.69	0.85	0.23	0.06	0.09	100.00
MM	Orthopyroxenite	52.65	0.21	1.26	0.78	17.71	0.47	24.91	1.85	0.15	0.02	0.00	100.00
MM	Nakhlite n=2	50.27	0.53	6.19	0.12	19.69	0.40	8.50	11.25	2.10	0.45	0.51	100.00
MM	NWA 5790/6148	55.00	0.82	14.43	0.00	17.25	0.26	0.44	4.28	5.44	1.11	0.97	100.00
MM	Regolith Breccia	48.40	1.00	10.72	0.30	16.63	0.40	10.92	7.01	2.81	0.50	1.29	100.00
MM	Shergottite basalt n=3	49.81	1.03	8.94	0.10	18.84	0.48	7.85	10.32	1.63	0.12	0.86	100.00
MM	Shergottite cumulate n=3	48.86	1.30	9.66	0.11	19.54	0.48	6.30	10.22	1.74	0.17	1.61	100.00
MM	Shergottite olv phyric n=3	48.70	0.67	5.89	0.42	18.85	0.48	16.68	6.84	0.89	0.07	0.51	100.00
MM	Shergottite poikilitic n=3	45.57	0.41	2.94	0.69	19.83	0.49	24.65	4.47	0.50	0.08	0.38	100.00
MERA	Husband Hill n=16	47.55	2.28	14.19	0.04	12.85	0.24	7.50	7.54	4.05	0.53	3.23	100.00

MERA	Plains Basalts n=9	47.15	0.57	11.27	0.63	18.72	0.41	9.65	7.99	2.81	0.16	0.64	100.00
MERA	Mazatzal n=5	47.96	0.79	10.09	0.39	19.39	0.39	9.14	7.44	2.99	0.42	1.00	100.00
MERA	West Spur n=18	48.82	0.89	10.76	0.20	16.63	0.22	12.71	5.11	3.22	0.34	1.09	100.00
MERA	Peace n=2	42.58	0.49	2.88	0.77	22.38	0.50	23.63	5.93	0.21	0.00	0.62	100.00
MERB	Average Soil n=9_avg	48.50	1.18	9.64	0.43	20.56	0.43	7.92	7.49	2.36	0.54	0.96	100.00
MERB	Matijevic Frm Average n=6	51.90	0.92	10.66	0.30	16.97	0.35	8.65	6.33	2.49	0.39	1.04	100.00
MERB	Shoemaker Frm Average n=15	49.00	1.14	10.02	0.24	19.42	0.50	8.49	6.82	2.60	0.52	1.26	100.00
MERB	Grasberg Frm Average n=5	50.65	1.10	9.25	0.30	21.55	0.23	5.72	6.70	2.46	0.80	1.24	100.00
MERB	Burns Frm Average n=15	48.86	1.00	8.31	0.24	20.45	0.37	9.47	7.04	2.23	0.71	1.33	100.00
MERB	Pre-Endv “Blue” n=6	50.52	0.68	12.81	0.28	14.62	0.40	10.63	6.02	2.68	0.28	1.09	100.00
MERB	Post-Endv “Blue” n=3	50.65	1.12	12.78	0.20	15.97	0.34	7.07	7.38	2.84	0.44	1.21	100.00
MERB	Pitted n=7	58.49	0.70	15.72	0.05	8.93	0.21	4.52	6.82	3.00	0.27	1.29	100.00
MERB	Bounce Rock	51.94	0.74	10.55	0.11	14.49	0.40	6.88	12.17	1.67	0.11	0.93	100.00
MERB	Tickbush	51.64	1.22	14.48	0.10	13.65	1.24	5.08	7.55	3.21	0.51	1.32	100.00
MERB	Hoover	47.67	1.10	8.54	0.25	21.68	0.39	7.39	8.71	2.31	0.61	1.35	100.00
MERB	Marquette Island n=2	48.17	0.62	12.29	0.50	17.02	0.37	11.20	5.93	2.55	0.42	0.93	100.00
MSL	Lowerre (Jake M)	52.93	0.56	16.75	0.07	11.89	0.21	3.18	5.90	5.58	2.31	0.62	100.00
MSL	Oswego (Bathurst)	44.96	0.93	8.37	0.56	23.42	0.52	9.11	6.41	2.82	2.05	0.84	100.00
MSL	Jum Jum	49.21	0.86	13.41	0.30	16.48	0.27	5.22	5.46	4.34	3.80	0.66	100.00
MSL	Thimble (Rocknest)	48.95	0.68	12.42	0.22	17.49	0.10	6.59	5.41	5.17	2.24	0.72	100.00
MSL	Secure (Et Then)	47.20	0.70	8.94	0.05	28.28	0.31	4.19	3.82	4.26	1.53	0.73	100.00
MSL	Wernecke (John Klein)	47.98	0.93	9.11	0.42	20.97	0.31	10.03	5.52	3.07	0.63	1.02	100.00
MSL	Eqalulik (Bell Island)	45.32	0.92	9.50	0.70	22.23	0.43	8.91	7.06	3.24	0.84	0.86	100.00
MSL	Heimdall (Mt. Bastion)	50.31	1.03	11.86	0.21	14.50	0.33	7.88	8.20	3.63	1.07	0.99	100.00
MSL	Mojave (Confidence Hills)	55.66	1.15	13.32	0.42	14.51	0.32	4.80	4.61	3.01	0.70	1.50	100.00
MSL	Buckskin (Buckskin)	74.06	1.64	6.63	0.11	4.79	0.11	3.75	4.21	2.39	0.89	1.41	100.00
MSL	Big Sky (Ronan)	47.27	1.01	10.57	0.46	18.95	0.44	9.28	7.48	3.05	0.51	0.98	100.00
MSL	Greenhorn (Greenhorn)	64.28	1.14	6.29	0.39	10.75	0.11	5.46	6.84	2.86	0.50	1.37	100.00
MSL	Clinton	56.96	0.37	17.73	0.06	6.05	0.13	3.60	7.56	5.48	1.44	0.64	100.00

4.2 Data & Methods

4.2.1 Data Sets

Every rover sent to the surface of Mars as of the publication of this paper has carried some form of the Alpha Particle X-ray Spectrometer. The first rover, Sojourner, of the 1996

Pathfinder mission, carried an Alpha Proton Spectrometer (APS), a precursor to the APXS (Rieder et al., 1997). Since the APS was not capable of detecting the full range of major rock-forming elements, and so is excluded from this analysis.

The APXS instrument that was used on both the Mars Exploration Rovers (MER) and the Mars Science Laboratory (MSL) utilizes a ^{244}Cm source to bombard a ~4 cm diameter target of soil or rock with alpha particles and x-rays (Gellert et al., 2004; Gellert et al., 2006; Grotzinger et al., 2012; Rieder et al., 2004; Rieder et al., 2003). The resulting x-ray fluorescence and backscattered protons are used to determine the relative abundance of the elemental constituents of the target. These signals can be translated into oxide weight percent abundances of major and minor rock forming oxides (SiO_2, TiO_2, Al_2O_3, Cr_2O_3, FeO, MnO, MgO, CaO, Na_2O, K_2O, P_2O_5, SO_3) and some trace elements (including Cl, Ni, Br, and Zn). This geochemical data set has been used to infer mineralogy and classify rock types, and has been a staple of surface exploration on Mars for over 20 years. To date over 1,450 APXS analysis have been taken with the MER (A: 220, B: 491) and MSL (742 as of April 4th, 2019) APXS. Not only does this represent a valuable, mineable data set for each location, the similarity of the instrumentation provides an ideal opportunity for a cross-site comparison of these data.

The geologic setting of each rover provides insights into different martian surface terrains. The Spirit rover (landed 2004, last contact 2010) landed in Gusev crater to examine layered lake units as observed from orbit (Arvidson, et al., 2004; Arvidson et al., 2008; Arvidson, et al., 2006; Crumpler et al., 2005; McSween et al., 2004; Morris et al., 2004; Squyres, et al., 2004); however, these units proved to be Amazonian aged basaltic lava flows. Ultimately, Spirit did strike aqueous “pay dirt” with the discovery of near pure opaline silica nodules in a

deposit interpreted to be a hydrothermal sinter (Arvidson et al., 2010; 2008; Ruff & Farmer, 2016).

The Opportunity rover (landed 2004, last contact 2018) was sent to Meridiani Planum to investigate a hematite signature observed from orbit (Arvidson, et al., 2003; 2004; Christensen et al., 2000; Squyres et al., 2003; 2004). The signature turned out to be hematite concretions that had weathered out their host rocks and accumulated in surface lag deposits (Arvidson, et al., 2006; Morris, 2006). The host rocks were bedded aeolian sulfate sandstones cemented by playa sourced sulfate cement (Clark et al., 2005; Grotzinger et al., 2005; McLennan et al., 2005; Squyres & Knoll, 2005). The rover began investigating new lithologies upon its arrival at Endeavour crater in 2014. Endeavour is a 22-km diameter crater whose rim exposes rocks older than the late-Noachian, early-Hesperian Burns formation (Arvidson et al., 2014; Crumpler et al., 2015; Squyres et al., 2012). The Curiosity rover (landed 2012, presently active) was sent to Gale crater, a 154 km diameter crater on the hemispherical dichotomy boundary that appears to be host to remnant sedimentary facies from a crater lake (Grotzinger et al., 2012; Grotzinger et al., 2014).

These missions were part of NASA's "follow the water" campaign, with the MER rovers successfully discovering evidence of surface aqueous minerals. MSL's mission expands the campaign to assessing the habitability of a past aqueous environment. Together these missions cover four distinct terrains: Amazonian lava flows, late-Noachian-early-Hesperian playa cemented sulfate sandstones, late Noachian syn-impact and pre-impact units, and an aeolian excavated crater lake. For this paper we have taken a sub-set of relatively soil/dust-free APXS targets representative of the major primary and secondary rock lithologies of each of the three landing sites: Gusev, Meridiani/Endeavour, and Gale (Tables 4.2 and 4.3).

Another extensive geochemical data set of martian materials are the martian meteorites. To date over 200 meteorites (Meyer, 2019) have been identified as coming from Mars (Bogard & Johnson, 1983; Bogard, et al., 1984). These achondrite meteorites were previously grouped into three classes on the basis of age, composition, and mineralogy. The shergottites, nakhlites, and chassignites, or "SNCs," were proven to have originated from Mars by comparing trapped martian atmospheric gases to those measured by Viking (Bogard & Johnson, 1983; Bogard et al., 1984; Lodders, 1998; Owen et al., 1977). The shergottites themselves can be grouped into five classes: basalt, basaltic cumulate, gabbroic, olivine-phyric, and poikilitic (Meyer, 2019). In addition, the oldest meteorite in the collection, ALH 84001, is a unique orthopyroxenite, and there is now a recently discovered class of regolith breccia martian meteorites (Agee et al., 2013; Beck et al., 2015; Cannon, et al., 2015; Humayun et al., 2013; Udry, et al., 2014; Wittmann et al., 2015). The current random sampling of martian materials launched to Earth covers a range of ultra-mafic and mafic mineralogies. To better contextualize the APXS data set a suite of martian meteorites are included in this analysis. Their oxide weight percentages have been derived from various analytical methods and the compositions presented here are averages of published literature compositions (Table 4.1).

4.2.2 Methods

In order to quantify the similarities across representative samples of three rover data sets and the martian meteorite literature we employ a statistical grouping model specifically designed and weighted for the APXS data set (Bouchard & Jolliff, 2016, 2018b). The statistical grouping quantifies similarities between samples on the basis of their oxide weight percentages. The analysis includes hierarchical clustering and a similarity index for one-to-one compositional comparisons.

The selected data are first passed through a hierarchical, group average, agglomerative clustering algorithm. This step builds dendrograms of similar targets with linkages based on the decreasing similarity of groups. This step provides a first look at the diversity of the data and allows us to assess super- and subclusters. The clustering is completed on the data after the dataset has been standardized for variance to reduce the impact of oxides with the greatest absolute range, while maintaining the integrity of the data geometry.

The data set is then passed through a reduced-χ^2, sum-of-squares-of-differences algorithm that is specifically weighted for the error inherent within the APXS instrument on a per-oxide basis. The reduced-χ^2 provides a one-to-one comparison of every composition in the form of a unitless Similarity Index (SI). Smaller SI values indicate more similar compositions, with a perfect match having an SI value of 0. Based on previous model validation using the well-studied Opportunity APXS data set, we have set cutoffs for three levels of similarity: highly similar targets are close enough in composition to be members of the same rock unit (SI values: 0-20), moderately similar targets are close enough in composition to be the same geologic unit with different dust contamination or derived from similar source materials (SI values: 20-40), and weakly similar targets (SI values: 40-60) (Bouchard & Jolliff, 2018b). Dust contamination is an important factor because the compositions represented by the APXS data sets are integrations of the entire field of view of the instrument, so targets that were ground into or brushed off with the Rock Abrasion Tool (RAT) and Dust Removal Tool (DRT) are preferred when available (Grotzinger et al., 2012; Squyres et al., 2003). The model is run initially with the complete 13 major oxides, and then again, with sulfur and chlorine removed and bulk composition normalized to 100 wt.%. The removal of S and Cl permits a comparison between potential unaltered and soil free rock protoliths under the premise that surface alteration of martian surface

materials may be primarily isochemical, with addition of sulfur and chlorine (e.g., as by volcanic gases) (McLennan, 2012; McLennan & Grotzinger, 2008; Ming, et al., 2008; Morris & Klingelhöfer, 2008).

The statistical aspects of this approach have been particularly designed for making comparisons with the APXS data set. Here, we apply it to quantitatively cross-compare the three sites of the rovers, contextualized by comparison to the eight classes of martian meteorites. Finally the rock suites and groupings in this study are compared to several traditional Mars compositional classification schemes for new insights (McSween et al., 2009).

Tables 4.4: The error weighed reduced-χ^2 similarity index of every representative target to every other target in this study. A perfect match has a similarity index value of zero, highly similar targets are 0-20, moderately similar targets are 20-40, and weakly similar targets are 40-60. These indexes were calculated with S and Cl.

Martian meteorite Similarity Index (+)	Chass	Ortho	Nakh	NWA	RegBr	SgBs	SgCm	SgOP	SgPk
MM_Chassigny n=2	0	2061	2155	2662	2387	2357	2483	2234	2226
MM_Orthopyroxenite		0	918	1284	1085	1108	1229	855	727
MM_Nakhlite n=2			0	985	378	192	292	249	595
MM_NWA 5790/6148				0	807	919	1047	874	999
MM_Regolith Breccia					0	146	328	179	326
MM_Shergottite basalt n=3						0	143	116	431
MM_Shergottite cumulate n=3							0	279	627
MM_Shergottite olv phyric n=3								0	175
MM_Shergottite poikilitic n=3									0

Spirit Similarity Index (+)	HH	PB	Maz	WS	Pce
MERA_Husband Hill n=16	0	138	105	130	1292
MERA_Plains Basalts n=9		0	74	173	1205
MERA_Mazatzal n=5			0	74	1072
MERA_West Spur n=18				0	1065
MERA_Peace n=2					0

Opportunity Similarity Index (+)	AvgS	Matj	Shoe	Gras	Brns	Pre-EB	Post-EB	Pitt	BoRk	TkBsh	Hvr	Mrqt
MERB_Average Soil n=9	0	53	18	72	654	102	73	467	459	183	99	88
MERB_Matijevic Average n=6		0	42	107	720	27	40	302	424	110	210	59

MERB_Shoemaker Average n=15			0	45	614	88	97	465	509	192	79	103
MERB_Grasberg Average n=5				0	595	194	180	520	589	270	71	216
MERB_Burns Average n=15					0	777	808	1110	1157	912	474	793
MERB_Pre-Endv "Blue" n=6						0	43	262	418	95	285	30
MERB_Post-Endv "Blue" n=3							0	243	314	49	270	48
MERB_Pitted n=7								0	500	160	696	366
MERB_Bounce Rock									0	311	638	393
MERB_Tickbush										0	384	130
MERB_Hoover											0	288
MERB_Marquette n=2												0

Curiosity Similarity Index (+)	Low	Osw	JJ	Thmb	Scr	Wrnk	Eqlk	Hmdl	Mjv	Bksk	BS	GnHn	Clnt
MSL_Lowerre (Jake M)	0	449	153	174	386	352	524	274	157	1149	421	366	442
MSL_Oswego (Bathurst)		0	158	163	172	176	45	204	364	1356	77	651	931
MSL_JumJum			0	90	173	234	174	100	100	1158	119	379	631
MSL_Thimble (Rocknest 3)				0	188	141	257	206	179	1179	213	457	697
MSL_Secure (Et Then)					0	263	260	382	264	1133	294	688	888
MSL_Wernecke (John Klein)						0	291	325	371	1364	268	646	946
MSL_Eqalulik (Bell Island)							0	149	372	1381	26	604	950
MSL_Heimdall (Mt. Bastion)								0	173	1240	61	289	626
MSL_Mojave (Confidence Hills)									0	967	278	262	559
MSL_Buckskin (Buckskin)										0	1334	911	1082
MSL_Big Sky (Ronan)											0	468	837
MSL_Greenhorn (Greenhorn)												0	506
MSL_Clinton													0

Tables 4.5: The error weighed reduced-χ^2 similarity index of every representative target to every other target in this study. A perfect match has a similarity index value of zero, highly similar targets are 0-20, moderately similar targets are 20-40, and weakly similar targets are 40-60. These indexes were calculated without S and Cl.

Martian meteorite Similarity Index (-)	Chass	Ortho	Nahk	NWA	RgBr	SgBs	SgCm	SgOp	SgPk
MM_Chassigny n=2	0	2337	2447	2744	2452	2469	2503	2340	2284
MM_Orthopyroxenite		0	1085	1116	966	1112	1164	842	604
MM_Nahklite n=2			0	761	130	29	56	127	450
MM_NWA 5790/6148				0	553	684	691	633	787
MM_Regolith Breccia					0	75	90	84	353
MM_Shergottite basalt n=3						0	12	134	492
MM_Shergottite cumulate n=3							0	181	535
MM_Shergottite olv phyric n=3								0	167

MM_Shergottite poikilitic n=3									0

Spirit Similarity Index (-)	HH	PB	Maz	WS	Pce
MERA_Husband Hill n=16	0	119	120	136	627
MERA_Plains Basalts n=9		0	10	93	396
MERA_Mazatzal n=5			0	72	397
MERA_West Spur n=18				0	415
MERA_Peace n=2					0

Opportunity Similarity Index (-)	AvgS	Matj	Shoe	Gras	Brns	Pre-EB	Post-EB	Pitt	BoRk	TkBsh	Hvr	Mrqt
MERB_Average Soil n=9_avg	0	43	7	33	10	91	47	480	141	142	13	54
MERB_Matijevic Average No Veneer n=6_avg		0	24	53	40	23	20	328	133	92	89	33
MERB_Shoemaker Average n=15_avg			0	37	9	59	35	444	149	122	32	33
MERB_Grasberg Average n=5_avg				0	41	128	62	425	181	143	49	102
MERB_Burns Average n=15_avg					0	85	62	503	167	174	24	48
MERB_Pre-Endv “Blue” n=6						0	37	296	159	95	153	22
MERB_Post-Endv “Blue” n=3							0	279	83	44	80	53
MERB_Pitted n=7								0	316	188	541	427
MERB_Bounce Rock									0	103	137	200
MERB_Tickbush										0	180	146
MERB_Hoover											0	105
MERB_Marquette n=2												0

Curiosity Similarity Index (-)	Low	Osw	JJ	Thmb	Scr	Wrnk	Eqlk	Hmdl	Mjv	Bksk	BS	GnHn	Clnt
MSL_Lowerre (Jake M)	0	475	115	203	427	353	428	173	96	1229	320	250	492
MSL_Oswego (Bathurst)		0	168	150	187	46	9	192	357	1489	50	605	1067
MSL_JumJum			0	46	184	96	146	84	71	1283	99	350	732
MSL_Thimble (Rocknest 3)				0	204	88	136	112	129	1305	99	382	801
MSL_Secure (Et Then)					0	164	215	396	285	1271	270	688	1048
MSL_Wernecke (John Klein)						0	43	127	206	1357	38	466	961
MSL_Eqalulik (Bell Island)							0	144	329	1503	24	571	1011
MSL_Heimdall (Mt. Bastion)								0	154	1379	58	267	697
MSL_Mojave (Confidence Hills)									0	1112	238	226	675
MSL_Buckskin (Buckskin)										0	1458	1029	1220
MSL_Big Sky (Ronan)											0	443	896
MSL_Greenhorn (Greenhorn)												0	560
MSL_Clinton													0

4.3 Resulting Rock Suites

4.3.1 Martian Meteorites

The most dissimilar cluster of targets consists of most of the martian meteorites, including the chassignites, orthopyroxenite, and the poikilitic shergottites (Figures 4.1 and 4.2). The only surface rock that groups with these targets is the Peace rock from Gusev. These targets are highly dissimilar to meteorites outside of their class, and collectively are grouped together because of their high dissimilarity to all other surface materials (Tables 4.4 and 4.5).

The nakhlites and the basaltic and cumulate shergottites form a loose super group of their own (Figures 4.1 and 4.2). The olivine-phyric shergottites cluster off of this loose super group. With S and Cl removed from the dataset, the shergottite basalts are highly similar to the cumulates with a SI of 12 and moderately similar to the nakhlites with a SI of 29 (Tables 4.5). This grouping of martian meteorites is more similar to surface rocks analyzed by the rovers than are the other classes of martian meteorites. The Bounce Rock erratic basalt from Meridiani Planum groups with this cluster as well (with and without S and Cl, Tables 4.4 and 4.5). Bounce Rock is dissimilar to almost all targets included in this analysis, but is most similar to the basalt and cumulate shergottites (261-278 with S and Cl, 50-66 without S and Cl, Tables 4.4 and 4.5). The only surface targets that have SI values within these ranges is the Gale Mt. Bastion (Heimdall) target (SI: 58, without S and Cl, Tables 4.5). Bounce Rock's mineralogy and composition has previously been compared to shergottite EETA 79001 lithology B (SI: 14 without S and Cl) (Bouchard & Jolliff, 2018b; Zipfel et al., 2011).

In preliminary analyses the meteorite NWA 5790/6148, which has been classified as a nakhlite (Meyer, 2019), did not group with the other nakhlites, and is more similar to the basalt and cumulate shergottites than to other nakhlites (Tables 4.4 and 4.5). For example, Nakhla and

Lafayette have an SI (without S and Cl) of 69, while NWA 5790/6148 has an SI of 1173 and 1070 when compared to NWA 5790 and 6148, respectively (Tables 4.5). For these reasons NWA 5790/6148 was not included in the nakhlite average and has been kept separate in the clusters and indexing. It is not similar to any of the target or meteorite groups in this analysis and groups with one of the clusters of Gale rocks (with and without S and Cl, Figures 4.1 and 4.2, Tables 4.4 and 4.5).

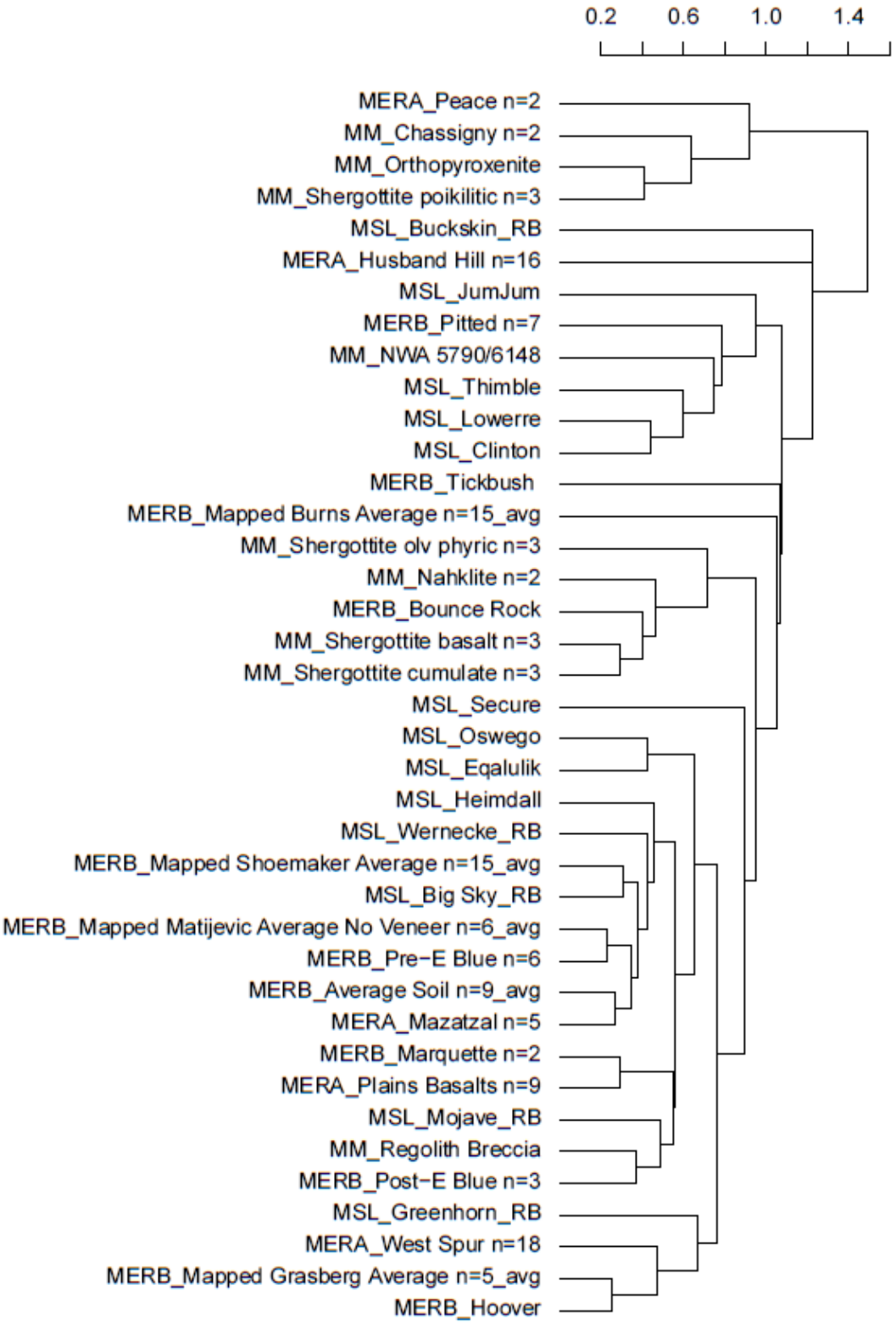

Figure 4.1 This is an agglomerative, group average, hierarchical cluster of the 39 representative targets and averages (representing 149 target compositions) included in this analysis with S and Cl. Compositions are labeled with their rover source (MERA for Spirit, MERB for Opportunity, MSL for Curiosity) or a MM for a martian meteorite. They also have a label for the number of targets that went into the summary (n=x).

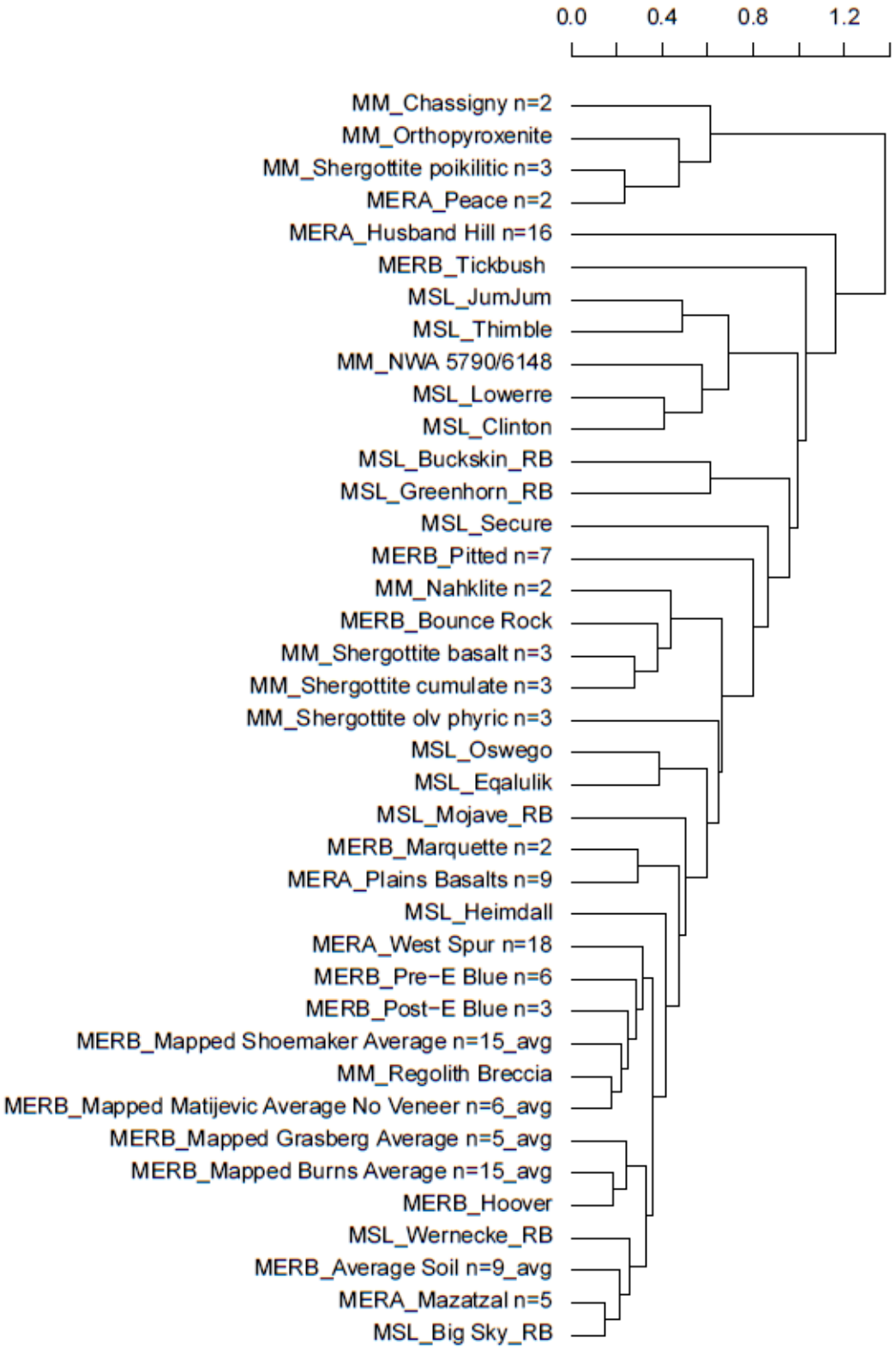

Figure 4.2 This is an agglomerative, group average, hierarchical cluster of the 39 representative targets and averages (representing 149 target compositions) included in this analysis with S and Cl removed. Compositions are labeled with their rover source (MERA for Spirit, MERB for Opportunity, MSL for Curiosity) or a MM for a martian meteorite. They also have a label for the number of targets that went into the summary (n=x).

The regolith breccia class of martian meteorite does not cluster with the other meteorites, instead, with S and Cl, it clusters with the Endeavour "blue," Gale Columbia Hills (Mojave), and Gusev plains basalts, and without S and Cl, it clusters with the Gusev West Spur rocks, and the Endeavour Shoemaker, Matijevic, and "blue" rocks (Figures 4.1 and 4.2). The regolith breccia class is more similar to surface materials than are the martian meteorites (Agee et al., 2013; Bouchard & Jolliff, 2018b; Cannon et al., 2015). The regolith breccia class is moderately similar to the average soil composition, the Endeavour Matijevic formation, Endeavour "blue" rocks, and Endeavour Hoover erratic, the Gusev plains basalts, and the Gale Mt. Bastion (Heimdall) rock class, and is highly similar to the Endeavour Shoemaker formation and Marquette Island rock, the Gusev Mazatzal basalts, and the Gale Ronan (Big Sky) rock class (without S and Cl, Tables 4.4 and 4.5).

4.3.2 Gusev Crater

The rock targets from the Spirit rover representing lithologic diversity of Gusev crater fall into three groupings along geographic lines (Figures 4.1 and 4.2). The 16 rock targets of Husband Hill cluster together, the 18 targets of the West Spur rocks cluster together, and 9 of the rock targets of the plains basalts form a cluster (Appendix Figures A4.1 and A4.2). The Mazatzal plains basalt did not consistently cluster with the other plains basalts so Mazatzal analyses were kept separated in averaged representative compositions (Figures 4.1, 4.2 and Tables 4.4, 4.5).

The Husband Hill targets cluster on their own, away from most of the other surface materials (Figures 4.1 and 4.2) and are the least similar Gusev rock suite to other surface rocks (Tables 4.4 and 4.5). The Husband Hill suite is most similar to the Mt. Bastion (Heimdall) Gale class of rocks (SI: 62 with S and Cl, and 49 without S and Cl, Tables 4.4 and 4.5). With S and Cl included, the West Spur class of Gusev rocks clusters with the Endeavour Grasberg formation

and the erratic Hoover rock, whereas without S and Cl, the group clusters with the Endeavour "blue" rocks, the Matijevic and Shoemaker formations, and the regolith breccia meteorites (Figures 4.1 and 4.2). Although the West Spur targets cluster differently depending on whether S and Cl are included, they cluster not far from the Gusev plains basalts and the Endeavour and Gale suites similar to those basalts. With S and Cl, the West Spur rocks are most similar to the Endeavour crater Shoemaker, Matijevic, and pre-Endeavour class of "blue" rocks (SI: 60, 64, and 65, Tables 4.4). Without S and Cl, the West Spur rocks are still moderately to weakly similar to those same Endeavour rocks (SI: 65, 48, and 34), but are also moderately similar to the Gale John Klein (Wernecke) class of rocks (SI: 39) and are highly similar to the Endeavour erratic Marquette Island (SI: 20, Tables 4.5).

The plains basalts of Gusev are more similar to select Endeavour and Gale rock suites than all other Gusev rocks in this study (Tables 4.4 and 4.5). With S and Cl, the plains basalts cluster with the Endeavour erratic Marquette Island and post-Endeavour "blue" basalts, the Gale Columbia Hills (Mojave) class of rocks, and the regolith breccia martian meteorites (Figure 4.1). Without S and Cl, the plains basalts form a couplet with Marquette Island, and along with the Gale Columbia Hills class (Mojave), branch off of the supercluster that includes the West Spur-Endeavour lithologies supercluster (Figure 4.2). The plains basalt suite is moderately similar to the Marquette Island erratic both with and without S and Cl (SI: 35, and 39, Tables 4.4 and 4.5). Without S and Cl, the plains basalt is moderately to weakly similar to many of the Endeavour lithologies and the Gale Bell Island (Eqalulik) rock class (Tables 4.5). As stated above, Mazatzal does not cluster with the other plains basalt rocks (Figures 4.1 and 4.2). With S and Cl, Mazatzal clusters with several Endeavour (Average Soil, Matijevic, Shoemaker, Pre-Endeavour "blue") and Gale rock suites (Ronan/Big Sky, Mt. Bastion/Heimdall, and John Klein/Wernecke). When S

and Cl are removed Mazatzal still clusters with some of the Gale rock suites (Ronan/Big Sky, and John Klein/Wernecke), and average soil. This subcluster is a member of a supercluster that includes the all four of the Endeavour lithology averages, both "blue" rock classes, the Hoover erratic, the regolith breccia martian meteorite, and the Gusev West Spur rock suite. The Gale Mt. Bastion (Heimdall) class of rocks is an outlier off of this supercluster. With S and Cl, the Mazatzal class of basalts is just as similar (SI: 74) to the West Spur rocks as they are to the other plains basalts; however, when S and Cl are removed Mazatzal is highly similar (SI: 10) to the plains basalts; Mazatzal has about twice as much K, S, and Cl as the other plains basalt rocks, and a lower Al content (Tables 4.2, 4.4 and 4.5).

The Peace rock clast is the most distinct rock composition of the Gusev suites included in this study (Figures 4.1 and 4.2). Both with and without S and Cl, it clusters with the dissimilar martian meteorites (chassignites, orthopyroxenite, and poikilitic shergottites). It is one of the most dissimilar rocks based on the Similarity Index with no values below 1,000 with S and Cl, and, with the exception of the poikilitic shergottites (92), 200 without S and Cl (Tables 4.4 and 4.5).

4.3.3 Gale Crater

This study uses eleven targets representative of eleven classes of Gale bedrock across the Bradbury and Lower Mount Sharp rock groups as reported by Thompson et al. (2016). When multiples of these classes were included in the analysis, they grouped with their classes so only the representative eleven targets were used in this analysis (Appendix Figures A4.1 and A4.2). Also included are two outliers in the APXS dataset, Jum Jum, a breccia-conglomerate with relatively high Na, Al, Si and low Fe and Mg and exceptionally high K for Gale rocks (Thompson et al., 2016), and Clinton, an igneous erratic basalt rock analyzed with the APXS

(Edwards et al., 2017). The Gale rocks are predominately sedimentary facies and do not group neatly according to geography like the Gusev basalts and also exhibit a greater range of compositions than the other rover sites (Figures 4.1 and 4.2).

There is one supercluster of Gale targets (Bradbury supercluster) that has the same members both with and without S and Cl; it includes the Rocknest (Thimble) and Jake M (Lowe) classes of bedrock as well as the Clinton and Jum Jum erratics, and the martian meteorite NWA 5970/6148 (Figures 4.1 and 4.2). With S and Cl, this "Bradbury supercluster," so named because it includes only Gale targets from the Bradbury group, also includes the Endeavour Si-rich pitted rock suite (Figure 4.1). The pitted rocks of Endeavour are relatively silica-rich for Mars (56 wt% SiO_2). Some of the targets in this super cluster also have a relative silica-enrichment: Lowerre (51 wt% SiO_2), Clinton (54 wt% SiO_2), and NWA 5790/6148 (55 wt% SiO_2). The pitted rocks also have a higher Al_2O_3 content (15 wt% Al_2O_3), similar to the others in the super cluster (12-17 wt% Al_2O_3), which are themselves higher than other Gale rocks (6-12 wt% Al_2O_3). These Gale rocks are predominately sedimentary rocks, but their protolith composition is likely more evolved than the other representative Gale targets. The supercluster is a loose grouping with the targets only slightly more similar to each other than they are to the other surface targets (Tables 4.4 and 5). With S and Cl included, Jum Jum is most similar to the Endeavour Matijevic, Shoemaker, and Grasberg formations, and "blue" rocks (SI: 61-94), as well as the Gale Thimble target (SI: 90, Tables 4.4). Without S and Cl, Jum Jum is still most similar to the same Endeavour rocks (SI: 53-79), but is moderately similar to Thimble (SI: 46, Tables 4.5). Clinton is dissimilar to all other targets in this analysis, but is most similar to the Pitted rocks both with (SI: 251) and without S and Cl (SI: 298, Tables 4.4 and 4.5).

The Lower Mount Sharp Gale targets mostly cluster with the Endeavour rocks, the plains basalts and West Spur rocks of Gusev crater, and several of the remaining Bradbury Group Gale classes (Figures 4.1 and 4.2). With S and Cl, the Ronan (Big Sky) and the Bradbury Group John Klein (Wernecke) and Mt. Bastion (Heimdall) targets form a subcluster with the Pre-Endeavour "blue" rocks, the Endeavour Shoemaker and Matijevic averages, average soil, and the Gusev Mazatzal basalts, while the Columbia Hills (Mojave) Gale class forms a subcluster with the Gusev plains basalt, the Pre-Endeavour "blue" rocks, and the regolith breccia martian meteorite (Figure 4.1). Off of these clusters branches the Bathurst (Oswego) and Bell Island (Eqalulik) Gale classes of rocks. Off of that supercluster is another cluster that includes the Greenhorn Gale class of bedrock with the West Spur Gusev rocks and the Hoover erratic. This collection of subclusters forms a supercluster, and off of that is the Et Then (Secure) class of Gale rocks. The Buckskin Gale rock class is unlike all other surface rocks and branches off of the linkage between the Husband Hill Gusev rocks and the other surface rocks. Buckskin is highly dissimilar to all of the targets included in this study with a SI >900 both with and without S and Cl (Tables 4.4 and 4.5). The other Gale targets are more similar to the surface rocks than Buckskin, but with the exception of Big Sky (highly similar to the average Shoemaker and Mazatzal basalts, moderately similar to average soil and Eqalulik, and weakly similar to the Hoover erratic), Heimdall (weakly similar to Mazatzal, and the Shoemaker average), and Eqalulik (weakly similar to Mazatzal, Oswego, and the Hoover erratic), they are not even weakly similar to those surface rocks (Tables 4.4 and 4.5). These values become more similar when the highly variable S (1-11 wt%) is normalized out (Tables 4.4 and 4.5).

Without S and Cl, the Ronan (Big Sky) and John Klein (Wernecke) class of Gale bedrock cluster with the average soil and Gusev Mazatzal rocks (Figure 4.2). Big Sky is highly similar to

Mazatzal and the plains basalts (SI: 2, 8) the martian meteorite regolith breccia (SI: 15), and the Endeavour average soil and average Shoemaker lithology (SI: 10, 12, Tables 4.5). It is also moderately similar to the Wernecke and Eqalulik Gale targets (SI: 38, 24). Wernecke is moderately similar to the Endeavour Shoemaker average (SI: 27), the average soil (SI: 37), the Marquette Island erratic and Mazatzal Gusev basalt (SI: 33, 33), and the Gusev West Spur rocks (SI: 39). Without S and Cl, off of that subcluster is a subcluster with the Endeavour Grasberg and Burns formation averages, and the Hoover erratic, and then another subcluster with the Gusev West Spur targets, the regolith martian meteorite breccia, and the rest of the Endeavour rock suites sans the pitted rocks (Figure 4.2). Branching off of these three subclusters is the Mt. Bastion class (Heimdall) of Gale rocks. Heimdall is highly similar to the post-Endeavour "blue" rocks (SI: 12) and moderately similar to the regolith breccia (SI: 37) and the Endeavour Matijevic average (SI: 39, Tables 4.5). Off of that supercluster and a grouping of the Gusev plains basalts and the Marquette Island erratic is the Confidence Hills (Mojave) Gale class, and then a couplet of the Bathurst (Oswego) and Bell Island (Eqalulik) classes. Oswego and Eqalulik are highly similar to each other (SI: 9). The only other targets to which Eqalulik is moderately similar are: Big Sky (SI: 24), the Mazatzal basalts (SI: 29), the average soil (SI: 32), the Gusev plains basalts (SI: 36), and the Hoover erratic (SI: 38). Oswego is not moderately similar, and Mojave is not weakly similar to any other targets (Tables 4.5). The Et Then (Secure) class of Gale rocks is an outlier off of the previously described supercluster of nakhlites and shergottites (Figure 4.2). Secure is even less similar to other surface targets than Oswego and Mojave (Tables 4.5). Without S and Cl, the Lower Mount Sharp classes Buckskin and Greenhorn branch off of Secure. Greenhorn is likewise dissimilar to the targets in this study, but not as dissimilar as Buckskin with a lowest SI value of 1029.

4.3.4 Endeavour Crater and Meridiani Planum

The Opportunity rover targets are reduced to rock formation averages and erratic outliers. This includes an average of the Meridiani Planum sulfate sandstones of the Burns formation, the impact breccia of the Shoemaker formation, the Matijevic formation, a pre-Endeavour impact lithologic group, , the post-Endeavour sedimentary lithology of the Grasberg formation, and an average of Meridiani soil (Bouchard & Jolliff, 2018b; Crumpler et al., 2015; Mittlefehldt, et al., 2018; Squyres et al., 2012). Also included are two groupings of fine-grained basaltic "blue" rocks grouped into pre-Endeavour and post-Endeavour impact groups, an average of pitted silica-rich rocks, and a collection of erratic crystalline rocks analyzed across the traverse (Bouchard, et al., 2019; Bouchard & Jolliff, 2018a, 2018b; Bouchard, et al., 2017).

With S and Cl, the average Shoemaker formation, Matijevic formation, soil, and pre-Endeavour class of "blue" rocks cluster with the Gusev Mazatzal basalt, and the Gale Ronan (Big Sky), John Klein (Wernecke), and Mt. Bastion (Heimdall) classes of rocks (Figure 4.1). The post-Endeavour "blue" class and Marquette Island erratic cluster with the Gale Columbia Hills class, the other Gusev plains basalts, and the regolith breccia martian meteorite (Figure 4.1). These two subclusters form a supercluster with several other Bradbury group Gale classes and a subcluster with Gusev West Spur, and the Endeavour Grasberg formation average and Hoover erratic. The Tickbush erratic and the Meridiani sulfate sandstone of the Burns formation are (unrelated) outliers of this supercluster. The only Endeavour target not within this supercluster are the Bounce Rock erratic, which groups with the shergottite/nakhlite supercluster, and the pitted class of rocks, which group off of a cluster with the Rocknest (Thimble) and Jake M (Lowerre) class of Gale rocks and the Clinton float (Figure 4.1).

With S and Cl included, the average soil is highly similar to the Gusev Mazatzal basalt (SI: 8) and the Shoemaker formation average (SI: 18), moderately similar to the Gale Ronan class (Big Sky, SI: 38), and weakly similar to the Matijevic formation average (SI: 53, Tables 4.4). The pre-Endeavour Matijevic formation average is moderately similar to both the pre- and post-Endeavor "blue" rock classes (SI: 27, SI: 40), and is weakly similar to the Shoemaker formation average (SI: 42), the Gusev Mazatzal basalts (SI: 47), and the Marquette Island erratic (SI: 59). The Shoemaker impact breccia formation is also highly similar to the Gusev Mazatzal basalts (SI: 11) and the Gale Ronan class (Big Sky SI: 18), and is weakly similar to the Grasberg formation (SI: 45) and the Gale Mt. Bastion class (Heimdall SI: 53, Tables 4.4). The post-Endeavour clastic Grasberg formation is only weakly similar to the Shoemaker formation from which it may be, at least in part, an erosional sediment (Bouchard & Jolliff, 2018b). The pre- and post-Endeavour "blue" rocks are weakly similar to each other when S and Cl are included (Tables 4.4). The pre-Endeavour "blue" rocks are moderately similar to the Marquette Island erratic (SI: 30), while the post-Endeavour class is weakly similar to Marquette Island (SI: 48), the Tickbush erratic (SI: 49), and the Gusev plains basalts (SI: 56). The sulfate sandstones of Meridiani Planum, the Burns formation, and the silica-rich pitted rocks are expectedly highly dissimilar to all other targets in this study (SI: 400-2600 & SI: 200-2900 respectively, Tables 4.4). Other than noted above, the Bounce Rock and Tickbush erratics are highly dissimilar to the rest of the targets in this study (Tables 4.4). The Hoover erratic is moderately similar to the Bell Island and Ronan classes of Gale rocks (Eqalulik SI: 42, Big Sky SI: 42). Of the erratics the Marquette Island rock is the most similar to other Endeavour rocks, specifically the pre-Endeavour "blue" rocks, and it is also moderately similar to the Gusev plains basalts (SI: 35).

When S and Cl are removed, the Grasberg, Burns, and soil average form a subcluster with the Hoover erratic, the Gusev Mazatzal basalt, and the Gale Ronan (Big Sky) and John Klein (Wernecke) classes of Gale rocks (Figure 4.2). The Matijevic and Shoemaker average form a neighboring subcluster with both of the Endeavour "blue" classes, the regolith breccia martian meteorite, and the Gusev West Spur class of rocks. Off of this supercluster branches the Gale Mt. Bastion (Heimdall) class, and then the Gusev plains basalt and Marquette Island erratic. The Bounce Rock erratic still groups with the same martian meteorites, and the pitted silica-rich rocks still branch off all of those clusters. The Tickbush erratic is the greatest outlier of the Endeavour targets (Figure 4.2).

When S and Cl are removed, some of the martian meteorite targets become more similar to the Meridiani/Endeavour surface targets (Tables 4.5). When S and Cl is removed, the regolith breccia class of martian meteorite becomes highly similar to the Marquette Island erratic (SI: 14) and the Shoemaker impact breccia formation (SI: 18), moderately similar to the Matijevic formation (SI: 27) and the pre-Endeavour "blue" rocks (SI: 28), and weakly similar to the post-Endeavour "blue" rocks (SI: 34) and the average Meridiani soil (SI 34, Tables 4.5). The Hoover erratic is moderately similar to the shergottite cumulates (SI: 24) and the shergottite basalts (SI: 33), and weakly similar to the nakhlites (SI: 59). The only other martian meteorites similar to Endeavour rocks are the shergottite basalts which, along with the shergottite cumulates, are weakly similar to the average soil (SI: 42 and SI: 42, Tables 4.5). The shergottite basalts are also weakly similar to the Bounce Rock erratic (SI: 50), and the Shoemaker formation average (SI: 57). The average soil is highly similar to the Shoemaker average (SI: 7) and the Hoover erratic (SI: 13), moderately similar to the Grasberg average (SI: 33), and weakly similar to the Matijevic average (SI: 43), the post-Endeavour "blue" rocks (SI: 47) and the Marquette Island erratic (SI:

54). The average soil is also highly to weakly similar to many targets beyond Endeavour craters as detailed in sections above (Tables 4.5).

Without S and Cl, the pre-Endeavour Matijevic formation average is moderately similar to the post-and pre-Endeavour "blue" rocks (SI: 20, SI: 35), the Shoemaker formation average (SI: 24), the Marquette Island erratic (SI: 33), as well as the Gusev Mazatzal basalt (SI: 39) and the Mt. Bastion class of Gale rocks (Heimdall, SI: 39). The Shoemaker formation is also highly similar to the Gusev Mazatzal basalt (SI: 8) and the Ronan class of Gale rocks (SI: 12), moderately similar to the Matijevic formation (SI: 24), the John Klein class of Gale rocks (Wernecke SI: 27), the Gusev plains basalts (SI: 30), the Hoover and Marquette Island erratics (SI: 32 and SI: 33), and the post-Endeavour "blue" rocks, and is weakly similar to other Endeavour and Gale rock classes (Tables 4.5). The clastic Grasberg formation is still most similar to the Shoemaker formation (SI: 37), and is weakly similar to the Hoover erratic (SI: 49) and the Gusev Mazatzal basalt (SI: 52). The pre- and post-Endeavour "blue" rocks are moderately similar to each other (SI: 37), but are both more similar to the pre-Endeavour Matijevic formation (SI: 23 and SI: 20, Tables 4.5). The post-Endeavour "blue" rocks are highly similar to the Mt. Bastion class of Gale rock (SI: 12), and are weakly similar to the Marquette Island erratic (SI: 53), the Gusev Mazatzal basalts (SI: 44), plains basalts (SI: 57) and Husband Hill rocks (SI: 59), and the Gale Ronan class (Big Sky SI: 47) and Jum Jum erratic (SI: 53). The pre-Endeavour "blue" rocks are much more similar to the Marquette Island erratic (SI: 22), and are moderately similar to the John Klein class of Gale rocks (Wernecke SI: 34), and weakly similar to the Mt. Bastion Gale rock class (Heimdall SI: 43).

Other than noted above, the Bounce Rock and Tickbush erratics are still dissimilar to all other targets with the exception of being weakly similar to the Mt. Bastion class of Gale rocks

(Heimdall SI: 58 and 51 respectively, Tables 4.5). The Hoover erratic is moderately similar to the Gusev Mazatzal basalt (SI: 23), the Ronan and Mt. Bastion classes of Gale rocks (SI: 28 and SI: 38), and the Gusev plains basalts (SI: 40). The Marquette Island erratic is highly similar to the Gusev West Spur rocks (SI: 20), and is moderately similar to the Gale Ronan and Mt. Bastion rock classes (SI: 31 and SI: 33) and the Gusev Mazatzal and other plains basalts (SI 32 and SI: 39). The silica-rich pitted rocks are as highly dissimilar to all other targets (SI: 120-2900) as expected (Tables 4.5). Sulfur is such an important component (average of 21 oxide wt%) of the sulfate sandstones of the Burns formation we won't read much into the S and Cl removed SI values.

4.4 Discussion

4.4.1 Martian Meteorites

To the first order this data set is unlike the surface data set, which does not contain ultra-mafic components, and a few rock suites can even be described as andesitic. With the noted exceptions described below, the martian meteorite collection is not a representative sampling of general martian surface materials. As expected, the chassignites and ALH 84001 were the most dissimilar martian materials, clustering at the farthest branch away of the other materials; however, it was surprising that the poikilitic shergottites (LEW 88516, ALH 77005, Roberts Massif 04261/04262) are also as dissimilar and do not cluster with the other shergottite materials (Figures 4.1 and 4.2). The poikilitic class of meteorites has significantly more MgO (22-28 oxide wt%) and less Al_2O_3 (~3 oxide wt%) than the other shergottites, values that are more similar to the chassignites and the orthopyroxenite. Poikilitic shergottites represent more than 20% of the martian meteorite population and have been interpreted as gabbroic intrusive rocks (McSween,

2015; Rahib, et al., 2018). This study groups them with other intrusive martian meteorite rocks and indicates that although they are a significant fraction of the meteorite population, they do not represent a significant component of martian surface materials.

Indigenous S and Cl are very low in concentration in martian meteorites (<0.5 wt% among those meteorites for which they been measured). When S and Cl are removed, the basalt and cumulate shergottite compositions are weakly similar to several surface materials including average soil (SI: 42), the Endeavour Shoemaker formation (SI:57-60), the Gusev Mazatzal and plains basalts (SI: 48-54, and 51-61), the Endeavour erratic Bounce Rock (SI: 50-66), and the Ronan class of Gale rocks (SI: 55-59, Tables 4.5). The Bounce Rock-basalt shergottite relationship has previously been documented (Zipfel et al., 2011). The basalt and cumulate shergottites are highly similar to each other (SI: 12) and moderately similar to the Endeavour Hoover erratic (SI: 33-24).

One martian meteorite class that is consistently and highly similar to surface materials is the paired regolith breccia group NWA 7034/7475/7533 (Agee et al., 2013; Beck et al., 2015; Cannon et al., 2015; Humayun et al., 2013; Udry et al., 2014; Wittmann et al., 2015). In this and previous studies the regolith breccia meteorites cluster and index with Endeavour materials (Bouchard & Jolliff, 2018b). When S and Cl are removed, it is especially similar to the Marquette Island “blue” erratic, the Mazatzal Gusev basalt, the Shoemaker and Matijevic formation rocks, and both classes of Endeavour “blue” rocks (SI: 14, 16, 19, 27, 28-34, Tables 4.5). It is also highly and moderately similar to the Ronan (SI: 15) and Mt. Bastion classes of Gale rocks, respectively (SI: 37). The regolith breccia class is the best representation of the martian surface in the martian meteorite collection.

The nakhlites are set of clinopyroxenites and three compositions were included in this study. Two of the nakhlites (Nakhla and Lafayette) cluster together and are averaged to represent the nakhlite class composition in this study. The nakhlite average branches off of the cluster that includes the Bounce Rock erratic and the cumulate and basalts shergottites, both with and without S and Cl (Figures 4.1 and 4.2), and they have a moderately and weakly similar SI value to the basalt and cumulate shergottite average, respectively (SI: 29, 56). These similarities separate the nakhlites from the other cumulate rocks martian meteorite population. The third nakhlite, NWA 5790/6148, segregates in both cluster and SI analysis (Figures 4.1 and 4.2, Tables 4.4 and 4.5). It has a highly dissimilar SI value to the other nakhlites (SI: 553-985). Also the other nakhlites have a mineralogy dominated by pyroxene (74-85 volume %), olivine (5-16 volume %), and mesostasis (5-11 volume %) in Nakhla and pyroxene (69-84 volume %), olivine (7-20 volume %), and mesostasis (9-11 volume %) in Lafayette (Lentz, Taylor, & Treiman, 1999), compared to pyroxene (51 volume %), olivine (9 volume %), and mesostasis (40 volume %) and minor magnetite, tridymite, Na-plagioclase, K-feldspar, and ilmenite in NWA 5790 (Jambon et al., 2010). The separation of this meteorite from the other clinopyroxenites reflects that the nakhlites are not as compositionally homogeneous as other martian meteorite groups. This analysis did include, and track, enriched, intermediate, and depleted isotope values for each meteorite class where available, and in this comparison of bulk compositions there was no noticeable discrimination of target relationships along isotopic lines.

4.4.2 Gusev Crater

The Gusev rock suite compositions neatly segregate along geographic lines into three groups, the plains basalts, the West Spur rocks, and the Husband Hill rocks. Of the three groups the Husband Hill group is the most unique suite, clustering as an outlier from the rest of the

surface materials both with and with S and Cl, with a higher average SI, and are only weakly similar to the Mt. Bastion class of Gale rocks (SI: 62 with S and Cl, 48 without, Figures 4.1 and 4.2, Tables 4.4 and 4.5). The Husband Hill rocks are on the north-west flank of one of the Columbia Hills segments explored by Spirit and are characterized by a relative enrichment in P and Ti (Arvidson, et al., 2006). West Spur rocks are the oldest unit explored by Sprit, the first unit encountered of the Columbia Hills, and are granular sedimentary rocks that may represent a mixture of the olivine bearing plains unit cemented together (Arvidson, et al., 2006). The West Spur rocks are more similar to the surface materials than other Gusev materials, clustering with Endeavour lithologies, and are also weakly similar to the average Shoemaker formation and Matijevic formation compositions (SI: 60-65, 64-48), but without S and Cl, the West Spur rocks are more similar to the Marquette Island erratic, the Pre-Endeavour class of "blue" rocks, and the John Klein class of Gale rocks (SI: 20, 34, 39, Tables 4.4 and 4.5).

The plains rocks of Gusev crater are olivine-bearing basalts (Including Humphrey, Adirondack, and Route 66 (Arvidson, et al., 2006; McSween et al., 2004). They cluster with the Marquette Island erratic (SI: 35-39) and other Endeavour crater lithologies such as the basaltic "blue" rocks (Figures 4.1 and 4.2). However, the Mazatzal basalt of the Gusev plains is even more similar to the Endeavour rocks, and so has been selected for further study in this analysis (Tables 4.4 and 4.5). With S and Cl included, Mazatzal is highly similar to the average Meridiani soil and the Endeavour Shoemaker formation (SI: 8 and 11), but not the Marquette Island erratic (SI: 78). When S and Cl are removed, the plains basalts become moderately similar to the average soil and Shoemaker formation (SI: 23 and 30), but are still not as highly similar as Mazatzal (SI: 6 and 8). Overall when S and Cl are removed, the plains basalts are more similar to the Endeavour rock lithologies than most of the Gale rocks, martian meteorites, and other Gusev

rocks with the exception of Mazatzal (Tables 4.4 and 4.5). With S and Cl included, Mazatzal is the only Gusev rock to be highly (SI: 19, Ronan class) and weakly similar (SI: 53-59, Bell Island and Mt. Bastion class) to Gale rocks. Both Mazatzal and the other plains basalts are still highly similar to the Ronan class of Gale rocks (SI: 8, and 2). Of the Gusev rocks Mazatzal is most similar to the other plains basalts but has a dissimilar SI of 74 with S and Cl included. This SI becomes highly similar (SI: 10) when S and Cl are removed, indicating that the factor of two enrichment in both S and Cl in Mazatzal accounts for these differences. Since Adirondack, Humphrey, and Mazatzal all have brushed and RAT-ground APXS measurements, this discrepancy is more than a shallow surface coating or alteration feature.

Of the 50 Gusev rock APXS target compositions included in this analysis, the two RAT ground analyses that represent the Peace rock are extreme outliers and cluster with the cumulate martian meteorites both and without S and Cl (Figures 4.1 and 4.2). The Peace rock is also one of the most dissimilar rocks in this study with a similarity index of 1016-1919 with S and Cl, and 242-2286 without S and Cl, with the single exception of the poikilitic shergottites (SI: 92, Tables 4.4 and 4.5). While the Peace class has iron bearing phases similar to the plains basalts among which it is located, it is enriched in S, Cl, Br, and magnetite relative to those rocks (Arvidson, et al., 2006; Squyres et al., 2006). Peace is also depleted in Si, Al, Na, and K relative to the plains basalts and has been indicated to be similar to the ultramafic cumulate lherzolite martian meteorites (Ming et al., 2006). The Peace class of rocks is interpreted as a layered sandstone composed of ultramafic sand, cemented by Mg- and Ca-sulfates potentially precipitated in an evaporative environment (Squyres et al., 2006). While the dissimilar composition, known mineralogy, and proposed origin precludes the interpretation of the Peace class as a cumulate

rock similar to martian meteorites, it does explain why this unique target clusters with the cumulate martian materials.

4.4.3 Gale Crater

Unlike the Gusev targets the Gale targets in this study are not neatly segregate based on geography, likely due to the predominately and diverse sedimentary nature of these rocks. The Gale targets include 11 representative samples of Gale rock classes of across the Bradbury and Lower Mt. Sharp formations, and two outlier erratics (Jum Jum and Clinton).

There is a loosely similar supercluster of Bradbury group targets that are collectively unlike other surface materials (Figures 4.1 and 4.2). This grouping includes the Jake M (Lowerre) and Rocknest (Thimble) classes of Gale rocks as well as the Jum Jum and Clinton outliers. Jake M is a class of dark and fine-grained float rocks with a pitted surface texture that may be a sedimentary rock with minimal processing and thus representative of its original igneous composition which plots as basaltic trachyandesite, trachyandesite, and phonotephrite fields in the TAS diagram (Schmidt et al., 2014; Stolper et al., 2013). The Rocknest targets have compositions that are intermediate between Jake M and John Klein rocks, but Rocknest is distinctly a sedimentary unit that may represent a mechanical mixture of Jake M and typical martian basalt material, an interpretation that is supported by this classification (Thompson et al., 2016). Jum Jum represents the Point Columb breccia conglomerate member of the Kimberly formation and could be classified as a Mt. Bastion class rock based on major element chemistry, but it has one of the highest K concentrations of Gale rocks, which more consistent with the Bathurst class of rocks (Thompson et al., 2016). However, based on both cluster analysis and SI classification of bulk chemistry, Jum Jum is the most similar to the Rocknest class of rocks (SI: 46-90 with and without S and Cl, Tables 4.4 and 4.5). None of these targets are weakly similar to

any other surface rocks in this study and cluster together based on their mutual dissimilarity. Additionally, the Lowerre, Thimble and Jum Jum targets are mostly more similar to each other than to any other targets (SI: 90-174 with S and Cl, 46-168 without S and Cl).

Clinton is an erratic float analyzed on the Gusev plains, is classified as a trachybasalt (Mg#: 27), and based on ChemCam analyses, is one of two endmember classes of igneous float rocks in Gale (Edwards et al., 2017). Both are interpreted as low-pressure, olivine-dominated fractionation of an Adirondack composition basalt (Edwards et al., 2017). Clinton clusters with the Gale targets as described above, but is one of the most dissimilar targets in this study (SI: 251-3247 with S and Cl, SI: 298-3293, without, Tables 4.4 and 4.5). Clinton is very dissimilar to the Jake M class of Gale igneous rocks (SI: 442 with S and Cl, and 492 without). Clinton and Jake M represent very different primary igneous lithologies collected within the Gale basin, and neither are similar to the basalt units of Gusev or Endeavour craters or the shergottite meteorites.

The Lower Mount Sharp Gale rock classes Ronan (Big Sky) and Confidence Hills (Mojave) cluster within the Endeavour/Mazatzal/Gusev plains basalts supercluster, and with the Bradbury classes Mt. Bastion (Heimdall) and John Klein (Wernecke, with and without S and Cl, Tables 4.4 and 4.5).

The Mt. Bastion class of coarse-grained sedimentary rocks are compositional intermediate between, and hypothesized to be a mixture of, John Klein composition sand and Jake M composition pebbles (Thompson et al., 2016). The Mt. Bastion target Heimdall is highly similar to the pre-Endeavour “blue” rocks, and moderately similar to the Endeavour Matijevic formation and the martian meteorite regolith breccia (Tables 4.4 and 4.5). The John Klein class of Gale rocks are mudstones that were examined at Yellow Knife Bay, and are determined to not have extensive open system alteration from their basaltic protolith (McLennan et al., 2014).

Without S and Cl, the John Klein target Wernecke is moderately to weakly similar to Endeavour rocks, excluding the Hoover and Bounce Rock erratics and the pitted rocks (SI: 23-90). The coarse and cross-bedded sandstone of the Lower Mt. Sharp class of Ronan rocks are compositionally similar to the John Klein rocks and are even more similar to Endeavour rocks, excluding the Hoover and Tickbush erratics and the pitted rocks (SI: 7-71 without S and Cl, (Thompson et al., 2016)). These relationships suggest a broad similarity between the protolith materials of the John Klein Gale and Endeavour basaltic materials. The Big Sky target of the Ronan class is also highly similar to Mazatzal and other Gusev plains basalts (SI: 2-8 without S and Cl), indicating a higher similarity between the Gusev basalt and Gale John Klein precursor basalts.

The Bathurst (Oswego) and Bell Island (Eqalulik) classes group together off of this supercluster (with and without S and Cl, Figures 4.1 and 4.2). These two classes are weakly similar to each other with S and Cl (SI: 45), and highly similar without (SI: 9, Tables 4.4 and 4.5). The Bathurst inlet is an exposure of sandstone bedrock that was encountered on the traverse towards Yellowknife Bay while Bell Island is a silt/sandstone also located near Yellowknife Bay (Thompson et al., 2016). These target's highly similar chemistry and geography indicate a likely common pre-digenetic source material. The Bradbury class, Et Then (Secure), is an outlier of these groups, and this vuggy float rock is dissimilar to all other targets in this study (Figures and 4.1 and 4.2, and Tables 4.4 and 4.5).

The Greenhorn class clusters with the Gusev West Spur rocks with S and Cl, and as a dissimilar pair with Buckskin without S and Cl (Figures 4.1 and 4.2). Each of these classes are highly dissimilar to all of the meteorite and other surface materials, but Buckskin is one of the most extreme outliers of the surface rocks in this study (SI: >900, Tables 4.4 and 4.5). The

Lower Mt. Sharp Buckskin and Greenhorn classes have the highest SiO_2 of the representative 11 Gale classes, and both fall within the andesite, dacite, and rhyolite TAS fields (Thompson et al., 2016). The Greenhorn class is interpreted as an altered Ronan sandstone, while the Buckskin mud/siltstone's Si enrichment may be representative of the primary igneous source (Morris et al., 2016; Thompson et al., 2016). These classes likely have separate origins, but are clustered together based on their common Si enrichment.

4.4.4 Endeavour Crater and Meridiani Planum

The Gusev Mazatzal basalts and the Gale Ronan class of rocks cluster with, and are highly similar to, the Endeavour Shoemaker impact breccia (SI: 11-8, 18-12 with and without S and Cl), and overall are more similar to Endeavour crater lithologies than most other non-Meridiani surface materials (Figures 4.1 and 4.2, and Tables 4.4 and 4.5). When S and Cl are removed, the Gusev plains basalts, John Klein class of Gale rocks, and the regolith breccia martian meteorites are most similar to the Endeavour materials (SI: 23-90, 23-96, 19-89 excluding erratics and pitted rocks, Tables 4.5). The Hesperian-aged Gusev basalts (Golombek et al., 2006) are most like the Shoemaker breccia and the average soil, which is itself a local martian average, indicating that the Gusev plains basalts could be a good representative typical martian crustal rock.

The Grasberg formation is a clastic bench unit first identified at Cape York as a sedimentary unit predominately on the interior rim of Endeavour crater (Crumpler et al., 2015). The Grasberg formation is younger than the Endeavour crater impact units and the Burns sedimentary unit by superposition, and has two lithologic units temporally separated by secondary alteration features (Crumpler et al., 2015). The statistical grouping model does not differentiate between the bulk chemistry of these two units, pointing towards a uniform source

across time (Bouchard & Jolliff, 2018b). The formation is also consistently most similar to the Shoemaker formation (SI: 37-45 with and without S and Cl) and average Meridiani soil (SI: 33 without S and Cl). These observations, compositional similarity and homogeneity in source composition of both members, support a local origin as a modified erosional unit of the Endeavour crater rim as opposed to a distal ash fall unit (Bouchard & Jolliff, 2018b).

The Matijevic formation is a fine-grained mudstone, determined to be a sedimentary layer that predates the Endeavour crater impact and is exposed in an erosional window at Cape York (Arvidson et al., 2014; Crumpler et al., 2015). The formation is distinct in composition from the other Endeavour crater lithologies with the exception of the lowest member of the overlying shoemaker breccia. This unit, the Copper Cliffs breccia, is interpreted to have included eroded Matijevic material based on compositional similarities and the inclusion of Matijevic spherules in the breccia (Bouchard & Jolliff, 2018b; Mittlefehldt, et al., 2018). However, this study highlights the high similarity in bulk composition between the fine grained, false color "blue" rocks of Endeavour crater and the Matijevic formation (SI: 20-40 without S and Cl, Tables 4.5). Noticeably, the Matijevic formation is more similar to the pre-Endeavour class of "blue" rocks than the post-Endeavour class. It is possible that the Matijevic exposure at Cape York is a package of eroded sediment from a block of pre-Endeavour "blue" basalts that was cemented over time into a mudstone by the mild aqueous environment evident by the presence of hematite spherules and "box-work" veins (Arvidson et al., 2014; Crumpler et al., 2015). This possible petrogenetic relationship between the Matijevic formation and the Pre-Endeavour "blue" rocks further strengthens the argument that the "blue" rocks are a basalt unit and not an impact melt sheet of Endeavour crater.

The Marquette Island erratic float rock encountered on the plains of Meridiani Planum that was neither a member of the local sulfate sandstones nor a meteorite (Farrand, Johnson, Bell III, Yingst, & Weitz, 2010; Mittlefehldt et al., 2010). It's false "blue" color in Pancam imagery, aphanitic texture, and composition are all similar to the suites of "blue" rocks of Endeavour crater (Bouchard et al., 2017). In this analysis we show the compositional similarity between Marquette Island and the Endeavour "blue" rock suites (Figures 4.1 and 4.2, and Tables 4.4 and 4.5). Marquette Island is more similar to the pre-Endeavour class (SI: 22 without S and Cl) than the post-Endeavour class (SI: 53 without S and Cl), which would be consistent if it is a high velocity projectile from a large local impact younger than the Burns emplacement. Both the Bopolu (19 km diameter, (Grant et al., 2016)) and Iazu (6.8 km diameter, (Powell, et al., 2017)) craters meet this requirement, and are < 3 and < 6 crater diameters from the location of the Marquette Island erratic. Based on a 45° ejection angle and other idealized launch conditions, a boulder could end up in the location of Marquette Island by being be ejected at 0.4-0.5 km/s from Bopolu crater or 0.2-0.3 km/s from Iazu crater. These velocities are well below the 5 km/s martian escape velocity, and both craters are capable of excavating beyond the ~115-260 meter depth of the Burns formation (Grant et al., 2016; Powell et al., 2017).

The Hoover erratic analyzed at Wdowiak ridge is not similar to either of the Endeavour "blue" rock suites despite appearing "blue" in false color Pancam and being in a similar location to the post-Endeavour "blue" rock Margaret brush. Hoover tends to cluster with the Endeavour rim sedimentary unit, the Grasberg formation (SI: 71-32 with and without S and Cl), but is more similar to the Bell Island and Ronan classes of Gale rocks (SI: 42-38, 42-28 with and without S and Cl, Tables 4.4 and 4.5). However, the high SO_3, Cl, and Zn compared to local rocks of

Wdowiak ridge suggest Hoover has an altered composition (Mittlefehldt, et al., 2018) which makes comparison of bulk APXS composition misleading.

As expected, the Bounce Rock erratic rock does not cluster with other Endeavour rocks but with the shergottite martian meteorites, and is most similar to the shergottite basalts and cumulates (SI: 50 and 66 without S and Cl, Tables 4.5). The lithology of Bounce Rock has previously been compared specifically to lithology B of the shergottite basalt EETA 79001 and Queen Alexandra Range 94201, which are included in the shergottite basalt and shergottite cumulate averages in this study (Zipfel et al., 2011).

The sulfate sandstone plains of Meridiani Planum, as represented in this analysis by the Burns formation, are very dissimilar to most other martian materials. The Cape Tribulation erratic Tickbush is a fine-grained homogenous texture, a generally basaltic composition, and a visual appearance in false color Pancam imagery similar to other Endeavour "blue" rocks (Bouchard et al., 2017). However, Tickbush is the most dissimilar single target of the rocks investigated by Opportunity, and so represents a distinctly unique rock suites.

The pitted rock units as observed on the rim overlooking Marathon Valley and within Perseverance Valley not only have distinct pitted textures and a "purple" hue is Pancam false color, but they are some of the most silica-rich rocks observed by the Opportunity rover (Chapter 3) (Bouchard et al., 2019; Tait et al., 2019). Based on the co-location of these units with the pre-Endeavour crater lithologies, it is likely that these rocks are also a pre-impact lithology. The rock pits and secondary alteration minerals are different between these two locations, which represents difference in secondary environments in Perseverance Valley and 80 meters up in the rim of Endeavour crater (Chapter 3) (Bouchard et al., 2019; Tait et al., 2019). The pitted rocks are far less competent than the "blue" rocks, are highly degraded in imagery, and are not

observed as float on the interior of Endeavour's rim. Stratigraphically the pitted rocks lie on top of the "blue" rock outcrop overlooking Marathon Valley, but it is unknown if this block/unit might be overturned. In Perseverance Valley the pitted rocks lie in a trough next to tabular "blue" rocks both in a linear outcrop running along the strike of the valley, but this could be a result of vertical displacement (Chapter 3) (Bouchard et al., 2019), mass wasting into the valley trough, or the two units could be tilted from their original orientation and the current expression is an erosional horizon. Overall these rocks are outliers in both clustering and similarity indices to all materials included in this analysis and represent a unique lithology (SI: 120-2900 with and without S and Cl, Figures 4.1 and 4.2, and Tables 4.4 and 4.5).

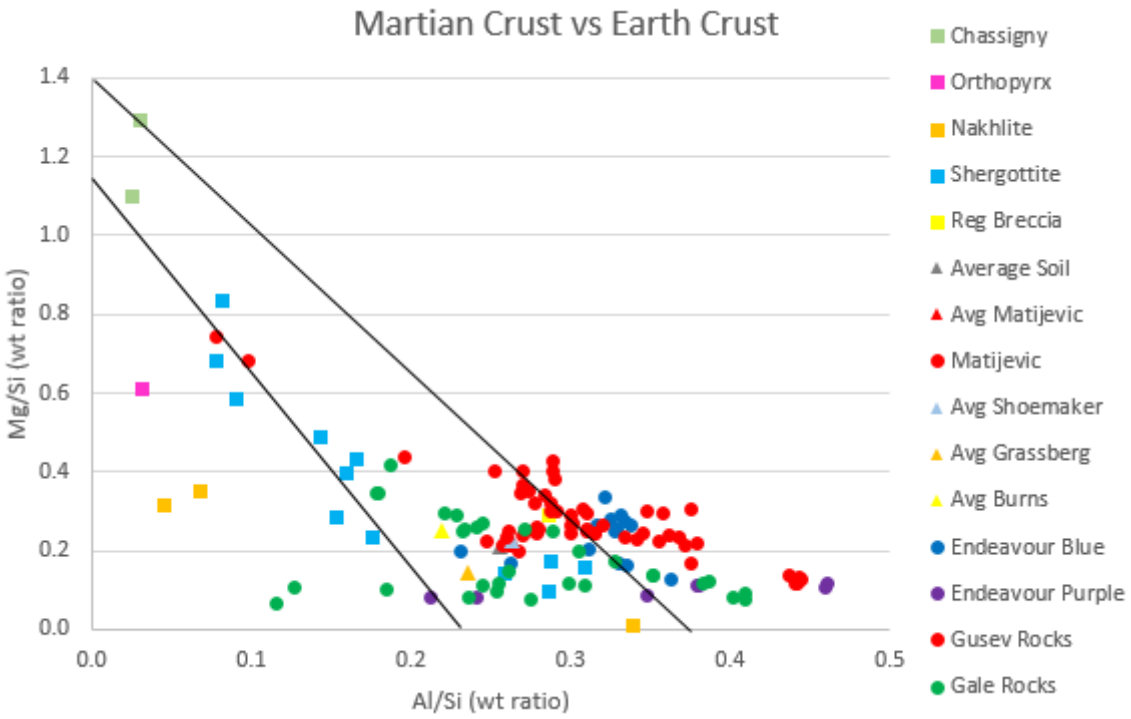

Figure 4.3 This plot contains the element weight ratios of the 149 representative target compositions included in this analysis. These lines have been used to discriminate martian rocks (left) and earth rocks (right). McSween et al (2009) argues that surface rocks don't discriminate along these lines like the martian meteorites do. I agree with this conclusion, however, the accepted "martian crust" composition line really only matches the shergottites, and doesn't even plot with several of the shergottites basalts (EETA 79001 lithology B and Dhofar 378) and basalt cumulates (Los Angeles and Queen Alexandra Range 94201).

4.4.5 Elemental Composition Comparisons

Al/Si vs Mg/Si wt. ratio plots have been used to discriminate martian and terrestrial crustal rock trends (Figure 4.3). McSween et al (2009) concluded that unlike the martian meteorites, robotic mission surface data does not plot on the "Mars" trend. Here we show that the "Mars" trend really only represents the Gusev Peace erratic and the shergottite meteorites (excluding basalts EETA 79001 lithology B and Dhofar 378, and cumulates Los Angeles and Queen Alexandra Range 94201, (Figure 4.3). Most of the surface materials intersect the "terrestrial" trend, and there may even be a third trend represented by the orthopyroxenite and nakhlite (excluding NWA 5970/6148) meteorites, and the Greenhorn and Buckskin classes of Gale crater rocks.

Fe (wt %) vs Mn (wt %) plots have been used to express trends associated with the mantle source composition of the martian meteorites (Figure 4.4). McSween et al (2009) argued that the data show a separate mantle trend for the rocks of Gusev crater. This study agrees with McSween's interpretation with the caveat that this mantle trend actually only applies to the shergottites, and adds that the Endeavour "blue" rocks (with the exception of the secondarily Mn-enriched Perseverance Valley "blue" rocks), the nakhlites (except NWA 5790/6148), and several Gale classes also plot on the Gusev mantle line (Figure 4.4). There may be even a third mantle trend represented by some Gusev and Gale targets and NWA 5790/6148. The Endeavour pitted rocks do not plot on any mantle trend, and thus their compositions may be more likely to be the result of alteration (Si and Mn enrichment and Fe depletion) of a basaltic source, a source that lies on the same mantle Fe-Mn trend as the Gusev basalts and the non-Mn enriched Endeavour "blue" rocks.

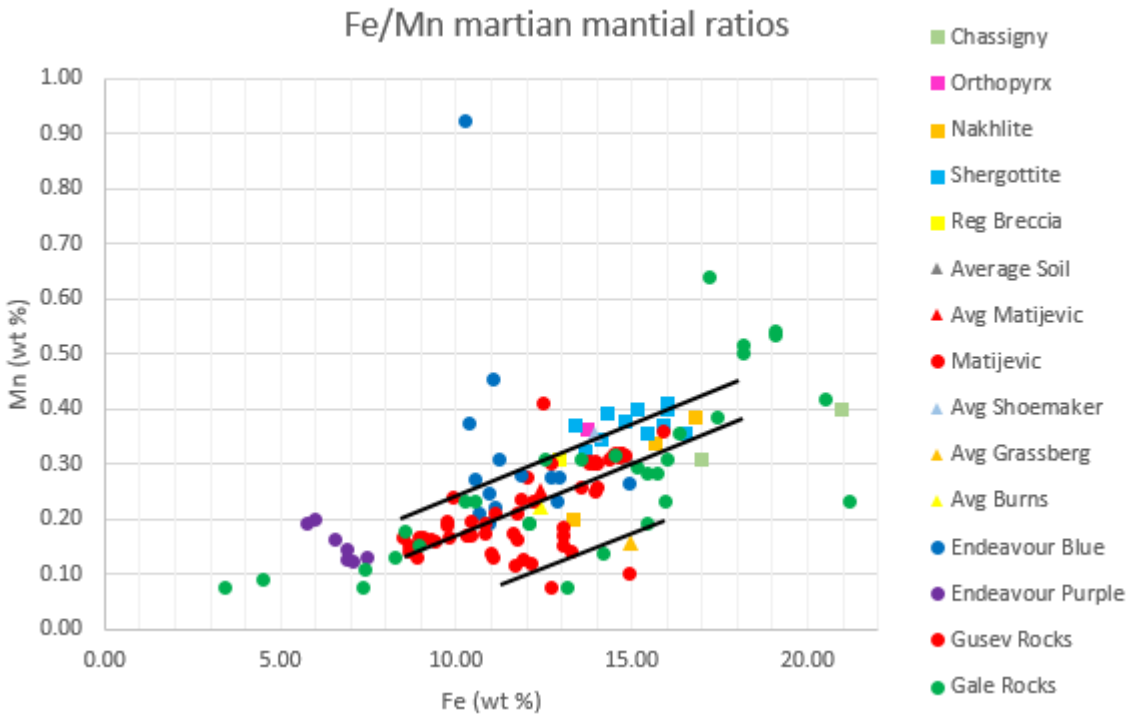

Figure 4.4 Weight % Fe vs. Mn of the 149 representative target compositions included in this analysis. The top line has been used to represent Fe/Mn ratio of the mantle source of the martian meteorites, McSween et al (2009) indicates that this implies a different mantle source than those of the Gusev rocks (red circles, middle line). The Endeavour "blue" rocks seem to fall on this line with the exception of the Perseverance Valley "blue" rocks, which have a Mn enrichment possibly due to secondary alteration. This study agrees with McSween's conclusion, but with the caveats that the first line only represents the shergottites, and that there are some Gusev targets that appear to define an even lower Fe/Mn ratio (bottom line). The pitted Endeavour rocks (purple circles) and several Gale sedimentary rocks (the Bathurst class, green circles) do not plot on any of the ratio lines but exhibits a Mn enrichment as well. The Endeavour erratic rock Tickbush (blue circle) has the highest Mn content of all targets in this study (0.9 wt%).

McSween et al (2009) also utilized an SiO_2 vs FeO/MgO plot to differentiate between mantle source regions of igneous rocks, in which most martian materials plot predominately as dry and tholeiitic as opposed to wet and calc-alkaline. The martian meteorite and APXS surface data used in this study predominantly agree with this interpretation (Figure 4.5). The exceptions are the silica-rich rocks, including the Lower Mt. Sharp Buckskin and Greenhorn classes of Gale rocks (rocks which span the andesite, dacite, and rhyolite fields in TAS diagrams (Thompson et al., 2016)), the silica-rich Endeavour pitted rocks, the olivine-phyric shergottites and the orthopyroxenite martian meteorites, and the Clinton igneous float rock. In the case of Greenhorn this silica enrichment has been inferred to suggest acid sulfate alteration (Thompson et al., 2016),

and the pitted rocks are not conclusively igneous rocks, so these targets are not reliable tracers for mantle composition. However, the martian meteorites, Clinton erratic, and to a lesser extent the Buckskin sedimentary rock, could be representative of samples of a previously underrepresented mantle composition indicative of hydrous melting. A more volatile-rich magma source has also been proposed for the Bradbury rocks (Schmidt et al., 2014), and modeling is also being used to suggest that the shergottites may have formed from a wetter magma (Balta & McSween, 2013). The martian crust has proven capable of producing similar rock dry, tholeiitic rock suites throughout geologic timescales (Noachian Pre-Endeavour "blue" to Hesperian Gusev Mazatzal basalts), as well as smaller units of more evolved and hydrous primary igneous materials (Clinton basalts, Buckskin protolith Gale rocks, orthopyroxenite and some olivine-phyric shergottites).

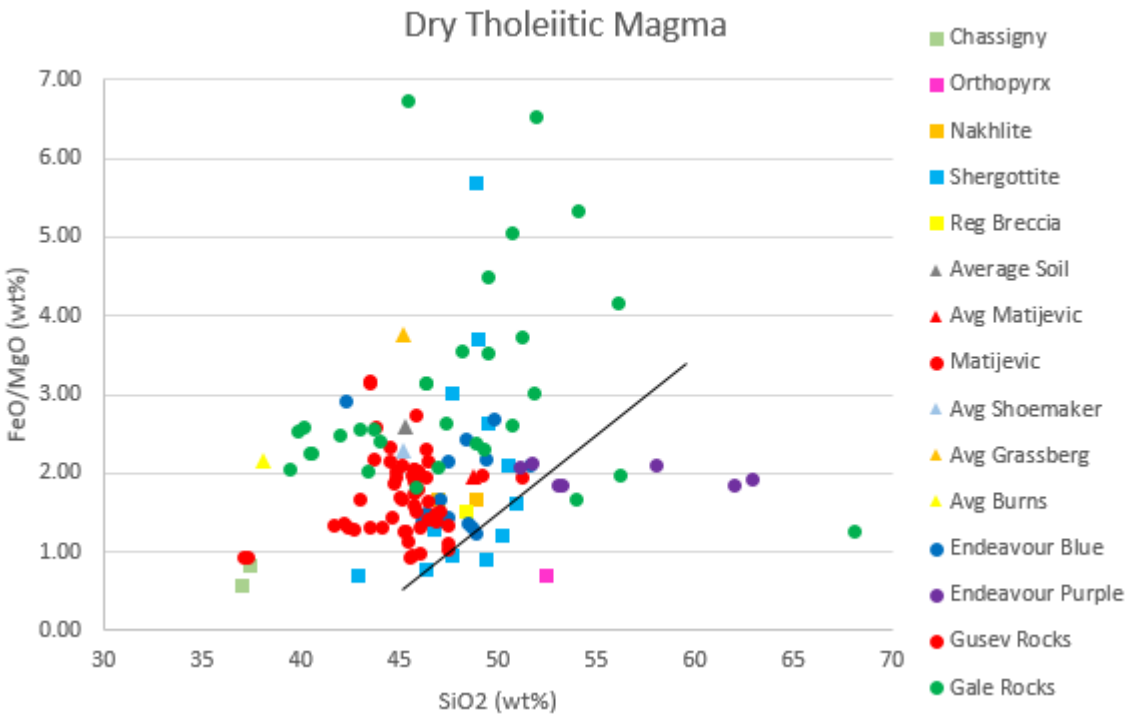

Figure 4.5 This plot contains oxide weight % and ratios of the 149 representative target compositions included in this analysis. The line represents the separation between inferred mantle source conditions, above the line is indicative of a dry and tholeiitic magma, and below is wet calc-alkaline mantle source (McSween 2009). These data agree with McSween's interpretation that the bulk martian mantle source is likely dry and tholeiitic. The outliers below the line include: the Buckskin and Greenhorn classes of Gale rocks (green circles), the Endeavour pitted rocks

(purple circles), the olivine-phyric shergottites (cyan squares) and the orthopyroxenite (pink square) martian meteorites, and an alkaline Gale basalt (Clinton, green circle). Some of these Si enrichments could be secondary alteration, while the definitively igneous rocks (Orthopyroxenite, olivine-phyric shergottites, and Clinton) that plot below this line could represent a more unique, wetter calc-alkaline magma source.

4.5 Conclusion

The cumulate martian meteorites, including the numerous gabbroic intrusive poikilitic shergottites, are highly dissimilar to the APXS rock suites investigated by rovers on the surface of Mars. This dissimilarity indicates that a significant fraction of the martian meteorites are not representative of martian surface materials. The other meteorite classes, especially the basaltic shergottites, are more similar to surface materials than other meteorites, but as a group are still only weakly similar to the Meridiani Plains erratic Hoover, the Gusev Mazatzal and plains basalts, and the Ronan and Mt. Bastion class of Gale rocks. The Meridiani Planum erratic Bounce Rock is highly similar to lithology B of the basaltic shergottite EETA 79001.

The bulk composition of the regolith breccia class of meteorite is much more representative of the surface materials as reported by the APXS, especially the Endeavour and Gusev crater basalts, and also the Ronan and Mt. Bastion class of rocks at Gale. In general, the martian meteorites are more similar to members of their own suite than to any other materials with the exception of highly dissimilar nakhlite meteorite NWA 5790/6148.

The predominately igneous rocks of Gusev crater form three discrete suites on the basis of geographic units, indicating discrete compositions between these Hesperian lava flows. The Husband Hill unit is the most unique suite of Gusev rocks, while the olivine bearing sedimentary unit and the oldest Gusev unit, the West Spur rocks, are more similar to Endeavour crater materials, specifically the pre-Endeavour crater “blue” basalt unit. The plains basalts of Gusev are most similar to Endeavour crater impact materials, but especially the Mazatzal class, which

differs slightly in compositional relationships from other plains basalts. All the Gusev plains basalts are highly similar to the Gale Ronan rock class, and moderately similar to the Gale John Klein and Bell Island rock classes. Peace, the ultramafic sandstone, is a unique compositional outlier and is one of the most dissimilar rocks in this study. It is more similar to the poikilitic shergottites than to other surface materials.

Most of the rocks of the sedimentary basin in Gale crater are not neatly separated by geography in the model as are the Gusev units. The Gale targets are generally less similar to the Endeavour and Gusev crater materials, not only the sedimentary units, but especially the alkaline Jake M and Clinton classes of igneous float rocks. Jake M and Clinton point to two discrete primary rock protoliths for Gale crater, both compositionally different than Endeavour, Gusev, and shergottite primary materials. The Clinton parent magma could possibly be fractionated from an Adirondack-type of magma (Edwards et al., 2017). The Jum Jum rock target is difficult to classify, but cluster and SI analysis suggests its bulk composition is most like the Rocknest class of rocks. However, the Ronan and Mt. Bastion classes of Gale rock are consistently some of the most similar materials to Gusev, Endeavour, and shergottite materials. Without S and Cl, the John Klein and Bell Island rock classes are also moderately similar to Endeavour and Gusev materials. These discrepancies indicate a diverse set of primary protoliths feeding into the Gale basin. The high similarity between the chemistry and geography of the Bathurst and Bell Island materials indicates a likely common sediment source material. The Gale mud/siltstones Buckskin and Greenhorn are highly dissimilar to all of the surface and meteorite materials in this study due to Si-enrichment based on (a) primary source (Buckskin) and (b) secondary alteration factors (Greenhorn).

The fine-grained, pre-Endeavour Matijevic formation is unique in composition from other Opportunity materials, but is most similar to the igneous suite of pre-Endeavour and similarly false colored “blue” rocks. It is possible that the exposure at Matijevic hill was sediment eroded from pre-Endeavour “blue” rock that was subsequently cemented and eventually host to spherule concretion formation (possibly reworked in a sedimentary depositional environment) and alteration veins. This relationship would imply a mid-late Noachian emplacement time for the pre-Endeavour “blue” rock suite prior the Endeavour crater impact, as opposed to an Endeavour crater impact melt sheet origin. On the basis of major and minor elemental composition and rock texture, the pre-Endeavour “blue” rock suite includes the basaltic outcrop overlooking Marathon Valley (Sgt. Charles Floyd), the San Miguel type outcrop within Perseverance Valley (Jornada Del Muerto), and the Marquette Island erratic. Marquette Island (Sol 2070-2075) was encountered in Meridiani Planum prior to arriving at the rim of Endeavour crater, sitting on top of the Burns formation that embays Endeavour crater. This location makes Marquette Island likely a high velocity projectile from a crater such as Bopolu or Iazu, and indicating that pre-Endeavour “blue” rock formation is not only a significant geographic unit spanning over 50 km, but could be a sample of the Middle-Noachian highland unit underlying the Meridiani plains (Tanaka et al., 2014) and thus one of the oldest rocks examined on the surface of Mars.

The internal homogeneity of the two clastic Grasberg formation units and its similarity to Meridiani soil and the Shoemaker impact breccia it overlies, points to a local erosional origin over a distal volcanic ash. The Endeavour erratics, Hoover, Bounce Rock, and Tickbush are not members of the pre-Endeavour “blue” rock suite, and Hoover may be a highly altered, local post-

Endeavour “blue” rock. Tickbush is the most dissimilar single target analyzed by Opportunity and represent a unique lithology not encountered elsewhere in the mission.

The silica-rich martian materials are indicative of a range primary and secondary processes. The Endeavour pitted rocks may be altered from a primary igneous source with a mantle source composition that has the same Fe-Mn trend as unaltered Endeavour “blue” rocks and the Gusev basalts. While the rocks which exhibit a likely primary silica-enrichment, such as martian meteorites ALH 84001 and some olivine-phyric shergottites, and the Gale Buckskin class of rock and Clinton basalt, could have been formed from a mantle source with a uniquely calc-alkaline chemistry.

Mars is predominately a one-plate, one-rock-type planet, with secondary alteration and sedimentary materials often not far removed from primary basaltic compositions. However, by comparing the well contextualized sample suites of three separate landing sites to each other and to the martian meteorites, we can gain a better understanding of the diversity of the martian crust.

Acknowledgements

We would like to thank NASA, the Jet Propulsion Laboratory, and other participating institutions of Mars Exploration Rover program for their support of the Opportunity mission, as well as the science, engineering, and operations teams. We would like to especially thank B. Farrand, L. Crumpler, D. Mittlefehldt, S. VanBommel, and R. Gellert for their productive conversations and collaboration in this work. Support for this work provided by NASA Earth and Space Sciences Fellowship grant 80NSSC17K0490 to M. Bouchard and JPL subcontract 1536058 to B. Jolliff.

4.6 References

Agee, C. B., Wilson, N. V., McCubbin, F. M., Ziegler, K., Polyak, V. J., Sharp, Z. D., . . . Elardo, S. M. (2013). Unique meteorite from early Amazonian Mars: Water-rich basaltic breccia Northwest Africa 7034. *Science, 339*(6121).

Arvidson, R. E., Anderson, R. C., Bartlett, P., Bell III, J. F., Blaney, D., Christensen, P. R., . . . Wilson, J. (2004). Localization and physical properties experiments conducted by Spirit at Gusev Crater. *Science, 305*, 821-824.

Arvidson, R. E., Anderson, R. C., Bartlett, P., III, J. F. B., Christensen, P. R., Chu, P., . . . Wilson, J. (2004). Localization and Physical Property Experiments Conducted by Opportunity at Meridiani Planum *Science, 306*(5702), 1730-1733.

Arvidson, R. E., Bell III, J. F., Bellutta, P., Cabrol, N. A., Catalano, J. G., Cohen, J., . . . Yen, A. S. (2010). Spirit Mars Rover Mission: Overview and selected results from the northern Home Plate Winter Haven to the side of Scamander crater. *Journal of Geophysical Research: Planets, 115*(E00F03).

Arvidson, R. E., Poulet, F., Morris, R. V., Bibring, J. P., Bell III, J. F., Squyres, S. W., . . . Wolff, M. (2006). Nature and origin of the hematite-bearing plains of Terra Meridiani based on analyses of orbital and Mars Exploration rover data sets. *Journal of Geophysical Research: Planets, 111*(E12S08).

Arvidson, R. E., Ruff, S. W., Morris, R. V., Ming, D. W., Crumpler, L. S., Yen, A. S., . . . McLennan, S. M. (2008). Spirit Mars Rover Mission to the Columbia Hills, Gusev Crater: Mission overview and selected results from the Cumberland Ridge to Home Plate. *Journal of Geophysical Research, 113*, E12S33. doi:10.1029/2008JE003183

Arvidson, R. E., Seelos, F. P., Deal, K. S., Koeppen, W. C., Snider, N. O., Kieniewicz, J. M., . . . Garvin, J. B. (2003). Mantled and exhumed terrains in Terra Meridiani, Mars *Journal of Geophysical Research, 108*(E12), 8073, DOI 8010.1029/2002JE001982.

Arvidson, R. E., Squyres, S. W., Anderson, R. C., Bell, J. F., III, Blaney, D., Brückner, J., . . . Yen, A. (2006). Overview of the Spirit Mars Exploration Rover Mission to Gusev Crater: Landing site to Backstay Rock in the Columbia Hills. *Journal of Geophysical Research, 111*(E2), 22. doi:10.1029/2005JE002499

Arvidson, R. E., Squyres, S. W., Bell III, J. F., Catalano, J. G., Clark, B. C., Crumpler, L. S., . . . Wolff, M. J. (2014). Ancient aqueous environments at Endeavour crater, Mars. *Science, 343*, 441-448. doi:DOI: 10.1126/science.1248097

Balta, J. B., & McSween Jr., H. Y. (2013). Application of the MELTS algorithm to Martian compositions and implications for magma crystallization. *Journal of Geophysical Research: Planets, 118*(12), 2502-2519. doi:10.1002/2013je004461

Balta, J. B., & Y. McSween, H. (2013). *Water and the composition of Martian magmas* (Vol. 41).

Beck, P., Pommerol, A., Zanda, B., Remusat, L., Göpel, C., Hewins, R., . . . Chevrier, V. F. (2015). A Noachian source region for the "Black Beauty" meteorite, and a source lithology for Mars surface hydrated dust? . *Earth and Planetary Science Letters, 427*, 104-111. doi:10.1016/j.epsl.2015.06.033

Bell, J. (2008). *The Martian Surface, Composition, Mineralology, and Physical Propertites*. United Kingdom: Cambridge Planetary Science.

Bogard, D. D., & Johnson, P. (1983). Martian Gases in an Antarctic Meteorite? *Science, 221*(4611), 651-654.

Bogard, D. D., Nyquist, L. E., & Johnson, P. (1984). Noble gas contents of shergottites and implications for the Martian origin of SNC meteorites. *Geochimica et Cosmochimica Acta, 48*(9), 1723-1739. doi:http://dx.doi.org/10.1016/0016-7037(84)90028-0

Bouchard, M. C., Jollif, B. L., & Farrand, W. H. (2019). Lithochemical Rock Suites of Perseverance Valley, Endeavour Crater, Mars. *Lunar and Planetary Science, 50*.

Bouchard, M. C., & Jolliff, B. L. (2016). Comparing MER Opportunity rock groups and martian meteorites using hierarchical clustering and a similarity index. *Lunar and Planetary Science Conference, 47*, #2551.

Bouchard, M. C., & Jolliff, B. L. (2018a). Rock suites of Endeavour crater, Mars: comparing Perseverance Valley to the floor of Spirit of St. Louis Crater. *Lunar and Planetary Science Conference, 49*, #2590.

Bouchard, M. C., & Jolliff, B. L. (2018b). A systematic method for classifying and grouping late Noachian and early Hesperian rock targets analyzed by the Mars Exploration Rover Opportunity at Endeavour crater, Mars. *Journal of Geophysical Research: Planets, 123*. doi:10.1029/2018JE005631

Bouchard, M. C., Jolliff, B. L., Farrand, W. H., & Mittlefehldt, D. W. (2017). Constraining the origin of basaltic volcanic rocks by Opportunity along the rim of Endeavour crater. *Lunar and Planetary Science Conference, 48*, #1608.

Cannon, K. M., Mustard, J. F., & Agee, C. B. (2015). Evidence for a widespread basaltic breccia component in the martian low-albedo regions from the reflectance spectrum of Northwest Africa 7034. *Icarus, 252*, 150-153. doi:10.1016/j.icarus.2015.01.016

Christensen, P. R., Bandfield, J. L., Clark, R. N., Edgett, K. S., Hamilton, V. E., Hoefen, T., . . . Smith, M. D. (2000). Detection of crystalline hematite mineralization on Mars by the

Thermal Emission Spectrometer: Evidence for near-surface water. *J. Geophys. Res., 105*(E4), 9623-9642.

Clark, B. C., Morris, R. V., McLennan, S. M., Gellert, R., Jolliff, B., Knoll, A., . . . Rieder, R. (2005). Chemistry and mineralogy of outcrops at Meridiani Planum. *Earth and Planetary Science Letters, 240*, 73-94.

Crumpler, L. S., Arvidson, R. E., Bell, J., Clark, B. C., Cohen, B. A., Farrand, W. H., . . . Yen, A. S. (2015). Context of ancient aqueous environments on Mars from in situ geologic mapping at Endeavour Crater. *Journal of Geophysical Research: Planets, 120*, 538-569. doi:10.1002/2014JE004699

Crumpler, L. S., Squyres, S. W., Arvidson, R. E., Bell, J. F., Blaney, D., Cabrol, N. A., . . . Fergason, R. (2005). Mars Exploration Rover geologic traverse by the Spirit rover in the plains of Gusev crater, Mars. *Geology, 33*(10), 809-812.

Edwards, P. H., Bridges, J. C., Wiens, R., Anderson, R., Dyar, D., Fisk, M., . . . Hutchinson, I. (2017). Basalt–trachybasalt samples in Gale Crater, Mars. *Meteoritics & Planetary Science, 52*(11), 2931-2410. doi:10.1111/maps.12953

Farrand, W. H., Johnson, J. R., Bell III, J. F., Yingst, R. A., & Weitz, C. M. (2010). Distinguishing Martian "Erratics" from Meteorites at Meridiani Planum Using Pancam: Comparing Marquette Island to Meridiani Cobbles. *Lunar and Planetary Science, 41*.

Gellert, R., Rieder, R., Anderson, R. C., Brückner, J., Clark, B. C., Dreibus, G., . . . Zipfel, J. (2004). Chemistry of rocks and soils in Gusev Crater from the alpha particle X-ray spectrometer. *Science, 305*, 829-832.

Gellert, R., Rieder, R., Brückner, J., Clark, B. C., Dreibus, G., Klingelhöfer, G., . . . Squyres, S. W. (2006). Alpha Particle X-Ray Spectrometer (APXS): Results from Gusev crater and calibration report. *Journal of Geophysical Research: Planets, 111*(E02S05), 1-32. doi:10.1029/2005JE002555

Golombek, M. P., Crumpler, L. S., Grant, J. A., Greeley, R., Cabrol, N. A., Parker, T. J., . . . Squyres, S. W. (2006). Geology of the Gusev cratered plains from the Spirit rover transverse. *J. Geophys. Res., 111*(E2), 27. doi:10.1029/2005JE002503

Grant, J. A., Parker, T. J., Crumpler, L. S., Wilson, S. A., Golombek, M. P., & Mittlefehldt, D. W. (2016). The degradational history of Endeavour crater, Mars. *Icarus, 280*, 22-36. doi:http://dx.doi.org/10.1016/j.icarus.2015.08.019

Grotzinger, J. P., Arvidson, R. E., Bell III, J. F., Calvin, W., Clark, B. C., Fike, D. A., . . . Watters, W. A. (2005). Stratigraphy and sedimentology of a dry to wet eolian depositional system, Burns formation, Meridiani Planum, Mars. *Earth and Planetary Science Letters, 240*, 11-72.

Grotzinger, J. P., Crisp, J., Vasavada, A. R., Anderson, R. C., Baker, C. J., Barry, R., . . . Wiens, R. C. (2012). Mars Science Laboratory Mission and Science Investigation. *Space Science Reviews, 170*(1), 5-56. doi:10.1007/s11214-012-9892-2

Grotzinger, J. P., Sumner, D. Y., Kah, L. C., Stack, K., Gupta, S., Edgar, L., . . . Yingst, A. (2014). A Habitable Fluvio-Lacustrine Environment at Yellowknife Bay, Gale Crater, Mars. *Science (New York, N.Y.), 343*(6169), 1242777-1242777. doi:10.1126/science.1242777

Humayun, M., Nemchin, A., Zanda, B., Hewins, R. H., Grange, M., Kennedy, A., . . . Deldicque, D. (2013). Origin and age of the earliest Martian crust from meteroite NWA 7533. *Nature, 503*, 513-516.

Jambon, A., Barret, J.-A., Bollinger, C., Sautter, V., Bourdouma, O., Greenwood, R. C., . . . Badia, D. (2010). Northwest Africa 5790. Top sequence of the Nakhlite pile. *Lunar and Planetary Science, 41*.

Lentz, R. C. F., Taylor, G. J., & Treiman, A. H. (1999). Formation of a martian pyroxenite: A comparative study of the nakhlite meteorites and Theo's Flow. *Meteoritics & Planetary Science, 34*(6), 919-932. doi:10.1111/j.1945-5100.1999.tb01410.x

Liu, Y., Balta, J. B., A. Goodrich, C., Y. McSween Jr, H., & A. Taylor, L. (2012). *New constraints on the formation of shergottite Elephant Moraine 79001 lithology A* (Vol. 108).

Lodders, K. (1998). A survey of shergottite, nakhlite, and chassigny meteorites whole-rock compositions. *Meteoritics & Planetary Science, 33*, A183-190.

McLennan, S. M. (2012). Geochemistry of Sedimentary Processes on Mars. In J. P. Grotzinger & R. E. Milliken (Eds.), *Sedimentary Geology of Mars* (Vol. 102, pp. 119-138): SEPM Spec.

McLennan, S. M., Anderson, R. B., Bell, J. F., Bridges, J. C., Calef, F., Campbell, J. L., . . . Yingst, R. A. (2014). Elemental Geochemistry of Sedimentary Rocks at Yellowknife Bay, Gale Crater, Mars. *Science, 343*(6169), 1244734. doi:10.1126/science.1244734

McLennan, S. M., Bell, J. F., III, Calvin, W. M., Christensen, P. R., Clark, B. C., de Souza, P. A., . . . Yen, A. (2005). Provenance and diagenesis of the evaporite-bearing Burns formation, Meridiani Planum, Mars. *Earth and Planetary Science Letters, 240*, 95-121.

McLennan, S. M., & Grotzinger, J. P. (2008). The sedimentary rock cycle of Mars. In J. Bell (Ed.), *The Martian Surface: Composition, Mineralogy and Physical Properties* (pp. 541-577). Cambridge: Cambridge University Press.

McSween, H. Y., Arvidson, R. E., Bell III, J. F., Blaney, D., Cabrol, N. A., Christensen, P. R., . . . Zipfel, J. (2004). Basaltic rocks analyzed by the Spirit rover in Gusev Crater. *Science, 305*, 842-845.

McSween, H. Y., Jr. (2015). Petrology on Mars. *American Mineralogist, 100*(11-12), 2380-2395. doi:10.2138/am-2015-5257

McSween, H. Y., Taylor, G. J., & Wyatt, M. B. (2009). Elemental Composition of the Martian Crust. *Science, 324*(736), 736-739. doi:10.1126/science.1165871

Meyer, C. (2019). *Mars Meteorite Compendium -- 2019* (Vol. JSC # 27672). Houston, Texas: Lyndon B. Johnson Space Center.

Ming, D. W., Mittlefehldt, D. W., Morris, R. V., Golden, D. C., Gellert, R., Yen, A., . . . Wang, A. (2006). Geochemical and mineralogical indicators for aqueous processes in the Columbia Hills of Gusev crater, Mars. *Journal of Geophysical Research: Planets, 111*(E2). doi:10.1029/2005je002560

Ming, D. W., Morris, R. V., & Clark, B. C. (2008). Aqueous alteration on Mars. In J. Bell (Ed.), *The Martian Surface: Composition, Mineralogy and Physical Properties* (pp. 519-540). Cambridge: Cambridge University Press.

Mittlefehldt, D. W., Crumpler, L. S., Grant, J. A., Arvidson, R. E., & Farrand, W. H. (2018). Noachian-aged pre-impact lithology exposed in Endeavour crater rim: Mars Exploration Rover Opportunity observations. *Geological Society of America Abstracts with Programs, 50*(6). doi:10.1130/abs/2018AM-318037

Mittlefehldt, D. W., Gellert, R., Herkenhoff, K. E., Morris, R. V., Clark, B. C., Cohen, B. A., . . . Team, t. A. S. (2010). Marquette Island: a distinct mafic lithology discovered by Opportunity. *Lunar and Planetary Science Conference, 41*, #2109.

Mittlefehldt, D. W., Gellert, R., VanBommel, S. J., Ming, D. W., Yen, A. S., Clark, B. C., . . . Rice, J. W. (2018). Diverse Lithologies and Alteration Events on the Rim of Noachian-Aged Endeavour Crater, Meridiani Planum, Mars: In-Situ Compositional Evidence. *Journal of Geophysical Research: Planets*(123). doi:10.1002/2017JE005474

Mittlefehldt, D. W. C., L. S., Grant, J. A., Arvidson, R. E., & Farrand, W. H. (2018). Noachian-aged pre-impact lithology exposed in Endeavour crater rim: Mars Exploration Rover Opportunity observations. *Geological Society of America Abstracts with Programs, 50*(6). doi:10.1130/abs/2018AM-318037

Morris, R. V., & Klingelhöfer, G. (2008). Iron mineralogy and aqueous alteration on Mars from the MER Mössbauer spectrometers. In J. Bell (Ed.), *The Martian Surface: Composition, Mineralogy and Physical Properties* (pp. 339-365). Cambridge: Cambridge University Press.

Morris, R. V., Klingelhöfer, G., Bernhardt, B., Schröder, C., Rodionov, D. S., de Souza Jr., P. A., . . . Arvidson, R. E. (2004). Mineralogy at Gusev Crater from the Mössbauer spectrometer on the Spirit rover. *Science, 306*, 833-836.

Morris, R. V., Vaniman, D. T., Blake, D. F., Gellert, R., Chipera, S. J., Rampe, E. B., . . . Schwenzer, S. P. (2016). Silicic volcanism on Mars evidenced by tridymite in high-SiO2 sedimentary rock at Gale crater. *Proceedings of the National Academy of Sciences of the United States of America, 113*(26), 7071-7076. doi:10.1073/pnas.1607098113

Morris, R. V. e. a. (2006). Mössbauer mineralogy of rock, soil, and dust at Meridiani Planum, Mars: Opportunity's journey across sulfate-rich outcrop, basaltic sand and dust, and hematite lag deposits. *Journal of Geophysical Research, 111*, E12S15. doi:10.1029/2006JE002791

Owen, T., Biemann, K., Rushneck, D. R., Biller, J. E., Howarth, D. W., & Lafleur, A. L. (1977). The composition of the atmosphere at the surface of Mars. *Journal of Geophysical Research (1896-1977), 82*(28), 4635-4639. doi:10.1029/JS082i028p04635

Powell, K. E., Arvidson, R. E., Zanetti, M., Guinness, E. A., & Murchie, S. L. (2017). The structural, stratigraphic, and paleoenvironmental record exposed on the rim and walls of Iazu Crater, Mars. *Journal of Geophysical Research: Planets, 122*(5), 1138-1156. doi:10.1002/2016je005196

Rahib, R. R., Udry, A., Combs, L. C., & Howarth, G. H. (2018). Formation and emplacement processes of martian poikilitic shergottite meteorites. *Lunar and Planetary Science, 49*.

Rieder, R., Gellert, R., Anderson, R. C., Brückner, J., Clark, B. C., Dreibus, G., . . . Zipfel, J. (2004). Chemistry of Rocks and Soils at Meridiani Planum from the Alpha Particle X-ray Spectrometer *Science, 306*(5702), 1746-1749.

Rieder, R., Gellert, R., Brückner, J., Klingelhöfer, G., Dreibus, G., Yen, A., & Squyres, S. W. (2003). The new Athena alpha particle X-ray spectrometer for the Mars Exploration Rovers. *J. Geophys. Res., 108*(E12). doi:10.1029/2003JE002150

Rieder, R. T., Economou, T., Wänke, H., Turkevich, A., Crisp, J., Brückner, J., . . . McSween, H. Y., Jr. (1997). The chemical composition of martian rocks and soil returned by the mobile Alpha Proton X-ray Spectrometer: Preliminary results from the X-ray mode. *Science, 278*, 1771-1776.

Ruff, S. W., & Farmer, J. D. (2016). Silica deposits on Mars with features resembling hot spring biosignatures at El Tatio in Chile. *Nature Communications, 7*, 13554. doi:10.1038/ncomms13554 https://www.nature.com/articles/ncomms13554#supplementary-information

Schmidt, M. E., Campbell, J. L., Gellert, R., Perrett, G. M., Treiman, A. H., Blaney, D. L., . . . Wiens, R. C. (2014). Geochemical diversity in first rocks examined by the Curiosity Rover in Gale Crater: Evidence for and significance of an alkali and volatile-rich igneous source. *Journal of Geophysical Research: Planets, 119*(1), 64-81. doi:10.1002/2013je004481

Squyres, S. W., Arvidson, R. E., Baumgartner, E. T., Bell, J. F., III, Christensen, P. R., Gorevan, S., . . . Romero, R. A. (2003). Athena Mars rover science investigation. *Journal of Geophysical Research, 108*(E12). doi:10.1029/2003JE002121

Squyres, S. W., Arvidson, R. E., Bell III, J. F., Clef III, F., Clark, B. C., Cohen, B. A., . . . Zacny, K. (2012). Ancient Impact and Aqueous Processes at Endeavour Crater, Mars. *Science, 336*, 570-576. doi:10.1126/science.1220476

Squyres, S. W., Arvidson, R. E., Bell, J. F. I., Brückner, J., Cabrol, N. A., Calvin, W., . . . Yen, A. (2004). The Spirit rover's Athena science investigation at Gusev Crater, Mars. *Science, 305*, 794-799.

Squyres, S. W., Arvidson, R. E., Blaney, D. L., Clark, B. C., Crumpler, L., Farrand, W. H., . . . Yen, A. (2006). Rocks of the Columbia Hills. *Journal of Geophysical Research: Planets, 111*(E2). doi:10.1029/2005je002562

Squyres, S. W., Grotzinger, J. P., Arvidson, R. E., Bell III, J. F., Calvin, W., Christensen, P. R., . . . Soderblom, L. A. (2004). In situ evidence for an ancient aqueous environment at Meridiani Planum, Mars. *Science, 306*, 1709-1714.

Squyres, S. W., & Knoll, A. H. (2005). Sedimentary rocks at Meridiani Planum: Origin, diagenesis, and implications for life on Mars. *Earth and Planetary Science Letters, 240*(1), 1-10.

Stolper, E. M., Baker, M. B., Newcombe, M. E., Schmidt, M. E., Treiman, A. H., Cousin, A., . . . Team, a. t. M. S. (2013). The petrochemistry of Jake_M: A martian mugearite. *Science, 341*(6153). doi:10.1126/science.1239463

Tait, A. W., Schröder, C., Farrand, W. H., Ashley, J. W., Cohen, B. A., Gellert, R., . . . Jollif, B. L. (2019). Exploring Origins of Pitted/Vesicular Rocks in Perseverance Valley, Endeavour Crater. *Lunar and Planetary Science, 50*.

Tanaka, K. L., Skinner, J. A., Dohm Jr., J. M., Irwin III, R. P., Kolb, E. J., Fortezzo, C. M., . . . Hare, T. M. (Cartographer). (2014). Geologic map of Mars

Thompson, L., Schmidt, M., Spray, J., Berger, J., Fairén, A., L. Campbell, J., . . . VanBommel, S. (2016). *Potassium-rich sandstones within the Gale impact crater, Mars: The APXS perspective: Potassium-rich sandstones on Mars*.

Udry, A., Balta, J. B., & McSween Jr., H. Y. (2014). Exploring fractionation models for Martian magmas. *Journal of Geophysical Research: Planets, 119*(1), 1-18. doi:10.1002/2013je004445

Udry, A., Lunning, N. G., McSween, H. Y., & Bodnar, R. J. (2014). Petrogenesis of a vitrophyre in the martian meteorite breccia NWA 7034. *Geochimica et Cosmochimica Acta, 141*, 281-293. doi:10.1016/j.gca.2014.06.026

Wittmann, A., Korotev, R. L., Jolliff, B. L., Irving, A. J., Moser, D. E., Barker, I., & Rumble III, D. (2015). Petrography and composition of Martian regolith breccia meteorite Northwest Africa 7475. *The Meteoritical Society, 50*(2), 326-352.

Zipfel, J., Schröder, C., Jollif, B. L., Gellert, R., Herkenhoff, K. E., Rieder, R., . . . Yen, A. S. (2011). Bounce Rock—A shergottite-like basalt encountered at Meridiani Planum, Mars. *Meteoritics & Planetary Science, 46*(Nr 1), 1–20. doi:10.1111/j.1945-5100.2010.01127.

Appendix

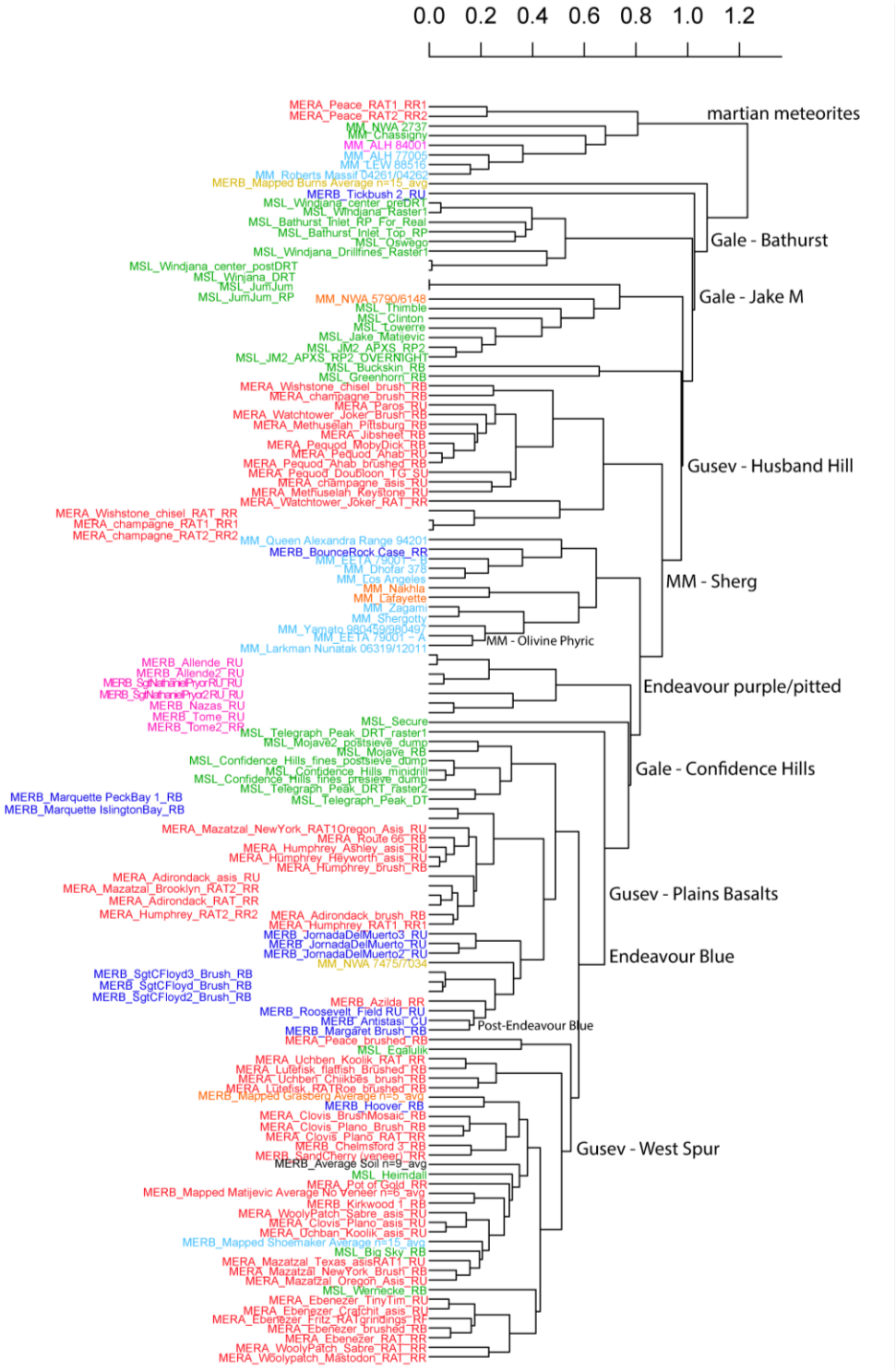

Figure A4.1: This is an agglomerative, group average, hierarchical cluster of all 131 targets and averages including S and Cl. Chassignite martian meteorites and Gale targets are in green, the orthopyroxenite martian meteorite and the Endeavour pitted rocks are in pink, the nakhlite martian meteorites and the Endeavour Grasberg formation average are in orange, the shergottite martian meteorites and the Endeavour Shoemaker formation average are in cyan, the regolith breccia meteorites and the Endeavour Burns formation average are in yellow, the Endeavour "blue" class of rocks are in blue, and the Gusev targets and Endeavour Matijevic formation average and targets are in red.

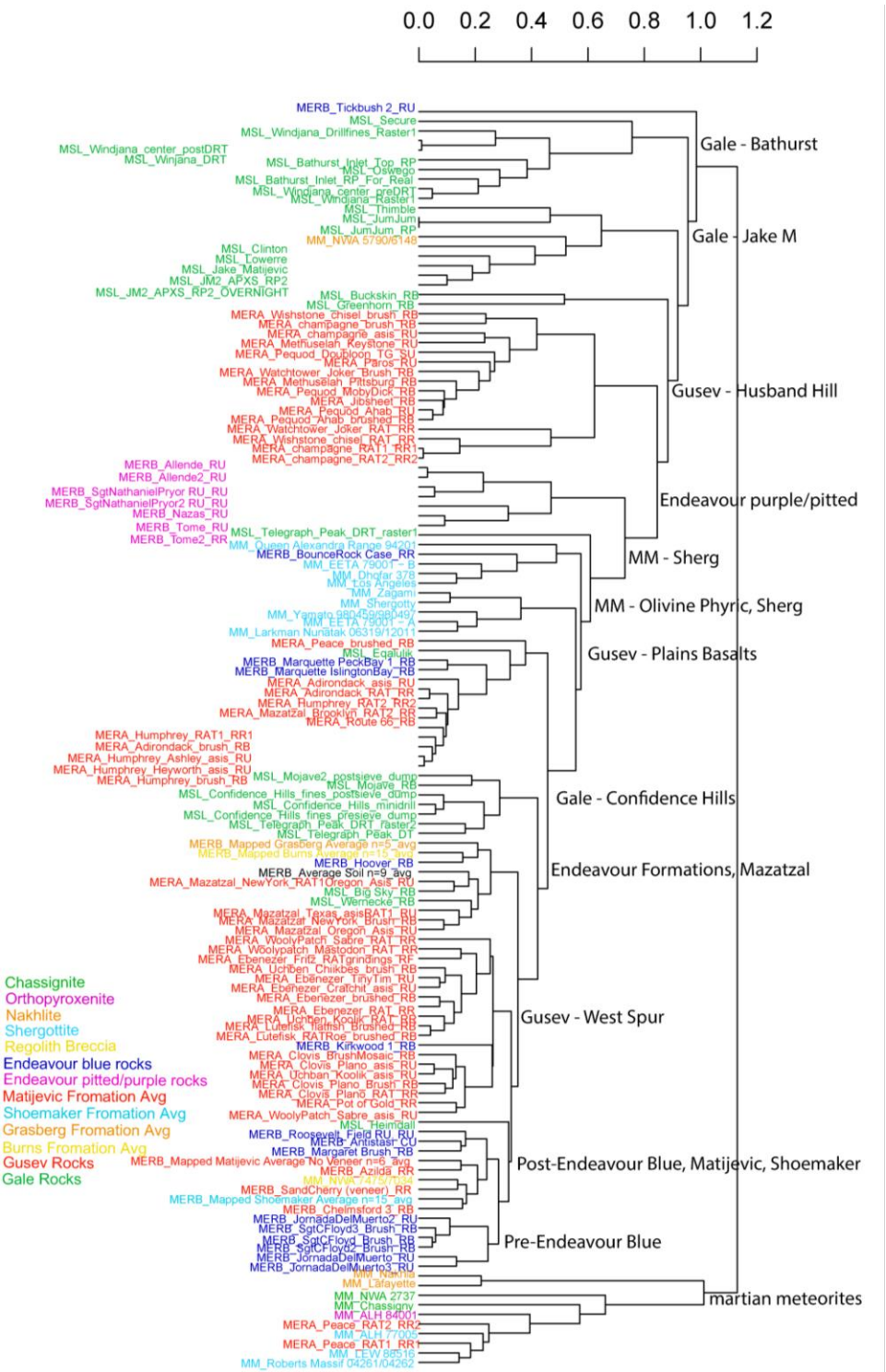

Figure A4.2: This is an agglomerative, group average, hierarchical cluster of all 131 targets and averages with S and Cl removed. Chassignite martian meteorites and Gale targets are in green, the orthopyroxenite martian meteorite and the Endeavour pitted rocks are in pink, the nakhlite martian meteorites and the Endeavour Grasberg formation average are in orange, the shergottite martian meteorites and the Endeavour Shoemaker formation average are in cyan, the regolith breccia meteorites and the Endeavour Burns formation average are in yellow, the Endeavour "blue" class of rocks are in blue, and the Gusev targets and Endeavour Matijevic formation average and targets are in red.